No. 099
December 1970

THE WAVE RESISTANCE OF AN AIR-CUSHION VEHICLE IN ACCELERATED MOTION

Lawrence J. Doctors
Som D. Sharma

This research was carried out under Office of Naval Research Contract No. N00014-67-A-0181-0018 Task No. NR 062-420.

THE DEPARTMENT OF NAVAL ARCHITECTURE AND MARINE ENGINEERING

THE UNIVERSITY OF MICHIGAN
COLLEGE OF ENGINEERING

THE WAVE RESISTANCE OF AN AIR-CUSHION VEHICLE IN ACCELERATED MOTION

by
Lawrence J. Doctors
and
Som D. Sharma

This research was carried out under
Office of Naval Research
Contract No. N00014-67-A-0181-0018
Task No. NR 062-420 (Code 438)

Department of Naval Architecture and Marine Engineering
College of Engineering
The University of Michigan
Ann Arbor, Michigan 48104

Report No. 099
December 1970

ABSTRACT

This report is concerned with the theoretical wave resistance of an air-cushion vehicle (ACV) traveling over water of uniform finite or infinite depth, in steady or unsteady motion. Referring first to steady motion, it is shown that the unrealistic oscillations in the wave resistance curve at low Froude numbers found by previous workers can be eliminated by using a smoothed out pressure distribution rather than one with sharp edges studied exclusively in the past. The main result of unsteady motion calculations is that the peak wave resistance in shallow water, even in moderately accelerated motion, is appreciably less than the corresponding steady-state value. In fact, cases have been found where an ACV starting from rest under the action of a constant thrust would seem to be unable to cross the critical depth Froude number on the basis of quasi-steady estimates of wave resistance, while the more elaborate unsteady calculations show that it has sufficient power to reach its final supercritical cruising speed. An interesting feature of unsteady motion is that besides wave resistance there is another mechanism transferring energy to the free surface which is here called the dynamic sustention power. Contrary to intuition, the wave resistance in unsteady motion over finite depth sometimes becomes negative at supercritical Froude numbers before finally approaching zero at infinite speed.

ACKNOWLEDGMENTS

This report is almost identical in content to a doctoral dissertation prepared by the first author at the University of Michigan under the general guidance of the second author. Other members of the doctoral committee were Professors Stanley J. Jacobs, Finn C. Michelsen, Horst Nowacki and T. Francis Ogilvie. We are specially grateful to Professor Ogilvie for many helpful suggestions at every stage of the project.

The practical problem of overcoming the critical Froude-number wave-resistance hump in shallow water was first suggested to us by Dr Sidney Davis and Dr Jerry Cuthbert of the Joint Surface Effect Ships Program Office in 1968. They also suggested the need for calculating the wave resistance of an air-cushion vehicle in accelerated motion.

The elaborate numerical calculations essential to this project would not have been feasible but for the excellent computing facilities maintained by the University of Michigan.

CONTENTS

LIST OF FIGURES

NOMENCLATURE

a	=	half length of craft
A	=	$1/2F^2$
A_F	=	frontal area of craft
b	=	half width of craft
c	=	velocity of ACV
C_D	=	drag coefficient
d	=	water depth
D	=	propeller diameter
D_A	=	aerodynamic drag
D_M	=	momentum drag
F	=	Froude number
F_d	=	depth Froude number
g	=	acceleration due to gravity
$\underset{\sim}{i}, \underset{\sim}{j}, \underset{\sim}{k}$	=	unit vectors in x, y, z direction
J	=	propeller advance ratio
k	=	wave number = $\sqrt{w^2 + u^2}$
k_0	=	fundamental wave number = g/c^2
K_Q	=	propeller torque coefficient
K_T	=	propeller thrust coefficient
L	=	length of pressure distribution
$\mathcal{L}$	=	Laplace transform operator
m	=	mass of ACV
$\dot{m}_A$	=	mass flow into air cushion

$\underset{\sim}{n}$ = unit normal to free surface, directed inwardly

N = propeller speed of revolutions

p = cushion pressure

p_0 = reference cushion pressure

P = power absorbed by propeller

P_e, P_o, Q_e, Q_o = Kochin functions defined by Eq. (3.14). They are different from the Kochin functions defined by Wehausen and Laitone (1960, p. 558) or by Eggers, Sharma and Ward (1967), being greater by the factor, $c\rho \cdot \cos\theta$.

P_{2D}, Q_{2D} = Two-Dimensional Kochin functions, cf. Eq. (3.28)

Q = propeller torque

R = wave resistance

s = distance traveled by ACV

S = area of pressure distribution

t = time

T = thrust of propulsor

w, u = induced longitudinal and transverse wave numbers

W = weight of ACV = mg

$\dot{W}_T$ = total rate of work done on water, cf. Eq. (3.9)

$\dot{W}_S$ = dynamic sustention power, cf. Eq. (3.11)

$\dot{W}_R$ = power to overcome wave resistance = cR

x, y, z = coordinate system fixed to ACV, cf. Fig. 1

x^* = longitudinal coordinate in fixed reference frame

α = longitudinal cushion fall-off parameter

β = transverse cushion fall-off parameter

γ = $\sqrt{gk \cdot \tanh(kd)}$

ε = water shallowness parameter

ζ = free surface elevation

η = propeller efficiency

θ = wave direction with respect to the x axis

ρ = water density

ρ_A = air density

τ = dummy time variable

ϕ = disturbance velocity potential in moving frame such that $\underset{\sim}{v} = \nabla\phi$

$\phi^{(n)}$ = n'th term of asymptotic expansion for ϕ

∇ = $\underset{\sim}{i}\frac{\partial}{\partial x} + \underset{\sim}{j}\frac{\partial}{\partial y} + \underset{\sim}{k}\frac{\partial}{\partial z}$

∇_{2D} = $\underset{\sim}{i}\frac{\partial}{\partial x} + \underset{\sim}{j}\frac{\partial}{\partial y}$

SUPERSCRIPTS

* = stationary frame variable

$'$ = dummy variable

$\tilde{}$ = Laplace or Fourier transform

$\cdot$ = $\frac{\partial}{\partial t}$

SUBSCRIPT

$_{\sim}$ = vector quantity

SUMMARY

This report is concerned with the theoretical wave resistance of an air-cushion vehicle (ACV) traveling over water of uniform finite or infinite depth, in steady or unsteady rectilinear motion.

It is conventional in such an analysis to model the ACV with a given pressure distribution applied to the free surface of an inviscid incompressible fluid and to use linearized boundary conditions on the free surface.

The results obtained by this approach in the past, while in good agreement with measurements at high Froude numbers, have raised two questions of practical significance. First, at low Froude numbers the theory predicts an infinite number of unrealistic humps and hollows in the wave resistance curve. Second, when the depth of water is small compared to the length of the ACV, the steady-state peak wave resistance at the critical depth Froude number becomes relatively high compared to the wave resistance at the cruising speed, which is typically supercritical.

It is shown that the unrealistic oscillations at low Froude numbers can be essentially eliminated by using a smoothed out pressure distribution in contrast to the sharp edged distribution used by previous workers. Moreover, for a rectangular distribution, this effect is mainly pro-

duced by the smoothing at the forward and after edges.

In resolving the second question, the primary consideration was that such peak resistance can only represent a transient phase in the practical operation of any ACV. This naturally suggests tackling the unsteady motion problem, also in the hope that in accelerated motion the extremely long shallow water waves may never have enough time to build up to their peak values.

The unsteady theory indeed shows that at reasonable accelerations, an ACV can pass the critical depth Froude number without encountering unreasonably high wave resistance.

It is seen that in unsteady motion, besides wave resistance, there is another mechanism transferring energy to the free surface. This is the dynamic sustention power and represents the work done by the pressure against the relative vertical motion of the free surface in order to maintain the altitude of the ACV. This is quite independent of the static lift power required to support the air-cushion vehicle - even at zero speed.

Results of several sample calculations are presented, including many for a two-dimensional pressure band which is relatively easy to compute, and exhibits the phenomena of interest in a very accentuated manner. Contrary to intuition, in two-dimensional unsteady motion, the wave resistance, and even the total rate of work done on the free surface (including sustention power) become negative at

some supercritical speed, before finally approaching zero at infinite speed. However, there should be no fundamental objection to this phenomenon, as the ACV is merely recovering some of the energy previously expended on the free surface.

It is found that the Froude number at which the maximum negative wave resistance occurs can be predicted by an application of the simpler shallow water theory - in which the phenomenon is further accentuated. No region of negative wave resistance was encountered for a three-dimensional pressure distribution.

Finally, several cases of the inverse problem have been calculated, which is aimed at determining the velocity pattern for an ACV starting from rest under the action of a propulsor of given thrust-speed characteristics. This is treated in two different ways: calculating the wave resistance in a truly unsteady manner, and on the simplified quasi-steady basis. All other components of drag are assumed to be strictly quasi-steady. The results show that the shape of the propeller thrust and torque coefficient curves has only a minor effect on the velocity pattern. On the other hand, the effect of overloading the ACV is found to have crucial effects on its ability to surpass the critical depth hump.

In this respect, the simpler quasi-steady calculations lead to unnecessarily pessimistic estimates of the velocity pattern. Under certain circumstances in relatively shallow

water, the quasi-steady analysis would suggest that the ACV could not overcome the critical hump with the available power, while the more elaborate unsteady calculations show that it has indeed adequate power to reach its final cruising speed.

1 - INTRODUCTION

1.1 - PREVIOUS WORK:-

The hydrodynamic aspects of an air-cushion vehicle (ACV) can be studied by assuming its action to be equivalent to that of a pressure distribution acting on the free surface of the water. This idealization neglects any physical contact of the lower edge of the craft with the water. It also assumes that the flow of air escaping under the periphery is inviscid, and therefore produces no spray.

Havelock, in some of his early papers (1909, 1914 & 1926) was the first to treat the theoretical problem of the wave resistance of a pressure distribution. His interest in pressure disturbances lay in a desire to represent the motion of a ship. As a results, most of the distributions that he chose to analyse were very smooth and were not typical of the ACV.

However, later on, Havelock (1932) derived the general expression for a pressure distribution traveling at a constant speed. In this paper, he also found the relationship between the pressure acting on the free surface, and the equivalent source distribution.

Lunde (1951a) extended the theoretical treatment to cover the case of an arbitrary distribution moving over finite depth. Other workers have obtained numerical results for pressure distributions which are directly applicable to the ACV. These

include Newman and Poole (1962) who considered the case of motion in a restricted waterway such as a canal. They calculated the two cases of a constant pressure acting over a rectangular area, and over an elliptical area. The most striking feature of their results is the very strong interaction between the bow and stern portions of the distribution. Particularly for the rectangular distribution (where the interaction would be greater), there are displayed a series of humps and hollows in the resistance curve. A hump occurs when the bow and stern wave systems are in phase and combine to give a trailing wave of a maximum height. A hollow occurs when the two wave systems are out of phase by half a wavelength giving a combined amplitude of a minimum height.

The interference effects are found to be stronger for large beam to length ratios, as would be expected from the above argument, since the wave motion becomes more nearly two-dimensional for a wide craft.

Barratt (1965) also computed the wave resistance of rectangular and elliptical pressure distributions, but for the case of unrestricted water. His results are to some extent similar to those for the canal. In deep water, the main (or "last") hump occurs at a Froude number given by $F = 1/\sqrt{\pi}$. In water of finite depth this hump is shifted to a lower Froude number, and for sufficiently shallow water occurs at a depth Froude number, F_d, equal to unity (i.e., at the critical speed). One difference between these two sets of results is

pointed out by Newman and Poole. For a canal of finite width, the theory predicts a discontinuity in the wave resistance at the critical depth Froude number. The resistance is higher just below the critical speed than just above it. However, for an infinitely wide canal, there is no discontinuity, but there is a sudden change in slope at the critical speed.

Havelock (1922) also presented some results for a very smooth pressure distribution over water of finite depth. These, too, clearly show the shift of the main hump and the increase in its magnitude in shallower water. Havelock's curves display only the main hump. The secondary and other humps do not occur because of his choice of pressure distribution.

Recently a number of experimental programs have been carried out in order to check the above-mentioned theoretical results. Chief workers in this field are Everest (1966a, 1966b & 1967) and Hogben (1966a). The main question pointed out in these papers is the resolution of the total drag on the ACV into its components. These components are often considered to be: Wave Resistance, Aerodynamic Drag, Momentum Drag and Water Contact Drag.

The aerodynamic drag (or profile drag) is assumed to be that resistance acting on the model if it were tested in a wind tunnel with the engines not running.

The momentum drag is that due to the change in direction of the air supplying the cushion as it enters the fan intakes.

In fact, we should consider two components here: Inlet Momentum Drag, and Outlet Momentum Drag. The outlet momentum drag is associated with the changes in direction and velocity of the air as it escapes from the cushion, and can be either positive or negative, depending on the trim of the craft.

The water contact drag is due to any touching of the lower edge of the craft, or of the skirts, with the water. Due to the extremely non-linear nature of this effect, the drag (or possibly thrust) due to spray from the cushion hitting the craft is usually included with it.

While the first three resistance components defined above may be studied from a theoretical approach, the water contact drag only lends itself to an experimental study. To this end, Everest (1966a) estimated the water-wetting resistance by eliminating it - using a thin polythene sheet floating on the water surface. This technique, however, introduces the question about the tensile forces in the sheet. The resistance breakdown is further discussed by Hogben (1966a) where he provides a careful definition of each component.

These experimental results were generally obtained by a dynamometer measuring the total drag. Then the aerodynamic, momentum and water contact drag components were estimated and subtracted in order to make a comparison with the theoretical wave resistance. The agreement appears to be quite good in regard to the range in values of the wave resistance. However, the large scatter in the data makes it difficult to

draw precise conclusions. The authors suggest that, in addition to the main hump, they can detect a secondary and possibly a third one, and that these are out of phase with the theoretical humps by no more than 0.05 on the Froude number scale.

An explanation given for the non-appearance of more humps is based on the fact that the lower speed humps predicted by the linearized theory correspond to a wave pattern whose maximum slope is too large from physical considerations. Hogben gave a two-dimensional argument (1965) showing that the maximum ratio of wave height to length is about 1/7. This would preclude the development of any humps above the third or fourth (depending on the cushion pressure).

Further experimental work by Everest, Willis and Hogben (1968 & 1969) dealt with the wave resistance of an ACV at an arbitrary angle of yaw. This problem was also studied theoretically by Murthy (1970). In these experiments, the wave resistance was measured directly from the wave pattern. As a result there is less scatter in the data since the rather doubtful technique of estimating the wetting drag is eliminated. The experimental results here are generally low compared with the theory, the difference being usually limited to about 10% but is occasionally as much as 50% at certain Froude numbers.

The outcome of these investigations is that the main hump drag is relatively large in relation to the installed propulsive power of typical ACVs. In addition, the prob-

lem is more acute in shallow water where the thrust margin of some craft has been found insufficient to surpass the hump. It has been found necessary from speed and economic considerations to operate in the cruising condition at a Froude number of at least 1.5. This is well above the hump speed and the wave resistance is accordingly smaller.

However, in a real situation, the craft does not operate steadily at the hump speed. In fact, the procedure is to accelerate through it as quickly as possible. Under a non-steady condition it appears quite reasonable to anticipate that the large amplitude wave pattern at the hump speed will not have time to establish itself - thus leading to a less aggravated problem in shallow water. Some experiments on a rectangular model by Everest (1966b) confirm this. Under certain conditions in finite depth he has found a reduced resistance peak.

1.2 - PRESENT STUDY:-

These considerations point towards a theoretical investigation of the wave resistance during accelerated motion. Already, the problem for a ship has been treated by Sretensky (1939), Lunde (1951b, 1953a & 1953b) and Shebalov (1966). These workers have derived the linearized result for the resistance, but produced no computed values. Wehausen (1964) computed the resistance of a ship model with a constant acceleration from rest up to a speed which was then held fixed.

His results, however, consist of asymptotic expressions for large values of the time, and there are no data for the resistance during the acceleration phase of the motion. Wehausen's interest stemmed from a desire to know the required length of a model ship test before the steady state resistance is achieved.

With regard to the unsteady motion of a surface pressure distribution, Havelock (1916) has computed the resistance of two particular distributions whose motion is suddenly established from rest, and then continued at a constant speed. On the other hand, Djachenko (1966) has derived an expression for the resistance of an arbitrary pressure distribution for a general acceleration pattern. He also presented some results for a two-dimensional distribution.

The transient problem is of interest mainly for two reasons. First, since a numerical solution to this problem will make it possible to calculate the resistance history as a function of the acceleration pattern, one could expect to find optimum acceleration programs that would reduce the peak wave resistance, or the peak total resistance.

Second, it is of interest to examine the inverse problem: the resulting motion under the action of a propulsive device of given thrust-speed characteristics. This is, of course, the more natural problem and any theoretical results could also be checked by experiment.

It is believed that there is more justification for applying the linearized theory to the transient, rather than

the steady, problem because of the diminished likelihood of an excessively steep wave system building up.

2 - THE POTENTIAL FUNCTION

2.1 - PROBLEM STATEMENT:-

The air-cushion vehicle will be represented by a pressure distribution $p(x,y)$ acting on the free surface, and traveling with the speed of the craft. Two right-handed coordinate systems will be used, as shown in Fig. 1. The system xyz moves with the craft, z being vertically upwards and x being in the direction of the rectilinear motion. The second axis system x^*yz is fixed in space. The relationship between the coordinates is then given by

$$x = x^* - s(t)$$

$$= x^* - \int_0^t c(\tau)\, d\tau, \qquad (2.1)$$

where c and s are the velocity of the model, and its distance traveled, respectively.

The velocity potential satisfies the Laplace equation:

$$\nabla^{*2}\, \phi^* = 0, \qquad (2.2)$$

where ϕ^* is the velocity potential in the stationary frame (such that the velocity is the positive gradient of the potential), and ∇^* also implies differentiation in this frame. If ϕ is the perturbation potential in the moving frame, we

may say that

$$\phi(x,y,z,t) = \phi^*(x^*,y,z,t), \tag{2.3}$$

if x and x^* correspond to the same point in space. From Eq. (2.1) we have

$$\frac{\partial}{\partial x^*} = \frac{\partial}{\partial x}, \tag{2.4}$$

so that Eq. (2.2) may be written as

$$\nabla^2\phi = 0. \tag{2.5}$$

The kinematic boundary condition on the free surface requires that a particle on it remains there. That is,

$$\frac{D}{Dt}\left[z - \zeta(x,y,t)\right]_{z=\zeta} = 0, \tag{2.6}$$

where ζ is the elevation of the surface. In terms of the moving coordinates we have

$$\frac{D}{Dt} = \frac{\partial}{\partial t} + (u - c)\frac{\partial}{\partial x} + v\frac{\partial}{\partial y} + w\frac{\partial}{\partial z},$$

where u, v and w are the perturbation velocities. Combining this with the exact kinematic condition, Eq. (2.6), and substituting for u, v and w:

$$\left[\phi_z - \zeta_t - (\phi_x - c)\zeta_x - \phi_y\zeta_y\right]_{z=\zeta} = 0.$$

At this stage the second order terms may be dropped, and the remaining terms written as a Taylor expansion about the

point $z = 0$:

$$\left(\left[\phi_z \right]_{z=0} + \left[\phi_{zz} \right]_{z=0} \zeta + \cdots \right) - \zeta_t + c\, \zeta_x = 0 \ .$$

Finally, the linearized kinematic condition on the free surface may be obtained by dropping the higher order quantities again:

$$\left[\phi_z \right]_{z=0} - \zeta_t + c\, \zeta_x = 0. \qquad (2.7)$$

The dynamic condition on the surface - the Bernoulli equation - in terms of the stationary coordinates is

$$\left[\phi^*_t + \frac{1}{2}(\phi^*_{x^*}{}^2 + \phi^*_y{}^2 + \phi^*_z{}^2) \right]_{z=\zeta} + \frac{p^*}{\rho} + g\zeta^* = f, \qquad (2.8)$$

where ρ is the water density and g is the acceleration due to gravity, while f is an arbitrary function of time. Again, we may drop the squared terms as these are of higher order. In addition, f may be put identically to zero without loss of generality. Also, from Eqs. (2.1) and (2.3) we have

$$\phi^*_t = \phi_t - c\, \phi_x \ .$$

Thus Eq. (2.8) reduces to

$$\left[\phi_t - c\,\phi_x\right]_{z=\zeta} + \frac{p}{\rho} + g\zeta = 0 \ .$$

As before we may expand the first term in a Taylor series about $z = 0$, and then drop the higher order terms to obtain the linearized dynamic condition:

$$\left[\phi_t - c\,\phi_x\right]_{z=0} + \frac{p}{\rho} + g\zeta = 0 \ . \qquad (2.9)$$

The combined free surface condition is obtained from Eqs. (2.7) and (2.9) after eliminating ζ :

$$\left[\phi_{tt} + c^2\phi_{xx} - 2c\,\phi_{xt} - \dot{c}\,\phi_x + g\,\phi_z\right]_{z=0} = c\,p_x/\rho \ . \qquad (2.10)$$

The last boundary condition to be satisfied is that there is no flow through the water bed:

$$\left[\phi_z\right]_{z=-d} = 0 \ , \qquad (2.11)$$

where d is the depth of the water.

2.2 - SOLUTION FOR THE POTENTIAL:-

The solution of this set of equations can be obtained by an application of the double Fourier transform pair:

$$\tilde{f}(w,u) = \frac{1}{2\pi} \int_{-\infty}^{\infty} dx \int_{-\infty}^{\infty} dy\ f(x,y)\ \exp(-i(wx + uy)) \tag{2.12}$$

$$\text{and} \quad f(x,y) = \frac{1}{2\pi} \int_{-\infty}^{\infty} dw \int_{-\infty}^{\infty} du\ \tilde{f}(w,u)\ \exp\ (i(wx + uy))\ ,$$

and the Laplace transform pair:

$$\tilde{f}(q) = \int_{0}^{\infty} f(t)\ \exp(-qt)\ dt$$

$$\text{and} \qquad f(t) = \frac{1}{2\pi i} \int_{\delta-i\infty}^{\delta+i\infty} \tilde{f}(q)\ \exp(qt)\ dq, \tag{2.13}$$

δ being a positive constant.

Using the rules for transforming a derivative, the Laplace equation (2.5), under the transformation (2.12), becomes:

$$(iw)^2\tilde{\phi} + (iu)^2\tilde{\phi} + \tilde{\phi}_{zz} = 0 \ ,$$

where $\tilde{\phi} = \tilde{\phi}(w,u;z,t)$.

Hence $$\tilde{\phi}_{zz} - k^2\tilde{\phi} = 0 \ ,$$

where $$k^2 = w^2 + u^2 \ . \qquad (2.14)$$

A solution for $\tilde{\phi}$ is

$$\tilde{\phi} = \tilde{A}(w,u;t)\ \cosh(kz + \tilde{B}(w,u;t)) \ , \qquad (2.15)$$

where $\tilde{A}$ and $\tilde{B}$ are, at the moment, arbitrary. $\tilde{B}$ may be found by transforming the bed condition, Eq. (2.11), giving

$$\left[\tilde{\phi}_z\right]_{z=-d} = 0 \ ,$$

and substituting Eq. (2.15). Thus

$$\left[\tilde{A}\cdot k\cdot\sinh(kz + \tilde{B})\right]_{z=-d} = 0 \ ,$$

giving $$\tilde{B} = kd$$

and $$\tilde{\phi} = \tilde{A}\ \cosh(k(z + d)) \ . \qquad (2.16)$$

Applying now the Fourier transform to the combined free surface condition, Eq. (2.10), and using $\tilde{\phi}$ given by Eq. (2.16), we obtain

$$\left[\tilde{A}_{tt}\cdot\cosh(k(z+d)) + c^2(iw)^2\tilde{A}\cdot\cosh(k(z+d))\right.$$

$$- 2c\cdot iw\cdot\tilde{A}_t\cdot\cosh(k(z+d)) - \dot{c}\cdot iw\cdot\tilde{A}\cdot\cosh(k(z+d))$$

$$\left. + gk\cdot\sinh(k(z+d))\right]_{z=0} = c\cdot iw\cdot\tilde{p}/\rho \ .$$

Or, more simply,

$$\tilde{A}_{tt} - 2icw\cdot\tilde{A}_t + \tilde{A}(\gamma^2 - c^2w^2 - i\dot{c}w) = icw\cdot\operatorname{sech}(kd)\cdot\frac{\tilde{p}}{\rho} \ , \quad (2.17)$$

in which $$\gamma^2 = gk\tanh(kd) \ . \quad (2.18)$$

A substitution that makes the coefficients in Eq. (2.17) constant has been found by Lunde (1951b). It is

$$\tilde{A}(w,u;t) = \tilde{\chi}(w,u;t)\ \exp(iw\cdot s(t)) \ . \quad (2.19)$$

After putting this in Eq. (2.17), and some simplification, one obtains

$$\tilde{\chi}_{tt} + \gamma^2\tilde{\chi} = icw\cdot\operatorname{sech}(kd)\cdot\frac{\tilde{p}}{\rho}\cdot\exp(-iw\cdot s(t)) \ .$$

We now take the Laplace transform, Eq. (2.13), of the previous equation to get

$$(q^2 + \gamma^2)\tilde{\chi} = iw \cdot \operatorname{sech}(kd) \cdot \frac{\tilde{p}}{\rho} \cdot L(c \cdot \exp(-iw \cdot s(t))) \ ,$$

where L is the Laplace transform operator. Thus

$$\tilde{\chi} = i \cdot \frac{w\tilde{p}}{\rho\gamma} \cdot \operatorname{sech}(kd) \cdot L(\sin \gamma t) \cdot L(c \cdot \exp(-iw \cdot s(t))) \ .$$

Using the convolution theorem to perform the inverse Laplace transform of this, we obtain

$$\tilde{\chi} = i \cdot \frac{w\tilde{p}}{\rho\gamma} \cdot \operatorname{sech}(kd) \int_0^t c(\tau) \cdot \sin(\gamma(t - \tau)) \cdot \exp(-iw \cdot s(\tau)) \, d\tau \ .$$

Eqs. (2.19) and (2.16) are now used, together with the above equation, to yield

$$\tilde{\phi} = i \cdot \frac{w\tilde{p}}{\rho\gamma} \cdot \frac{\cosh(k(z + d))}{\cosh(kd)} \int_0^t c(\tau) \cdot \sin(\gamma(t - \tau)) \cdot$$

$$\cdot \exp(iw(s(t) - s(\tau))) \, d\tau \ . \qquad (2.20)$$

The double Fourier transform, Eq. (2.12), can be used to express $\tilde{p}$ in Eq. (2.20) in terms of p, and then the

inverse transform is taken to give the disturbance potential, ϕ , in terms of the moving coordinate system, xyz :

$$\phi(x,y,z,t) = \frac{i}{4\pi^2\rho} \iint_{S'} p' \, dS' \int_0^t c(\tau) \, d\tau \int_{-\infty}^{\infty} dw \int_{-\infty}^{\infty} du$$

$$\frac{w \cdot \cosh(k(z + d))}{\sqrt{gk \cdot \tanh(kd)} \cdot \cosh(kd)} \cdot \sin\left[\sqrt{gk \cdot \tanh(kd)} \cdot (t - \tau)\right] \cdot$$

$$\cdot \exp\left[i(w(x - x' + s(t) - s(\tau)) + u(y - y'))\right] . \quad (2.21)$$

Here $k^2 = w^2 + u^2$ as before, and $p' = p'(x',y')$, defined over the area S' , while x' and y' are dummy coordinates in the moving reference frame.

3 - THE WAVE RESISTANCE AND SUSTENTION POWER

3.1 - DEFINITIONS:-

In this section expressions for the wave resistance will be derived. Also the computer studies showed that under certain circumstances this resistance could become negative. Hence it is of interest to examine the total rate of energy input to the water, as well.

Using the stationary frame of reference, the wave resistance may be defined as the horizontal component of the cushion pressure force acting on the free surface. Thus

$$R = \iint_{S^*} p^*(x^*,y,t)\ \zeta^*_{x^*}\ dx^* dy\ ,$$

where the superscript * indicates that the variable is given in terms of the fixed frame. This formula may be expressed in the moving frame as

$$R = \iint_{S} p(x,y)\ \zeta_x\ dx\ dy\ . \qquad (3.1)$$

Now the power input to the water (in the fixed frame) is

$$\dot{W}_T = \iint_{S^*} p^*(x^*,y,t)\ \underset{\sim}{n}^* \cdot \underset{\sim}{v}^*\ dS^* , \qquad (3.2)$$

where $\underset{\sim}{n}$ is the unit normal vector at the free surface and directed inwardly, and $\underset{\sim}{v}$ is the velocity of the particles of water on the surface. By definition

$$\underset{\sim}{n}^* = (\zeta^*_{x^*}\ \underset{\sim}{i} + \zeta^*_y\ \underset{\sim}{j} - \underset{\sim}{k})/\sqrt{1 + (\zeta^*_{x^*})^2 + (\zeta^*_y)^2} \qquad (3.3)$$

and

$$\underset{\sim}{v}^* = \phi^*_{x^*}\ \underset{\sim}{i} + \phi^*_y\ \underset{\sim}{j} + \phi^*_z\ \underset{\sim}{k} . \qquad (3.4)$$

In the stationary reference frame, the kinematic condition on the free surface is

$$\left[\frac{D}{Dt}\ (z - \zeta^*(x^*,y,t))\right]_{z=\zeta^*} = 0 ,$$

or

$$\left[\phi^*_z - \zeta^*_{x^*}\ \phi^*_{x^*} - \zeta^*_y\ \phi^*_y - \zeta^*_t\right]_{z=\zeta^*} = 0 . \qquad (3.5)$$

In addition, we have

$$dS^* = dx^* dy \sqrt{1 + (\zeta^*_{x^*})^2 + (\zeta^*_{y})^2} \ . \qquad (3.6)$$

If we now combine Eqs. (3.2) to (3.6), we obtain

$$\dot{W}_T = - \iint_{S^*} p^*(x^*,y,t) \ \zeta^*_t \ dx^* dy \ . \qquad (3.7)$$

A transformation to the moving frame is now in order, and using the relation

$$\zeta^*_t = \zeta_t - c \ \zeta_x \ , \qquad (3.8)$$

the final expression for the total rate of work done on the water results:

$$\dot{W}_T = \iint_{S} p(x,y) \left[c \ \zeta_x - \zeta_t \right] dx \ dy \ . \qquad (3.9)$$

Note that the expressions for the resistance and total power (Eqs. (3.1) and (3.9)) are exact - they have not been linearized. The total power contains the power required to overcome the wave resistance:

$$\dot{W}_R = c\ R\ . \qquad (3.10)$$

The other part of the total power we shall call the sustention power:

$$\dot{W}_S = -\iint_S p(x,y)\ \zeta_t\ dx\ dy\ . \qquad (3.11)$$

Thus the sustention power represents the rate at which work is done by the cushion pressure against any vertical motion of the free surface, and is positive for an average downward movement. This power term should not be confused with the power required to provide the air cushion. The sustention power would come from changes in gravitational potential energy of the ACV, as it heaves and trims during the unsteady motion. During steady motion, the position of the free surface does not move relative to the craft. In this case the sustention power is zero.

3.2 - WAVE RESISTANCE:-

We use Eq. (3.1) defining the resistance, and the dynamic condition on the free surface, Eq. (2.9).

$$R = \frac{1}{g} \iint_S p \left(\left[c\, \phi_{xx} - \phi_{tx} \right]_{z=0} - p_x/\rho \right) dx\, dy \ .$$

After integrating with respect to x, the last term in the integrand gives

$$- \frac{1}{2\rho g} \int \left[p^2 (x,y) \right]_{x=-\infty}^{\infty} dy \ ,$$

which is zero for any typical distribution. We may now substitute the expression for ϕ given by Eq. (2.21), and after some reduction, obtain

$$R = \frac{1}{4\pi^2 \rho g} \iint_S p\, dS \iint_{S'} p'\, dS' \int_0^t c(\tau)\, d\tau \int_{-\infty}^{\infty} dw \int_{-\infty}^{\infty} du$$

$$w^2 \cdot \cos\left[\sqrt{gk \cdot \tanh(kd)} \cdot (t - \tau) \right] \cdot$$

$$\cdot \exp\left[i\left(w(x - x' + s(t) - s(\tau)) + u(y - y') \right) \right] . \qquad (3.12)$$

Since we only require the real part of this equation, we rewrite the exponent factor as

$$\text{factor} = \cos\Big[w(x - x' + s(t) - s(\tau)) + u(y - y')\Big]$$

$$= \cos\Big[w(x - x') + u(y - y')\Big]\cdot\cos\Big[w(s(t) - s(\tau))\Big]$$

$$- \sin\Big[w(x - x') + u(y - y')\Big]\cdot\sin\Big[w(s(t) - s(\tau))\Big] .$$

The second term on the right hand side is odd with respect to the pair $x - x'$ and $y - y'$, and therefore contributes nothing to the integral. Expanding the first term, now,

$$\text{factor} = \Big[\cos(w(x - x'))\cdot\cos(u(y - y'))$$

$$- \sin(w(x - x'))\cdot\sin(u(y - y'))\Big]\cdot\cos\Big[w(s(t) - s(\tau))\Big] .$$

This time the second term is odd with respect to w and u, and therefore gives no contribution. We may expand the factor a third time to yield

$$\text{factor} = \Big[\cos(wx)\cdot\cos(wx') + \sin(wx)\cdot\sin(wx')\Big]\times$$

(continued over)

$$\times\Big[\cos(uy)\cdot\cos(uy') + \sin(uy)\cdot\sin(uy')\Big]\times$$

$$\times\cos\Big[w(s(t) - s(\tau))\Big] .$$

If we place this factor back into Eq. (3.12), the desired expression for the resistance is obtained:

$$R = \frac{1}{\pi^2\rho g}\int_0^t c(\tau)\,d\tau\int_0^\infty dw\int_0^\infty du\; w^2\Big[P_e^{\,2} + P_o^{\,2} + Q_e^{\,2} + Q_o^{\,2}\Big]\times$$

$$\times\cos\Big[\sqrt{gk\cdot\tanh(kd)}\cdot(t - \tau)\Big]\cdot\cos\Big[w(s(t) - s(\tau))\Big] , \quad (3.13)$$

where
$$\begin{matrix}P_e\\P_o\end{matrix} = \iint_S p(x,y)\;\begin{matrix}\cos\\\sin\end{matrix}(wx)\;\begin{matrix}\cos\\\sin\end{matrix}(uy)\;dx\,dy \quad (3.14)$$

and
$$\begin{matrix}Q_e\\Q_o\end{matrix} = \iint_S p(x,y)\;\begin{matrix}\sin\\\cos\end{matrix}(wx)\;\begin{matrix}\cos\\\sin\end{matrix}(uy)\;dx\,dy .$$

It is interesting to compare Eq. (3.13) with the ex-

pression obtained by Lunde (1951b) for a ship. An additional term consisting of a fourfold integral, and being simply proportional to the instantaneous acceleration, occurs in his formula. It represents a type of added mass, and is zero if the singularity distribution lies on the free surface. This is the case of a pressure distribution.

3.3 - TOTAL POWER:-

The total power is defined by Eq. (3.9). Using the kinematic condition, Eq. (2.7), the power may be written as

$$\dot{W}_T = - \iint_S p \left[\phi_z\right]_{z=0} dx\, dy \ .$$

The equation for ϕ , Eq. (2.21), is now substituted to give

$$\dot{W}_T = \frac{-i}{4\pi^2 \rho g} \iint_S p\, dS \iint_{S'} p'\, dS' \int_0^t c(\tau)\, d\tau \int_{-\infty}^{\infty} dw \int_{-\infty}^{\infty} du$$

$$w \cdot \sqrt{gk \cdot \tanh(kd)} \cdot \sin\left[\sqrt{gk \cdot \tanh(kd)} \cdot (t - \tau)\right] \cdot$$

$$\cdot \exp\left[i(w(x - x' + s(t) - s(\tau)) + u(y - y'))\right] .$$

This expression may now be simplified in a manner identical to that used on Eq. (3.12) for the resistance. We then obtain for the total rate of work done on the water by the pressure:

$$\dot{W}_T = \frac{1}{\pi^2 \rho g} \int_0^t c(\tau)\, d\tau \int_0^\infty dw \int_0^\infty du\; w \cdot \sqrt{gk \cdot \tanh(kd)} \times$$

$$\times \left[P_e^{\,2} + P_o^{\,2} + Q_e^{\,2} + Q_o^{\,2} \right] \times$$

$$\times \sin\left[\sqrt{gk \cdot \tanh(kd)} \cdot (t - \tau) \right] \cdot \sin\left[w(s(t) - s(\tau)) \right] . \quad (3.15)$$

3.4 - STEADY STATE WAVE RESISTANCE:-

The steady state resistance may be obtained from Eq. (3.13) by letting the velocity of the model be constant for a long time. For example, if we take the velocity of the craft to be suddenly established, and then fixed at a value c, the time integral in Eq. (3.13) may be carried out analytically to give

$$R = \frac{c}{2\pi^2 \rho g} \int_0^\infty w^2 \, dw \int_0^\infty du \left[P_e^{\,2} + P_o^{\,2} + Q_e^{\,2} + Q_o^{\,2} \right] \times$$

$$\times \left[\frac{\sin(\gamma + wc)t}{\gamma + wc} + \frac{\sin(\gamma - wc)t}{\gamma - wc} \right] , \qquad (3.16)$$

with $\gamma^2 = gk \cdot \tanh(kd)$

$$= g\sqrt{u^2 + w^2} \cdot \tanh(\sqrt{u^2 + w^2} \cdot d) \ ,$$

as before.

We want to know the value of R for very large time. As $t \to \infty$, the oscillations (about zero) due to the sine terms increase, so that there is no contribution to the integral except when

$$\gamma - w c = 0 \ . \qquad (3.17)$$

Eq. (3.17) gives the relationship between the transverse and longitudinal wave numbers for waves which travel at the speed of the model. We may now quote the following result from Wehausen (1964) or Wehausen and Laitone (1960, p. 477):

$$\lim_{t \to \infty} \int_a^b f(x) \frac{\sin(x - x_0)t}{x - x_0} dx = \pi f(x_0) \quad \text{if} \quad a < x_0 < b .$$

It is required here that f is smooth in the neighborhood of $x = x_0$, and that $f(x)/x$ is absolutely integrable in the range. The theorem below may then be derived from this result:

$$\lim_{t \to \infty} \int_a^b f(x) \frac{\sin g(x)t}{g(x)} dx = \pi \sum_i f(x_i)/|g'(x_i)|, \quad (3.18)$$

where x_i are the zeros of $g(x)$, assuming that $a < x_i < b$ and $g'(x_i) \neq 0$.

First we rewrite Eq. (3.16) in terms of polar coordinates:

$$\begin{aligned} w &= k \cos \theta , \\ u &= k \sin \theta , \\ \frac{\partial(w,u)}{\partial(k,\theta)} &= k , \end{aligned} \quad (3.19)$$

and then apply the second theorem to the k integral. It is seen that if

$$g(k,\theta) = \gamma - w c ,$$

or $$g(k,\theta) = \sqrt{gk\cdot\tanh(kd)} - ck\cdot\cos\theta \ ,$$

then $$\left|\frac{\partial}{\partial k}\, g(k,\theta)\right| = \frac{1}{2}c\cdot\cos\theta\left[1 - k_0 d\cdot\sec^2\theta\cdot\mathrm{sech}^2(kd)\right] ,$$

where k is the solution of

$$k - k_0\sec^2\theta\cdot\tanh(kd) = 0 \ , \qquad (3.20)$$

with $$k_0 = g/c^2 \ . \qquad (3.21)$$

If we now make the necessary substitutions detailed above, Eq. (3.16) reduces to the following single integral for the resistance of an ACV during steady motion:

$$R = \frac{1}{\pi\rho g}\int_{\theta_1}^{\pi/2} \frac{k^3\cos\theta}{1 - k_0 d\cdot\sec^2\theta\cdot\mathrm{sech}^2(kd)}\times$$

$$\times\left[P_e^{\,2} + P_o^{\,2} + Q_e^{\,2} + Q_o^{\,2}\right] d\theta \ . \qquad (3.22)$$

Here the lower limit for θ is taken as θ_1, the smallest positive value of θ which can satisfy Eq. (3.20) for a real k. It is given by

$$\theta_1 = 0 \qquad \text{for} \quad k_0 d > 1 \quad \text{(subcritical speed)}$$
$$= \arccos \sqrt{k_0 d} \quad \text{for} \quad k_0 d < 1 \quad \text{(supercritical speed)} \tag{3.23}$$

Eq. (3.22) is the same as that given by Barratt (1965). It may also be reexpressed as an integral with respect to the wave number k, through the connecting relationship given by Eq. (3.20). The result is

$$R = \frac{k_0}{2\pi\rho g} \int_{k_1}^{\infty} \frac{k \tanh(kd)}{\sqrt{1 - k_0 \tanh(kd)/k}} \left[P_e^{\,2} + P_o^{\,2} + Q_e^{\,2} + Q_o^{\,2} \right] dk \, . \tag{3.24}$$

Here k_1 is given by the solution of

$$k_1 = k_0 \tanh(k_1 d) \quad \text{if} \quad k_0 d > 1 \, ,$$
$$\text{or} \qquad k_1 = 0 \qquad \text{if} \quad k_0 d < 1 \, . \tag{3.25}$$

It may be noted in passing, that we could obtain the steady state value of the total power, Eq. (3.15), in a similar manner. In that case, after integrating Eq. (3.15) with respect to time, we would get the following expression, instead of Eq. (3.16):

$$\dot{W}_T = \frac{c}{2\pi^2\rho g}\int_0^\infty w\,dw\int_0^\infty du\;\gamma\cdot\left[P_e{}^2 + P_o{}^2 + Q_e{}^2 + Q_o{}^2\right]\times$$

$$\times\left[-\frac{\sin(\gamma + wc)t}{\gamma + wc} + \frac{\sin(\gamma - wc)t}{\gamma - wc}\right].$$

As in the case for R, the only contribution to $\dot{W}_T$, as $t \to \infty$, is given by the second sine term. And this occurs when $\gamma = wc$. It is clear then, as the steady-state condition is achieved, that

$$\dot{W}_T = cR$$

$$= \dot{W}_R,$$

as required.

3.5 - TWO-DIMENSIONAL WAVE RESISTANCE:-

It is of interest to study the wave resistance of a two-dimensional band of pressure since this shows up clearly the interference effects of the transverse wave system.

A possible method of solving this problem would be to set up a two-dimensional analog of Sec.(2) - for the potential,

ϕ , - and then solve this. However, it is simpler to consider a pressure distribution independent of y , and then let the beam approach infinity. Thus we assume that

$$p(x,y) = p_{2D}(x) \quad \text{for} \quad -b < y < b \ . \tag{3.26}$$

The Kochin functions (see also the Nomenclature), Eq. (3.14), become

$$\begin{aligned} P_e &= \frac{2 \sin(bu)}{u} P_{2D} \ , \\ P_o &= 0 \ , \\ Q_e &= \frac{2 \sin(bu)}{u} Q_{2D} \\ \text{and} \qquad Q_o &= 0 \ , \end{aligned} \tag{3.27}$$

where the two-dimensional Kochin functions are given by

$$\begin{matrix} P_{2D} \\ Q_{2D} \end{matrix} = \int_L p_{2D}(x) \begin{matrix} \cos \\ \sin \end{matrix} (wx) \, dx \ , \tag{3.28}$$

L being the length of the distribution.

Let us now consider the u integral in Eq. (3.13) for the wave resistance. We have, for the wave resistance per unit width,

$$R_{2D} = R/2b$$

$$= \frac{1}{\pi^2 \rho g} \int_0^t c(\tau)\, d\tau \int_0^\infty dw\, w^2 \cdot \left[P_{2D}^{\,2} + Q_{2D}^{\,2} \right] \times$$

$$\times \cos\left[w(s(t) - s(\tau)) \right] \times$$

$$\times \left[\int_0^{1/\sqrt{b}} + \int_{1/\sqrt{b}}^\infty \right] \cos\left[\sqrt{gk \cdot \tanh(kd)} \cdot (t - \tau) \right] \frac{2 \sin^2(bu)}{bu^2}\, du \,,$$

in which we have broken the u integral into two subranges as indicated. After a change of variable, the first of these u integrals becomes

$$I_1 = 2 \int_0^{\sqrt{b}} \cos\left[\sqrt{g \sqrt{w^2 + \phi^2/b^2} \cdot \tanh\left(\sqrt{w^2 + \phi^2/b^2} \cdot d \right)} \cdot (t - \tau) \right] \times$$

$$\times \frac{\sin^2 \phi}{\phi^2}\, d\phi \,.$$

As $b \to \infty$, this simplifies to

$$I_1 = 2 \cos\left[\sqrt{gw \cdot \tanh(wd)} \cdot (t - \tau) \right] \int_0^\infty \frac{\sin^2 \phi}{\phi^2}\, d\phi \,.$$

This integral is given, for example, in Gradshteyn and Ryzhik (1965, p. 414, 3.741, Formula 3). Thus

$$I_1 = \pi \cos\left[\sqrt{gw \cdot \tanh(wd)} \cdot (t - \tau)\right] .$$

We shall now examine the second of the u integrals, I_2 . It is easily seen that

$$|I_2| \leq \int_{1/\sqrt{b}}^{\infty} \frac{2}{bu^2}\, du = 2/\sqrt{b} .$$

Thus, as $b \to \infty$, $I_2 = 0$.

The formula for the two-dimensional wave resistance may now be written as the following double integral:

$$R_{2D} = \frac{1}{\pi\rho g} \int_0^t c(\tau)\, d\tau \int_0^{\infty} dw\, w^2 \cdot \left[P_{2D}^{\,2} + Q_{2D}^{\,2}\right] \times$$

$$\times \cos\left[\sqrt{gw \cdot \tanh(wd)} \cdot (t - \tau)\right] \cdot \cos\left[w(s(t) - s(\tau))\right]. \quad (3.29)$$

3.6 - TWO-DIMENSIONAL TOTAL POWER:-

The procedure for finding the limiting expression for the total power, Eq. (3.15), in the case of two-dimensional flow, is identical to that given in Sec. (3.5). The result is

$$\dot{W}_{T_{2D}} = \frac{1}{\pi\rho g}\int_0^t c(\tau)\,d\tau \int_0^\infty dw\; w\sqrt{gw\cdot\tanh(wd)}\cdot\left[P_{2D}^{\,2} + Q_{2D}^{\,2}\right]\times$$

$$\times\sin\left[\sqrt{gw\cdot\tanh(wd)}\cdot(t-\tau)\right]\cdot\sin\left[w(s(t)-s(\tau))\right] . \qquad (3.30)$$

3.7 - TWO-DIMENSIONAL STEADY-STATE WAVE RESISTANCE:-

We now derive the two-dimensional limit of Eq. (3.22). The procedure followed is similar to that in Sec. (3.5) and the result is

$$R_{2D} = \frac{k^2}{\rho g\,[1 - k_0 d\cdot\mathrm{sech}^2(kd)]}\left[P_{2D}^{\,2} + Q_{2D}^{\,2}\right] , \qquad (3.31)$$

k being the solution of $k = k_0\tanh(kd)$. (3.32)

If $k_0 d < 1$ (the supercritical speed condition), then there is no real solution of Eq. (3.32), and the wave resistance is zero.

4 - STEADY-STATE RESULTS

4.1 - PRESSURE DISTRIBUTION USED:-

As mentioned in Sec. (1), it was felt that it would be necessary to allow the cushion pressure to drop to zero within a finite distance at the periphery of the craft. The actual details of this fall-off are discussed by Hogben (1966b) and Alexander (1967) for a periperal jet ACV, and by Jones (1966) for a plenum chamber machine.

However, it is unlikely that the precise way the pressure drops to zero is crucial. Rather, the essential parameter is a measure of the fall-off distance. The restriction of planform shape to a rectangular one was made, since the smoothing effects of an elliptical design were studied by Barratt and Newman. The general pressure distribution given below allows the fall-off distances to be individually varied:

$$p(x,y) = \frac{1}{4} p_0 \left[\tanh \alpha(x + a) - \tanh \alpha(x - a)\right] \times$$

$$\times \left[\tanh \beta(y + b) - \tanh \beta(y - b)\right] . \qquad (4.1)$$

Here p_0 is the nominal pressure, a is the half-length and b is the half-beam. The smoothness of the cushion

pressure fall-off at the edges is a function of the fall-off parameters α and β. A large value of α implies a rapid drop at the bow and stern edges. On the other hand, if β is large, then the cushion pressure decays rapidly at the sides. This function is shown in Fig. 2.

As a particular case, we may consider the limit as $\beta \to \infty$. Then the pressure is given by

$$p = \frac{1}{2} p_0 \left[\tanh \alpha(x + a) - \tanh \alpha(x - a) \right]$$

$$\text{for} \quad -b < x < b \qquad (4.2)$$

$$= 0 \qquad \text{otherwise.}$$

This could represent a so-called sidewall air-cushion vehicle or captured air bubble (CAB). In these craft, the cushion is physically restrained at the sides so that the pressure falls abruptly.

Another particular case occurs when both $\alpha \to \infty$ and $\beta \to \infty$. Then

$$p = p_0 \quad \text{for} \quad -a < x < a$$

$$\text{and} \quad -b < y < b \qquad (4.3)$$

$$= 0 \quad \text{otherwise.}$$

This case of a constant pressure acting over a rectangular area is one commonly used by previous workers.

It is advantageous to obtain analytic expressions for the Kochin functions, Eq. (3.14). Due to symmetry in the chosen expression for p, it is clear that

$$P_o = Q_e = Q_o = 0 \ . \tag{4.4}$$

Furthermore, Eq. (4.1) allows us to compute P_e as the product of two separate, but similar, integrals over x and y, respectively. The contour used for evaluating the integral is shown in Fig. 3. We write the x integral as

$$I_x = Real \int_{-\infty}^{\infty} \left[\tanh \alpha(x + a) - \tanh \alpha(x - a) \right] e^{iwx} \, dx \ . \tag{4.5}$$

Because of the finite lengths of the paths of integration for I_1 and I_3 in Fig. 3, it is clear that as $M \to \infty$, $I_1 = I_3 = 0$. Also, along C_2, points corresponding to x on C are given by $x + i\pi/\alpha$. It can then be shown from Eq. (4.5) that

$$I_2 = - e^{-\pi w/\alpha} \ I \ . \tag{4.6}$$

There are two simple poles lying inside the contour, and after applying the usual residue theorem, and some simplification, it is found that

$$I_x = 2\,\frac{\pi\,\sin(aw)}{\alpha\,\sinh(\pi w/2\alpha)} \tag{4.7}$$

The y integral in P_e may be written down by inspection, so that the final result for the Kochin function is

$$P_e = p_0\,\frac{\pi\,\sin(aw)}{\alpha\,\sinh(\pi w/2\alpha)}\cdot\frac{\pi\,\sin(bu)}{\beta\,\sinh(\pi u/2\beta)}\ . \tag{4.8}$$

P_e has well defined limits for the cases specified by Eqs. (4.2) and (4.3).

Finally, by integrating the pressure distribution, one obtains the weight of the ACV:

$$W = 4\,p_0\,ab\ . \tag{4.9}$$

4.2 - NONDIMENSIONAL COEFFICIENTS:-

The wave resistance coefficient used is defined by

$$R_c = \frac{R}{W}\cdot\frac{\rho g a}{p_0}\ , \tag{4.10}$$

and the power coefficient by

$$\dot{W}_c = \frac{\dot{W}}{W}\cdot\frac{\rho\sqrt{ga}}{p_0} \tag{4.11}$$

4.3 - RESULTS:-

The programs used for computing the steady-state resistance are documented by Doctors (1970, Sec. (10.1)).

Some curves for the wave resistance are shown in Figs. 4 to 7 inclusive. In these diagrams, the variable used for the abscissa is $A = 1/(2F^2)$. This results in the low speed interference oscillations having a period approaching a constant value of 2π .

With regard to the ordinate, an arcsinh scale is occasionally used to improve the presentation of the results. This transformation is defined by

$$y_p = C_1 \operatorname{arsinh}(C_2 y) , \qquad (4.12)$$

where y is the number to be plotted and y_p is the distance on the figure. C_1 and C_2 are constants.

In Fig. 4a, the effect of smoothing on a two-dimensional pressure band, that is, reducing the value of the parameter αa , is illustrated. For $\alpha a = \infty$, we have a sharp pressure distribution and the amplitude of the oscillations of the wave resistance remains unchanged with increasing A (decreasing speed). The theory predicts an infinite number of these oscillations between zero speed and any finite velocity. The curve is a sine wave and this result was obtained by Lamb (1932, p. 403).

For finite values of the pressure fall-off parameter, αa , the oscillations die out with decreasing speed. If

$\alpha a = 5$, then there are only three major humps. The humps and hollows are caused by the interference of the bow and stern wave systems, which are purely transverse in this example. The interference is not affected by the smoothing. However, the smoothing reduces the amplitude of the waves generated by the bow and stern.

Fig. 4b shows the effect of smoothing a two-dimensional pressure band for a finite depth. The resistance is zero for supercritical speeds (when $F_d > 1$) because free waves cannot travel faster than the critical speed.

Three cases are illustrated in Fig. 5a. Case 1, with $\alpha a = \beta a = \infty$, represents a sharp pressure distribution with a beam to length ratio of 0.5 traveling over deep water. The unrealistic oscillations obtained by previous workers are confirmed. It should be noted that for low speeds the amplitude of the oscillations asymptotically approaches unity - the same as for the two-dimensional case. Thus the transverse waves become relatively more important in this speed range. Case 3, with $\alpha a = \beta a = 5$, has smoothing applied on all four edges, and once again, only about three or four humps occur. While typical values of αa and βa would have to be found from measured pressure distributions, this curve could represent an actual ACV. Finally, Case 2 only has smoothing at the bow and stern - equivalent to a sidewall ACV. The result is almost the same as for Case 3, showing that the wave pattern is essentially produced by the fore and aft portions of the cushion - and not the sides.

The effect of smoothing equally on all four edges is also displayed in Fig. 5b. The sharply edged case is compared with those of three different amounts of smoothing. The diagram shows that for $\alpha a = \beta a > 5$ an unnaturally large number of low speed humps and hollows occur.

Fig. 5c shows the same three cases of Fig. 5a, but for a finite depth. The chief difference now is that the main hump is pushed to the right and occurs near the critical depth Froude number. The low speed humps are only marginally affected.

The effect of varying the beam to length ratio is depicted in Fig. 6. Fig. 6a is for deep water. The general effect is an increase in the maxima of the resistance coefficient for increasing beam, since the transverse waves assume greater importance as the two-dimensional case is approached. At the same time, the minima are reduced for the same reason. A secondary effect is a shift in the location of the oscillations. As the beam increases, this shift is to the right (i.e., to lower Froude numbers). In the two-dimensional limit the hollows occur precisely at values of $A = n\pi$, where n is an integer.

The result of varying the beam is again shown in Fig. 6b, but now for a finite depth. Similar effects are shown in the low speed range, away from the neighborhood of the critical speed. However, the position of the critical speed hump is hardly affected. For finite beams it occurs at a slightly lower speed than for the two-dimensional case.

Fig. 7 illustrates the result of varying the depth of water. Each of the five diagrams is for a different beam to length ratio. They show how the critical depth hump resistance increases with decreasing depth. For the two-dimensional case, this peak resistance varies as the inverse square of the depth. However, for finite beam to length ratios, this maximum drag does not increase nearly as rapidly in shallow water.

Another aspect brought out by these diagrams is the rate at which the resistance curves for different depths, but the same beam, converge at large values of A. Thus, for values of A greater than 3, the case of $d/a = 1$ is indistinguishable from the deep water case. And at $d/a = 0.5$, the resistance curve is essentially the same as that for any greater depth, provided that A is greater than 6.

5 - CALCULATIONS FOR ACCELERATED MOTION

5.1 - TWO-DIMENSIONAL RESULTS:-

Sample results for accelerated motion are shown in Figs. 8 to 18. All but Fig. 9 were computed by programs listed by Doctors (1970, Sec. (10.2)). Although these programs can handle general acceleration patterns, only calculations corresponding to a constant acceleration are presented here.

Various two-dimensional results are given in Figs. 8 to 12. Fig. 8 shows the effect of varying the level of acceleration for a smooth pressure band over deep water. There are only two humps displayed when the acceleration is non-zero. The third and higher order humps have been smoothed out by the unsteady motion. Furthermore, with increased acceleration up to $0.2g$, the second last hump is also practically lost. The last or major hump is also somewhat reduced, but evidently any significant reduction can only be achieved by an application of an unnaturally high acceleration.

The location of the humps is also affected by the acceleration. With increasing acceleration, the oscillations are delayed to higher Froude numbers.

The case of a sharp two-dimensional pressure band is shown in Fig. 9. A complete curve could not be computed because of the (apparently) infinitely many oscillations that

occur in the region where A is just less than 5 (for the case of $\dot{c}/g = 0.05$). The last two humps, and the last hollow, correspond in position with those displayed for a smooth pressure band in Fig. 8. Thus, the smoothing does not affect the positions of the oscillations - as was also evident for steady motion.

The resistance coefficient is constant and equal to unity for $A > 5$. The significance of this point lies in the fact that the ACV has traveled one craft length when $A = 5$, at an acceleration of $0.05g$.

From geometrical considerations, it is clear that there can be no interference effects between the bow and stern transverse waves until the craft has moved this distance. Up to this point in time, the bow and stern individually produce a wave train of varying wavelength (depending on the instantaneous velocity), but of constant amplitude. Let us call this amplitude ζ_0. Then, before the band has moved one length, there are two wave trains produced, each containing energy per unit area proportional to ζ_0^2. The wave resistance of the two waves in this speed range is then proportional to $2\zeta_0^2$, and is constant.

When the band has traveled one length, the stern waves of finite wavelength start to run into the bow system that was produced at the start of the motion. These latter waves have a vanishingly small length. As a result, there is an infinite accumulation of the interference oscillations in the resistance curve just to the left of $A = 5$.

However, later on in the motion, the two wave systems have a relatively more similar wavelength, or frequency, and then have a capability of combining to give a maximum amplitude of almost $2\zeta_0$, or a minimum amplitude near zero. Hence, the wave resistance can fluctuate between $(\sim 0)^2$ and $(\sim 2\zeta_0)^2$ at the higher speeds. So the peak interference resistance is almost twice as high as the constant value occuring before the band has traveled one length.

For a general acceleration level, the point where the oscillations start is given by

$$A_1 = g/4\dot{c} \ . \qquad (5.1)$$

Hence, for higher accelerations, A_1 is smaller and the oscillations are displaced further to the left. This explains the general effect of acceleration on the location of the humps and hollows in Fig. 8.

Resistance curves for a smooth distribution appear again in Fig. 10, but the water now has a finite depth. The reduction in magnitude of the peaks is even more marked. Indeed, while the maximum steady-state resistance increases without limit in shallower water, the peak resistance coefficient for accelerated motion is more nearly fixed. Thus the relative reduction during unsteady motion is accentuated.

The location of the unsteady finite depth humps is affected in the same way as in deep water, being delayed to a higher speed.

The most striking phenomenon, however, is that for all the finite depth cases studied, the wave resistance becomes negative beyond a certain velocity. The resistance then asymptotically approaches zero from below.

Other interesting features of the two-dimensional case are presented in Figs. 11 and 12. These show the total power, resistance power and sustention power - which were discussed in Secs.(3.1) and (3.3). The total power, being the sum of the other two, represents the total rate at which work is being done on the water. It was computed in order to see if it remained positive when the resistance became negative. Fig. 11 shows these three powers as a function of time, for different acceleration levels over deep water. It is seen that a hump in the resistance power or total power curves generally corresponds to a hollow in the sustention power curve. It may also be noted that the sustention power is relatively small compared with the two other quantities.

Passing now to the case of finite depth, Fig. 12, we notice that the total power also becomes negative, and at approximately the same point in time as the resistance changes sign. In shallower water, these two points approach each other. At a depth to half-length ratio of 0.25, the points where the total power and resistance power become negative are indistinguishable.

In interpreting the occurrence of negative total power, it should be borne in mind that the total energy input to the

water, integrated from zero time, is always positive. However, at very high speeds the ACV begins to recover from the wave pattern some of the energy previously expended in forming it. The location of the negative hump in the resistance curve is further discussed in Sec. (6.6).

5.2 - THREE-DIMENSIONAL RESULTS:-

Some computed cases for a three-dimensional pressure distribution are shown in Figs. 13 to 18.

The resistance over deep water is shown in Fig. 13. The similarity to the two-dimensional analog in Fig. 8 is to be noted. The three-dimensional resistance is generally about half that of the two-dimensional case (for this beam to length ratio). Also the oscillations occur at slightly higher Froude numbers, due to the additional effect of the diverging waves. These same two differences display themselves in the steady-state results in Fig. 6.

The influence of acceleration on the resistance of a three-dimensional ACV over finite depth (Fig. 14) is seen to be remarkably less than for the corresponding two-dimensional situation. Again, it must be remembered that the steady-state two-dimensional results showed stronger phenomena than the three-dimensional ones. Principally, these were stronger interference oscillations, and zero resistance beyond the

critical speed.

Of chief interest in Fig. 14, compared with Fig. 10, is the lack of any speed range in which the resistance is negative. This indicates that the transverse component of the wave pattern is less important than the previous steady-state results implied.

The three-dimensional results, nevertheless, show a substantial reduction in the peak resistance during accelerated motion, particularly for the shallower situations.

Beyond the last hump, the curves of resistance for different levels of acceleration converge rapidly, as the speed increases. Beyond $A \doteqdot 0.5$ ($F \doteqdot 1.0$) the acceleration has little effect.

For the sake of completeness, curves of total power, resistance power and sustention power are given in Figs. 15 and 16. The deep water case (Fig. 15), again, is similar to the two-dimensional case in Fig. 11. The finite depth results in Fig. 16 do not differ considerably from the deep water results of the previous figure - in contrast to the two-dimensional results discussed before. In finite depth the three-dimensional sustention power approaches zero somewhat faster that in infinitely deep water.

A comparison of the resistance power for different rates of acceleration is made in Fig. 17 (deep water) and Fig. 18 (finite depth). For accelerated motion over deep water, there is a slight increase in peak power to overcome resistance. This is because the resistance peaks remain essenti-

ally the same in magnitude, but are shifted to a higher speed.

At a depth to half-length ratio of 1.0, the resistance power peaks are also higher in accelerated motion. A significant reduction in the maximum resistance power occurs only at a depth to half-length ratio of 0.25.

Thus we have a situation in which the resistance hump is considerably diminished in water of finite depth. However, the new location of the hump greatly reduces any saving in the power needed to overcome it.

6 - APPLICATION OF SHALLOW WATER THEORY

6.1 - PREAMBLE:-

It is well known that the first-order shallow water theory produces less realistic results for ship wave resistance than the linearized theory for finite depth. Thus Michell (1898) and Tuck (1966) showed that it predicted zero resistance for a body traveling at less than the critical speed. The advantage in shallow water theory lies in the possibility of extending it to obtain higher order approximations to the flow, where the complexity of the finite depth results would preclude this.

The theory was employed in this case to predict the location of the negative resistance hump displayed in the unsteady two-dimensional results.

6.2 - DERIVATION OF POTENTIAL:-

The procedure is essentially the same as for the case of finite depth, since the same set of equations, namely Eqs. (2.5), (2.7), (2.9) and (2.11), are to be satisfied.

In the spirit of the shallow water approximation, we shall assume an asymptotic expansion for the disturbance

potential, viz:

$$\phi = \sum_{n=1}^{\infty} \phi^{(n)} \quad , \tag{6.1}$$

where $$\phi^{(n+1)} = o(\phi^{(n)}) \quad . \tag{6.2}$$

Furthermore, we shall follow Tuck and simply take

$$\phi^{(n)} = O(\varepsilon^n) \quad . \tag{6.3}$$

Here ε is the parameter denoting the shallowness of the water so that its definition could be

$$x, y = O(1) \; ; \quad z = O(\varepsilon) \quad , \tag{6.4}$$

x , y , z being inside the fluid region.

It follows from Eq. (6.4) that differentiation can change the order of magnitude of a quantity. Thus

$$\frac{\partial}{\partial x}, \frac{\partial}{\partial y} = O(1)$$

$$\text{and} \quad \frac{\partial}{\partial z} = O(\varepsilon^{-1}) \quad . \tag{6.5}$$

We may now substitute the expansion, Eq. (6.1), into the Laplace equation, Eq. (2.5). Due to the assumptions of

Eqs. (6.3) and (6.5), we may separate the lowest order term in Eq. (2.5). Thus

$$\phi^{(1)}_{zz} = 0 \ . \tag{6.6}$$

Similarly, the bed condition, Eq. (2.11), yields

$$\left[\phi^{(1)}_{z}\right]_{z=-d} = 0 \ . \tag{6.7}$$

From Eqs. (6.6) and (6.7) we see that $\phi^{(1)}$ is not a function of z, i.e.

$$\phi^{(1)} = A^{(1)}(x,y) \ . \tag{6.8}$$

The series, Eq. (6.1), is now substituted in the kinematic condition, Eq. (2.7). Also, the Laplace equation gives

$$\phi^{(1)}_{z} = \phi^{(2)}_{z} = 0 \tag{6.9}$$

and

$$\phi^{(3)}_{z} = -(z + d)\, \nabla^2_{2D} A^{(1)} \ , \tag{6.10}$$

where

$$\nabla^2_{2D} = \frac{\partial^2}{\partial x^2} + \frac{\partial^2}{\partial y^2} \ .$$

So the condition becomes

$$\left[\phi^{(3)}{}_z\right]_{z=0} - \zeta^{(1)}{}_t + c\,\zeta^{(1)}{}_x = 0 \ , \qquad (6.11)$$

where $\zeta^{(1)}$ is the first approximation to the value of ζ .

The last boundary condition needed is the dynamic condition on the free surface, Eq. (2.9). This results in

$$\left[\phi^{(1)}{}_t - c\,\phi^{(1)}{}_x\right]_{z=0} + p/\rho + g\,\zeta^{(1)} = 0 \ . \qquad (6.12)$$

The last three equations are utilized to produce the equation to be solved for $A^{(1)}$:

$$-gd\left[\left(1 - \frac{c^2}{gd}\right) A^{(1)}{}_{xx} + A^{(1)}{}_{yy}\right] + A^{(1)}{}_{tt} -$$

$$- 2c\,A^{(1)}{}_{xt} - \dot{c}\,A^{(1)}{}_x = \frac{c}{\rho}\,p_x \ . \qquad (6.13)$$

The method of solution for $A^{(1)}$ is similar to that used in Sec. (2.2) for ϕ . A double Fourier transform (Eq. (2.12)) with respect to x and y is made, and this is followed by the substitution given by Eq. (2.19). The result of these two operations is

$$\tilde{\chi}_{tt} + gd(w^2 + u^2)\tilde{\chi} = \frac{icw}{\rho}\cdot\tilde{p}\cdot\exp(-iw\cdot s(t)) \ . \qquad (6.14)$$

The similarity between the previous equation and the corresponding one for finite depth should be observed. The Laplace transform (Eq. (2.13)) of Eq. (6.14) is taken, and the convolution theorem applied. Then the double inverse Fourier transform is used to give the first approximation to the shallow water potential:

$$\phi^{(1)}(x,y,z,t) = \frac{i}{4\pi^2\rho\sqrt{gd}} \iint_{S'} p' \, dS' \int_0^t c(\tau) \, d\tau \int_{-\infty}^{\infty} dw \int_{-\infty}^{\infty} du$$

$$\frac{w}{k} \cdot \sin[\sqrt{gd} \cdot k \cdot (t - \tau)] \times$$

$$\times \exp[i(w(x - x' + s(t) - s(\tau)) + u(y - y'))], \quad (6.15)$$

with $$k^2 = w^2 + u^2 \ .$$

6.3 - WAVE RESISTANCE:-

The first approximation to the resistance is just

$$R^{(1)} = \iint_S p\, \zeta^{(1)}_x \, dS \ .$$

The dynamic condition on the free surface, Eq. (6.12), is now employed, as detailed in Sec. (3.2). The final result, after simplification is

$$R^{(1)} = \frac{1}{\pi^2 \rho g} \int_0^t c(\tau)\, d\tau \int_0^\infty dw \int_0^\infty du\, w^2 \cdot \left[P_e^{\,2} + P_o^{\,2} + Q_e^{\,2} + Q_o^{\,2} \right]$$

$$\times \cos[\sqrt{gd} \cdot k \cdot (t - \tau)] \cdot \cos[w(s(t) - s(\tau))] \ . \qquad (6.16)$$

It is interesting to compare this result with that for finite depth, namely Eq. (3.13). The shallow water result can be obtained simply by letting $d \to 0$ in the latter to the extent that $\tanh(kd)$ is replaced by kd .

The steady state resistance can be obtained either as the limit of Eq. (6.16) as $t \to \infty$ (if the velocity is held

constant), or by allowing d to approach zero in Eq. (3.24). The result follows:

$$R^{(1)} = \frac{1}{2\pi\rho g} \cdot \frac{F_d^{\,2}}{\sqrt{F_d^{\,2} - 1}} \int_0^\infty w^2 \cdot (P_e^{\,2} + P_o^{\,2} + Q_e^{\,2} + Q_o^{\,2})\, dw \ ,$$

where $$P_e = P_e(w,u) \ , \text{ etc.}, \tag{6.17}$$

and $$u = w \cdot \sqrt{F_d^{\,2} - 1} \ . \tag{6.18}$$

The relation between the transverse and longitudinal wave numbers, Eq. (6.18), shows that there is a fixed angle between the wavefronts and the y axis. This angle is given by

$$\theta = \arccos(1/F_d) \ . \tag{6.19}$$

If $F_d < 1$ there are no free waves satisfying Eq. (6.19) and the wave resistance is zero.

6.4 - ELEVATION OF THE FREE SURFACE:-

The free surface elevation may be found from substituting the potential, Eq. (6.15), into the dynamic condition, Eq. (6.12). Employing the standard rules for differentiating an integral expression, it is found that

$$\zeta^{(1)} = -\frac{p}{\rho g} + \frac{1}{4\pi^2 \rho g} \iint_{S'} p' \, dS' \int_{0}^{t} c(\tau) \, d\tau \int_{-\infty}^{\infty} dw \int_{-\infty}^{\infty} du$$

$$w \cdot \cos[\sqrt{gd} \cdot k \cdot (t - \tau)] \times$$

$$\times \sin[w(x - x' + s(t) - s(\tau)) + u(y - y')] \; . \qquad (6.20)$$

On the other hand, if we restrict our attention to pressure distributions which are symmetric about the x and y axes, such that

$$P_o = Q_e = Q_o = 0 \; ,$$

then Eq. (6.20) may be simplified to

$$\zeta^{(1)} = -\frac{p}{\rho g} + \frac{1}{\pi^2 \rho g} \int_0^\infty dw \int_0^\infty du \int_0^t c(\tau) \cdot w \cdot P_e \times$$

$$\times \cos[\sqrt{gd} \cdot k \cdot (t - \tau)] \cdot \sin[w(x + s(t) - s(\tau))] \cdot \cos(uy)\, d\tau \ . \qquad (6.21)$$

6.5 - STEADY-STATE RESULTS:-

A comparison of shallow water and finite depth theory is made in Fig. 19. The case of a smooth three-dimensional pressure distribution is depicted in Fig. 19a. It is seen that a depth to half-length ratio of 0.25 is essentially shallow if $1/F_d^2 < 0.5$.

The wave resistance of a sharp three-dimensional distribution is shown in Fig. 19b. The convergence of the finite depth resistance to the shallow water one is perhaps not so rapid here. An interesting feature of the shallow water result is the knuckle in the resistance curve at $F_d^2 = 5$. (The other sudden changes in slope in the

curve are due to the fact that a finite number of points have been computed to define it.) For this pressure distribution, it is possible to perform the integration in Eq. (6.17) analytically. Using Gradshteyn and Ryzhik (1965, p. 451, 3.828, Formula 9), the result may be written down as

$$R_c = \frac{a}{b}\cdot\frac{F_d^2}{2(F_d^2 - 1)^{3/2}} \qquad \text{if} \quad F_d > F_{d_1}$$

$$= \frac{F_d^2}{2(F_d^2 - 1)} \qquad \text{if} \quad F_d < F_{d_1} , \tag{6.22}$$

where $F_{d_1} = \sqrt{a^2/b^2 + 1}$.

Thus, the resistance is continuous at a depth Froude number equal to F_{d_1} but the slope is not. It is easily verified that when $F_d = F_{d_1}$, the wave pattern appears as in Fig. 20. Apparently there is a reinforcement between the bow and stern wave systems at this particular speed, causing the observed knuckle.

In Fig. 19a a slight hump is also discernible at this depth Froude number, but due to the finite values of the pressure fall-off parameters the slope of the resistance curve is continuous.

6.6 - ACCELERATED MOTION:-

In order to examine the phenomena exhibited in the two-dimensional wave resistance curves of Sec. (5.1), we shall consider the free surface elevation due to the motion of a pressure band given by Eq. (4.2). The Kochin function, P_e, given by Eq. (4.8) is then substituted into Eq. (6.21). The two-dimensional limit as $b \to \infty$ is obtained, by use of Eq. (3.18) to evaluate the u integral and the result is

$$\zeta^{(1)} = -\frac{p}{\rho g} + \frac{p_0}{\rho g \alpha} \int_0^\infty dw \int_0^t c(\tau) \cdot w \cdot \cos[\sqrt{gd} \cdot w \cdot (t - \tau)] \times$$

$$\times \sin[w(x + s(t) - s(\tau))] \cdot \frac{\sin(aw)}{\sinh(\pi w/2\alpha)} \, d\tau \, . \qquad (6.23)$$

We now apply the formulas for the products of sines and cosines, twice, to give

$$\zeta^{(1)} = -\frac{p}{\rho g} + \sum_{i,j=\pm 1} \sum i \cdot \frac{p_0}{4\rho g \alpha} \int_0^\infty dw \int_0^t c(\tau) \cdot w \times$$

$$\times \frac{\cos[w(\sqrt{gd} \cdot (t - \tau) + j(x + s(t) - s(\tau) - ia))]}{\sinh(\pi w/2\alpha)} \, d\tau \, . \qquad (6.24)$$

In Eq. (6.24), i and j are the signs of the appropriate factors and there are a total of four terms in the double

summation.

The w integral may now be done using Gradshteyn and Ryzhik (1965, p. 511, 4.111, Formula 2):

$$\zeta^{(1)} = - \frac{p}{\rho g} + \sum_{i,j=\pm 1} \sum i \cdot \frac{\alpha p_0}{4\rho g} \int_0^t c(\tau) \times$$

$$\times \operatorname{sech}^2[\alpha(\sqrt{gd}\cdot(t - \tau) + j(x + s(t) - s(\tau) - ia))]\, d\tau \ . \quad (6.25)$$

Further restricting our interest to a sharp pressure band, so that $\alpha \to \infty$, it is seen that the integrand is zero except when

$$\sqrt{gd}\cdot(t - \tau) + j(x + s(t) - s(\tau) - ia) = 0 \ . \quad (6.26)$$

Let us say that this occurs when $\tau = t_1$ and the velocity of the band is $c(t_1) = c_1$, while the distance traveled is $s(t_1) = s_1$. In the neighborhood of $\tau = t_1$, we put

$$\tau = t_1 + \tau' \ ,$$

where τ' is small as $\alpha \to \infty$. The argument of the hyperbolic secant in Eq. (6.25) may then be reexpressed in the region where $\tau \doteqdot t$. It is just

$$\tau'' = - \alpha(\sqrt{gd} + jc_1)\tau' \ .$$

This substitution is now made in Eq. (6.25) to give

$$\zeta^{(1)} = -\frac{p}{\rho g} - \sum_{i,j=\pm 1} \sum i \cdot \frac{p_0 c_1}{4\rho g(\sqrt{gd} + jc_1)} \times$$

$$\times \int_{\infty \cdot \mathrm{sgn}(\sqrt{gd}+jc_1)}^{-\infty \cdot \mathrm{sgn}(\sqrt{gd}+jc_1)} \mathrm{sech}^2 \tau'' \, d\tau'' \, . \qquad (6.27)$$

In this integral, the upper limit should be replaced by zero if $t_1 = t$, and similarly for the lower limit, if $t_1 = 0$. We then obtain

$$\zeta^{(1)} = \frac{p_0}{\rho g}\left[- H(a - |x|) + \frac{1}{2} \sum_{i,j=\pm 1} \sum \frac{i \cdot \varepsilon \cdot F_{d_1}}{|1 + j \cdot F_{d_1}|} \right] . \qquad (6.28)$$

Here $\varepsilon = 1$ if $0 < t_1 < t$

$= \frac{1}{2}$ if $t_1 = 0$ or $t_1 = t$ (6.29)

$= 0$ if $t_1 < 0$ or $t_1 > t$,

and H is the Heaviside step function.

The wave resistance of this sharp pressure band may be derived from the formula:

$$R^{(1)}_{2D} = p_0 \sum_{\ell=\pm 1} \ell \left[\zeta^{(1)}\right]_{x=\ell a} .$$

The resistance coefficient then follows:

$$R_C = \frac{1}{4} \sum_{i,j,\ell=\pm 1} \sum \sum \frac{i\ell \cdot \varepsilon \cdot F_{d_1}}{|1 + j \cdot F_{d_1}|} , \qquad (6.30)$$

and t_1 is now the solution of

$$\sqrt{gd} \cdot (t - t_1) + j(s(t) - s(t_1) + (\ell - i)a) = 0. \qquad (6.31)$$

The shallow water resistance is plotted as a function of time in Fig. 21. This is for a constant acceleration. At one point the resistance becomes infinite, and at another it becomes negatively infinite. This second peak corresponds closely with the negative hump predicted by the finite depth theory for the same depth and acceleration (Fig. 12e). Apparently the positive hump does not show up in finite depth

theory. It should be noted that the positive hump in the shallow water theory is smoother than the negative one in the sense that the latter has an infinite discontinuity in function value.

Fig. 22 shows the shape of the water surface at different stages of the motion of Fig. 21. Initially, the depression is due only to the static pressure under the pressure band. As time progresses a pile of water builds up ahead of the bow and this develops into an infinite peak at the critical depth Froude number ($F_d = 1$). At the same time, a negative peak develops just inside the stern. The pair of peaks causes the positive hump shown in Fig. 21.

Beyond the critical speed these peaks cannot keep up with the ACV, and are seen to move back relative to it. At a second critical point in time, the bow peak passes under the stern of the pressure band and the resistance suddenly drops to minus infinity. Thereafter, the water surface in the vicinity of the ACV levels out, and the wave resistance approaches zero.

An inspection of Eq. (6.30) shows that the peaks in the resistance curve occur when $j = -1$ and $F_{d_1} = 1$. Looking now at Eq. (6.31), this can happen when:

$\underline{\ell = i}$: $\qquad t = t_1 \ , \quad F_d = 1 \ .$

This is the case of the positive peak. The other possibility is:

$\underline{\ell = -i}$: $\sqrt{gd}\cdot(t - t_1) - (s - s_1 \pm 2a) = 0$.

This case corresponds to the negative peak. Of the two conditions represented by the latter equation, the only one that satisfies the relationship $0 < t_1 < t$ is

$$\sqrt{gd}\cdot(t - t_1) - (s - s_1 - 2a) = 0 \ . \qquad (6.32)$$

Eq. (6.32) gives the value of t when the spike of water generated at the bow passes under the stern of the pressure band.

If we now return to the special case of a constant acceleration $\dot{c}$, Eq. (6.32) becomes a quadratic in t. The depth Froude number which locates the negative hump is then given by the formula:

$$F_d = 1 + 2\sqrt{a\dot{c}/gd} \ . \qquad (6.33)$$

Eq. (6.33) is plotted in Fig. 23, together with some points representing the location of the negative hump for a finite depth. As expected, the agreement is better for shallower depths and sharper pressure distributions.

7 - THE INVERSE PROBLEM

7.1 - PROBLEM STATEMENT:-

An object of interest in the design of an ACV is to know the attainable acceleration pattern as a function of the characteristics of the propulsor. Hence, other items of concern, such as the acceleration margin at the hump speed, may be deduced.

In order to make the study realistic, one must include all the components of resistance. These were described in Sec. (1.1). We use Newton's law to obtain

$$T - D_A - D_M - R = m\dot{c} \ , \qquad (7.1)$$

where T is the thrust available, D_A is the aerodynamic or profile drag, D_M is the momentum drag and m is the mass of the craft. The problem definition could be made more elaborate by including, for example, an estimate of the water contact resistance. It is emphasized here that this break-down into drag components is only an idealization of the true situation in which there are interactions among them.

In Eq. (7.1), the terms on the left-hand side are functions of speed, or acceleration pattern - which are unknown. We shall assume the following forms of these resistance components:

$$D_A = \frac{1}{2} C_D A_F \rho_A c^2 , \tag{7.2}$$

and

$$D_M = \dot{m}_A c , \tag{7.3}$$

where C_D is the aerodynamic drag coefficient of the craft based on A_F, the frontal area, while ρ_A is the air density and $\dot{m}_A$ is the mass flow rate into the air cushion. The program used to solve Eq. (7.1) is described by Doctors (1970, Sec. (10.3)).

Let us now limit the numerical investigation to a single craft. The data are given meaning by relating them to a particular (dimensional) machine, below. The results will also apply to any scale model of this craft.

DIMENSIONAL VARIABLE				DIMENSIONLESS VARIABLE	
ρ	=	1.94	slugs/ft.^{3}	(base unit)	
g	=	32.2	ft./sec.^{2}	(base unit)	
a	=	20	ft.	(base unit)	
b	=	10	ft.	b/a	= 0.5
α	=	0.25	ft.$^{-1}$	αa	= 5
β	=	0.25	ft.$^{-1}$	βa	= 5
W	=	25,000	lbf.	ρga/p_0	= 40
ρ_A	=	0.002425	slugs/ft.^{3}	$\rho_A a^3/m$	= 0.025
$C_D A_F$	=	160	ft.^{2}	$C_D A_F \rho_A a/2m$	= 0.005
$\dot{m}_A$	=	7.384	slugs/sec.	$\dot{m}_A\sqrt{a}/m\sqrt{g}$	= 0.0075

7.2 - RESULTS FOR UNSTEADY MOTION:-

Fig. 24 shows the effect of applying three different constant thrust levels to the ACV. At the hump speed the wave resistance is of the same order as the two other drag components combined. Only one other minor hump is displayed, as was also the case for a constant acceleration level. Thus the character of the wave resistance curve is not grossly affected by the nature of the acceleration pattern - provided it is reasonably smooth. At the lowest thrust level (0.06 of the craft weight) the acceleration margin at the hump is only about 0.02g which could be inadequate for a practical machine.

The same craft running over finite depth is presented in Fig. 25. Similar general trends are displayed. However, the thrust margin at the hump speed is slightly reduced, but thereafter the wave resistance drops somewhat faster than in deep water.

The corresponding velocity patterns are shown in Figs. 26 and 27. The curves are quite smooth despite the humps in the wave resistance. The effect of depth is seen to be small for this case - the drop in velocity in the region of the hump due to finite depth is less than 10%.

Some calculations were also performed using an engine-driven airscrew to push the craft rather than a constant-thrust device. The propeller used was a four-bladed Clark Y Section screw (Propeller Reference Number 5868-9). The characteristics of this propeller were measured by Hartman

and Biermann (1937). The diameter, D , was 10 ft. and the blades had a nominal angle of 20° at the three-quarter radial point. The table below lists the thrust and torque coefficients, K_T and K_Q , as a function of the advance ratio, J , where

$$K_T = T/\rho_A N^2 D^4 \quad , \tag{7.4}$$

$$K_Q = Q/\rho_A N^2 D^5 \tag{7.5}$$

and $$J = c/ND \quad . \tag{7.6}$$

Here Q is the propeller torque and N its speed in revolutions per unit time.

J	K_T	K_Q	J	K_T	K_Q
0	0.187	0.0189	0.6	0.120	0.0158
0.1	0.185	0.0188	0.7	0.097	0.0138
0.2	0.181	0.0186	0.8	0.072	0.0114
0.3	0.175	0.0185	0.9	0.045	0.00764
0.4	0.161	0.0180	1.0	0.016	0.00366
0.5	0.140	0.0170			

Fig. 28 shows the variation of drag components with time, assuming that the propeller absorbs a power, P , given by

$$P = 3.804 \times 10^5 \text{ ft.lbf./sec.} \quad (692 \text{ H.P.}) ,$$

or $$P/ma^{1/2}g^{3/2} = 0.6 .$$

The results are very similar to those in Fig. 24 for a constant thrust. This is because the propeller advance ratio is still small at the hump speed - and up to this speed K_T and K_Q are almost constant.

The case of a constant propeller speed of revolution is treated in Fig. 29. Fig. 29a shows the resistance components when the propeller runs at a speed given by

$$N = 25.38 \text{ r.p.s.} ,$$

or $$N\sqrt{a/g} = 20 .$$

Again, the thrust drops only slightly in the speed range involved, so the results are similar to those for a constant thrust, or a constant engine power. In Figs. 29b and 29c the craft is overloaded by 50% and 100%, respectively. Only the weight (and cushion pressure) were increased, and all the other dimensional data were held fixed. Since the wave drag is proportional to the square of the cushion pressure, this component becomes relatively more important in cases of

overload. For the 100% overload situation, the machine barely surpasses the hump.

The case of the same propeller speed of revolution, but over finite depth, is handled in Fig. 30. For a normal load (Fig. 30a), or a 50% overload (Fig. 30b), the drag components follow quite closely the corresponding curves for deep water given in Figs. 29a and 29b, respectively. However, for a 100% overload (Fig. 30c) the situation is quite different in finite depth.

Here the craft apparently does not overcome the resistance hump in the time shown. At first, it seems to only just cross the (unsteady) hump. Then the wave resistance rises - probably because the almost zero acceleration at this time allows the shallow water wave pattern to build up, thus approaching a nearly steady state. The total drag (being essentially the same as the wave resistance now) is greater than the thrust so that the craft decelerates to below the hump speed. Without extending the calculation to a greater time limit, it is difficult to predict whether the ACV would cross the hump, approach a steady-state sub-hump speed, or settle down into a repetitive cycle.

The velocity pattern for the above-mentioned three loadings is shown in Figs. 31 and 32. In deep water (Fig. 31) it is seen that while a 50% overload is tolerable for this craft, a 100% overload could prevent hump speed being achieved in practice. In finite depth (Fig. 32) the region of deceleration for a 100% overload is now more clearly revealed.

The main assumption here is that the propeller and engine characteristics at any instant of an unsteady motion can be estimated on a quasi-steady basis using only the instantaneous craft speed, thus ignoring inertia and time history effects. (In fact, the only quantity treated in a truly unsteady fashion here is the wave resistance.) The calculated results, retrospectively, seem to confirm the validity of this assumption. The required changes in propeller speed of rotation (under the constraint of constant power) and thrust (under the constraint of constant propeller speed) are indeed quite small. Thus the system of the propeller and engine is effectively operating at a nearly steady state.

7.3 - QUASI-STEADY RESULTS:-

One might now consider the effect of a further simplification, namely the assumption that the wave resistance can also be treated on a quasi-steady basis. In other words, the wave resistance (as well as the other drag components) at any instant of the unsteady motion is assumed to be independent of acceleration and time history - and just equal to the steady-state value at the instantaneous velocity. This technique could make use of the steady-state results previously calculated in Sec. (4.3), which incidentally

require much less computational effort.

Fig. 33 is the quasi-steady analog of Fig. 24 and shows the drag components over deep water for three different thrust levels. There is generally little difference in the resultant motion because, as was seen in Sec. (5.2), the magnitude of the hump resistance in deep water is only slightly affected by this range of acceleration. Moreover, the low speed unsteady resistance curve tended to pass through the average value of the oscillating steady-state resistance curve, and the effect of small local oscillations in resistance tends to be averaged out in the resultant velocity pattern.

The effect of finite depth is shown in Fig. 34. The difference compared with the truly unsteady calculation (Fig. 25) is more discernible now - because of the higher steady-state hump encountered in the quasi-steady calculations. This aspect is more clearly seen in Figs. 35 and 36 which display the velocity patterns for deep water and finite depth, respectively. For comparison, the unsteady curves are also shown. In deep water there is little difference, but for $d/a = 0.5$, the patterns separate slightly more at the hump speed for the reasons cited above.

The result of employing the propeller previously described (with a constant speed of revolution) is shown in Fig. 37 (deep water) and Fig. 38 ($d/a = 0.25$). As was noted in Sec. (7.2), there is no new effect displayed when compared to a constant thrust device. Below the hump speed, the

propeller produces an almost constant thrust. In deep water the quasi-steady and unsteady results (Fig. 29) are again similar.

For $d/a = 0.25$, the motion of a normally loaded craft compares with that for the unsteady calculation (Fig. 30a). However, for a 50% overload, the quasi-steady calculation predicts that the ACV can only achieve a sub-hump speed while the unsteady theory (Fig. 30b) shows that the ACV, in fact, has a practical thrust margin to surpass the hump resistance. In the case of 100% overload the unsteady result (Fig. 30c) shows that the machine is in a marginal position regarding its ability to achieve a practical cruising speed. The quasi-steady calculation, on the other hand, would indicate that the craft considerably lacks the ability to cross the hump - it would seem to have only about half of the thrust required.

The velocity patterns for a constant propeller speed of revolution are shown in Fig. 39 (deep water) and Fig. 40 ($d/a = 0.25$). These clearly indicate the marked difference between the predictions of the quasi-steady and unsteady calculations - particularly for finite depth.

8 - CONCLUDING REMARKS

8.1 - CONCLUSIONS:-

A large number of results have been presented, and the reader is referred to the appropriate section for the details. However, some general remarks should now be made, and the first of these concerns the degree of smoothing required to eliminate the low speed oscillations in the steady-state wave resistance curves.

Reference is now made to Fig. 2 showing the pressure distribution. We shall take $\beta a = \infty$ since this parameter hardly affects the resistance. The slope of the free surface at the center of the bow ($x = a$, $y = 0$), at zero speed, is then given by

$$\zeta_x = \frac{\alpha p_0}{2\rho g}\left[1 - \operatorname{sech}^2(2\alpha a)\right] .$$

For $\alpha a > 2$ the second term may be dropped to give

$$\zeta_x \doteq \frac{\alpha p_0}{2\rho g} . \qquad (8.1)$$

Some calculations by Jones (1966), for example, indicate that this slope is of the order of unity. Furthermore, for typical ACVs, the ratio $\rho g a/p_0$ is about 40. Hence

Eq. (8.1) would yield $\alpha a = 80$ as a general value. The conclusion in this regard then, is that a reasonable amount of smoothing is not sufficient by itself to eliminate the low speed humps and hollows. Other effects, such as nonlinearity and real fluid properties, may have to be invoked to explain the discrepancy.

It is evident, however, that the use of low values of αa and βa (about 5) does improve the agreement between calculated and observed steady-state wave resistance curves, especially at lower speeds. Thus the use of such values, even if unnecessary from the point of view of accurate pressure modelling, could still be justified if αa and βa are regarded as semi-empirical factors introduced to effectively eliminate the unrealistic linear effects at low Froude numbers. Two advantages will accrue.

First, the inverse problem can be treated with more confidence since it requires a continuous calculation of wave resistance for the entire speed range beginning from zero and one can avoid the unrealistic phenomena which would occur for a sharp pressure distribution.

Second, the computational effort involved in evaluating the various integrals is considerably reduced due to the exponential decay of the integrands at infinity if αa and βa are finite and small. In fact the corresponding calculations for a sharp pressure distribution would be formidable, as discussed in Sec. (8.2). Thus there is also a practical and economical advantage in the use of these adjustable constants.

Most of the figures show a marked similarity between the two- and three-dimensional results. Thus the transverse wave system plays a large role in contributing to the energy radiation for the usual beam to length ratios of ACVs. On the other hand, the diverging waves are sufficiently important to prevent the occurrence of negative wave resistance during accelerated motion of the craft from rest in finite depth.

The effect of acceleration level on the wave resistance is quite marked. Normal accelerations of up to 0.1g are sufficient to eliminate most of the low speed humps. Also, the high resistance peak at the critical depth Froude number is limited to a much smaller value in accelerated motion.

However the resistance peak is displaced to a higher speed so that the power needed to overcome it is hardly diminished, except in very shallow water.

On the other hand, the practical design of an ACV results in the propulsive efficiency being a maximum near the design speed. At low speeds, up to the hump, the thrust is essentially constant. Hence the critical thing <u>is</u> the peak wave resistance - and not the peak power to overcome it. This was borne out by a comparison of the unsteady and quasi-steady theories for the solution of the inverse problem in finite depth. Under certain circumstances the ACV could easily cross the hump, even though the quasi-steady theory predicted otherwise.

8.2 - FUTURE WORK:-

It would be worthwhile to run some experiments to verify the calculations for accelerated motion. Either the direct or inverse case could be tested since the theory is equally valid for both. Correction for the additional drag components is one of the problems to be contended with.

A particular case that should be examined is the two-dimensional one. It should be interesting to see how accurately the theory predicts the phenomenon of negative wave resistance.

A few comments should also be addressed to the problem of computing the integral in Eq. (3.13). The convergence of this integral deteriorates for large values of t, α and β. This is because of the exponential decays in the Kochin function, Eq. (4.8). The Gauss-Laguerre quadrature rules used are based on these decays. Thus the majority of the resistance curves for accelerated motion, given in the figures, employed a rule of order 2048 for the w integral, and a rule of order 16 for the u integral. However, an estimation of the truncation error showed that, in fact, only the first 102 and 9 points, respectively, were needed for a three-figure accuracy. Generally, a 129-point trapezoidal rule was used in the τ integral.

This combination of rules was found to be the best, although it would be useful to investigate other numerical quadrature schemes.

Because of the limitations of the numerical method -

specially for large t - an alternative technique of evaluating the integral should be considered. For values of the velocity somewhat greater than the main hump speed, it should be possible to construct an asymptotic expression for the wave resistance (for large t). For the inverse problem, the asymptotic formula would have to be based on an extrapolated velocity pattern (which could be corrected iteratively).

Finally, it may be remarked, that a nonlinear theoretical treatment of the problem would reveal more about the low speed oscillations in the resistance curve predicted by the linear theory.

Following Wehausen (1963), one could assume the potential to be a power series in terms of a perturbation parameter such as $p_0/\rho ga$ or $p_0/\rho c^2$. It should then be fairly straightforward to construct a linear scheme of successively higher approximations as has already been done for the case of a ship in steady motion. In fact, there is good reason to believe that due to the absence of the hull boundary condition, the numerical evaluation of the resulting integrals here would be somewhat simpler than for a ship.

9 - BIBLIOGRAPHY

Alexander, A.J.: "Static Hovercraft over Water", J. Royal Aeronautical Soc., **71**, pp. 719 - 721 (1967).

Barratt, M.J.: "The Wave Drag of a Hovercraft", J. Fluid Mechanics, **22**, Part 1, pp. 39 - 47 (1965).

Davis, P.J. and Rabinowitz, P.: Numerical Integration, Waltham, Mass., Blaisdell Pub. Co., 230 pp. (1967)

Djachenko, V.K.: "The Wave Resistance of a Surface Pressure Distribution in Unsteady Motion", Proc. Leningrad Shipbuilding Inst. (Hydrodynamics and Theory of Ships Division). Translated by M. Aleksandrov and L.J. Doctors, Dept. Naval Architecture and Marine Engineering, University of Michigan, Ann Arbor, Michigan, Report 44, 12 pp. (1966)

Doctors, L.J.: "The Wave Resistance of an Air-Cushion Vehicle", Ph.D. Thesis, Dept. Naval Architecture and Marine Engineering, University of Michigan, 261 pp. (1970).

Eggers, K.W.H., Sharma, S.D., and Ward, L.W.: "An Assessment of Some Experimental Methods for Determining the Wavemaking Characteristics of a Ship Form", Trans. Soc. Naval Architects and Marine Engineers, **75**, pp. 112 to 157 (1967).

Everest, J.T.: "The Calm Water Performance of a Rectangular Hovercraft", National Physical Laboratory (Ship Division), Report 72, 12 pp. + 29 figs. (1966).

- "Shallow Water Wave Drag of a Rectangular Hovercraft", National Physical Laboratory (Ship Division), Report 79, 8 pp. + 19 figs. (1966).

- , and Hogben, N.: "Research on Hovercraft over Calm Water", Trans. Royal Inst. Naval Architects, **109**, pp. 311 - 326 (1967).

- , and Willis, R.C.: "Experiments on the Skirted Hovercraft Running at Angles of Yaw with Special Attention to Wave Drag", National Physical Laboratory (Ship Division), Report 119, 8 pp. + 15 figs. (1968).

- , and Hogben, N.: "A Theoretical and Experimental Study of the Wavemaking of Hovercraft of Arbitrary Planform and Angle of Yaw", Trans. Royal Inst. Naval Architects, **111**, pp. 343 - 365 (1969).

Fox, L. and Parker, I.B.: Chebyshev Polynomials in Numerical Analysis, London, Oxford Univ. Press, 205 pp. (1968).

Gradshteyn, I.S. and Ryzhik, I.M.: Table of Integrals, Series and Products, New York, Academic Press (Translation from the Russian), 1086 pp. (1965).

Hartman, E.P. and Biermann, D.: "The Aerodynamic Characteristics of Full-Scale Propellers Having 2, 3 and 4 Blades of Clark Y and R.A.F. 6 Airfoil Sections", N.A.C.A. Technical Report 640, 23 pp. (1937).

Havelock, T.H.: "The Wave-Making Resistance of Ships: A Theoretical and Practical Analysis", Proc. Royal Soc. London, Series A, **82**, pp. 276 - 300 (1909).

- "Ship Resistance: The Wave-Making Properties of Certain Travelling Pressure Disturbances", Proc. Royal Soc. London, Series A, **89**, pp. 489 - 499 (1914).

- "The Initial Wave Resistance of a Moving Surface Pressure", Proc. Royal Soc. London, Series A, **93**, pp. 240 to 253 (1916).

- "The Effect of Shallow Water on Wave Resistance", Proc. Royal Soc. London, Series A, **100**, pp. 499 - 505 (1922).

- "Some Aspects of the Theory of Ship Waves and Wave Resistance", Trans. North-East Coast Inst. Engineers and Shipbuilders, **42**, pp. 71 - 83 (1926).

- "The Theory of Wave Resistance", Proc. Royal Soc. London, Series A, **138**, pp. 339 - 348 (1932).

Hogben, N.: "Wave Resistance of Steep Two-Dimensional Waves", National Physical Laboratory (Ship Division), Report 55, 9 pp. + 5 figs. (1965).

Hogben, N.: "An Investigation of Hovercraft Wavemaking", J. Royal Aeronautical Soc., **70**, pp. 321 - 329 (1966).

- "Hovering Craft over Water", National Physical Laboratory (Ship Division), Tech. Memorandum 119, 78 pp + 29 figs. (1966)

IBM: "Programmers' Manual - System/360 Scientific Subroutine Package (360A - CM - 03X) Version III", Number H20 - 0205 - 3, 454 pp. (1968).

Jones, D.I.G.: "Hovering Performance of Plenum Chamber GEMs over Land and Water", J. Aircraft, **3**, pp. 333 - 337 (1966).

Lamb, H.: Hydrodynamics, New York, Dover Pubs., 738 pp. (1945). Originally: Cambridge, Cambridge Univ. Press (1932).

Lunde, J.K.: "On the Linearized Theory of Wave Resistance for a Pressure Distribution Moving at Constant Speed of Advance on the Surface of Deep or Shallow Water", Skipsmodelltanken, Norges Tekniske Høgskole, Trondheim, Medd. 8, 48 pp. (1951). In English.

- "On the Linearized Theory of Wave Resistance for Displacement Ships in Steady and Accelerated Motion", Trans. Soc. Naval Architects and Marine Engineers, **59**, pp. 25 - 85 (1951).

Lunde, J.K.: "The Linearized Theory of Wave Resistance and its Application to Ship-Shaped Bodies in Motion on the Surface of a Deep, Previously Undisturbed Fluid", Skipsmodelltanken, Norges Tekniske Høgskole, Trondheim, Medellelse 23 (1953). Translation: Soc. Naval Architects and Marine Engineers, Tech. and Research Bulletin 1 - 8, 70 pp. (1957).

- "A Note on the Linearized Theory of Wave Resistance for Accelerated Motion", Skipsmodelltanken, Norges Tekniske Høgskole, Trondheim, Medellelse 27, 14 pp. (1953).

Michell, J.H.: "The Wave Resistance of a Ship", Philosophical Mag. London, Series 5, **45**, pp. 106 - 123 (1898).

Murthy, T.K.S.: "The Wave Resistance of a Drifting Hovercraft", Hovering Craft and Hydrofoil, **9**, pp. 20 - 24 (1970).

Newman, J.N. and Poole, F.A.P.: "The Wave Resistance of a Moving Pressure Distribution in a Canal", Schiffstechnik, **9**, pp. 21 - 26 (1962). In English.

Rektorys, K., ed.: Survey of Applicable Mathematics, Cambridge, Mass., M.I.T. Press, 1369 pp. (1969).

Shebalov, A.N.: "Theory of Ship Wave Resistance for Unsteady Motion in Still Water", Proc. Leningrad Shipbuilding Inst. (Hydromechanics and Theory of Ships Division). Translated by M. Aleksandrov and G. Gardner, Dept. Naval Architecture and Marine Engineering, University of Michigan, Ann Arbor, Michigan, Report 67, 14 pp. (1966).

Sretensky, L.N.: "On the Theory of Wave Resistance", Trudy Tsentral. Aero-Gidrodinam. Inst., **348**, 28 pp. (1939). In Russian.

Stroud, A.H. and Secrest, D.: Gaussian Quadrature Formulas, Englewood Cliffs, N.J., Prentice-Hall Inc., 374 pp. (1966).

Tuck, E.O.: "Shallow Water Flows Past Slender Bodies", J. Fluid Mechanics, **26**, Part 1, pp. 81 - 95 (1966).

Wehausen, J.V. and Laitone, E.V.: Water Waves, **9** of Encyclopedia of Physics, ed. by S. Flügge, Berlin, Springer-Verlag, pp. 446 - 778 (1960).

Wehausen, J.V.: "An Approach to Thin-Ship Theory", International Seminar on Theoretical Wave Resistance, University of Michigan, Ann Arbor, Michigan, pp. 821 - 855, (1963).

- "Effect of the Initial Acceleration Upon the Wave Resistance of Ship Models", J. Ship Research, **7**, 3, pp. 38 to 50 (1964).

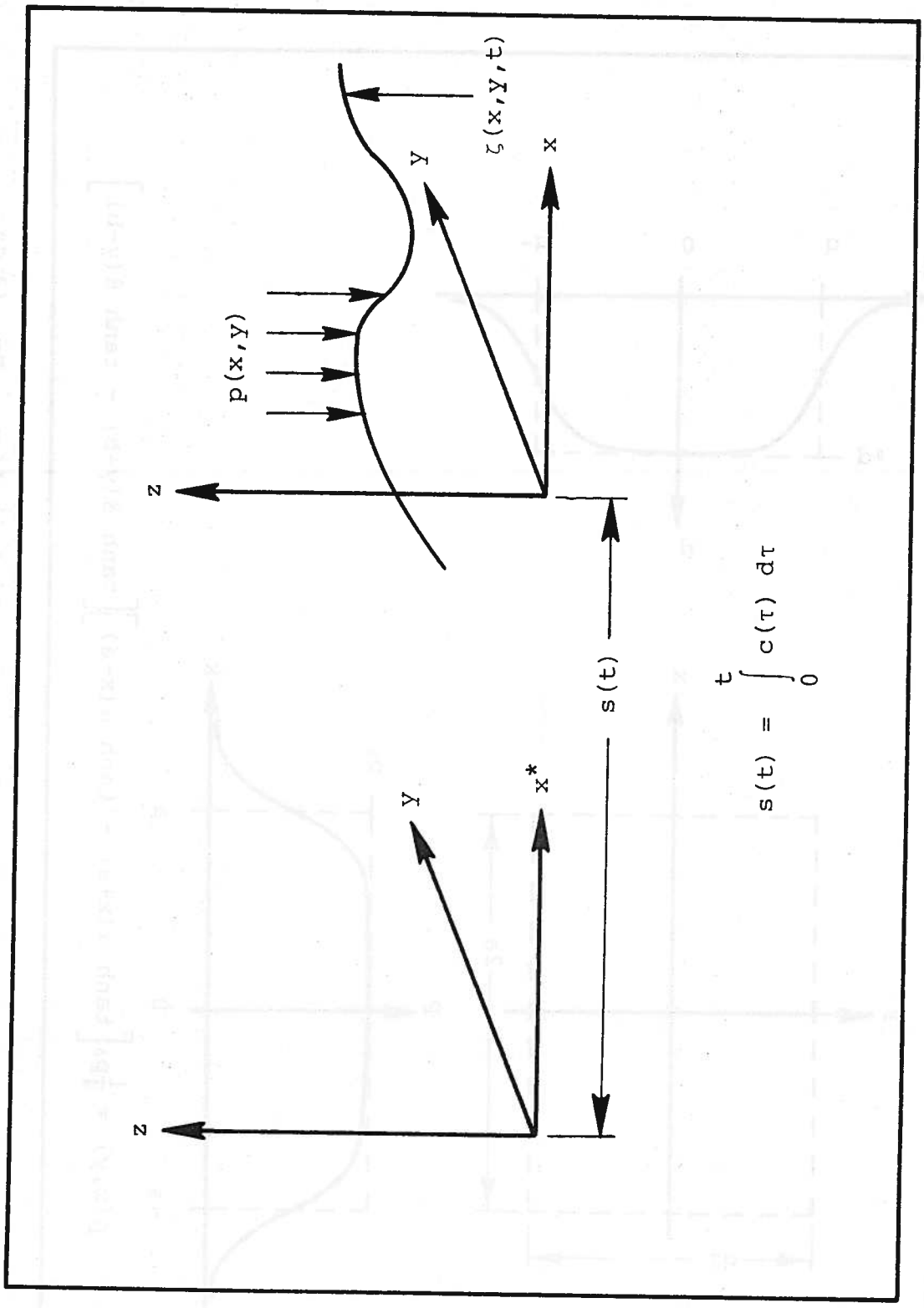

Fig. 1 The Two Coordinate Systems

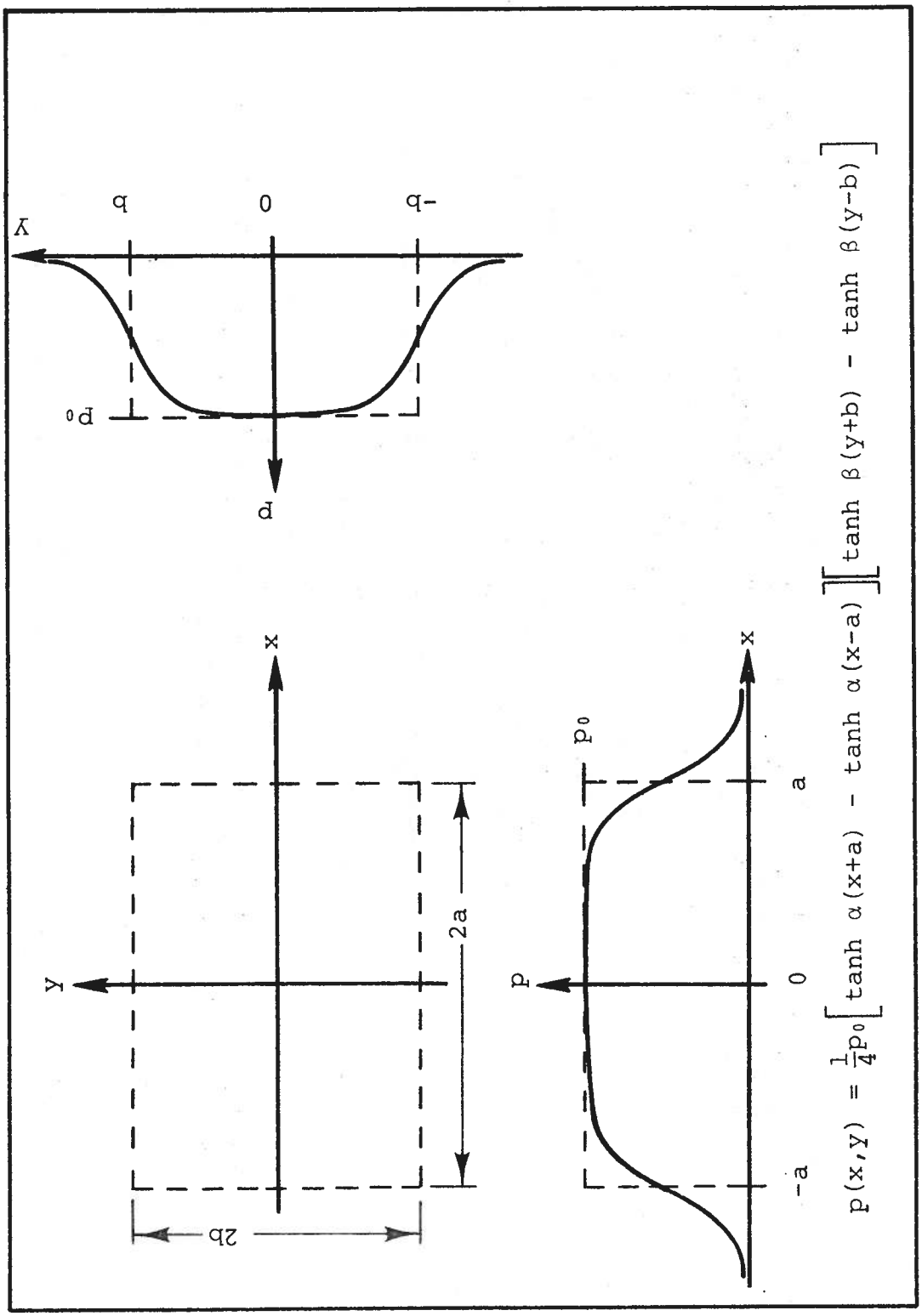

Fig. 2 The Double Tanh Pressure Distribution - Eq. (4.1)

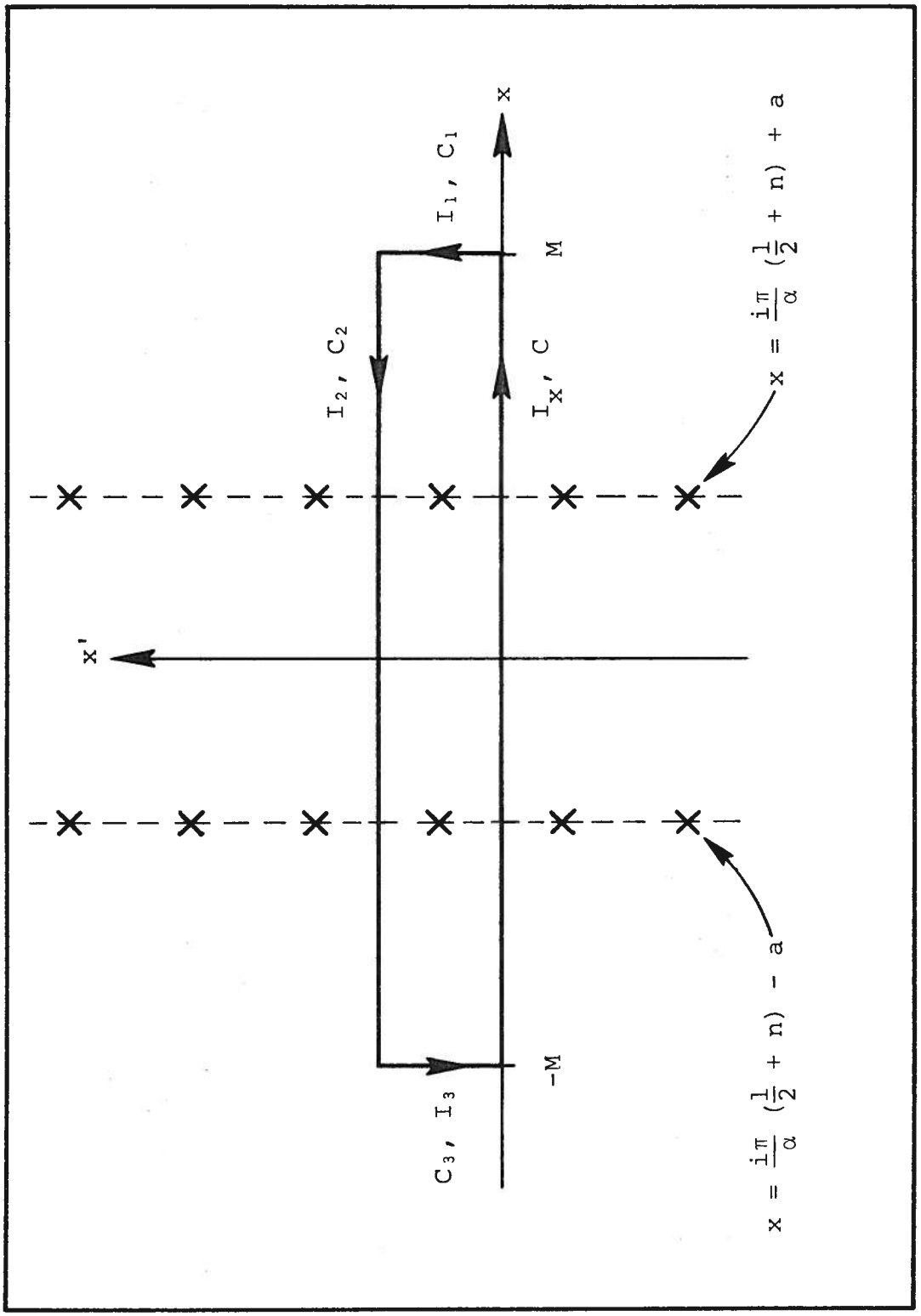

Fig. 3 Contour for Evaluating the Kochin Function

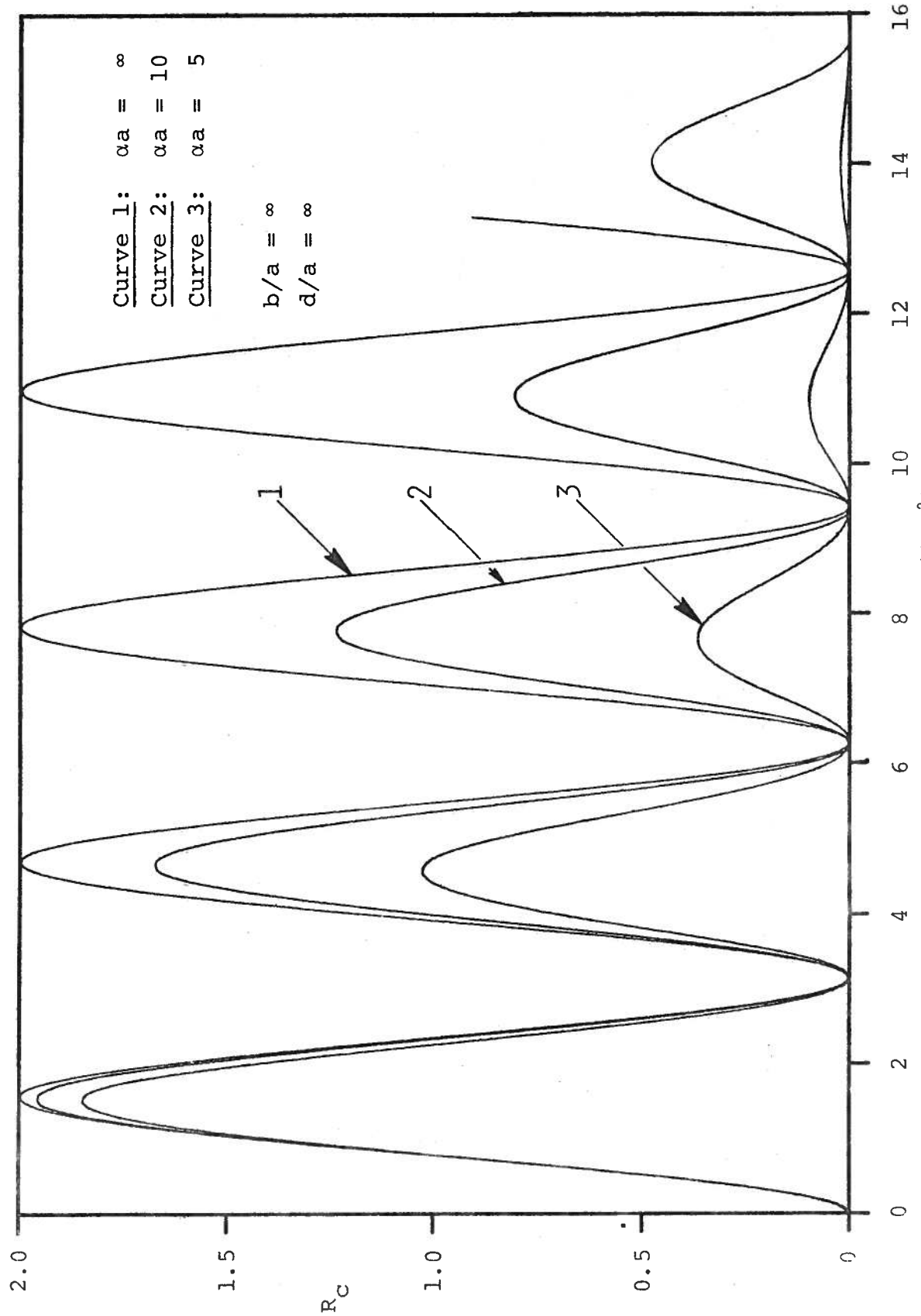

Fig. 4 2D Wave Resistance Showing the Effect of Smoothing, (a) Deep Water

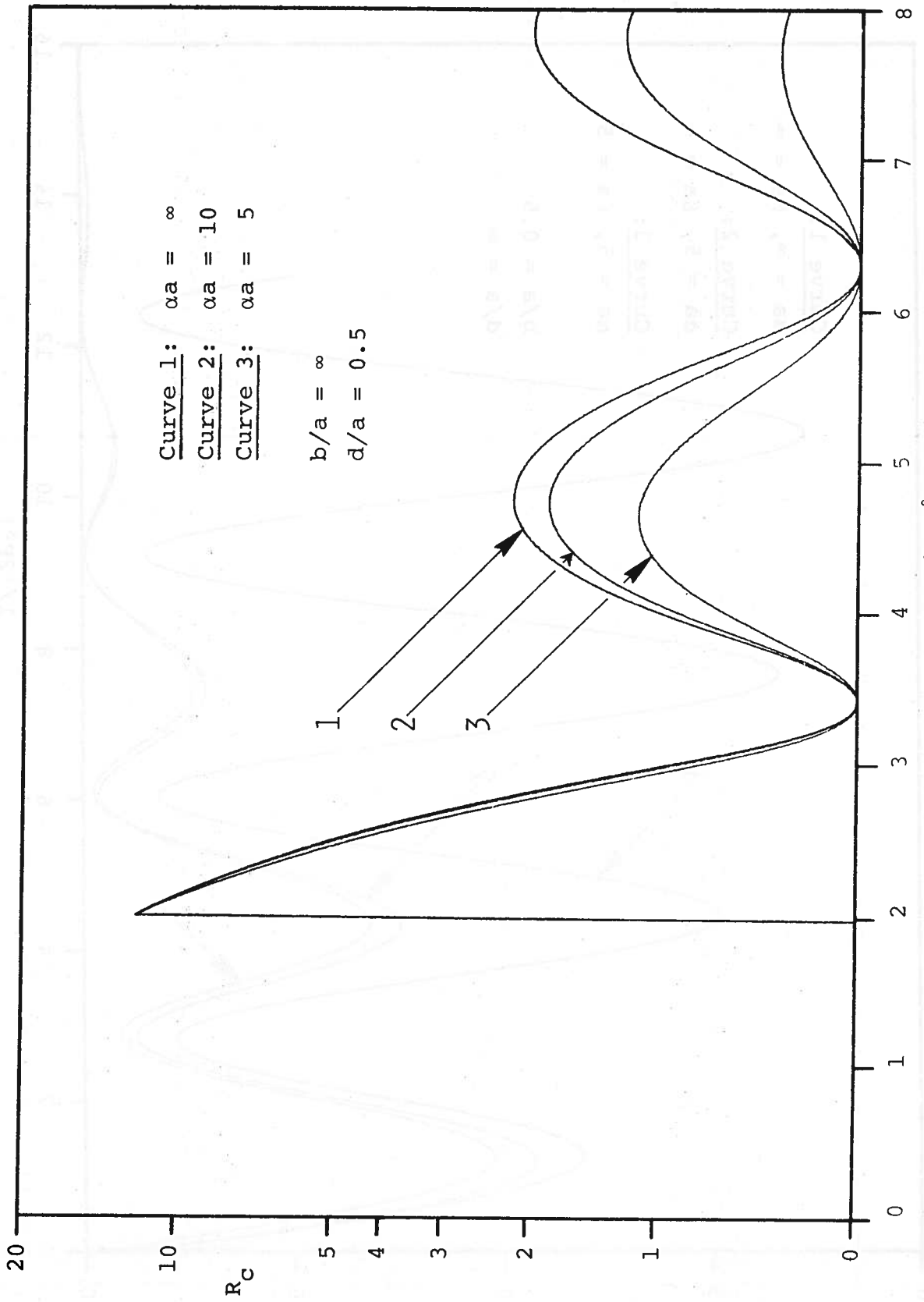

Fig. 4 (cont.) (b) Finite Depth

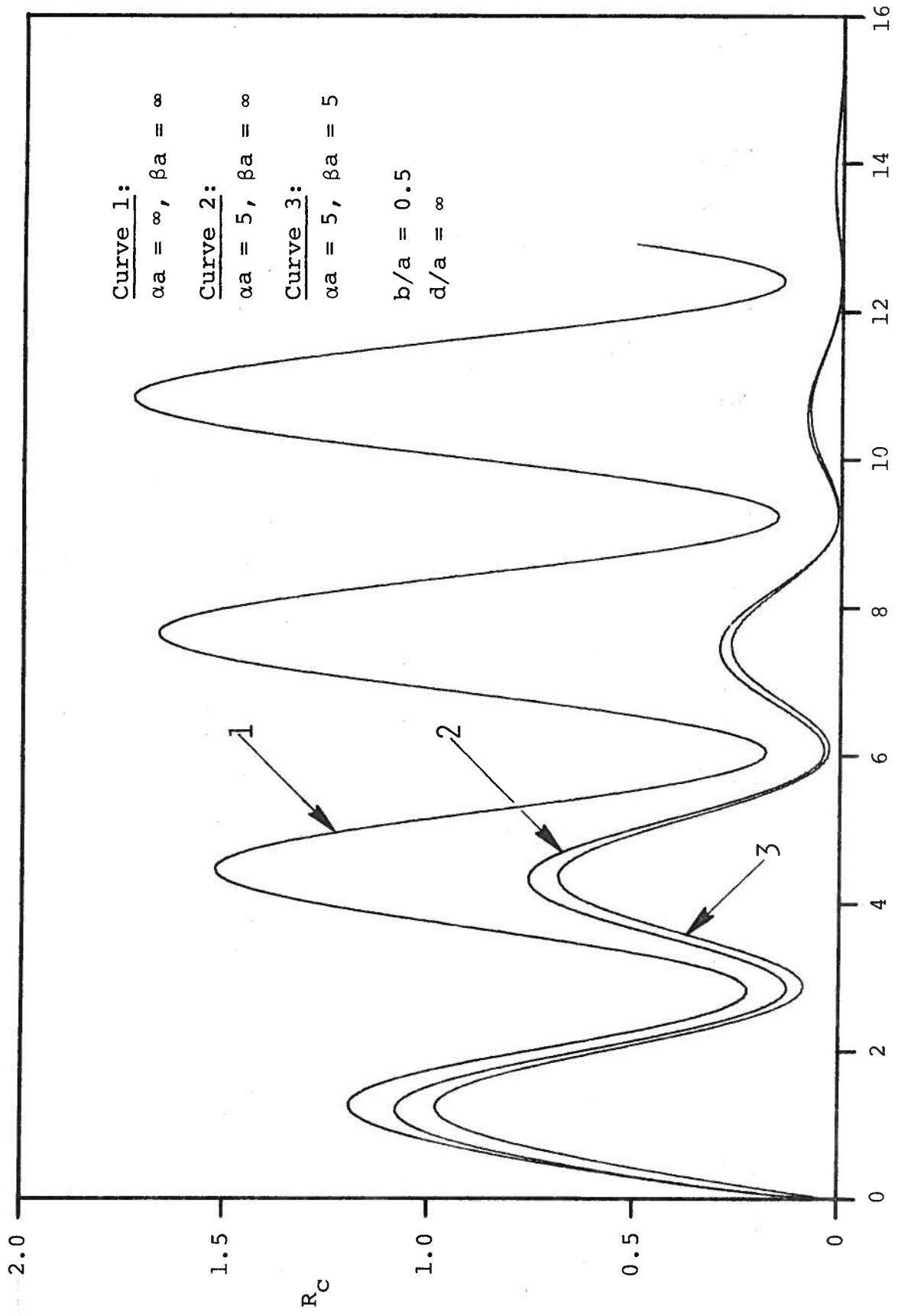

Fig. 5 3D Wave Resistance Showing the Effect of Smoothing, (a) Deep Water 1

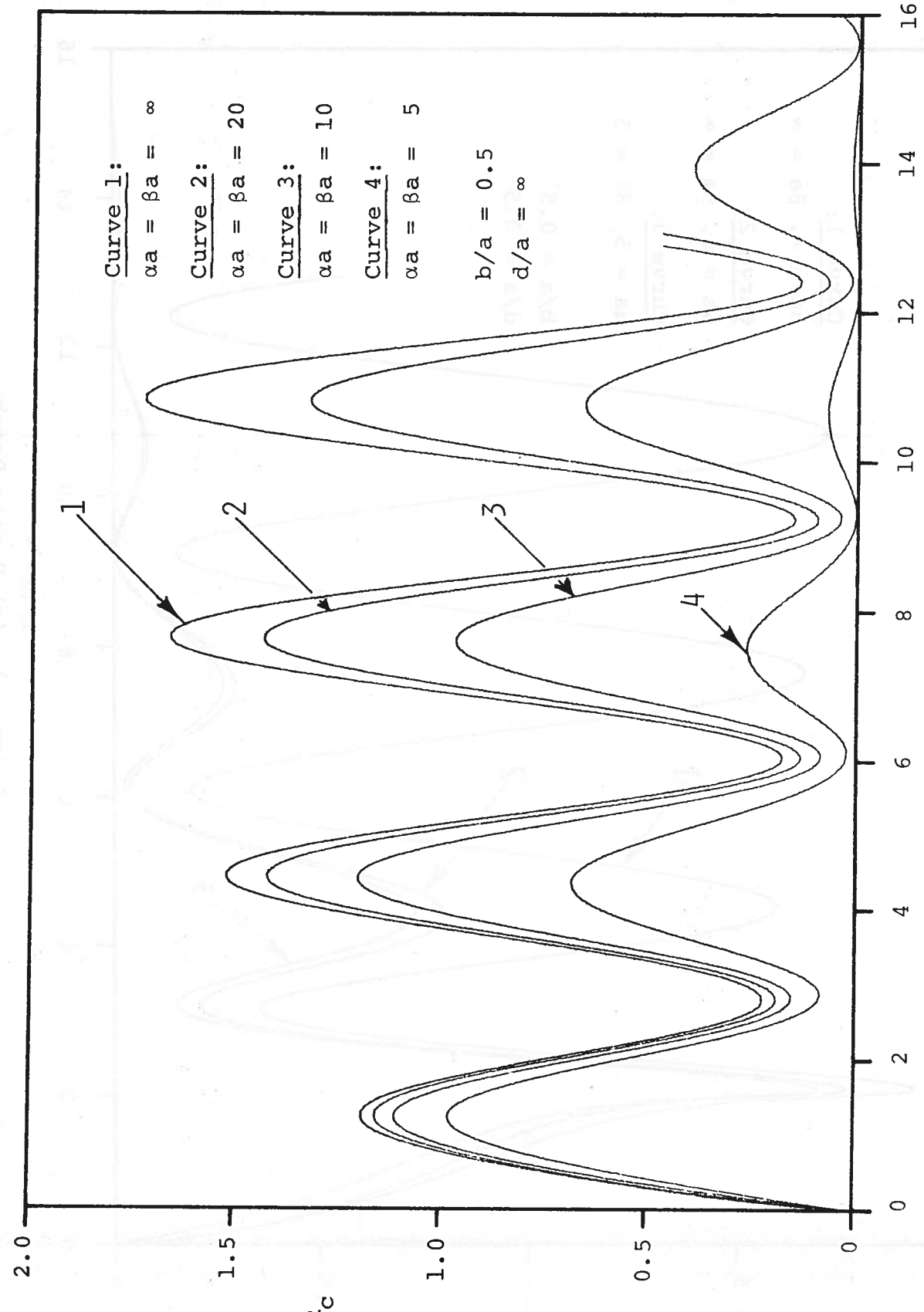

Fig. 5 (cont.) (b) Deep Water 2

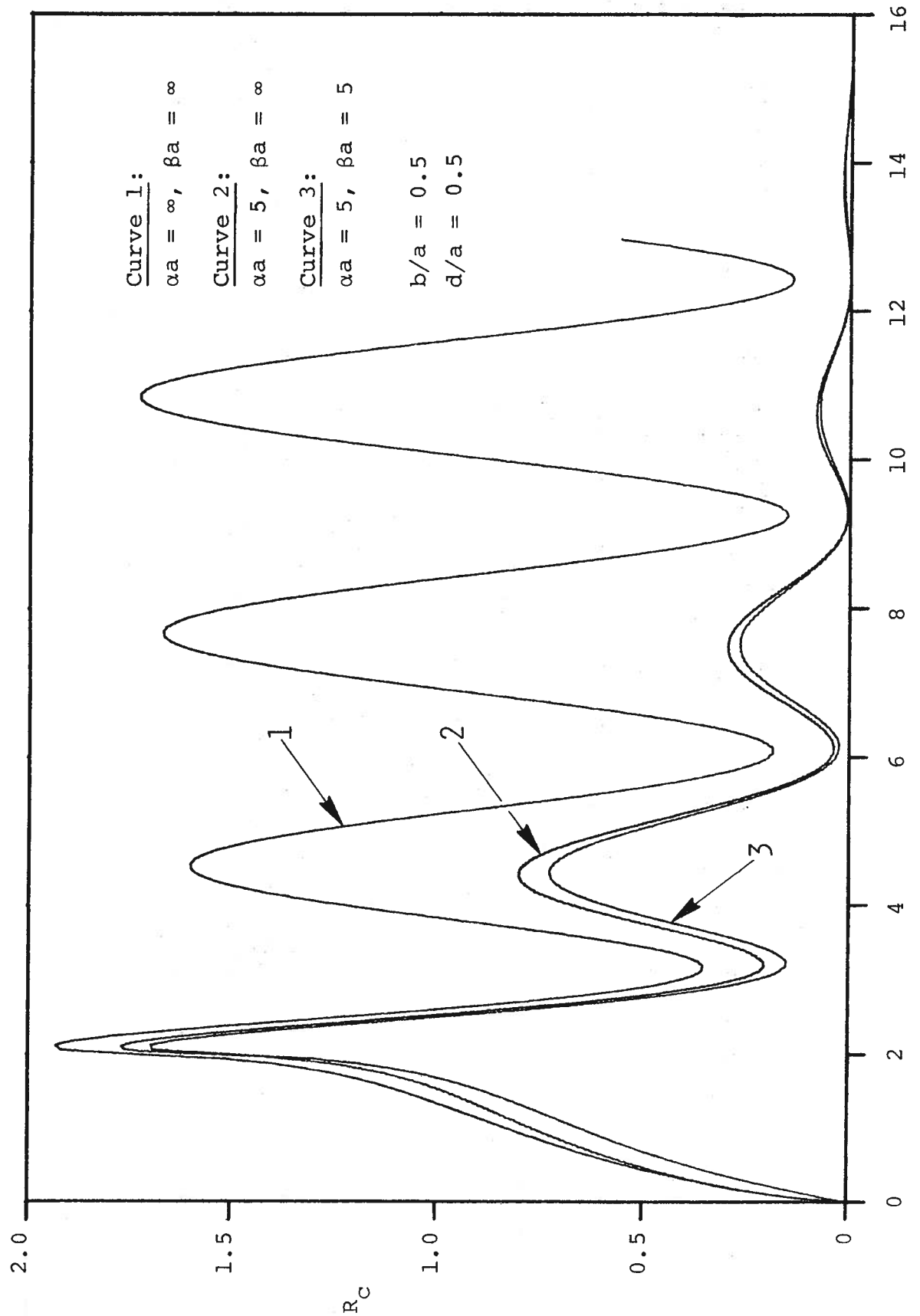

Fig. 5 (cont.) (c) Finite Depth

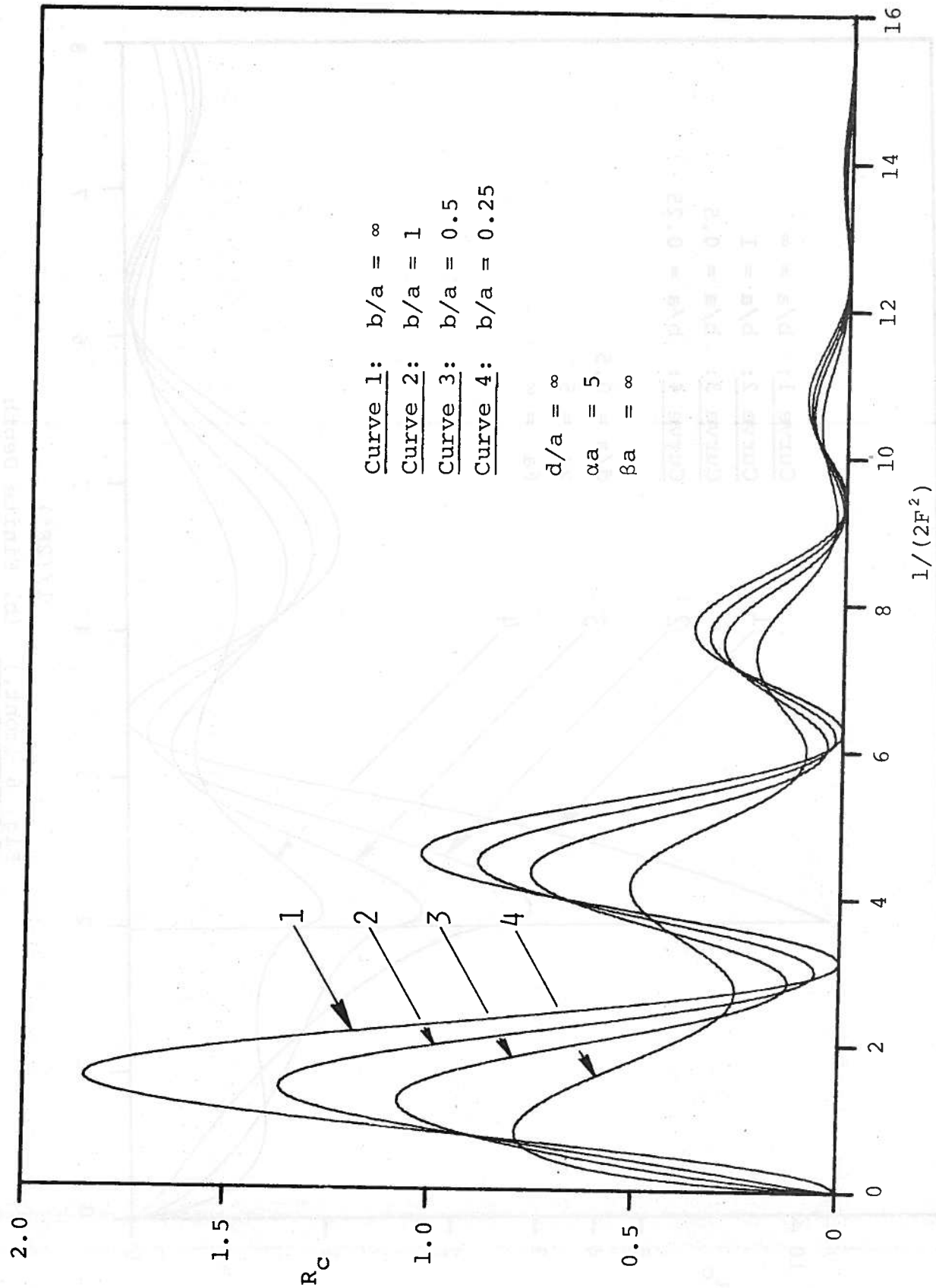

Fig. 6 3D Wave Resistance - Beam/Length Variation, (a) Deep Water

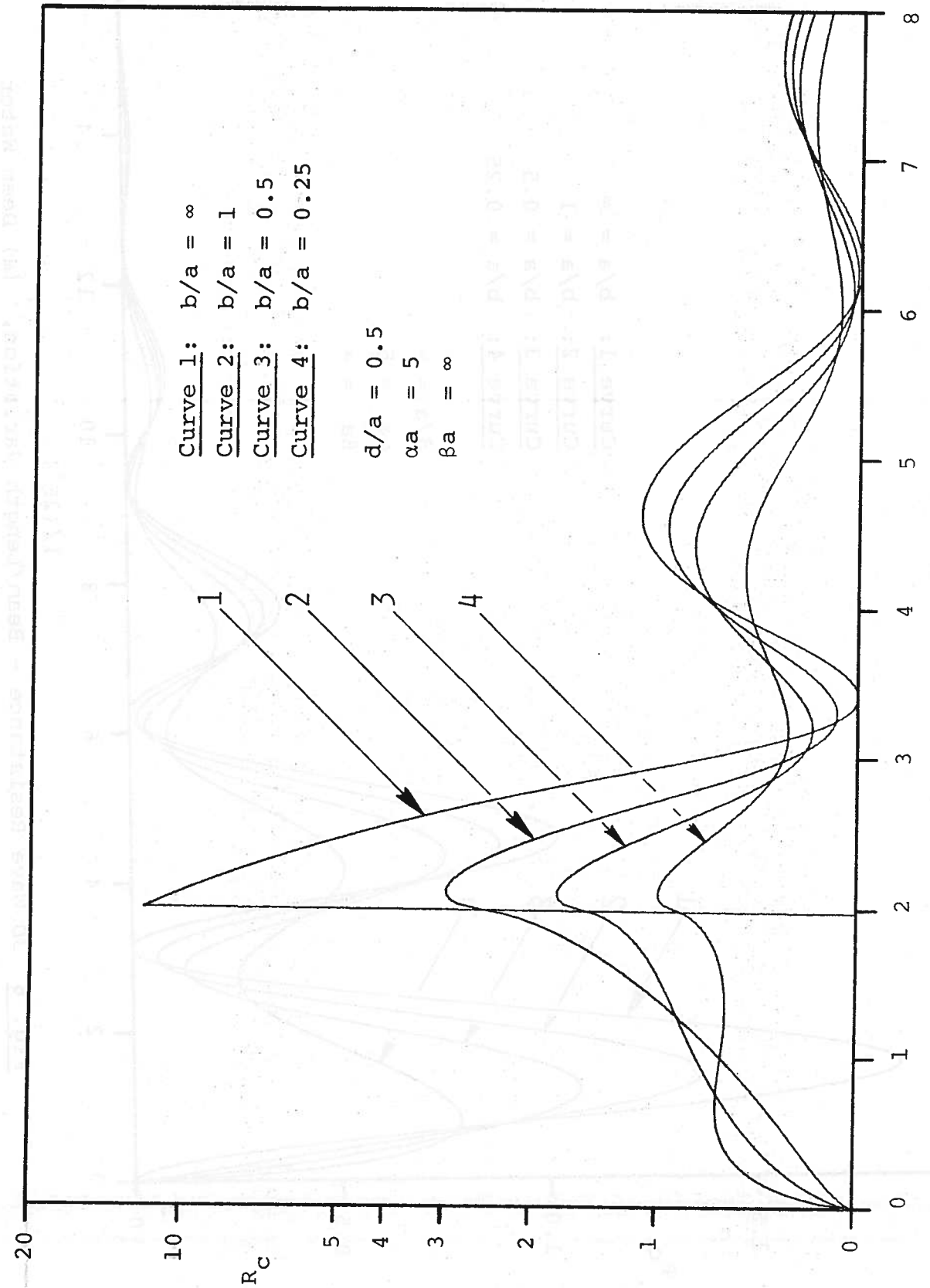

Fig. 6 (cont.) (b) Finite Depth

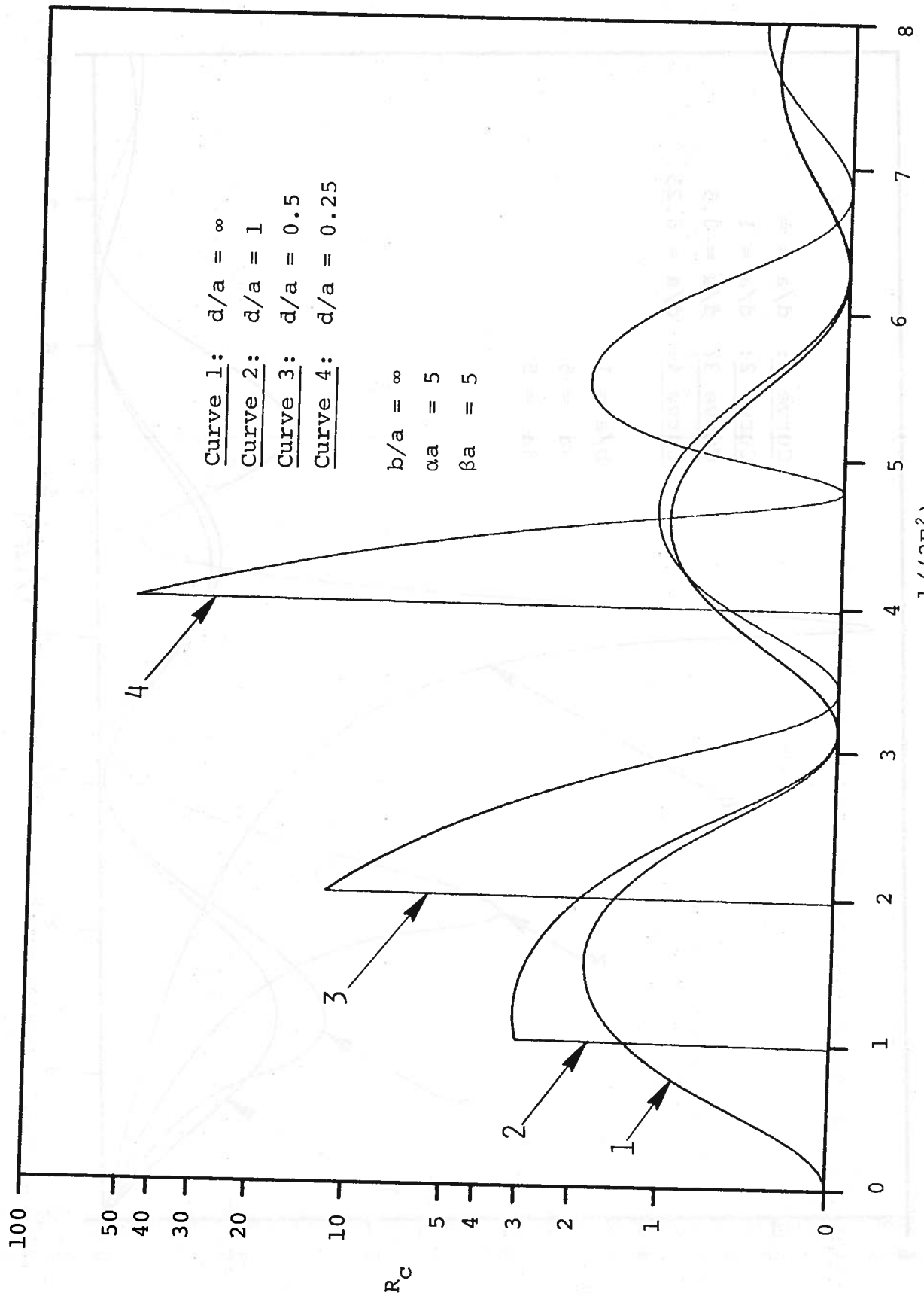

Fig. 7 3D Wave Resistance - Depth Variation, (a) b/a = ∞ (2D Limit)

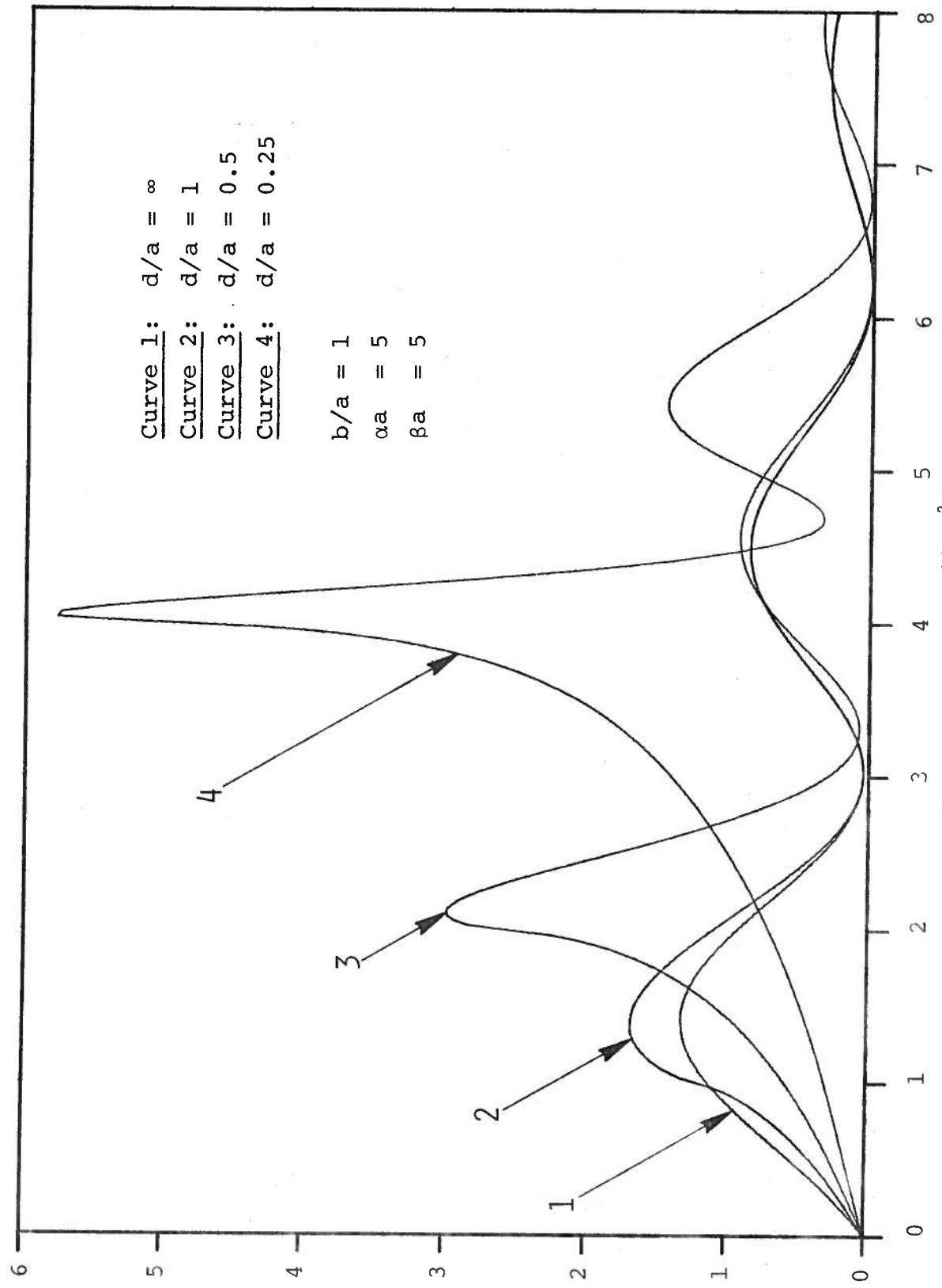

Fig. 7 (cont.) (b) b/a = 1

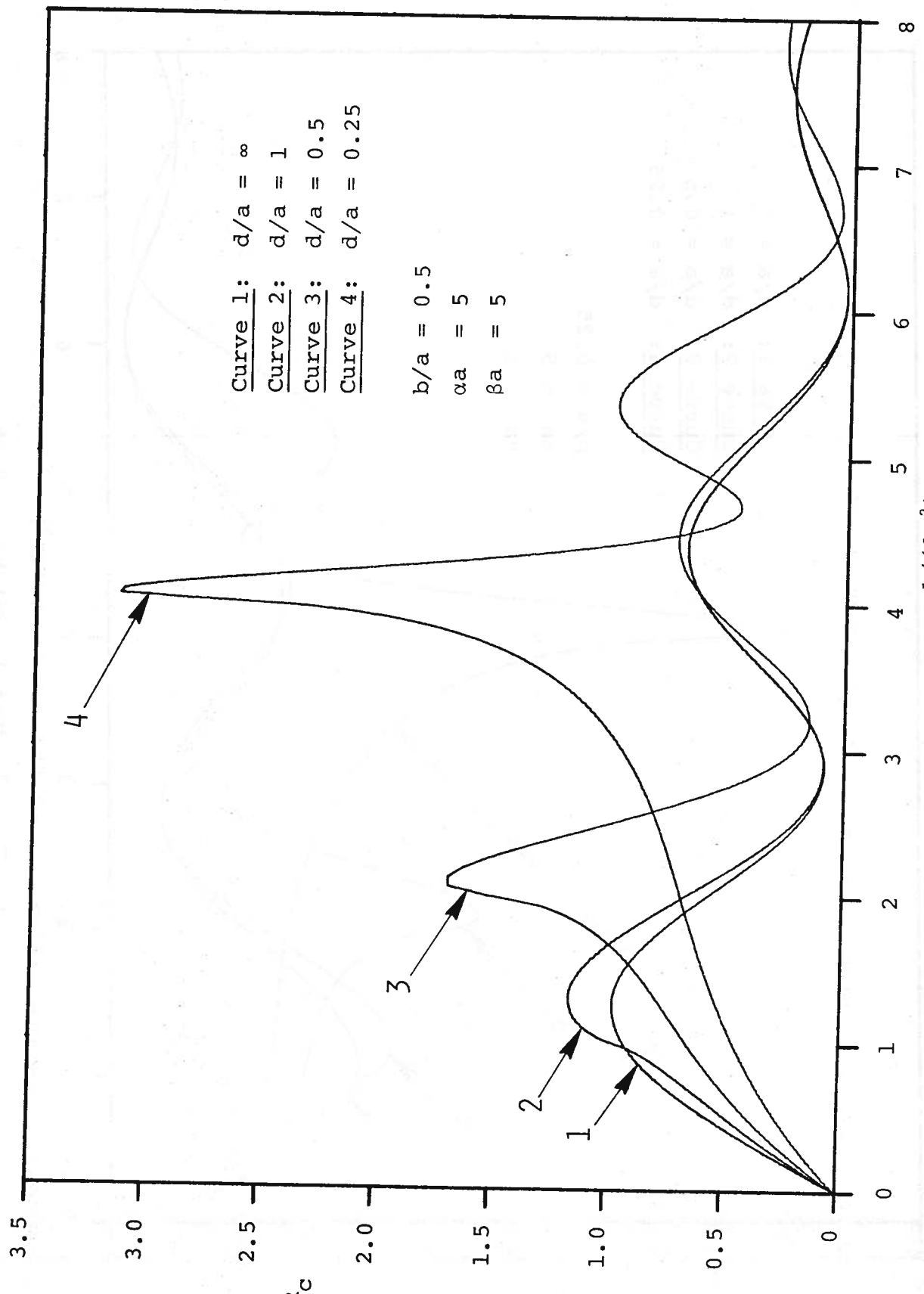

Fig. 7 (cont.) (c) b/a = 0.5

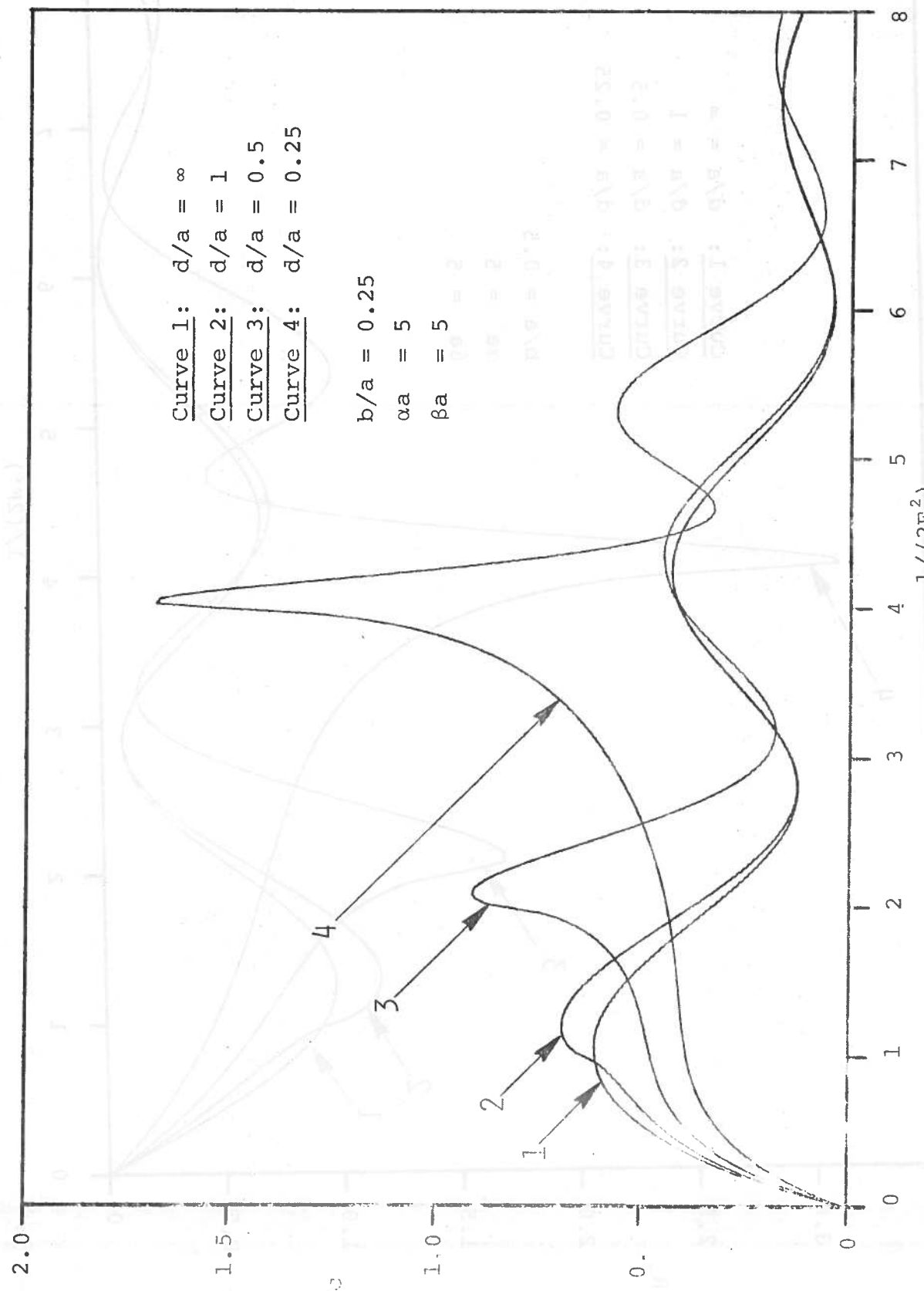

Fig. 7 (cont.) (d) b/a = 0.25

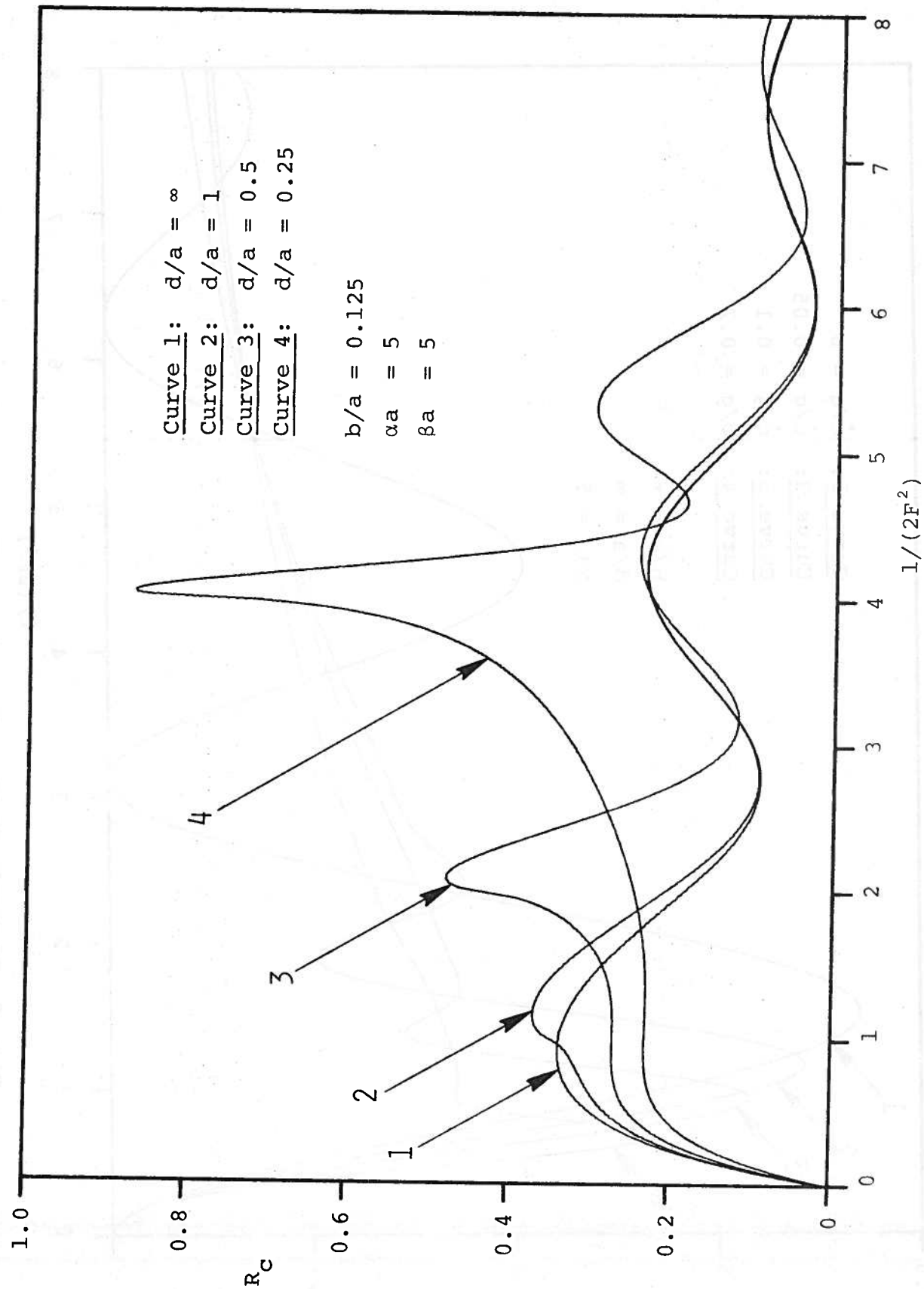

Fig. 7 (cont.) (e) b/a = 0.125

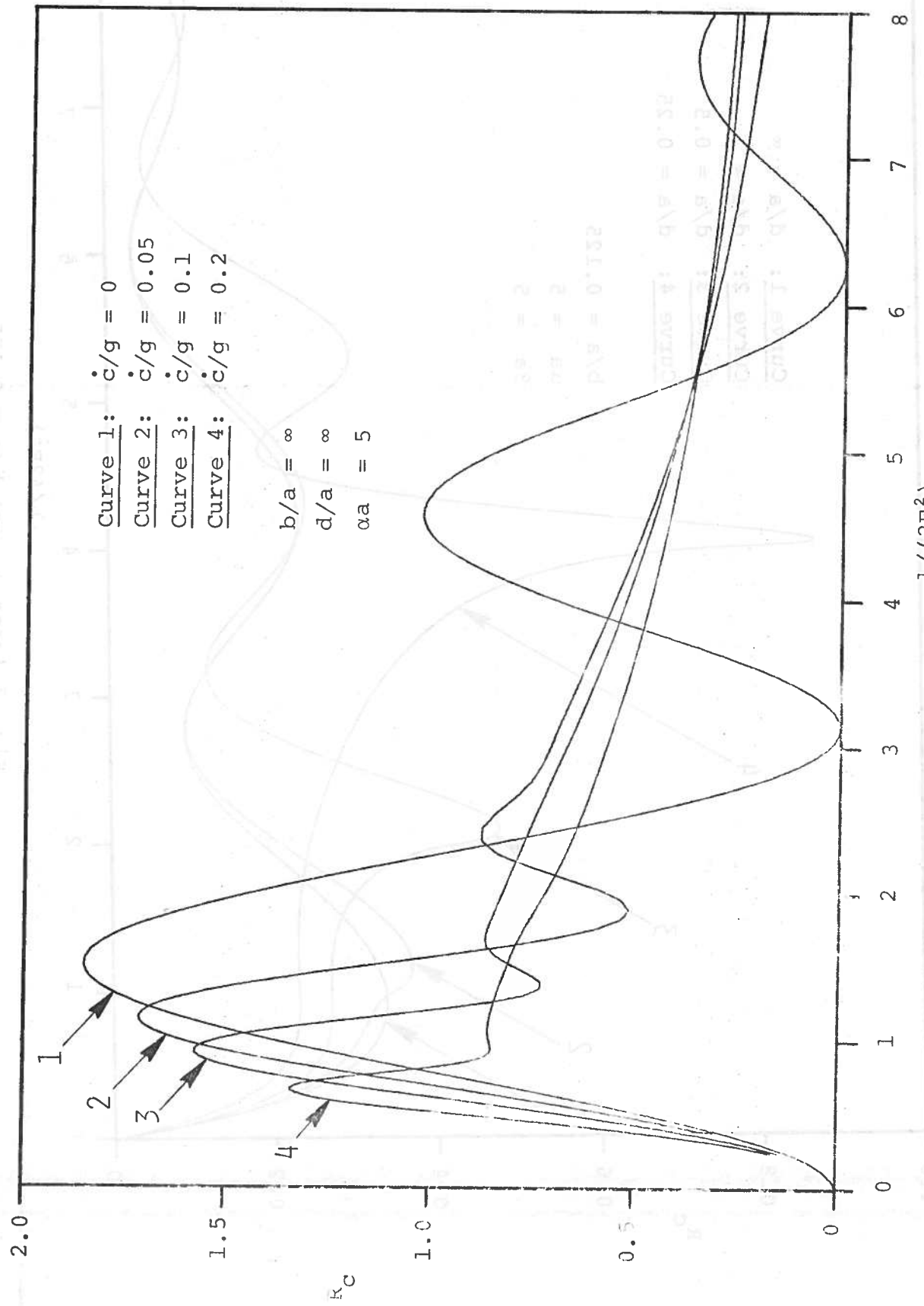

Fig. 8 Unsteady 2D Wave Resistance (Smooth) in Deep Water

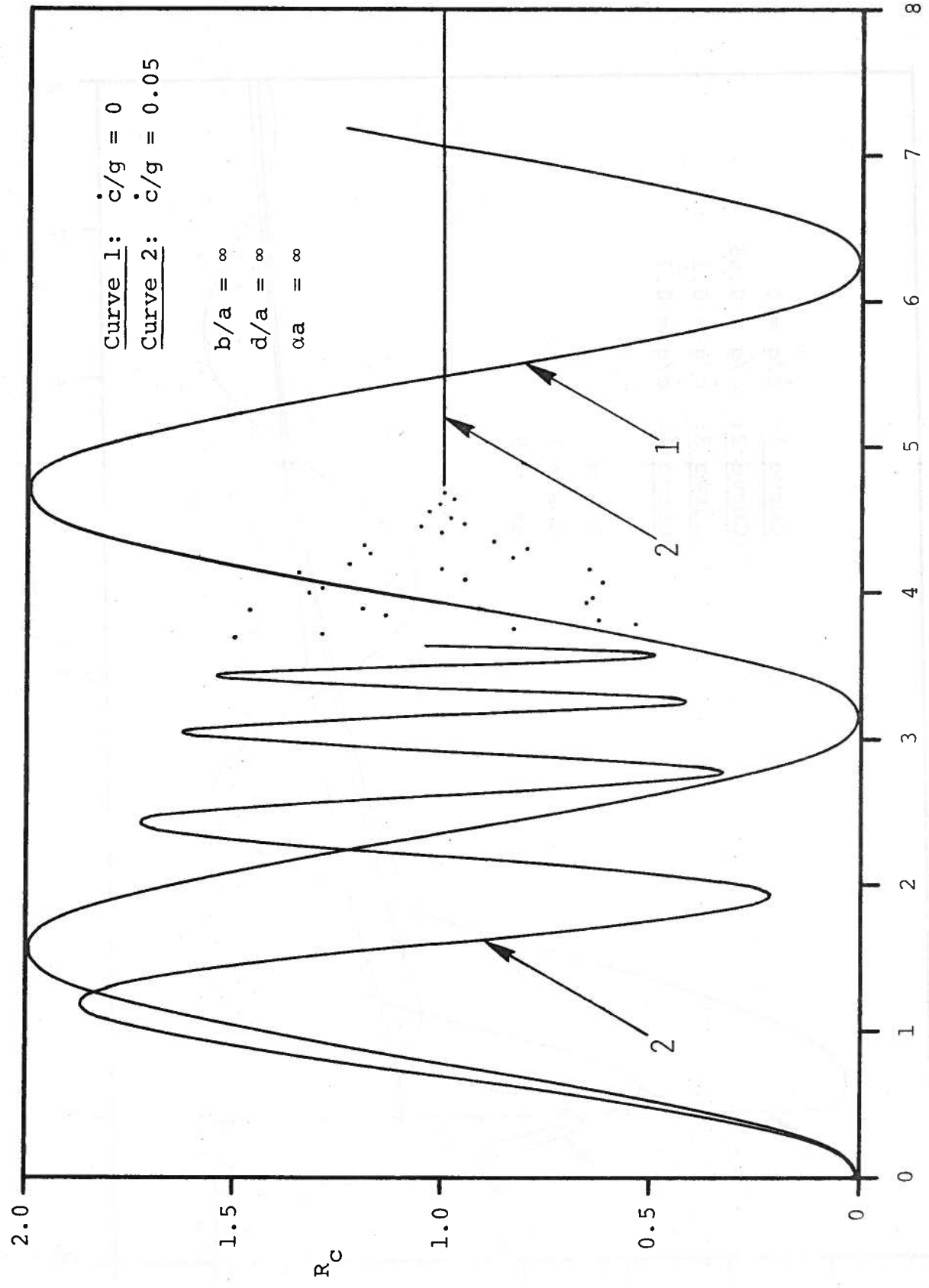

Fig. 9 Unsteady 2D Wave Resistance (Sharp) in Deep Water

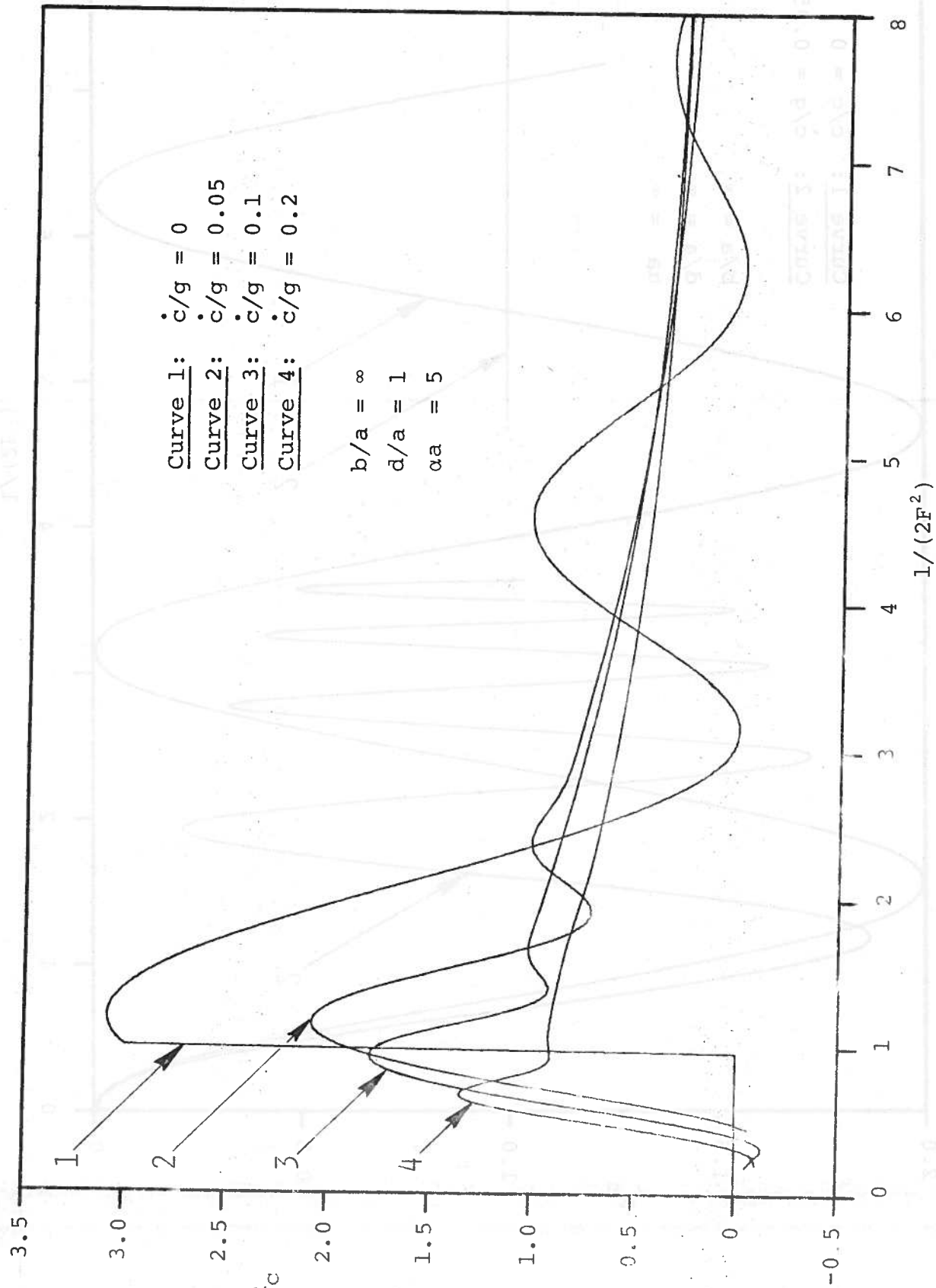

Fig. 10 Unsteady 2D Wave Resistance in Finite Depth, (a) d/a = 1

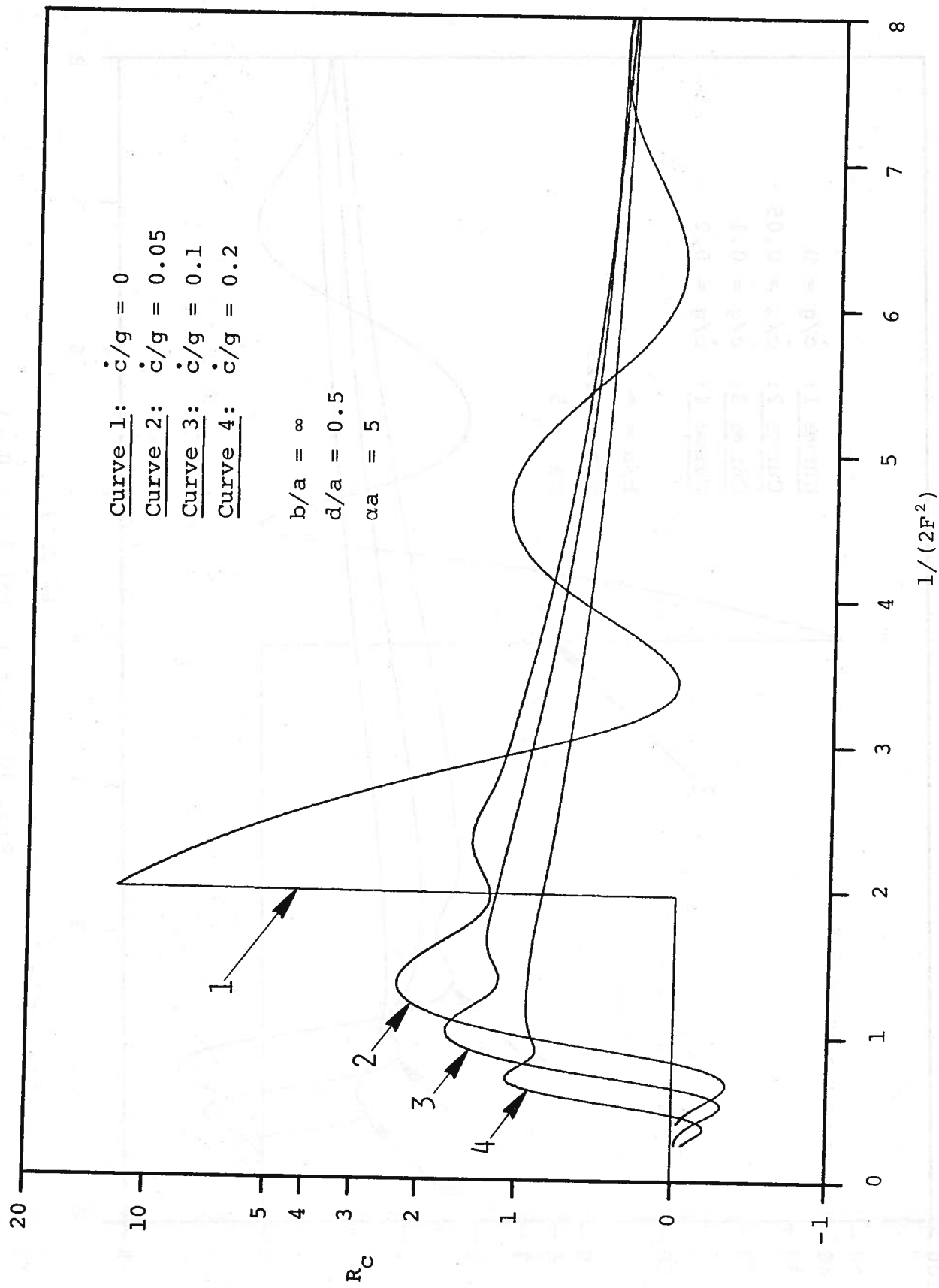

Fig. 10 (cont.) (b) d/a = 0.5

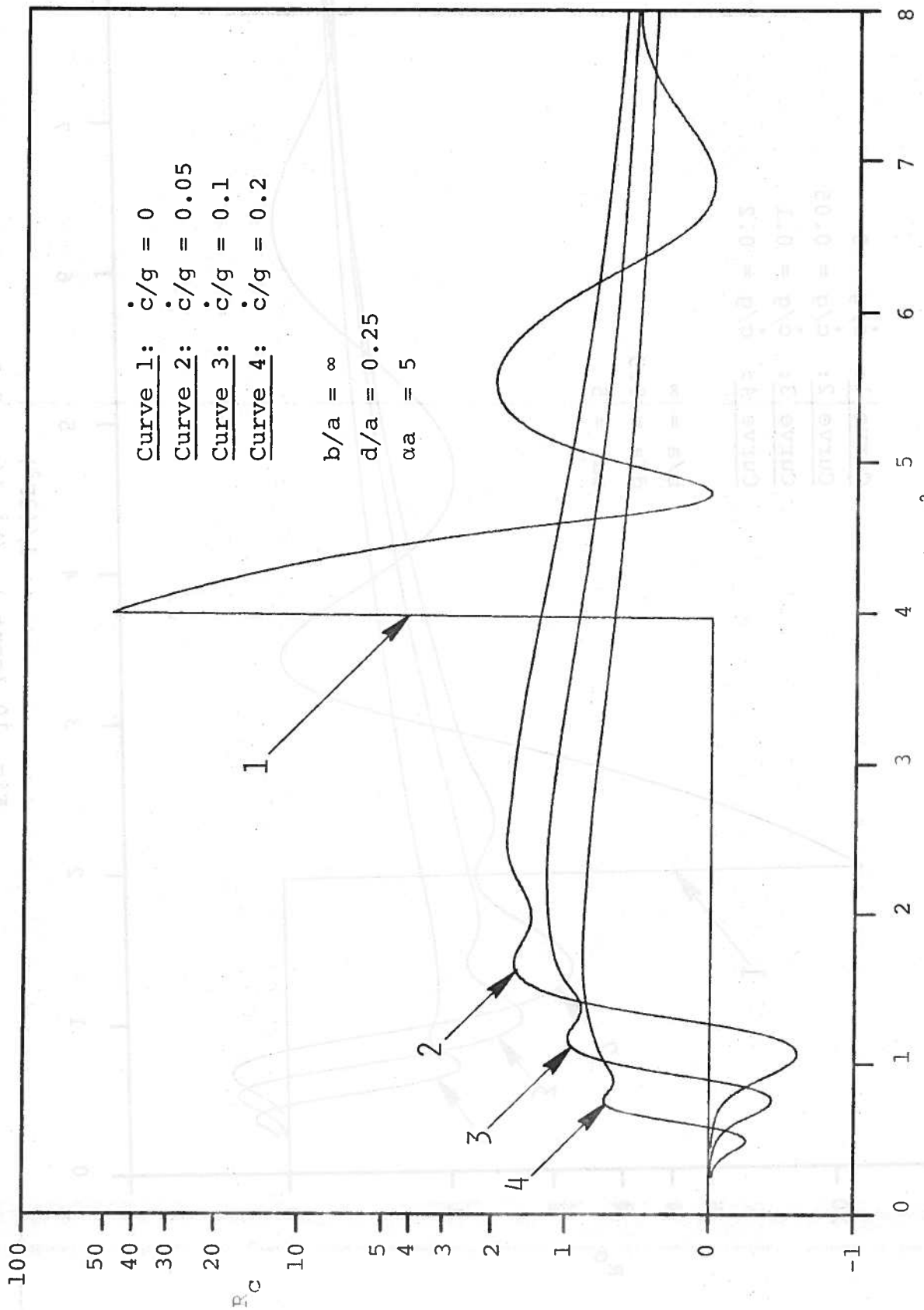

Fig. 10 (cont.) (c) d/a = 0.25

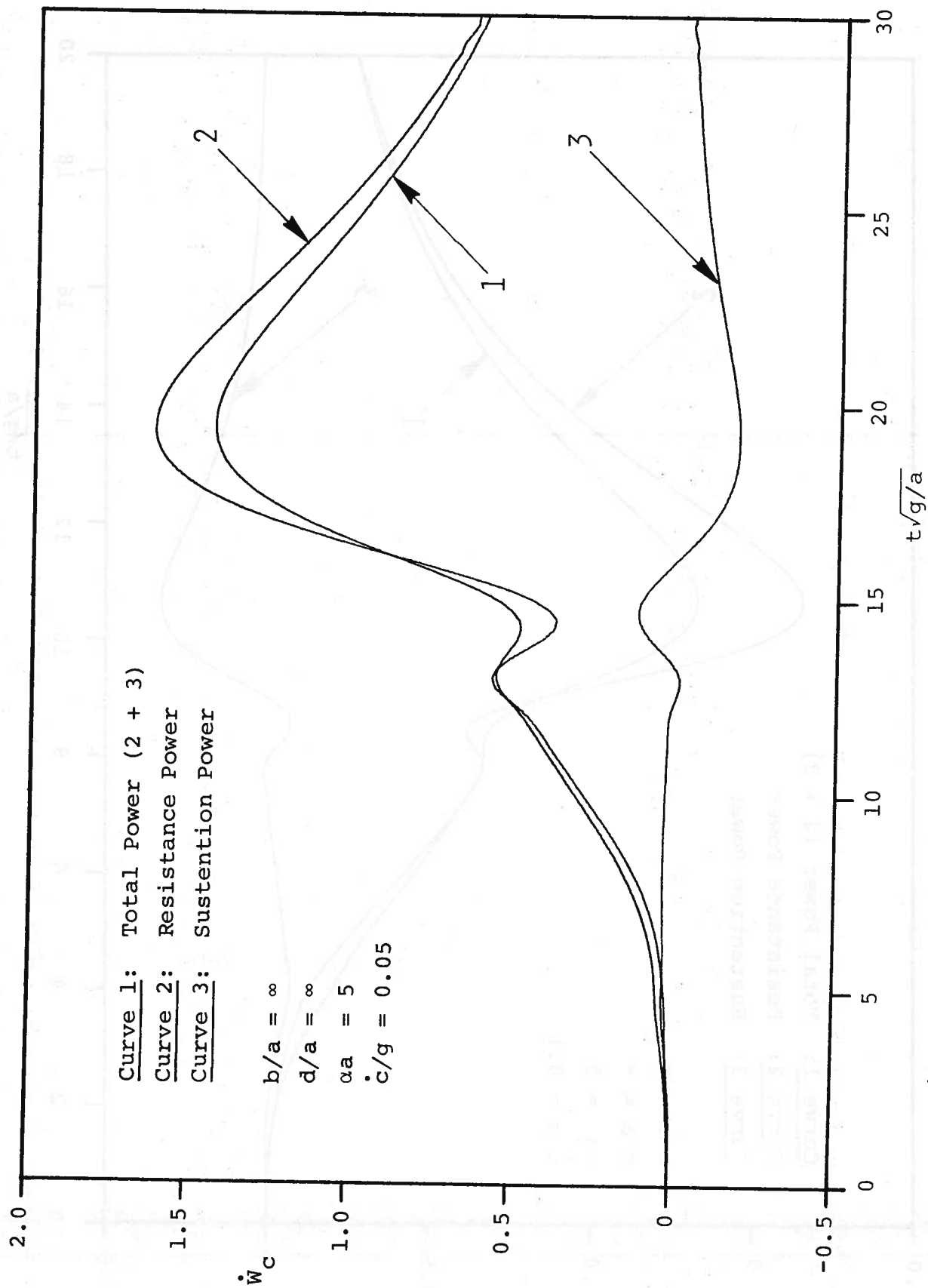

Fig. 11 Comparison of 2D Powers in Deep Water, (a) $\dot{c}/g = 0.05$

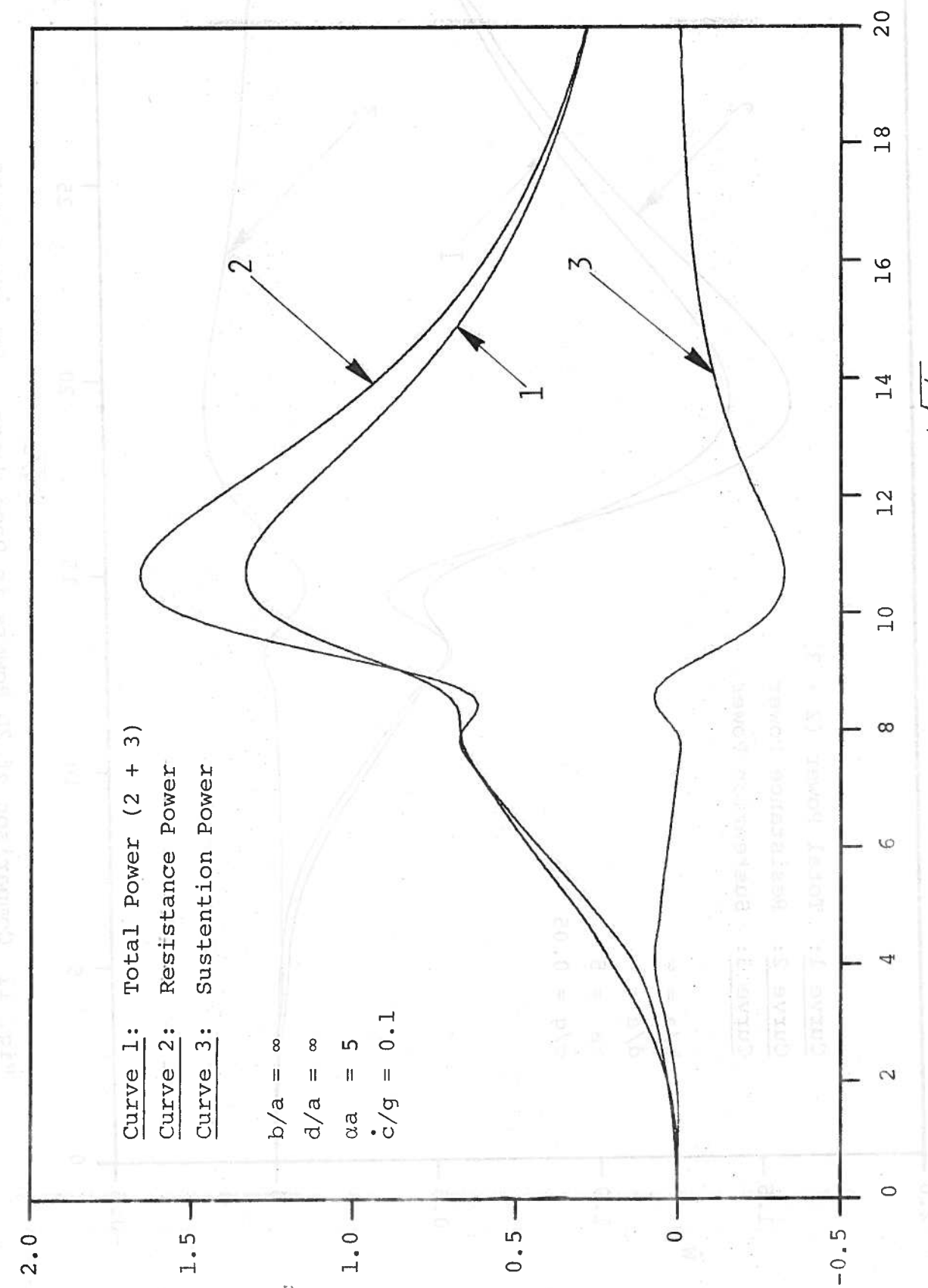

Fig. 11 (cont.) (b) $\dot{c}/g = 0.1$

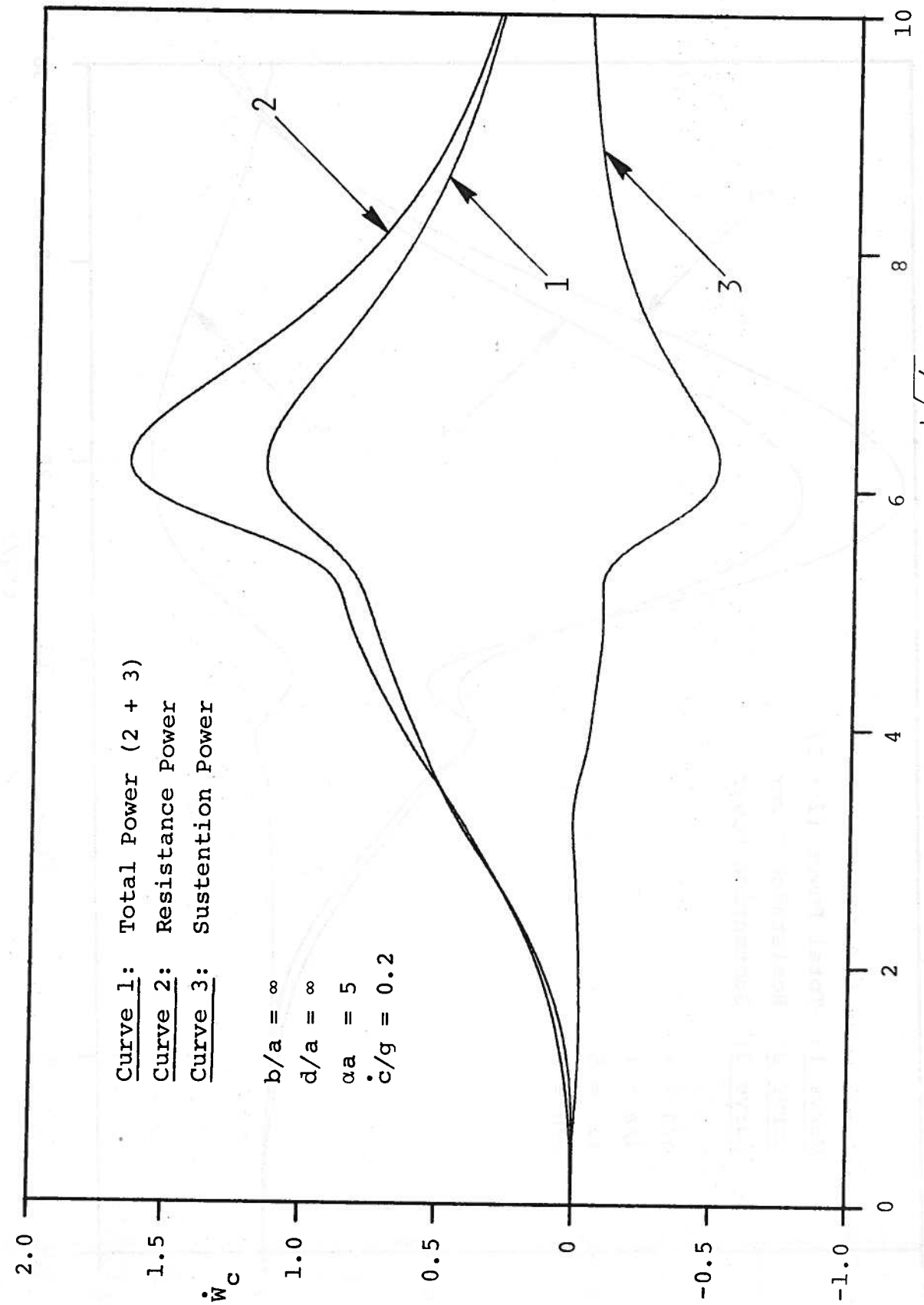

Fig. 11 (cont.) (c) $\dot{c}/g = 0.2$

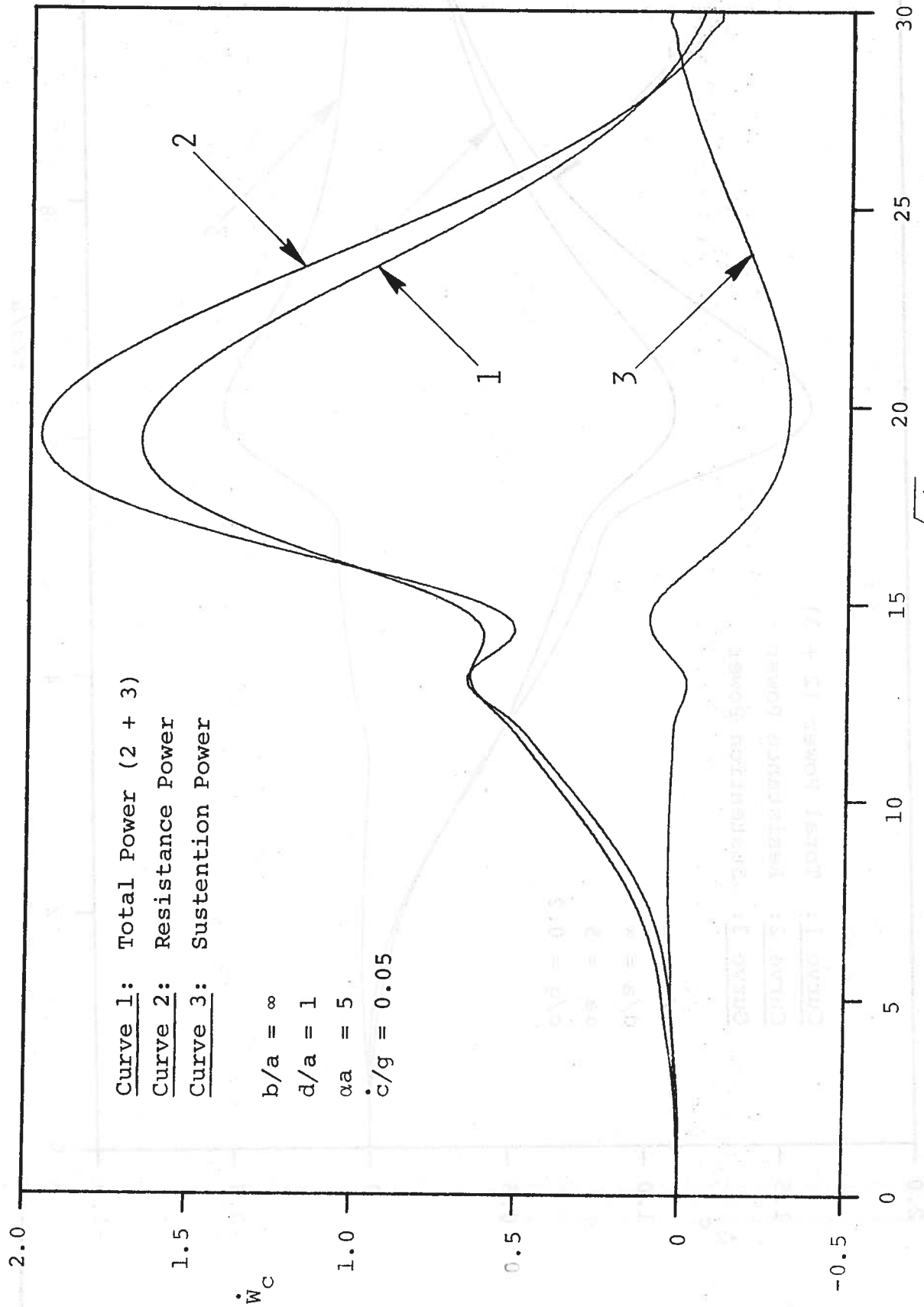

Fig. 12 Comparison of 2D Powers in Finite Depth, (a) $\dot{c}/g = 0.05$, $d/a = 1$

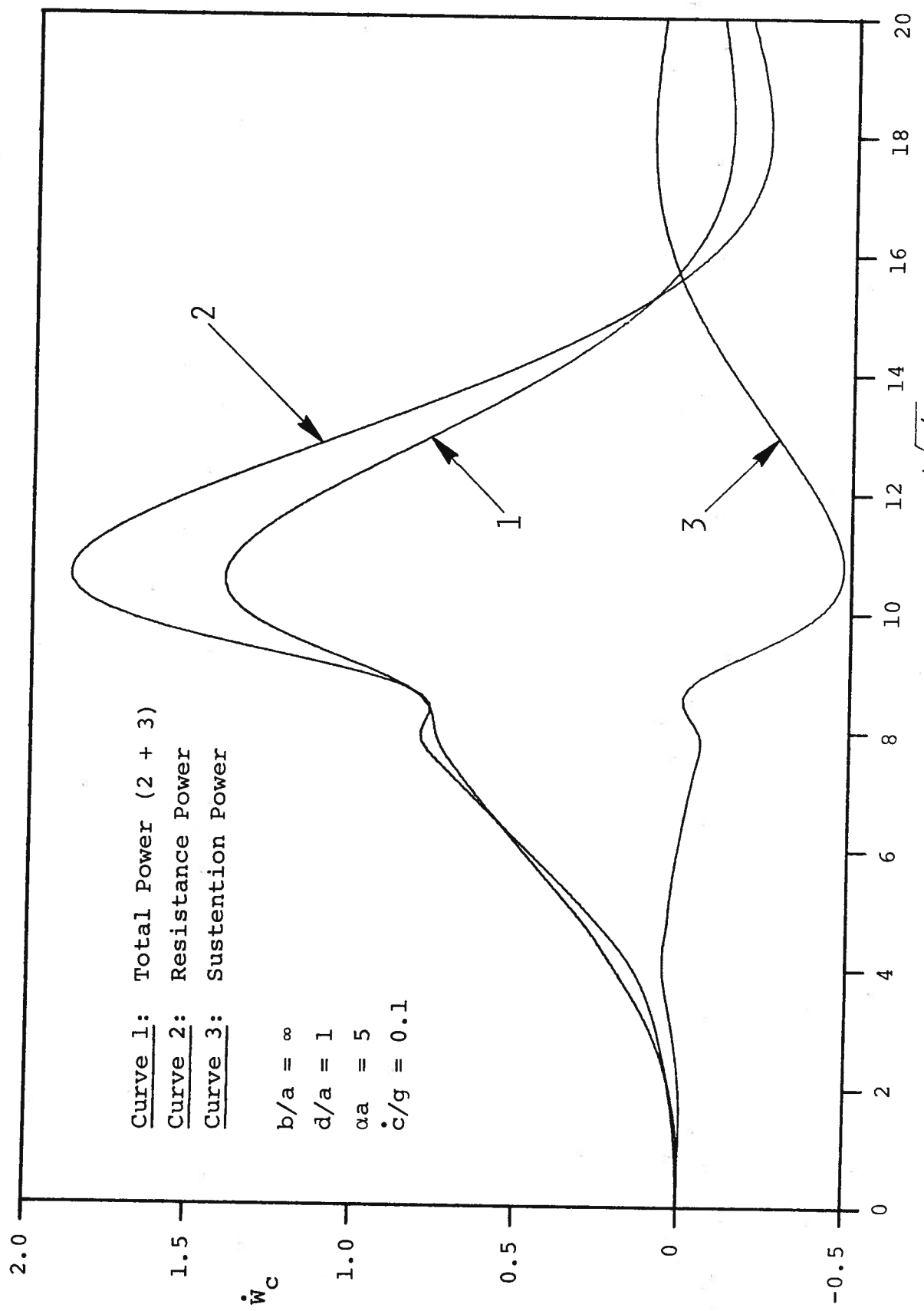

Fig. 12 (cont.) (b), $\dot{c}/g = 0.1$, $d/a = 1$

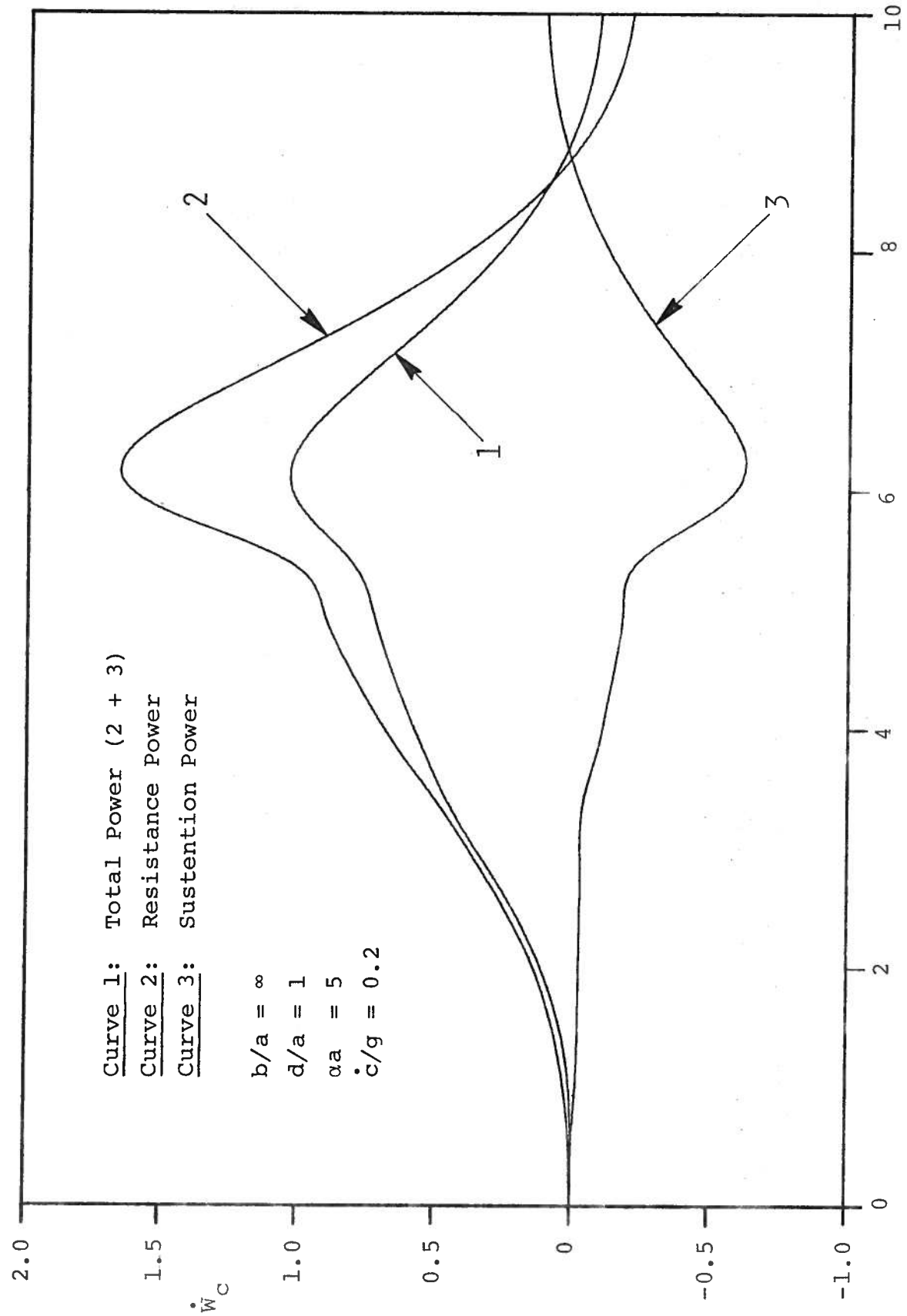

Fig. 12 (cont.) (c) $\dot{c}/g = 0.2$, $d/a = 1$

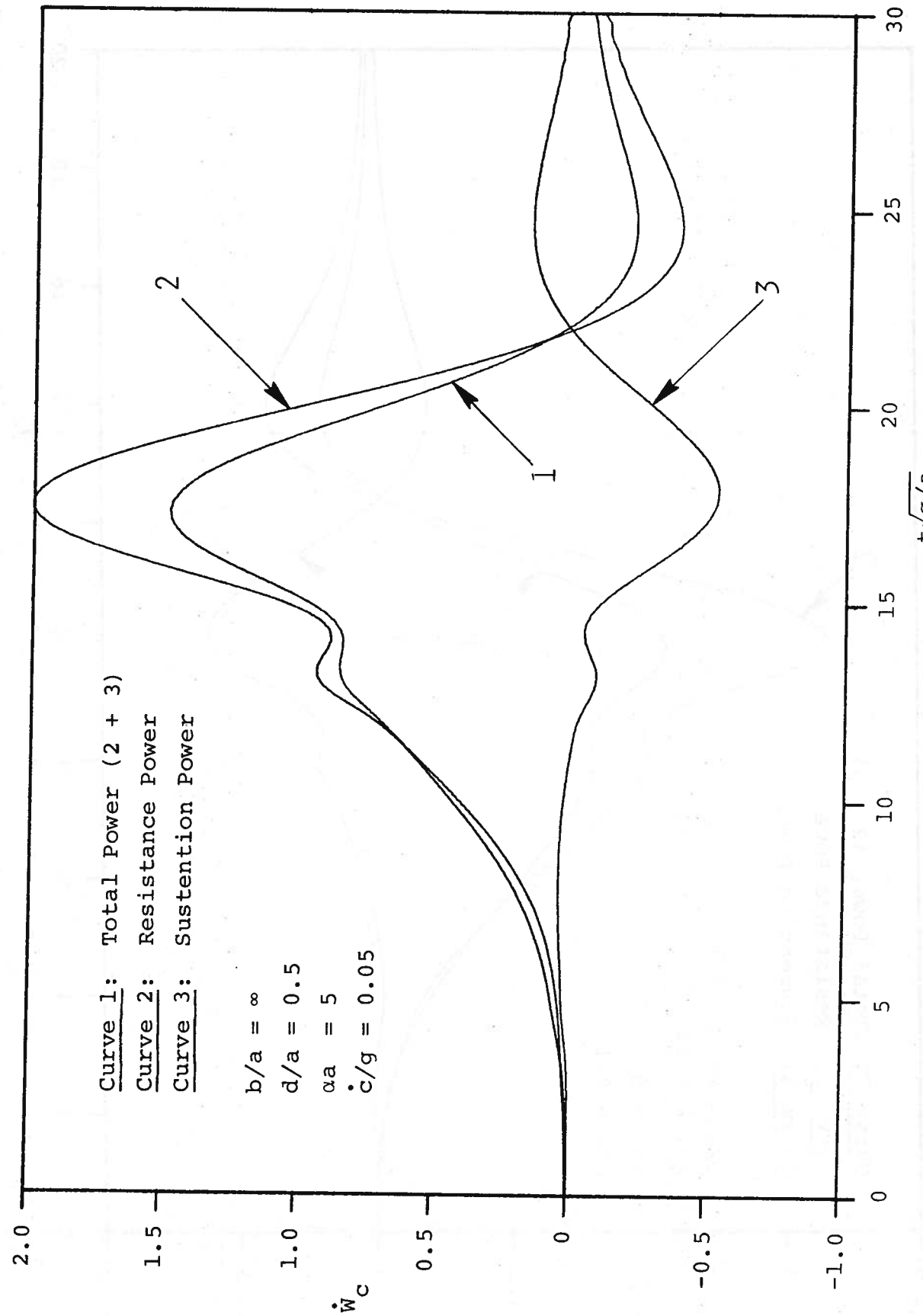

Fig. 12 (cont.) (d) $\dot{c}/g = 0.05$, $d/a = 0.5$

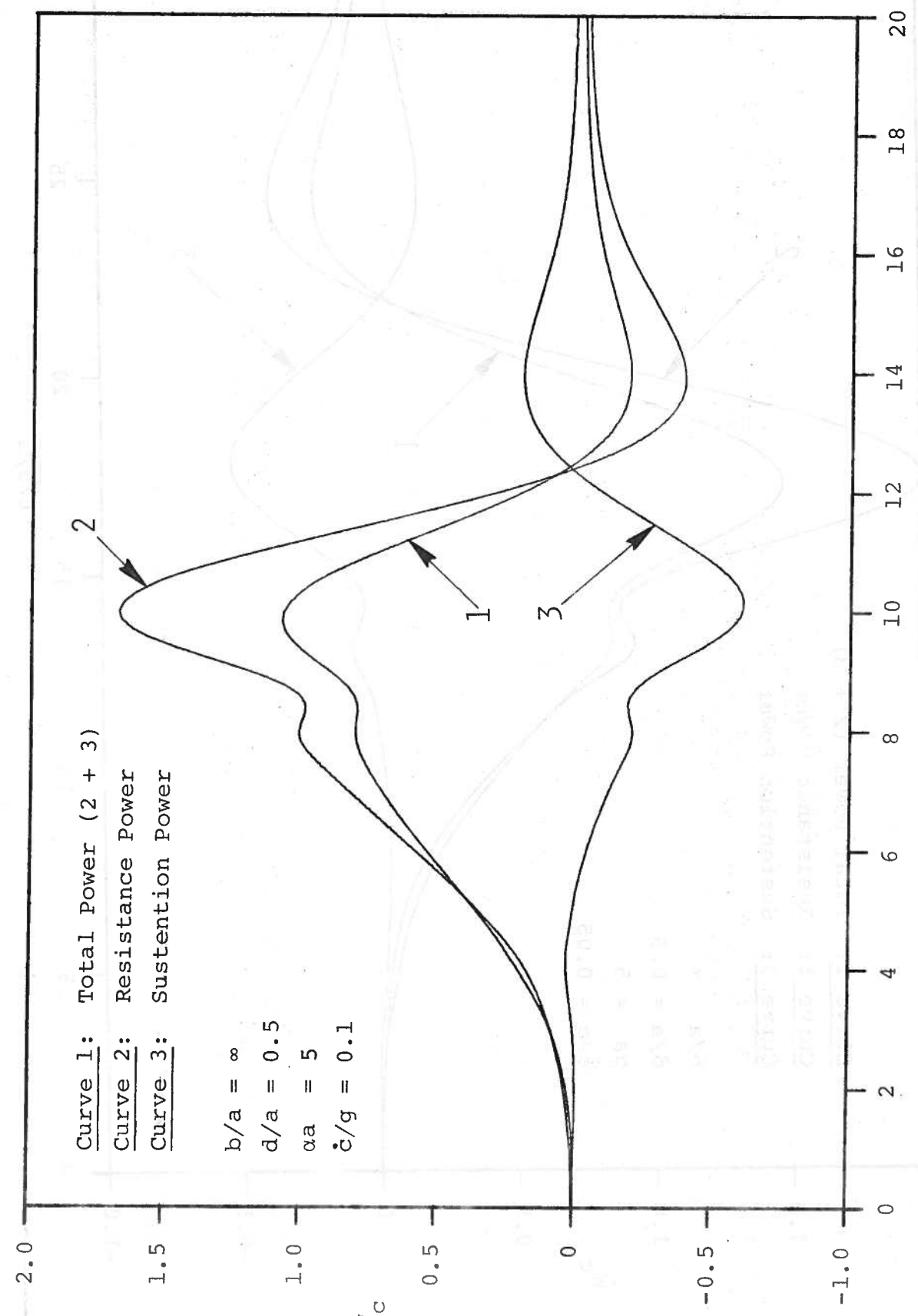

Fig. 12 (cont.) (e) $\dot{c}/g = 0.1$, $d/a = 0.5$

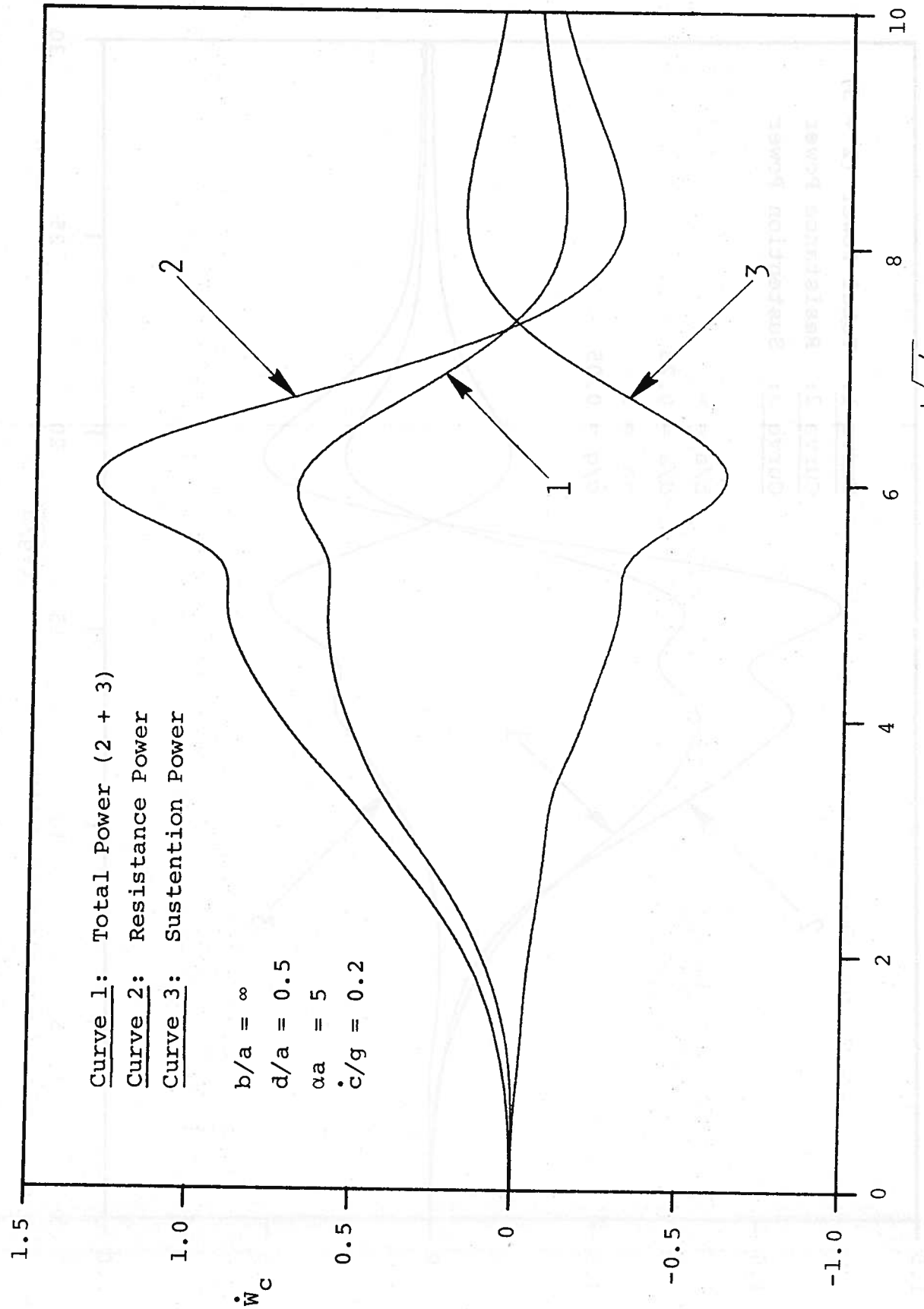

Fig. 12 (cont.) (f) $\dot{c}/g = 0.2$, $d/a = 0.5$

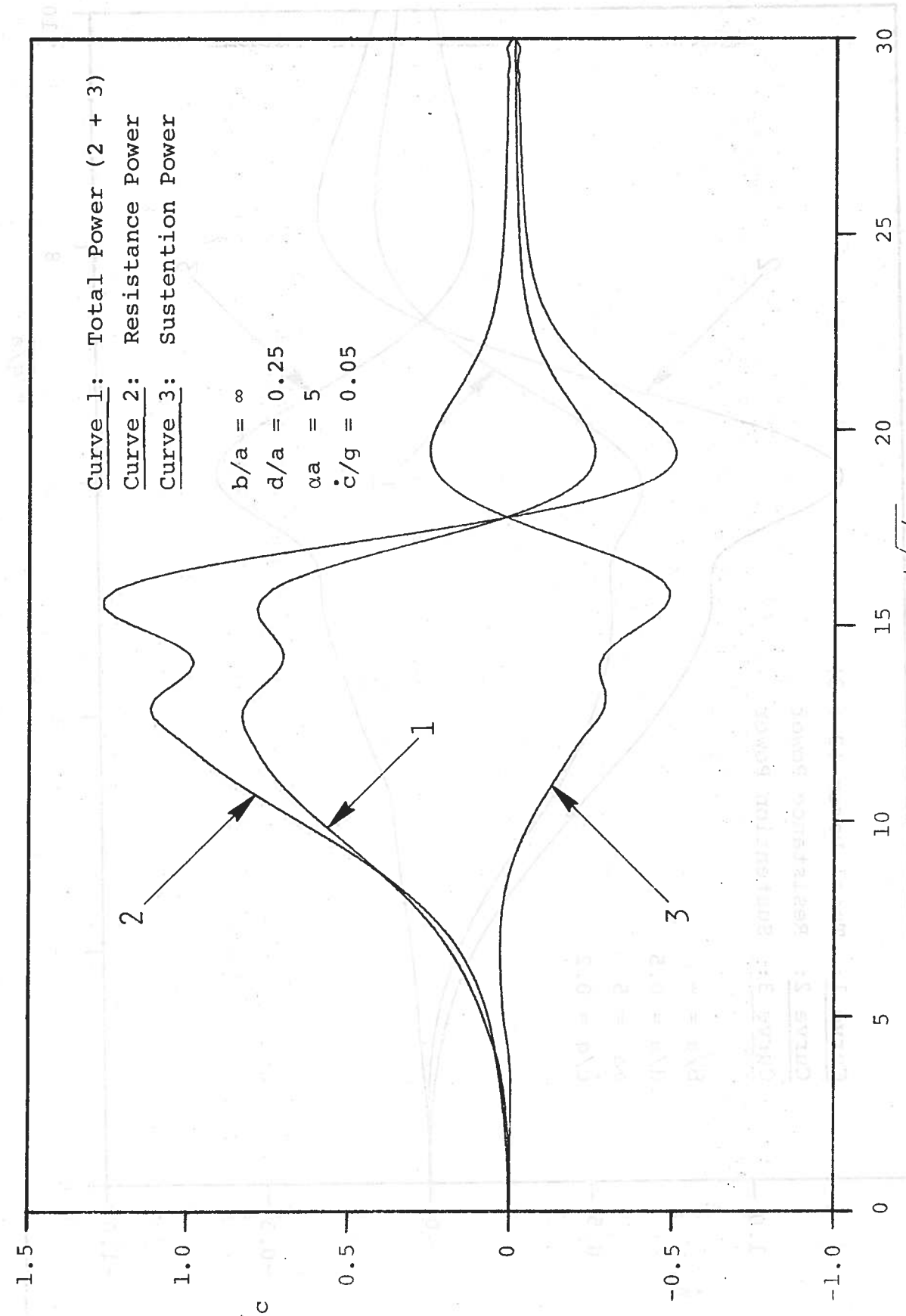

Fig. 12 (cont.) (g) $\dot{c}/g = 0.05$, $d/a = 0.25$

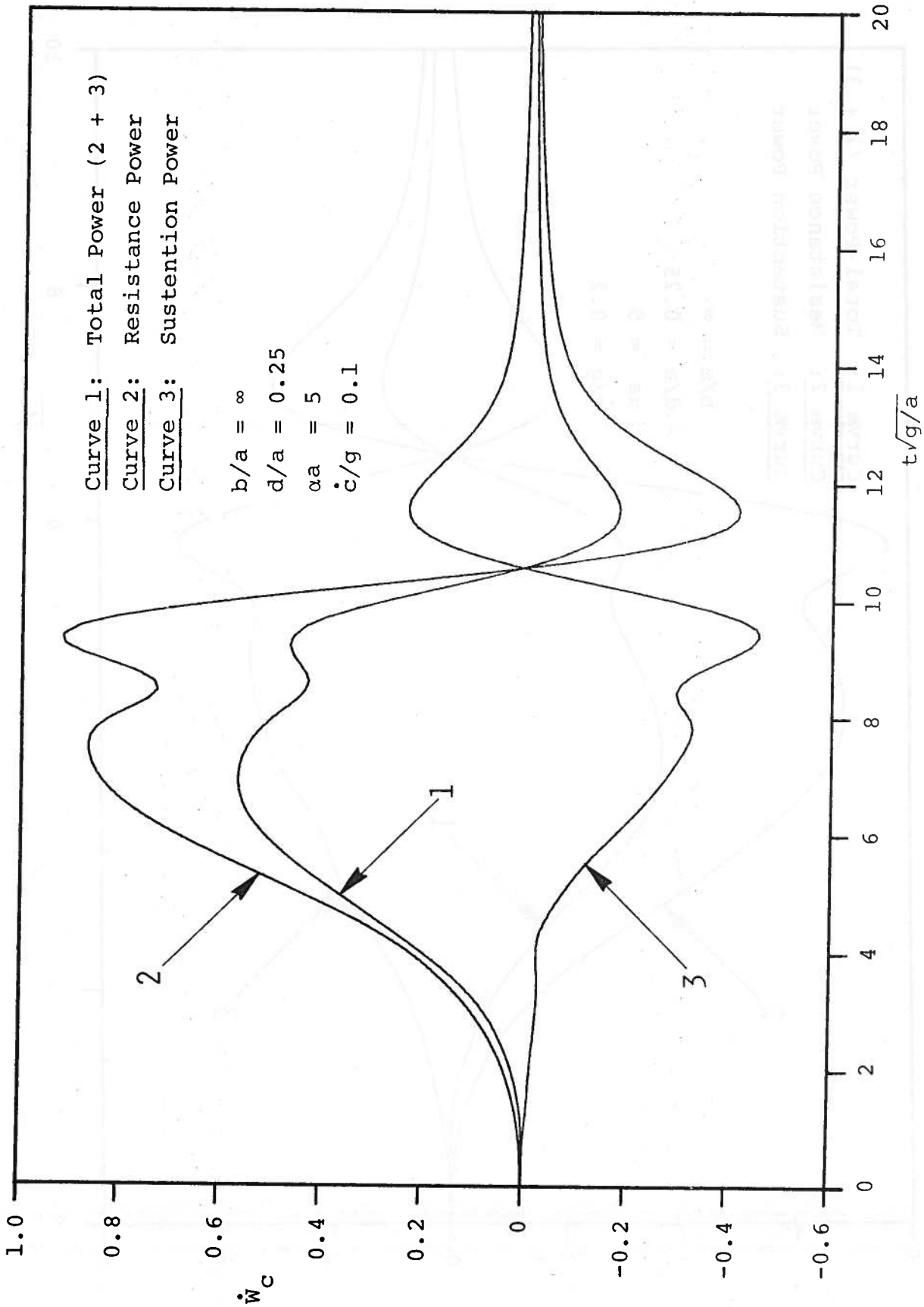

Fig. 12 (cont.) (h) $\dot{c}/g = 0.1$, $d/a = 0.25$

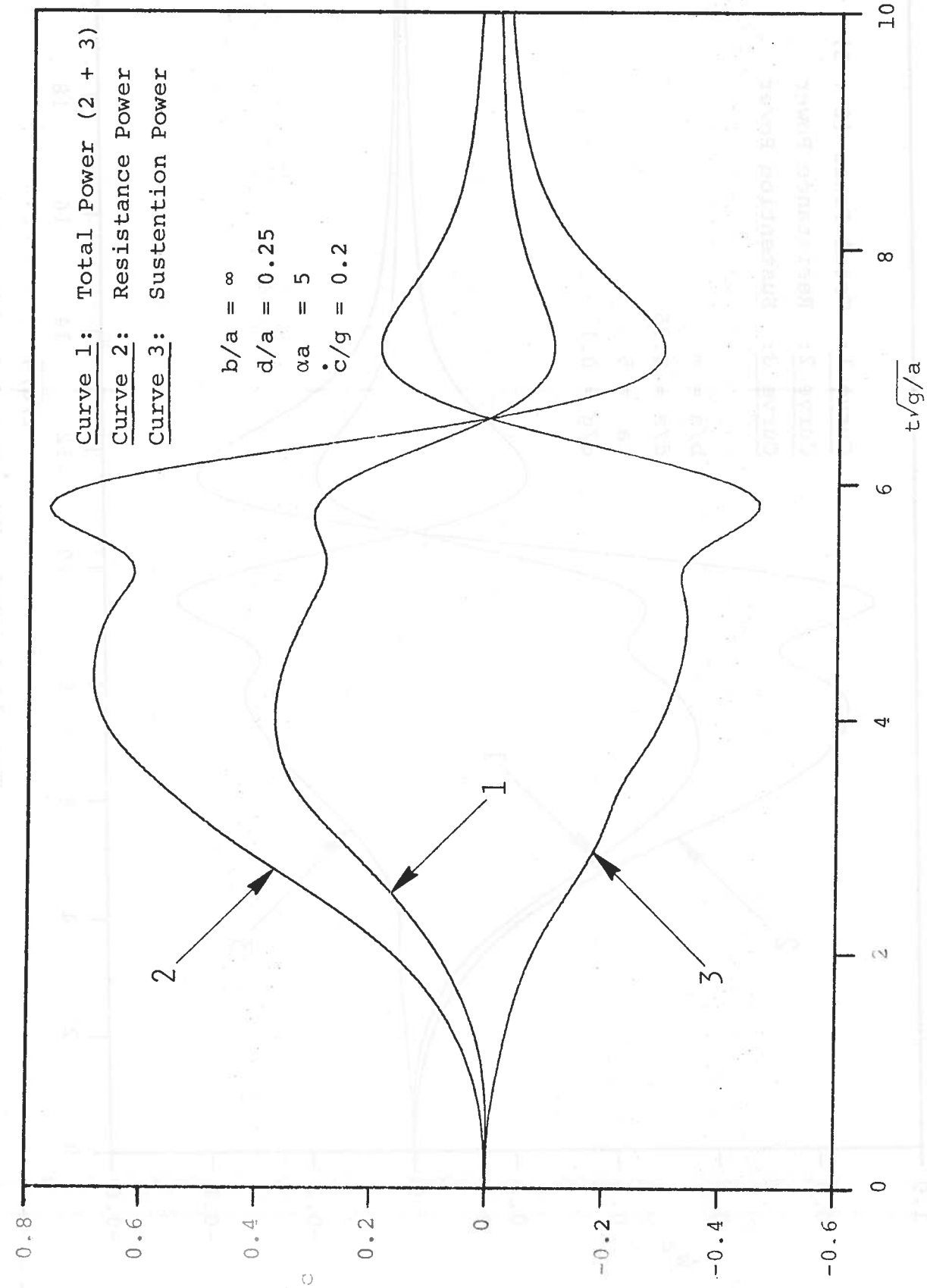

Fig. 12 (cont.) (i) $\dot{c}/g = 0.2$, $d/a = 0.25$

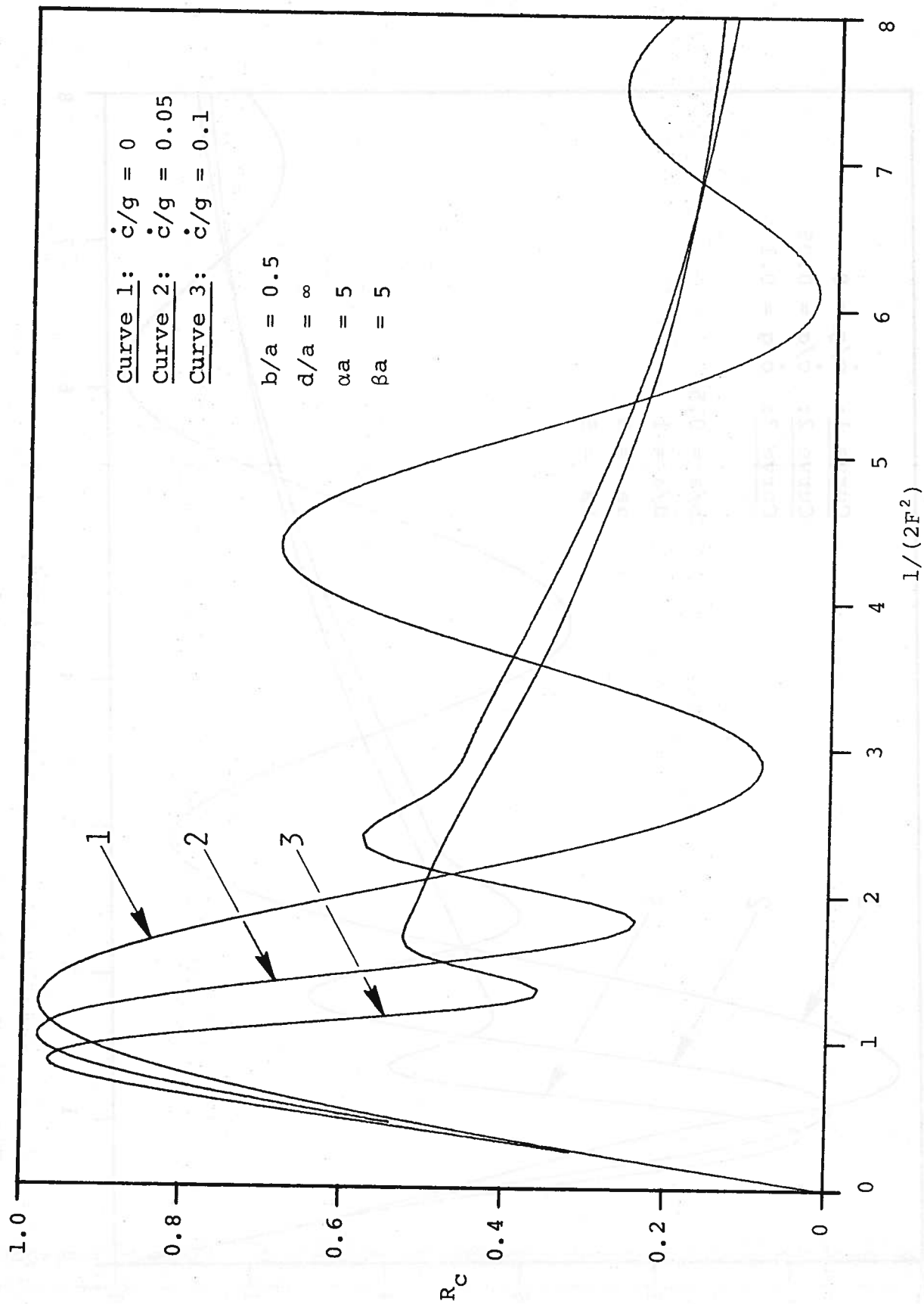

Fig. 13 Unsteady 3D Wave Resistance in Deep Water

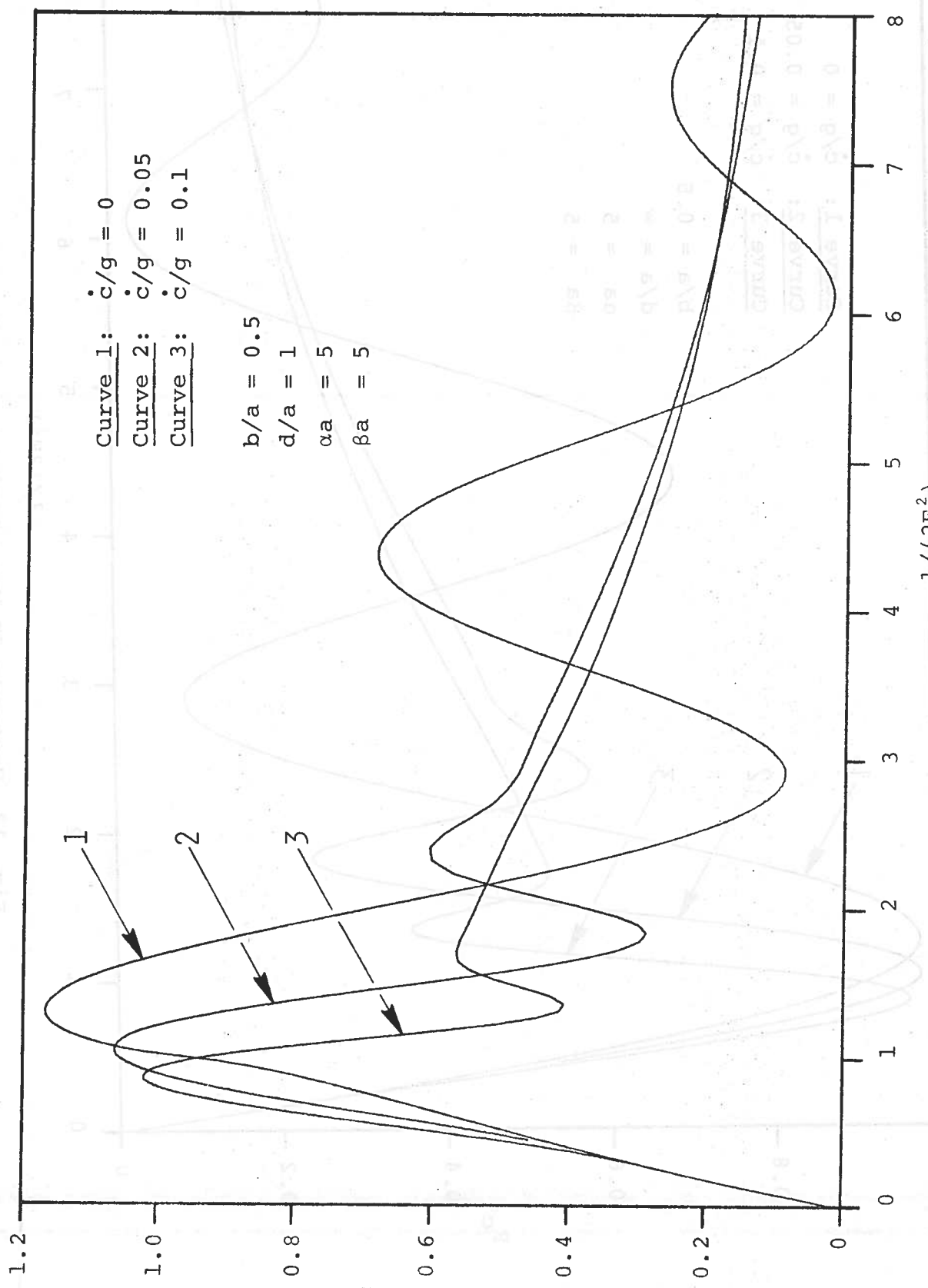

Fig. 14 Unsteady 3D Wave Resistance in Finite Depth, (a) d/a = 1

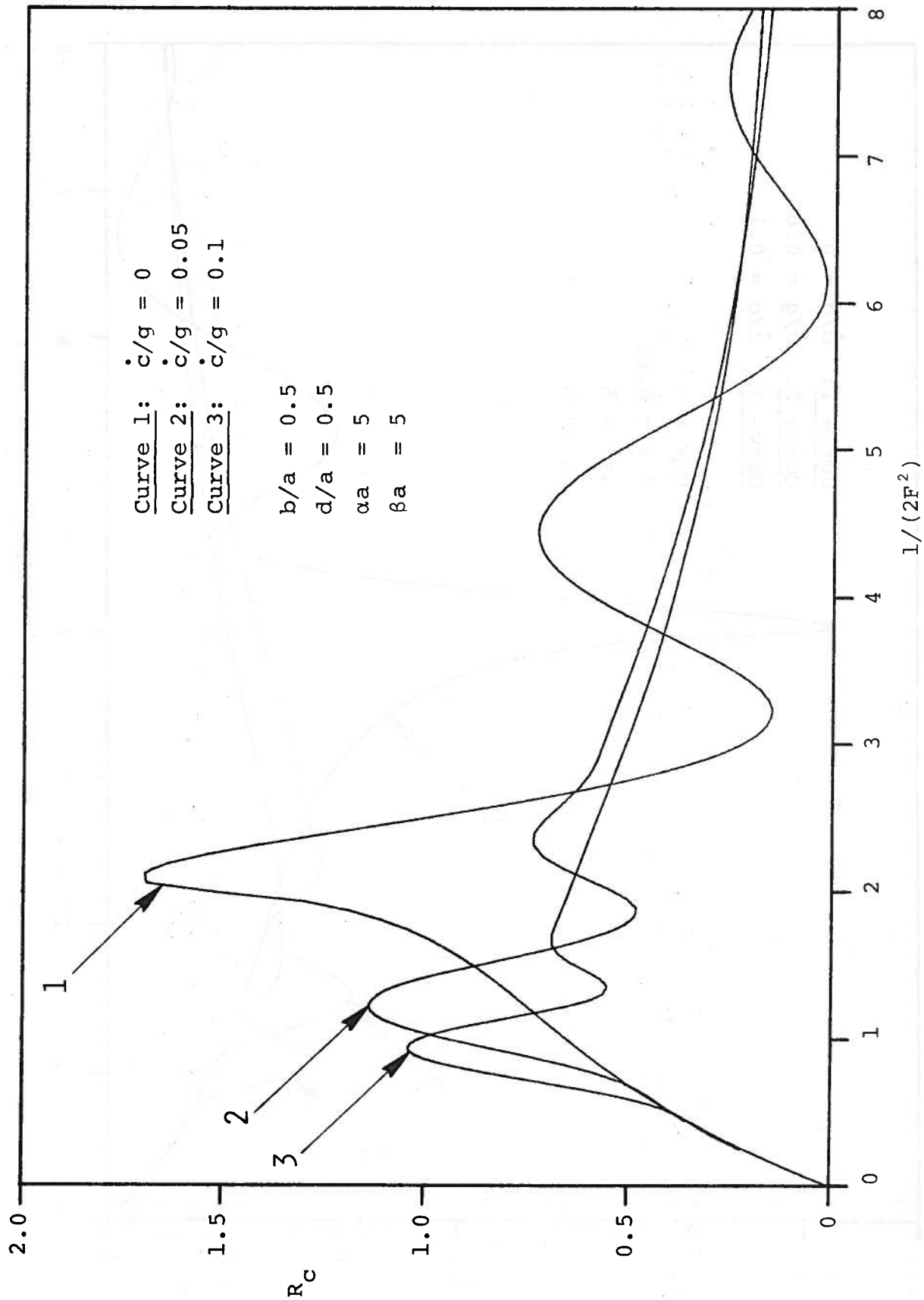

Fig. 14 (cont.) (b) d/a = 0.5

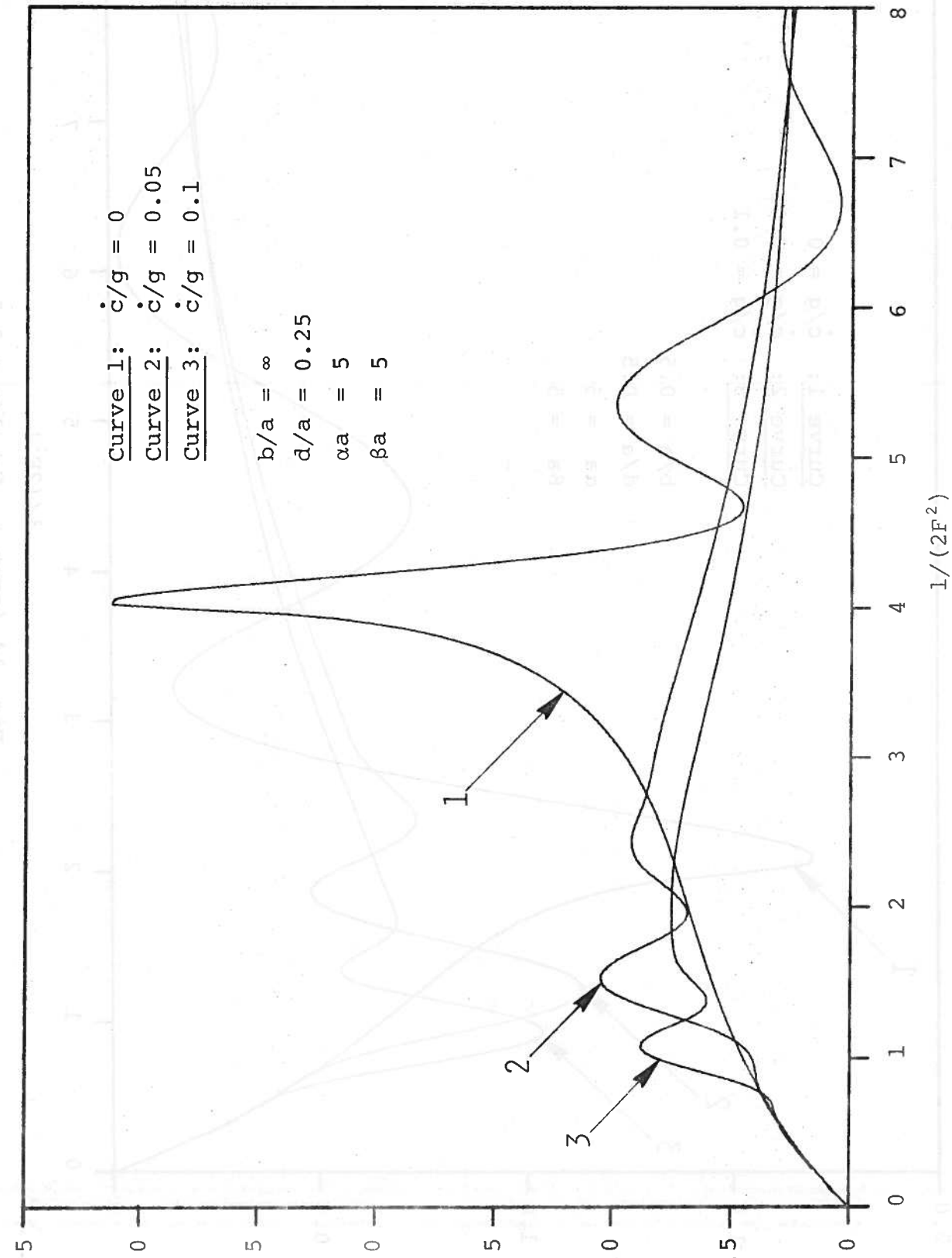

Fig. 14 (cont.) (c) 1/a = 0.25

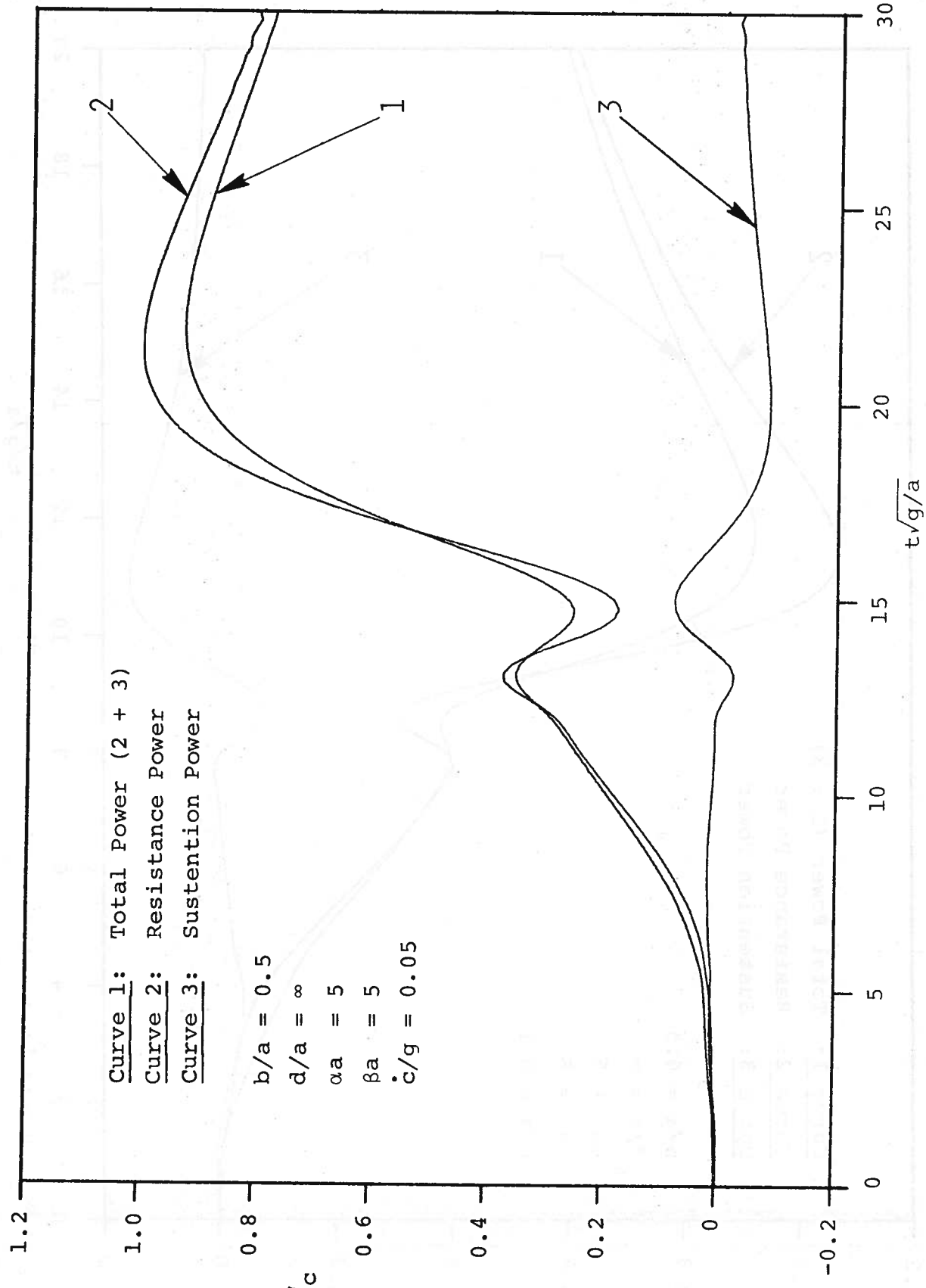

Fig. 15 Comparison of 3D Powers in Deep Water, (a) $\dot{c}/g = 0.05$

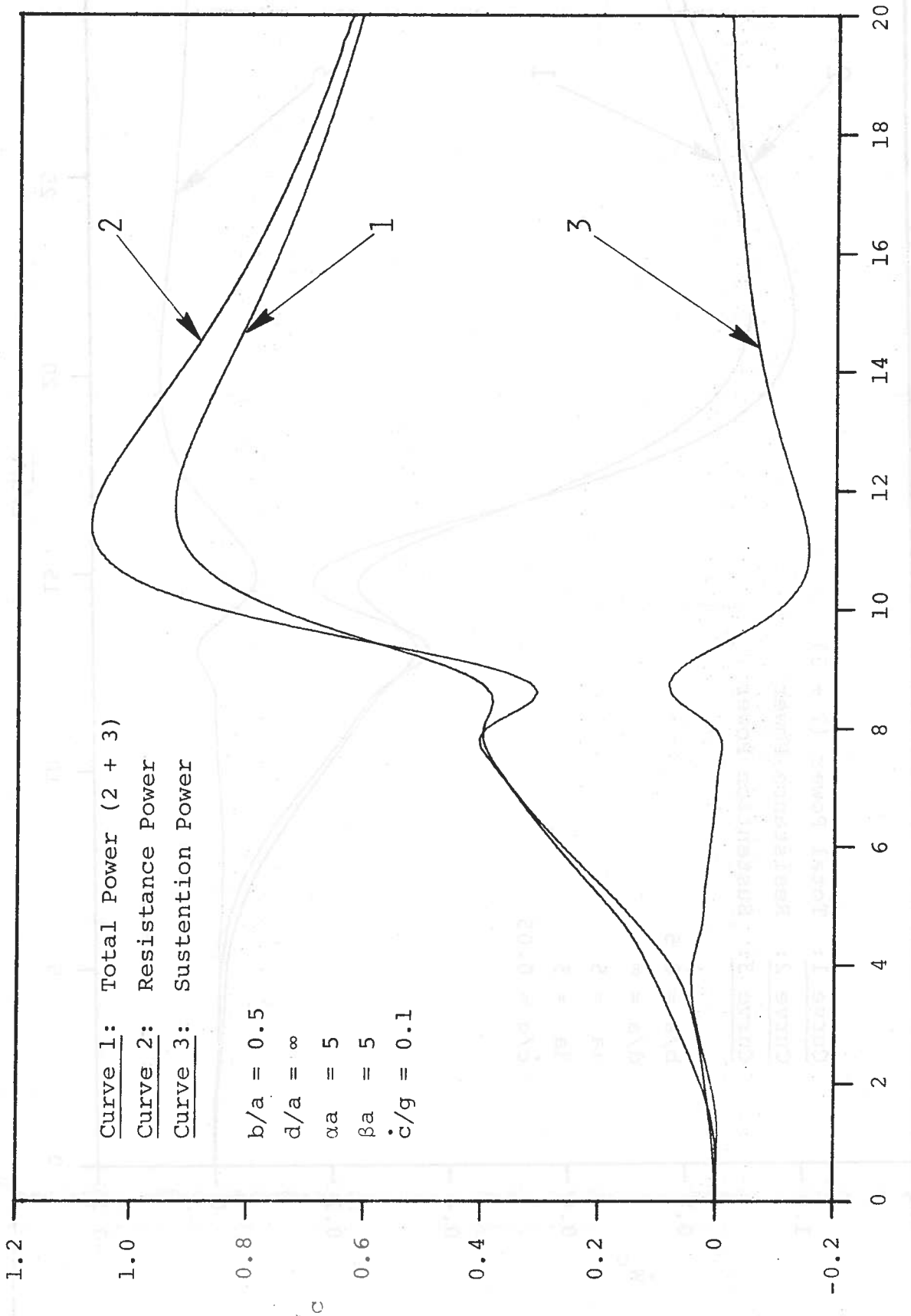

Fig. 15 (cont.) (b) $\dot{c}/g = 0.1$

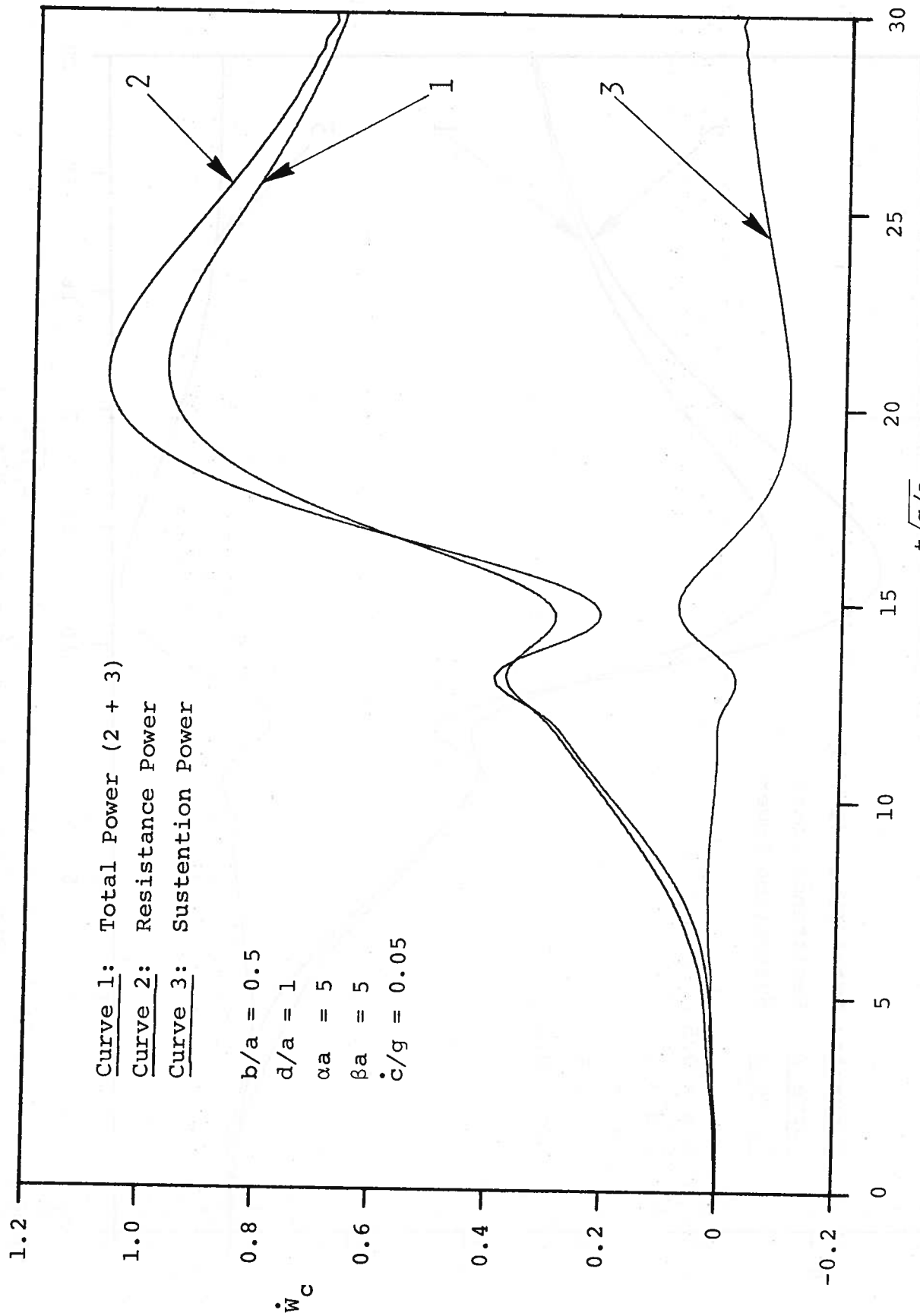

Fig. 16 Comparison of 3D Powers in Finite Depth, (a) $\dot{c}/g = 0.05$, $d/a = 1$

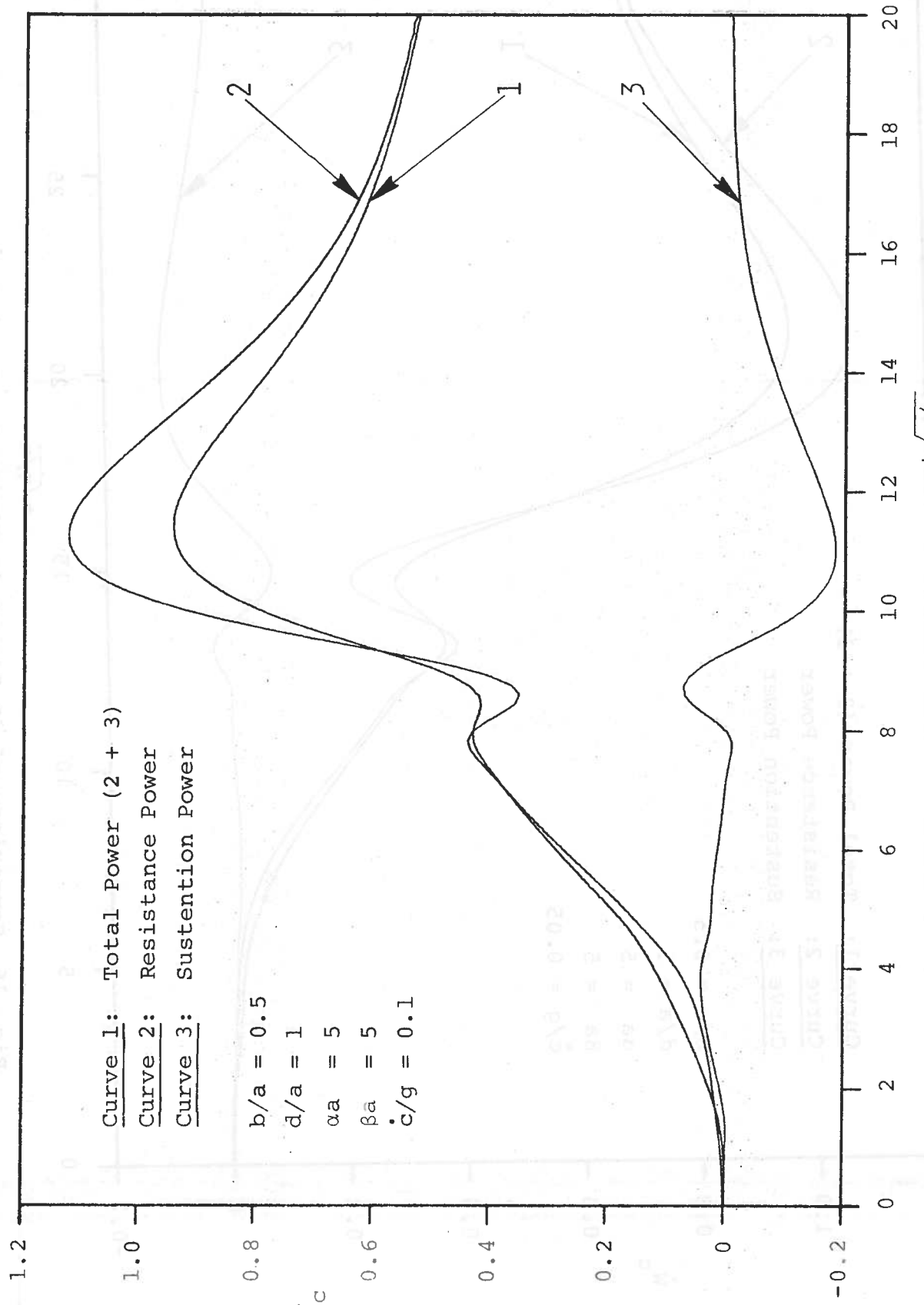

Fig. 16 (cont.) (b) $\dot{c}/g = 0.1$, $d/a = 1$

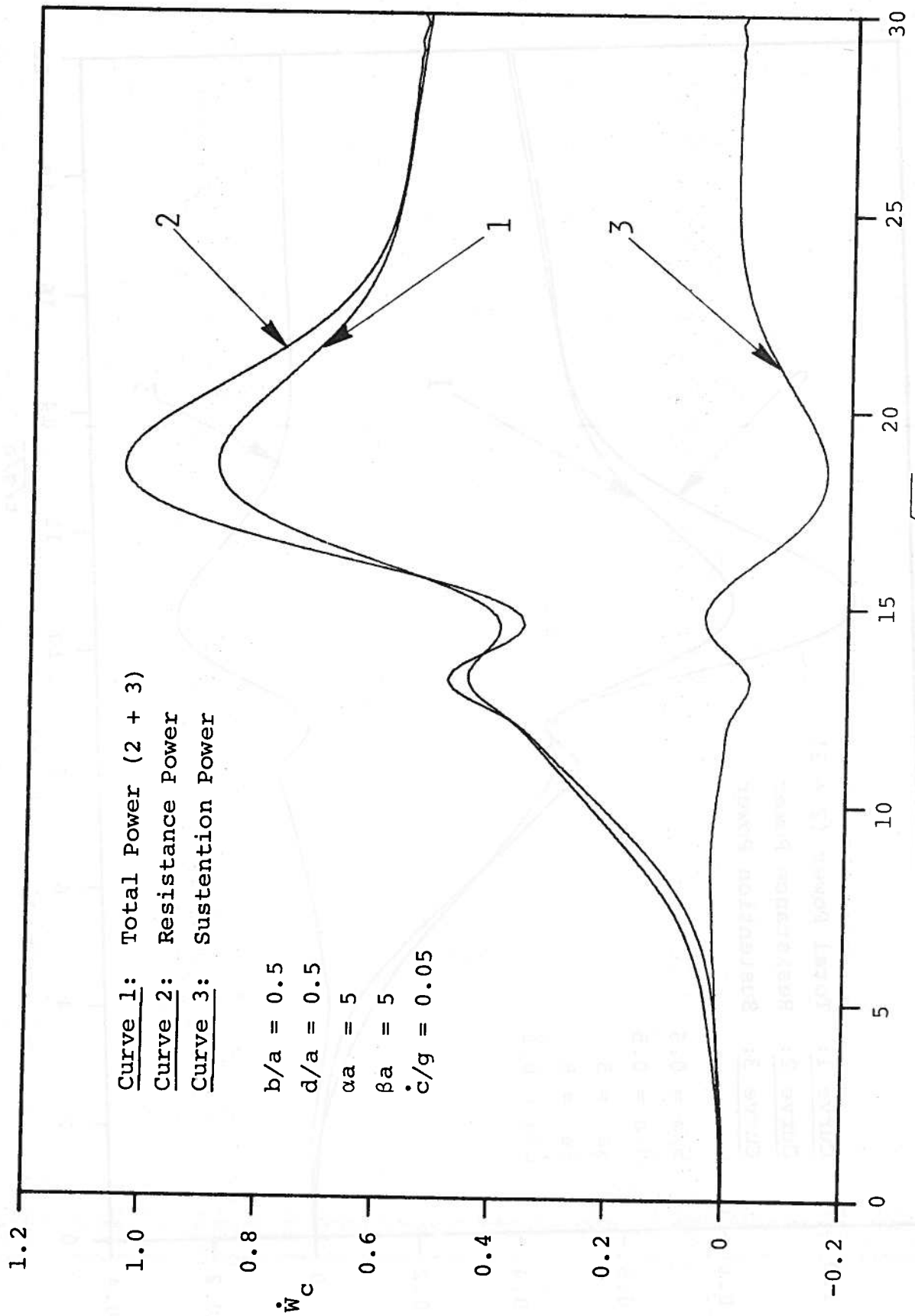

Fig. 16 (cont.) (c) $\dot{c}/g = 0.05$, $d/a = 0.5$

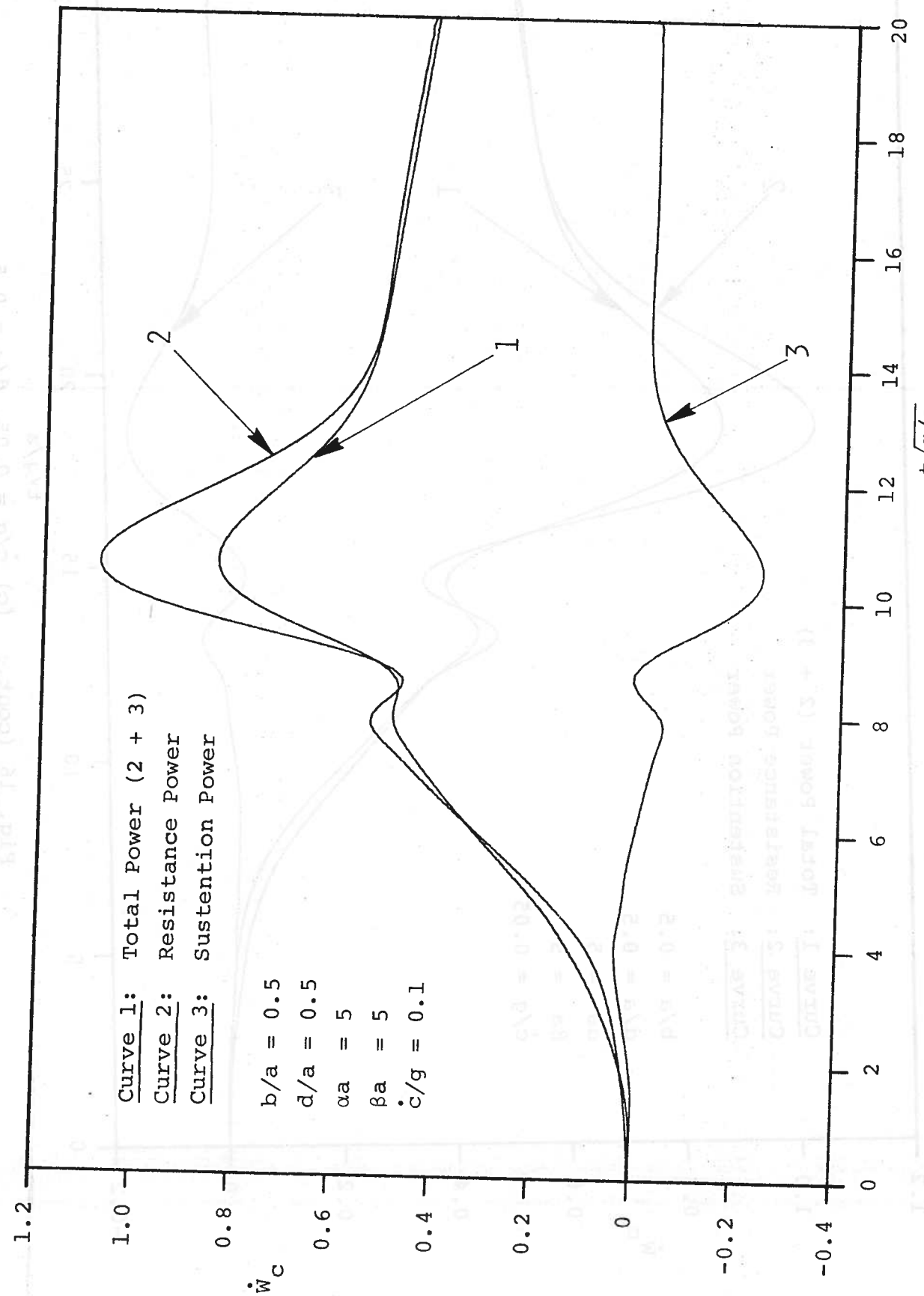

Fig. 16 (cont.) (d) $\dot{c}/g = 0.1$, $d/a = 0.5$

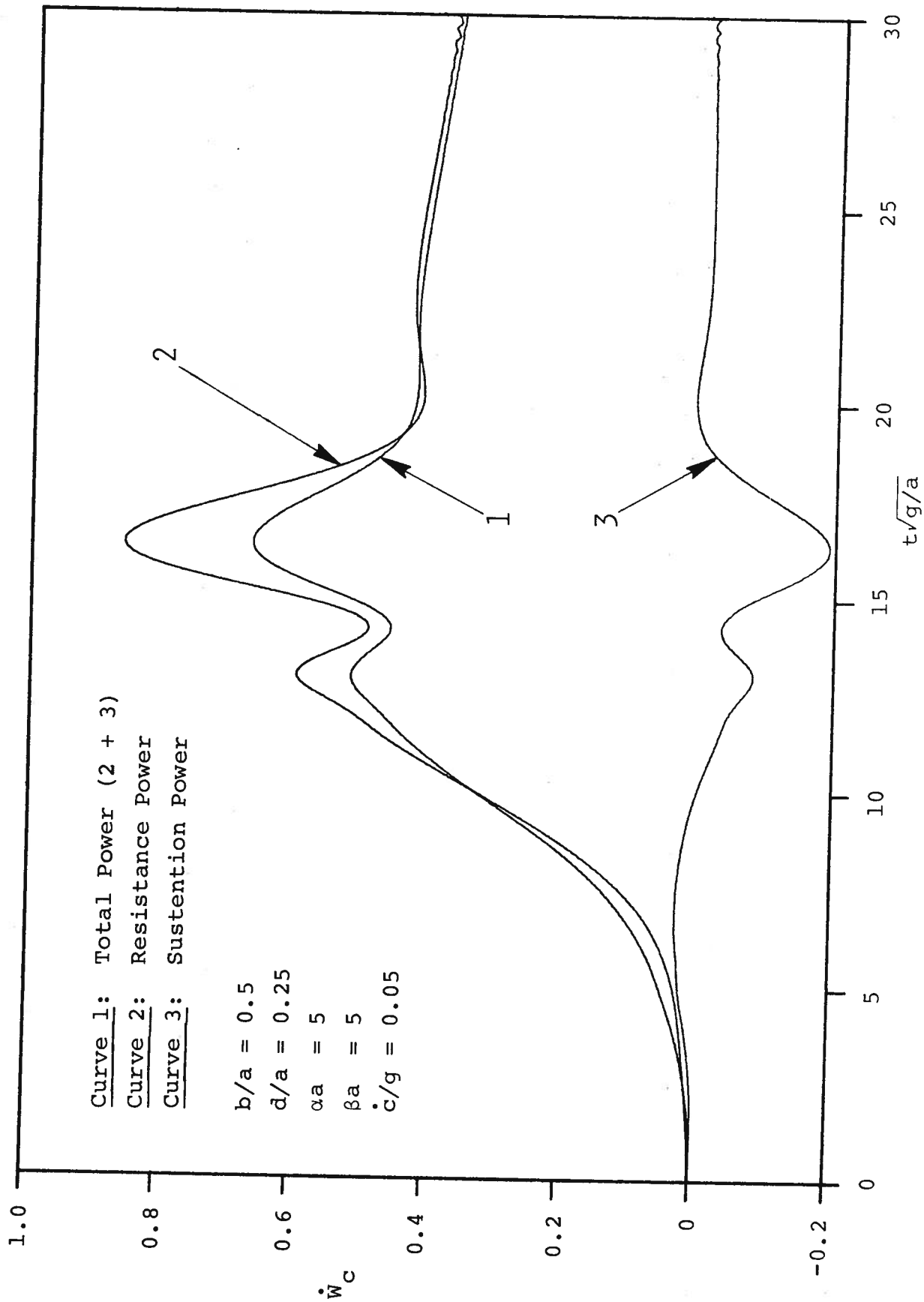

Fig. 16 (cont.) (e) $\dot{c}/g = 0.05$, $d/a = 0.25$

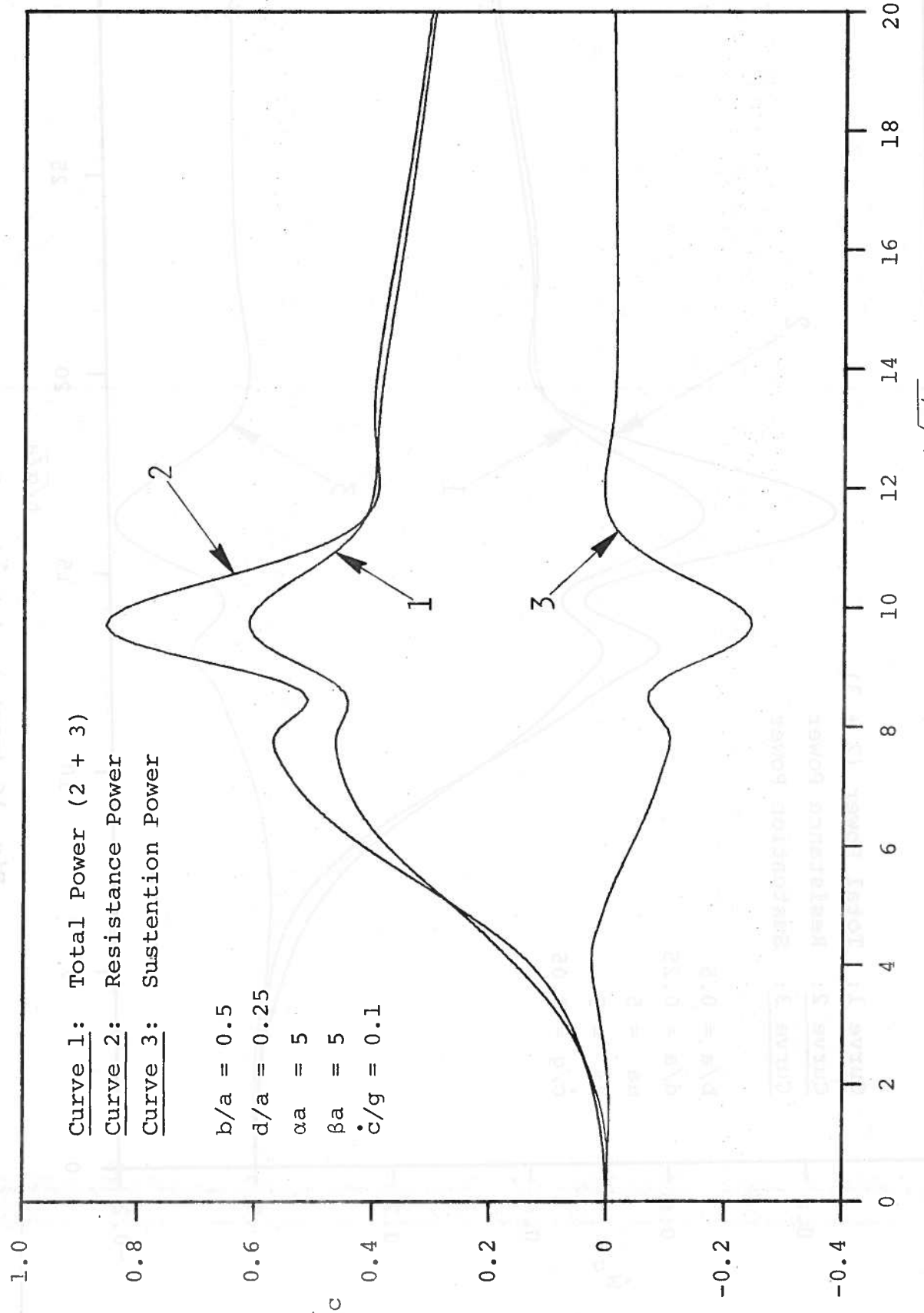

Fig. 16 (cont.) (f) $\dot{c}/g = 0.1$, $d/a = 0.25$

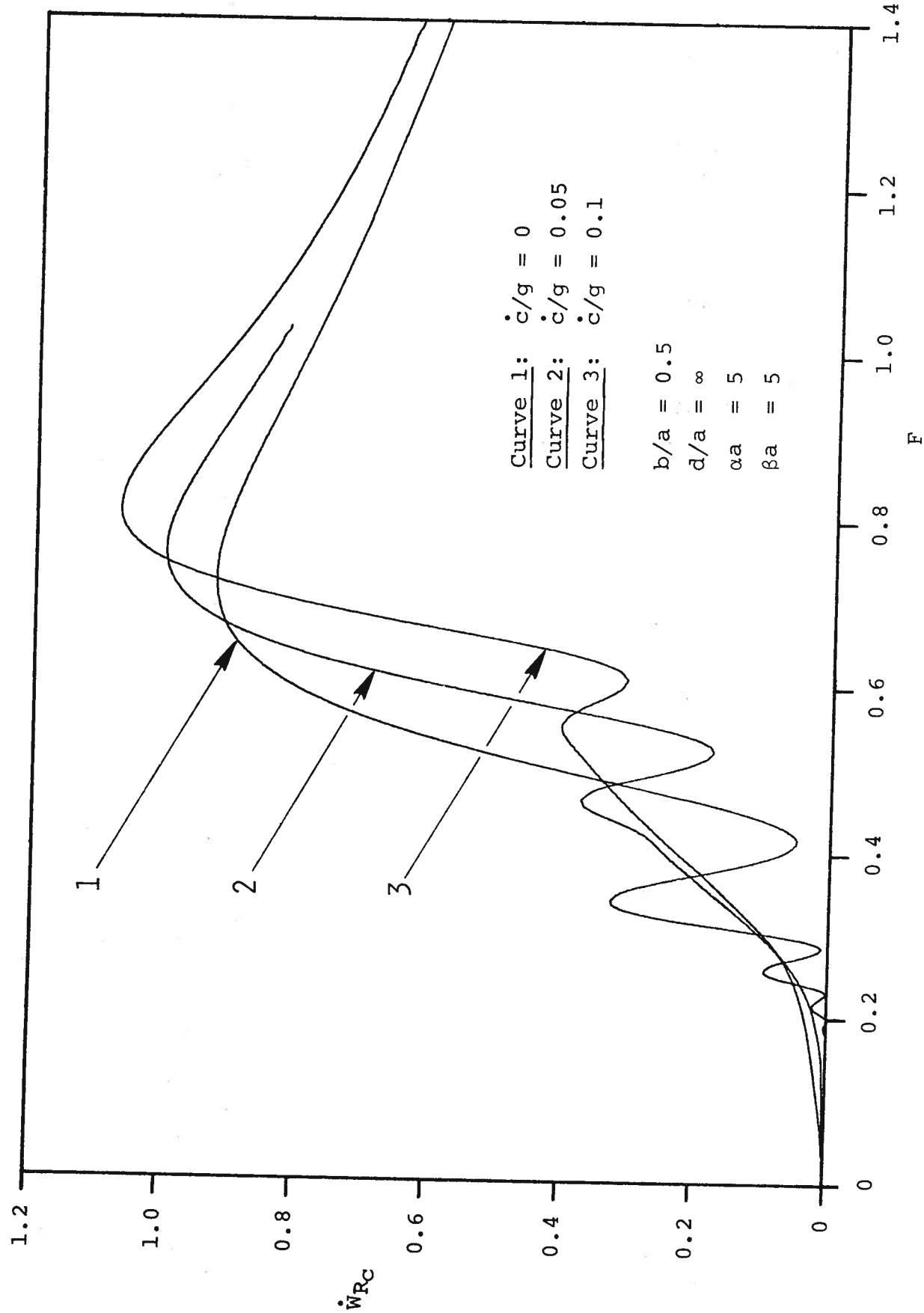

Fig. 17 3D Resistance Power in Deep Water

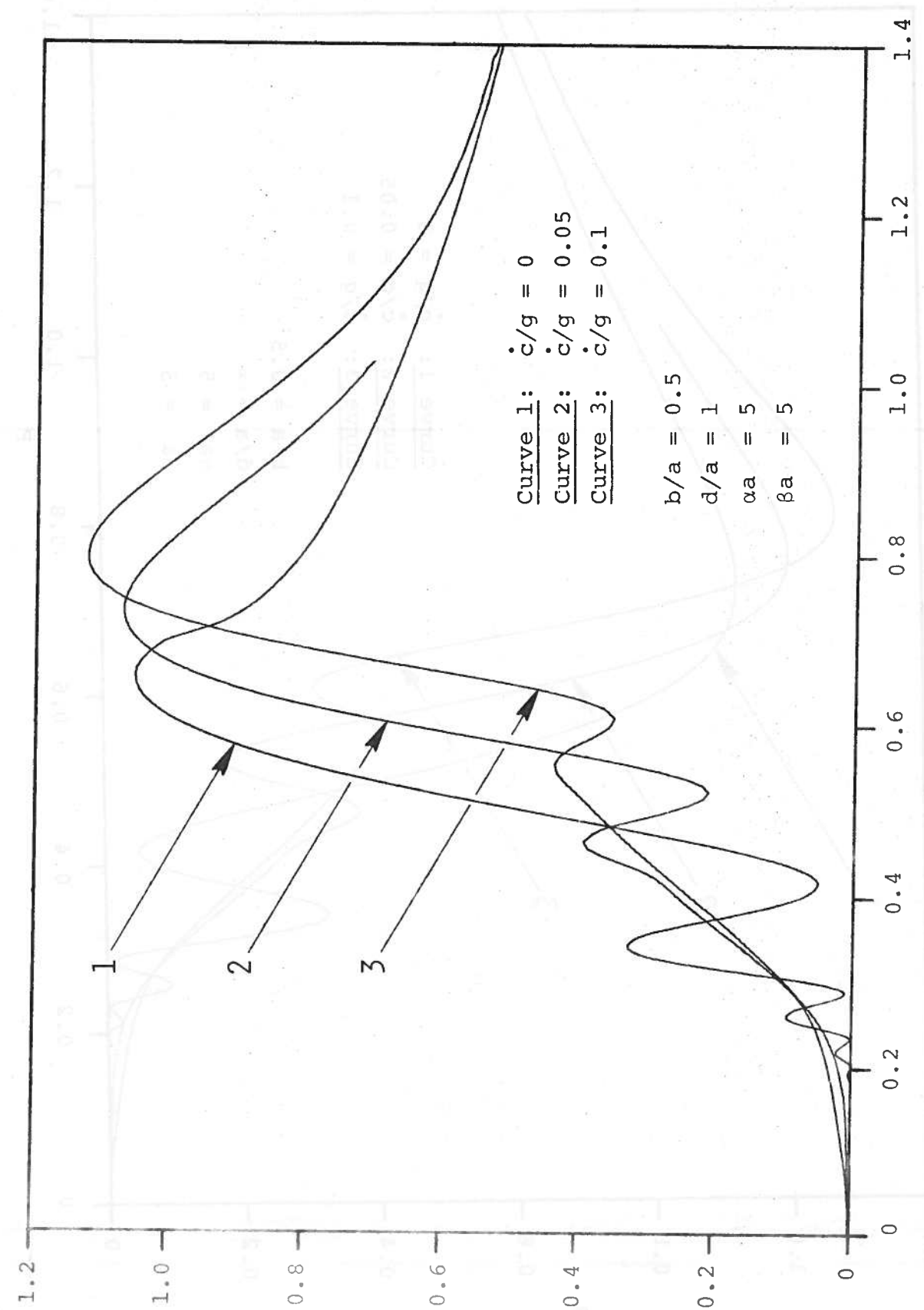

Fig. 18 3D Resistance Power in Finite Depth, (a) d/a = 1

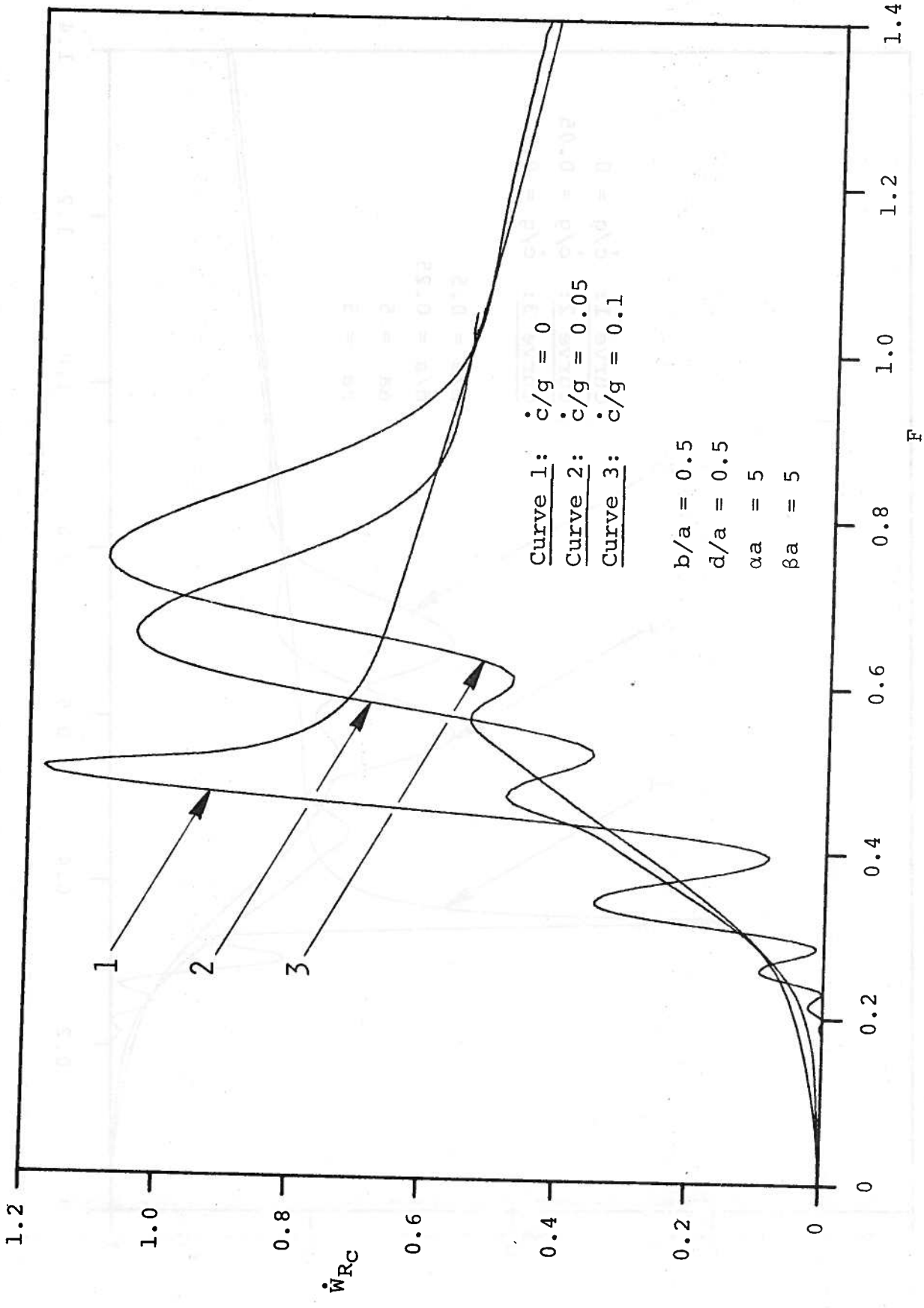

Fig. 18 (cont.) (b) d/a = 0.5

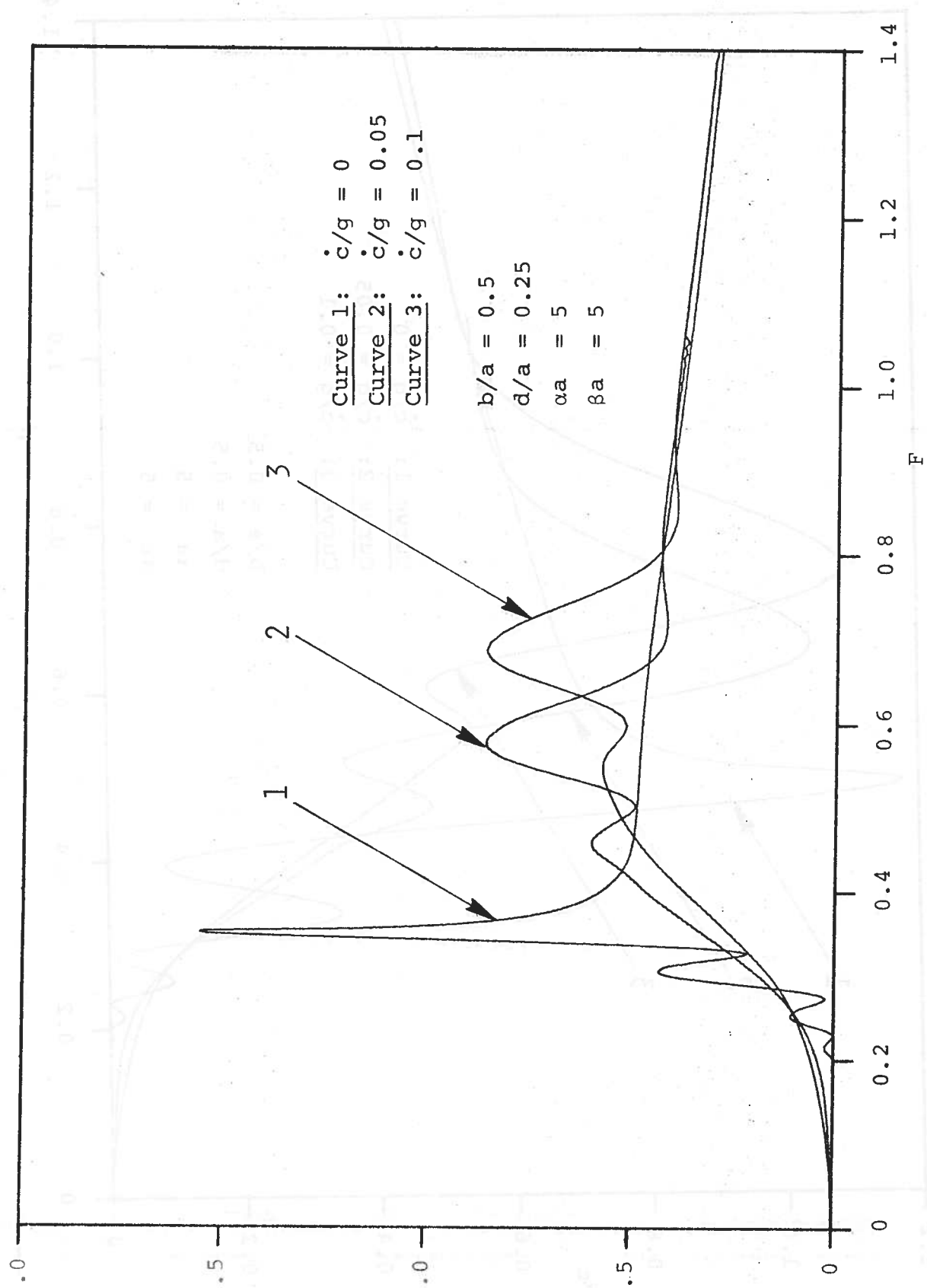

Fig. 18 (cont.) (c) d/a = 0.25

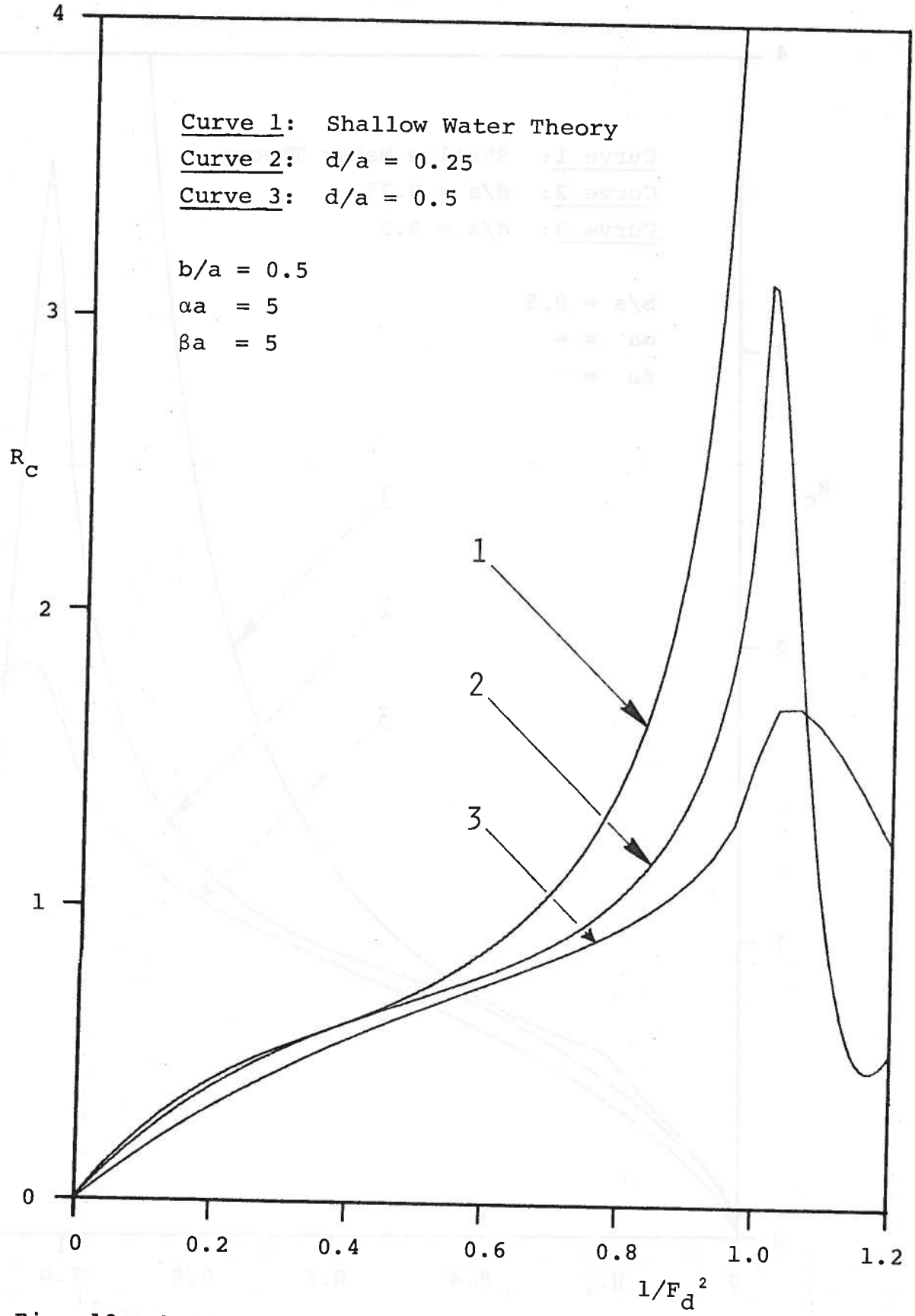

Fig. 19 Shallow Water Wave Resistance, (a) $\alpha a = \beta a = 5$

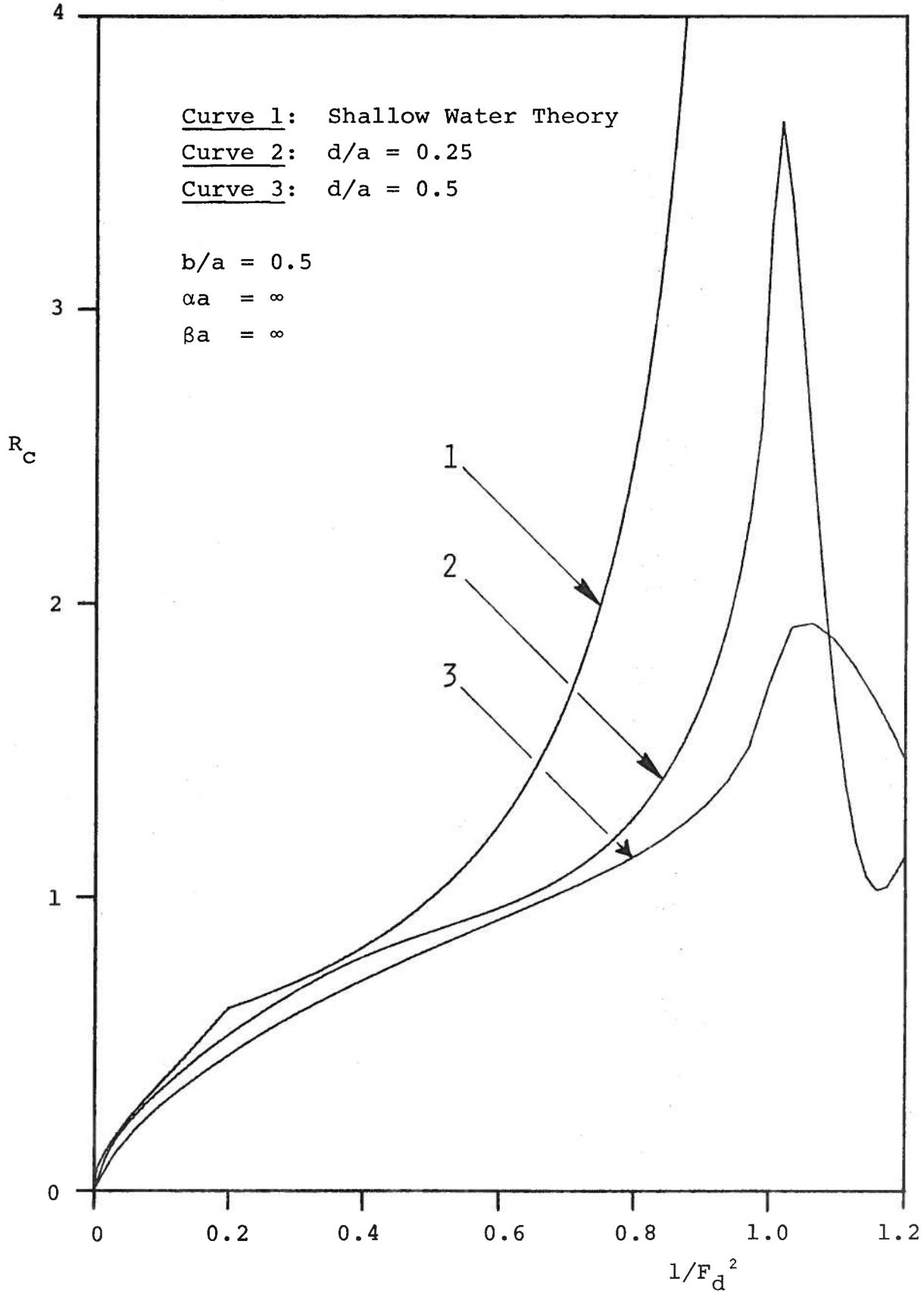

Fig. 19 (cont.) (b) $\alpha a = \beta a = \infty$

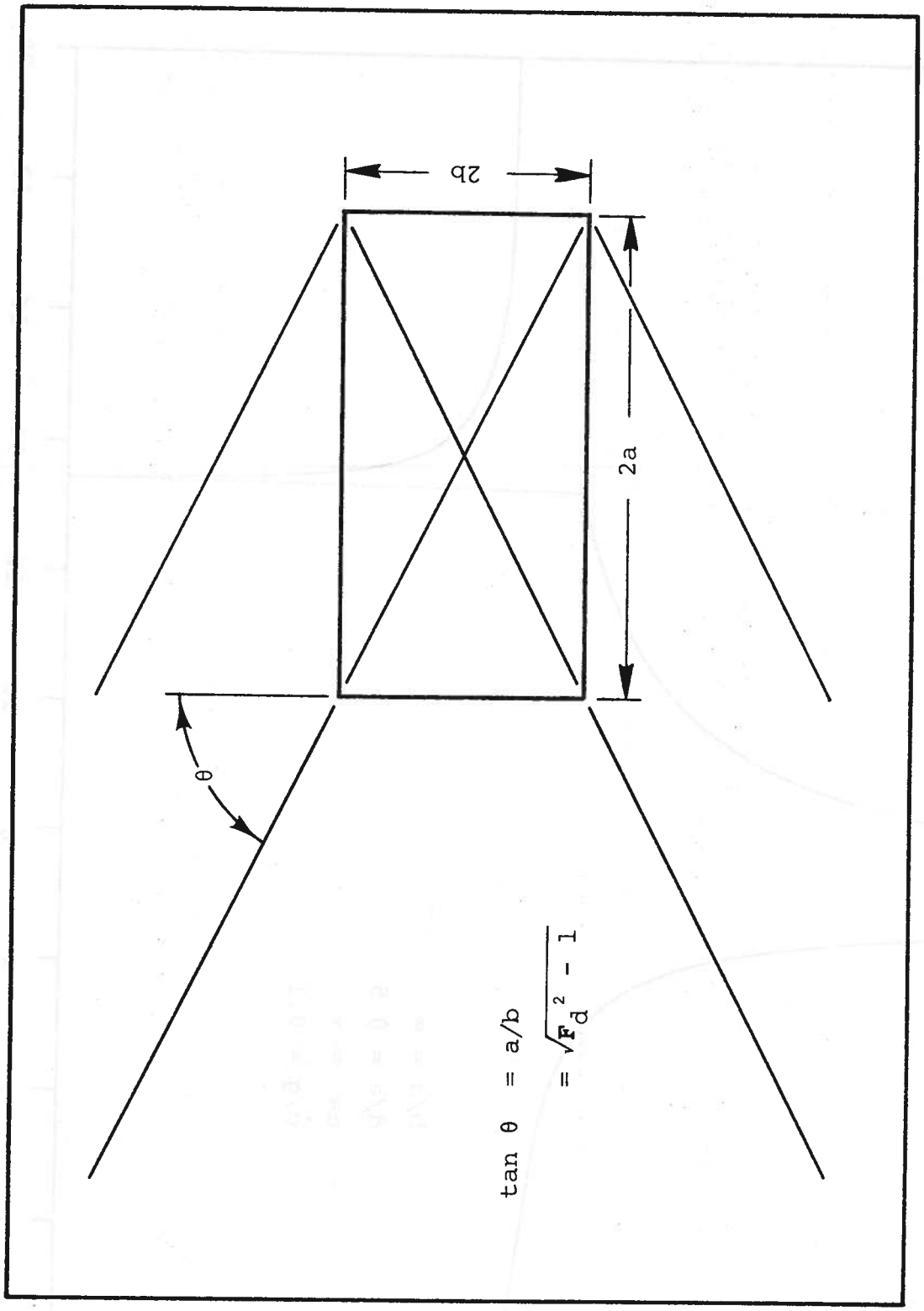

Fig. 20 Shallow Water Bow and Stern Wave Interference

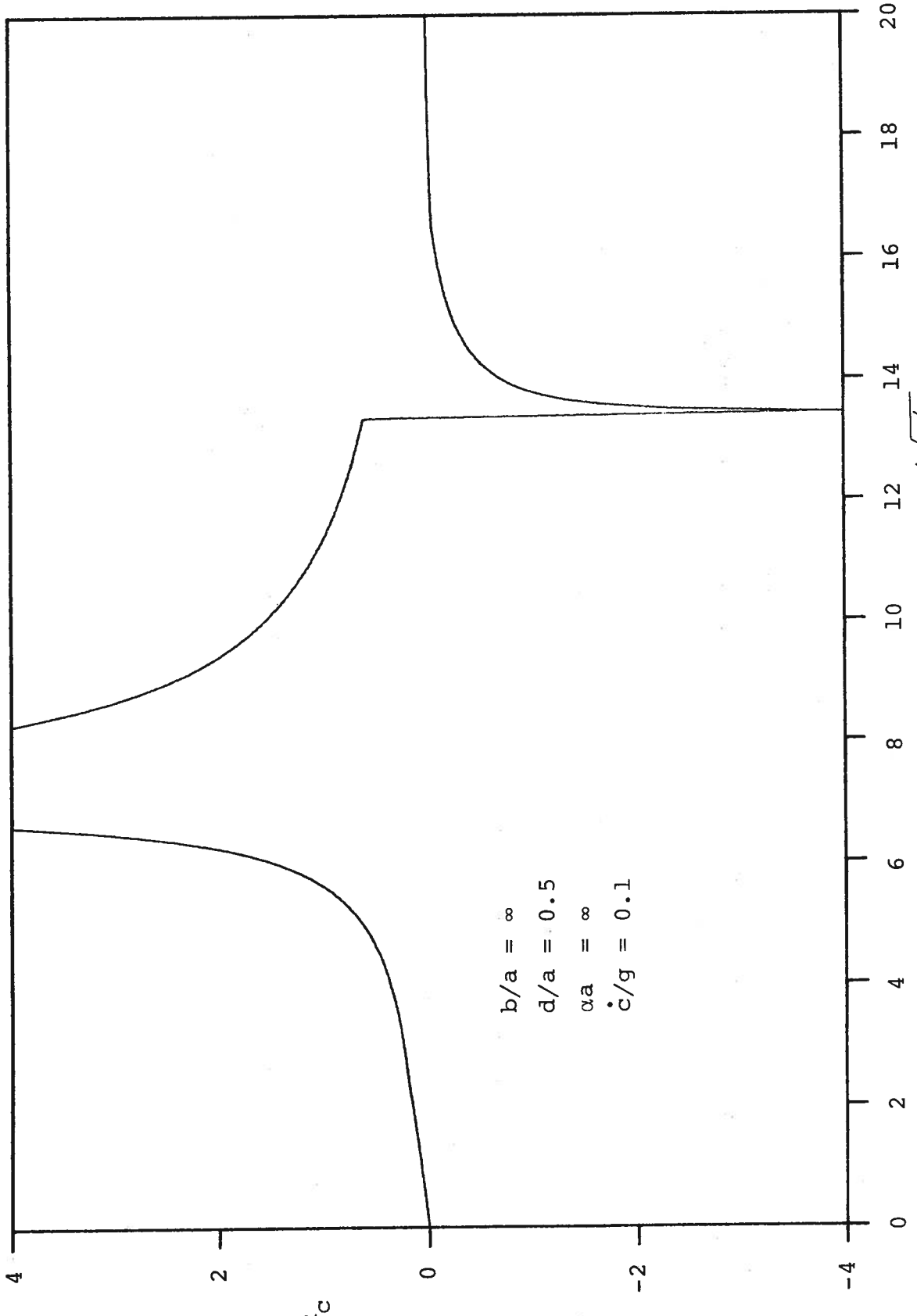

Fig. 21 Shallow Water 2D Wave Resistance (Unsteady)

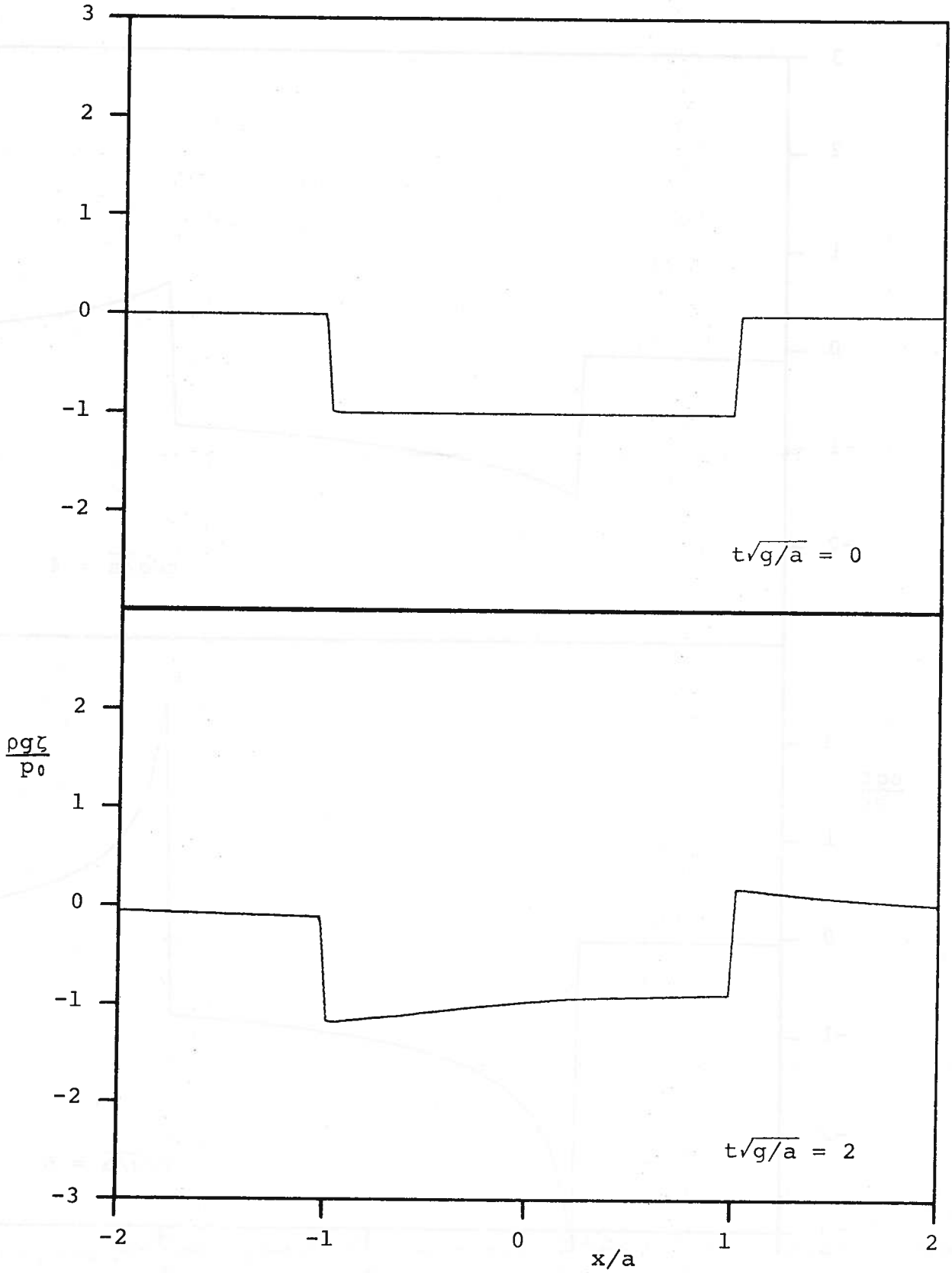

Fig. 22 Shallow Water Unsteady Free Surface Elevation (2D) for Fig. 21, (a) For $t\sqrt{g/a} = 0(2)18$

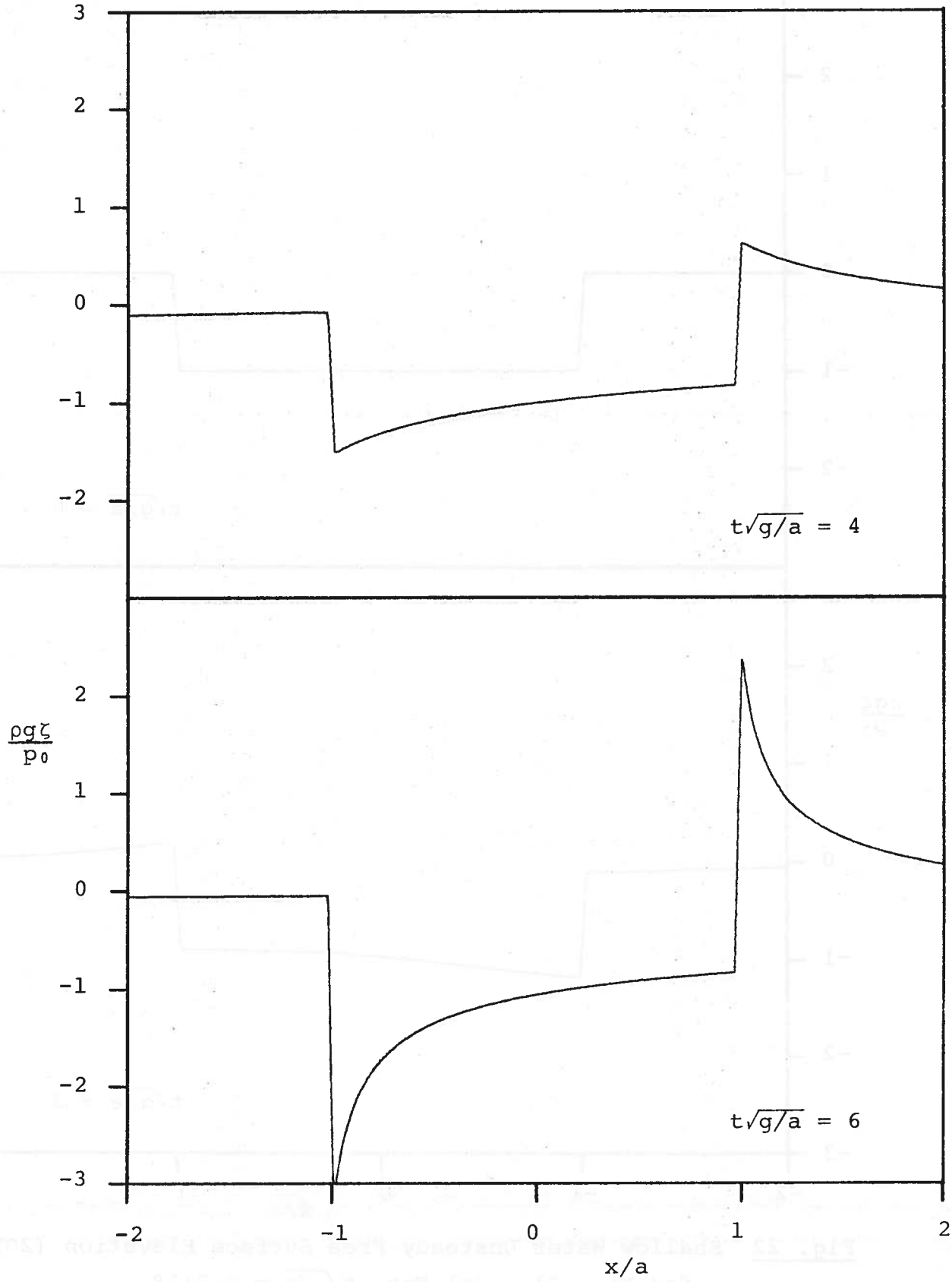

Fig. 22 (a) (cont.)

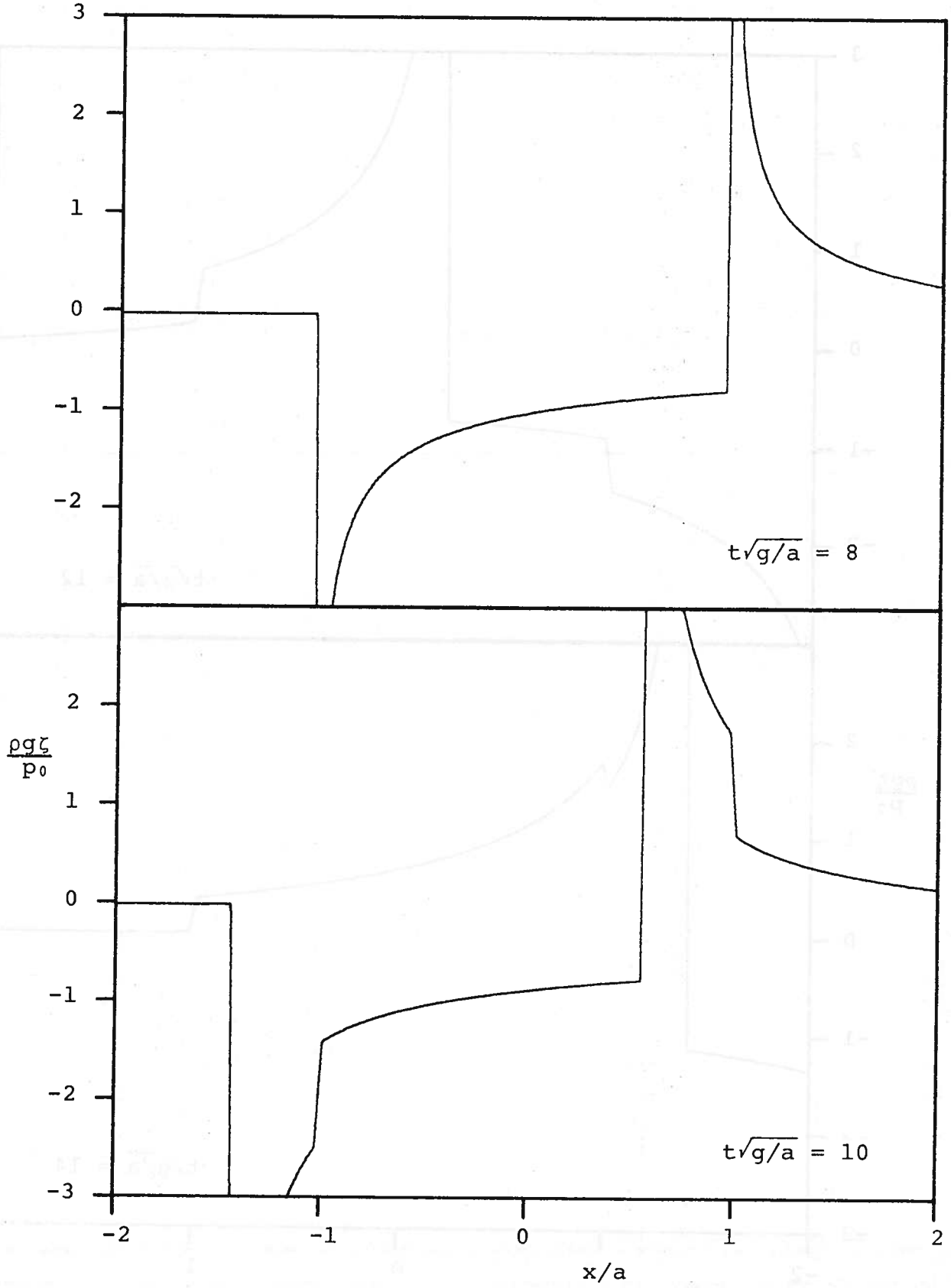
3
2
1
0
-1
-2
$t\sqrt{g/a} = 8$
$\frac{\rho g \zeta}{p_0}$
2
1
0
-1
-2
-3
$t\sqrt{g/a} = 10$
-2
-1
0
1
2
x/a

Fig. 22 (a) (cont.)

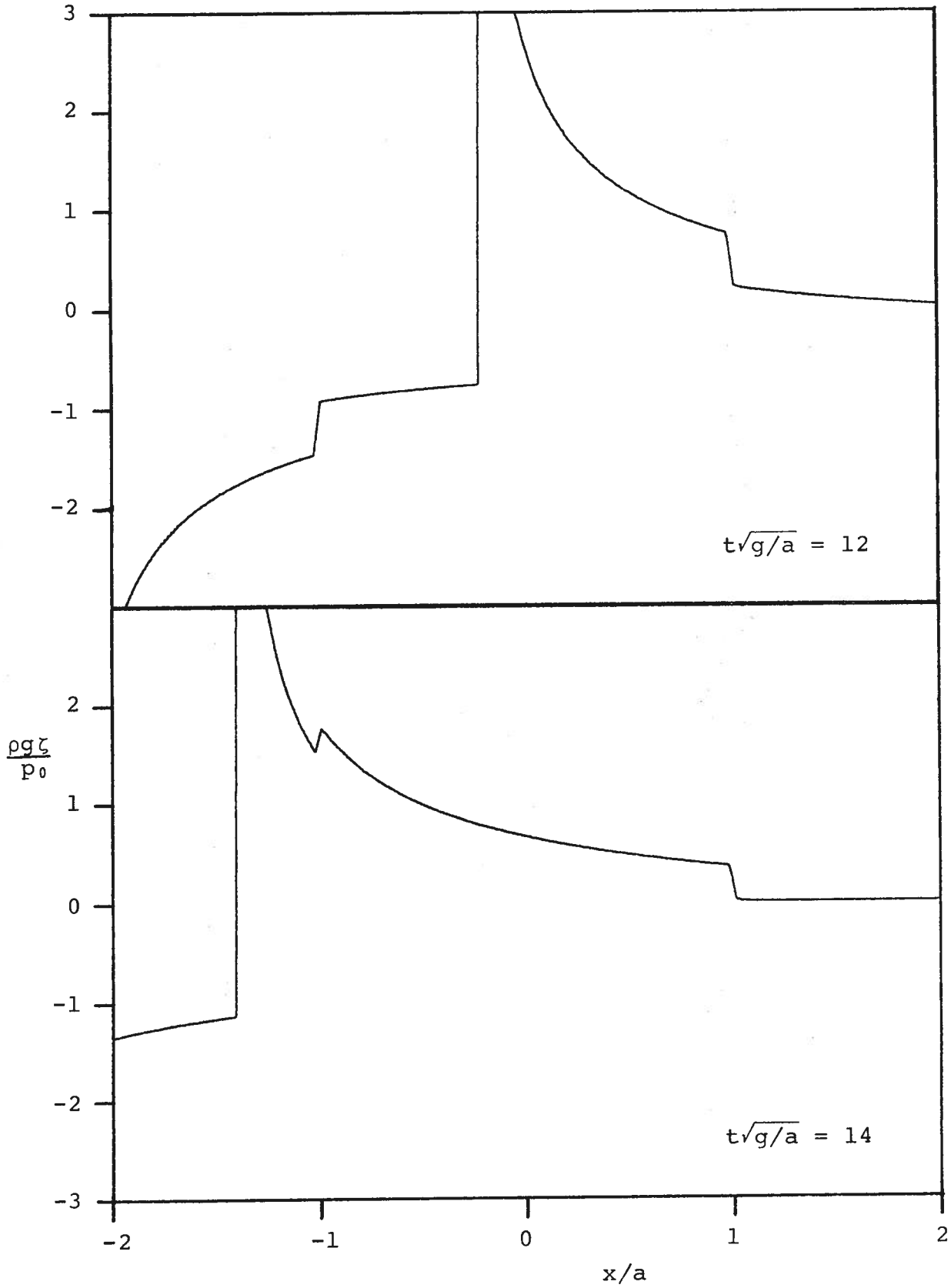
3
2
1
0
-1
-2
$t\sqrt{g/a} = 12$
2
1
0
-1
-2
-3
$t\sqrt{g/a} = 14$
$\frac{\rho g \zeta}{p_0}$
-2
-1
0
1
2
x/a

Fig. 22 (a) (cont.)

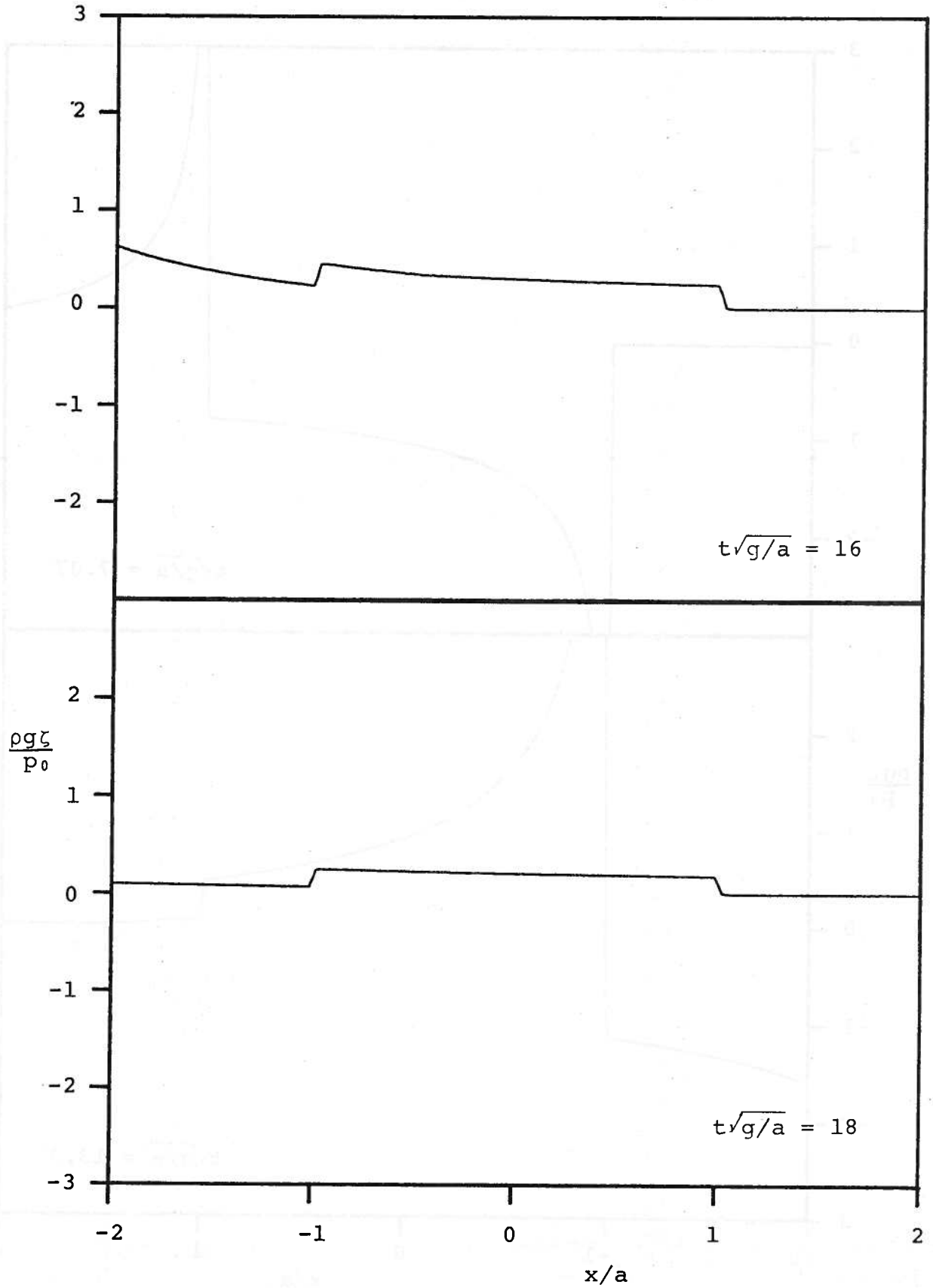
3
2
1
0
-1
-2
$t\sqrt{g/a} = 16$
2
1
0
-1
-2
-3
$\frac{\rho g \zeta}{p_0}$
$t\sqrt{g/a} = 18$
-2
-1
0
1
2
x/a

Fig. 22 (a) (cont.)

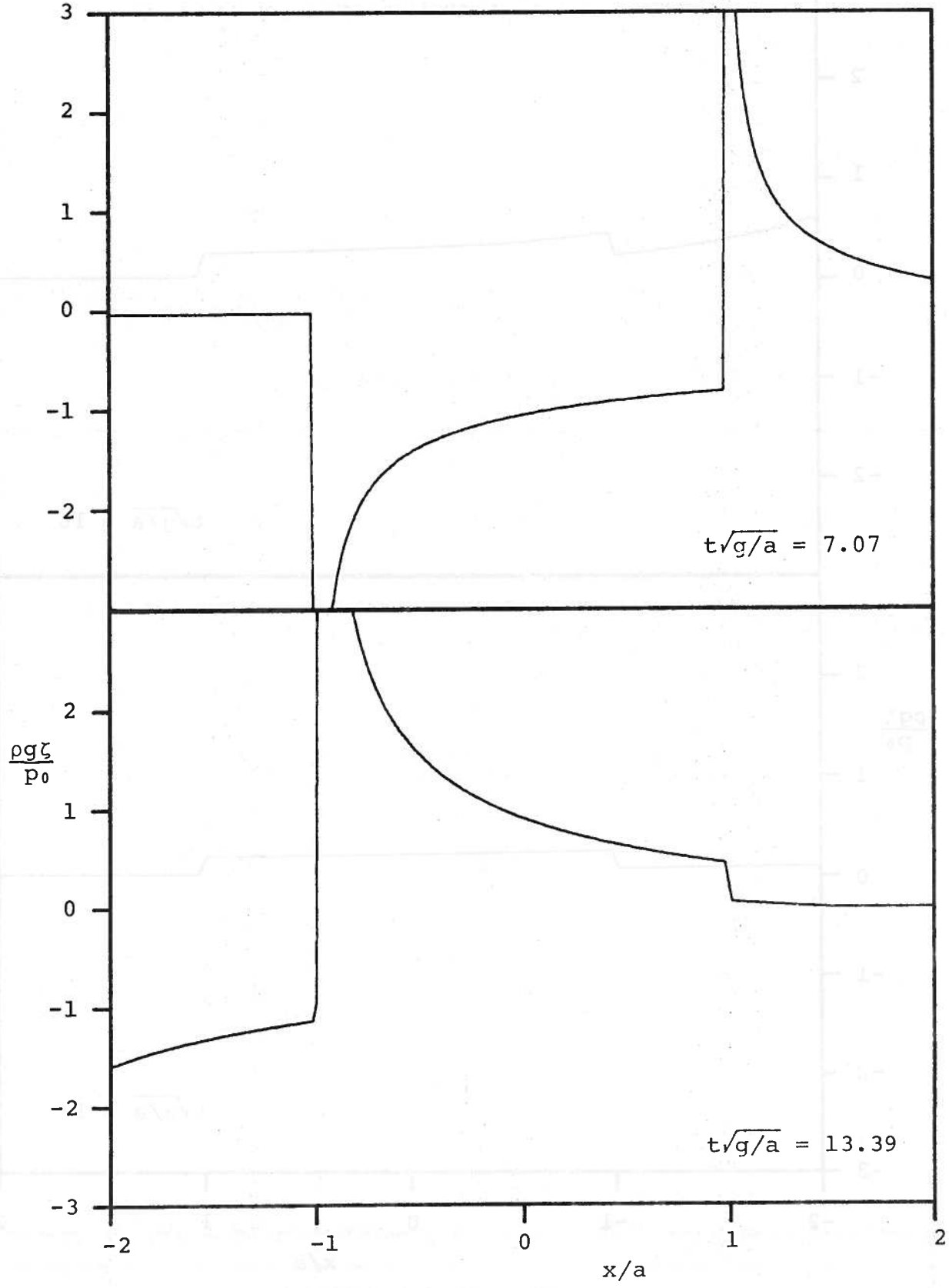

Fig. 22 (cont.) (b) For $t\sqrt{g/a}$ = 7.07 and 13.39

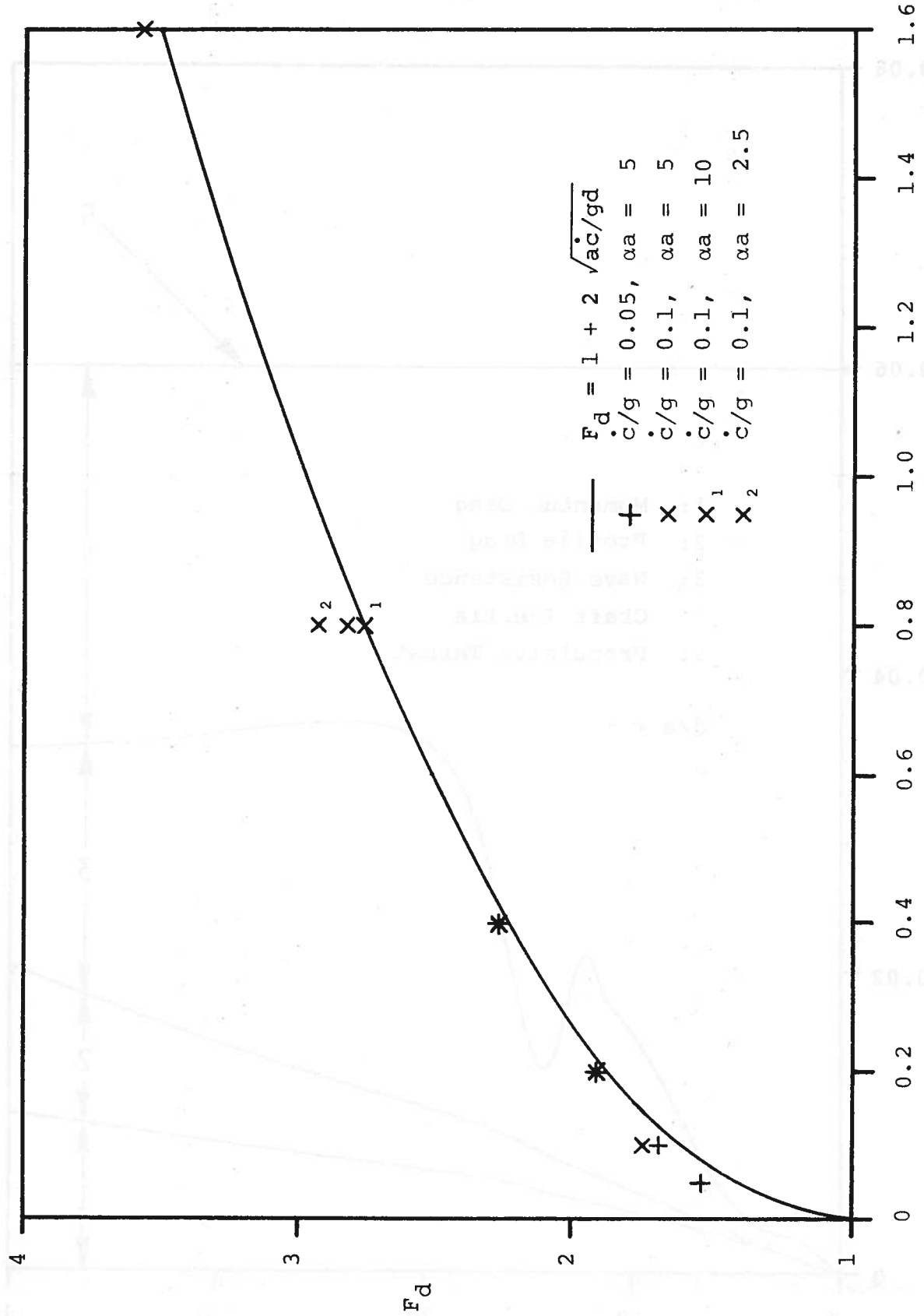

Fig. 23 Second Critical Depth Froude Number

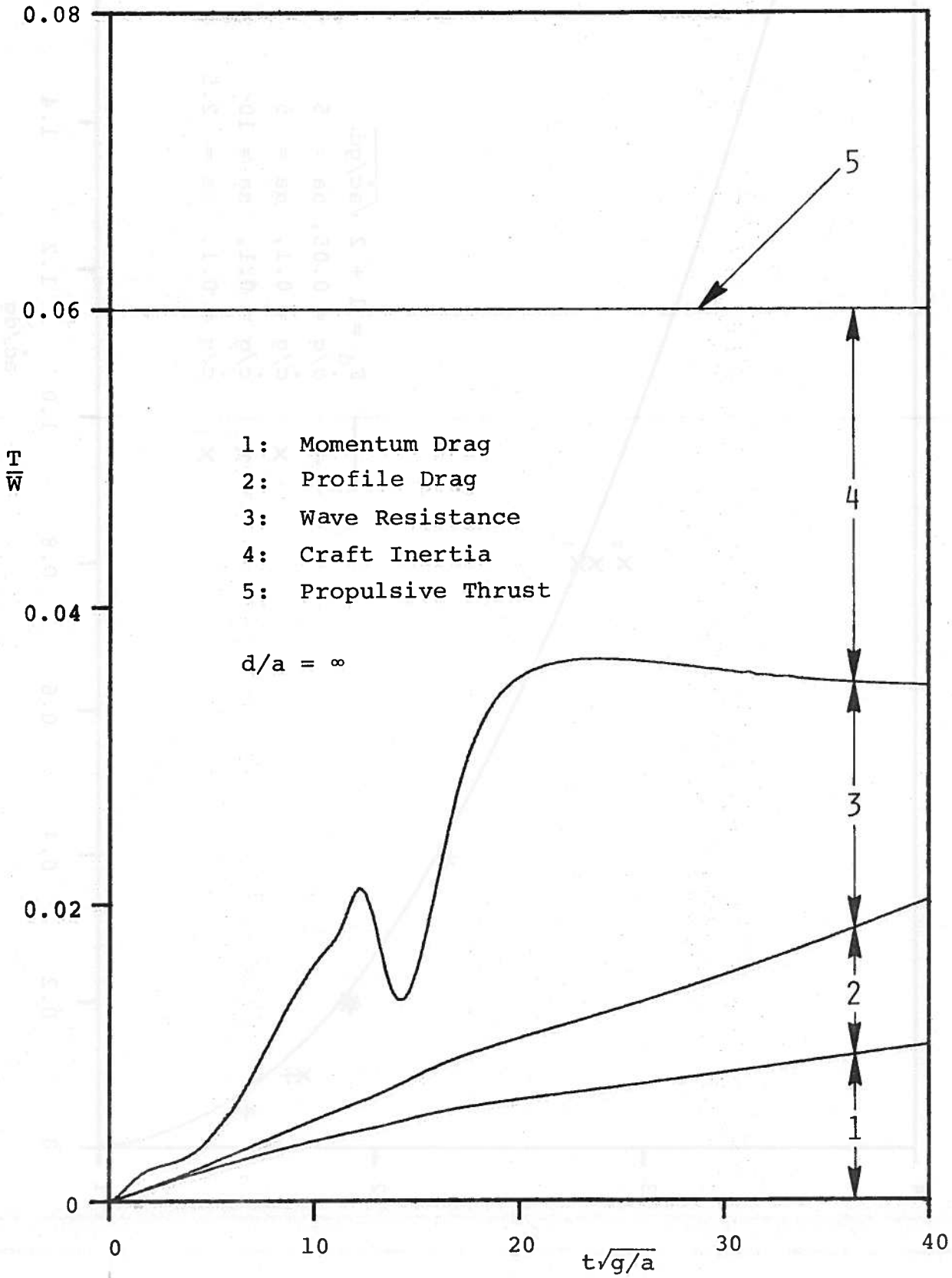

Fig. 24 Drag Components in Deep Water (Constant Thrust)
(a) T/W = 0.06

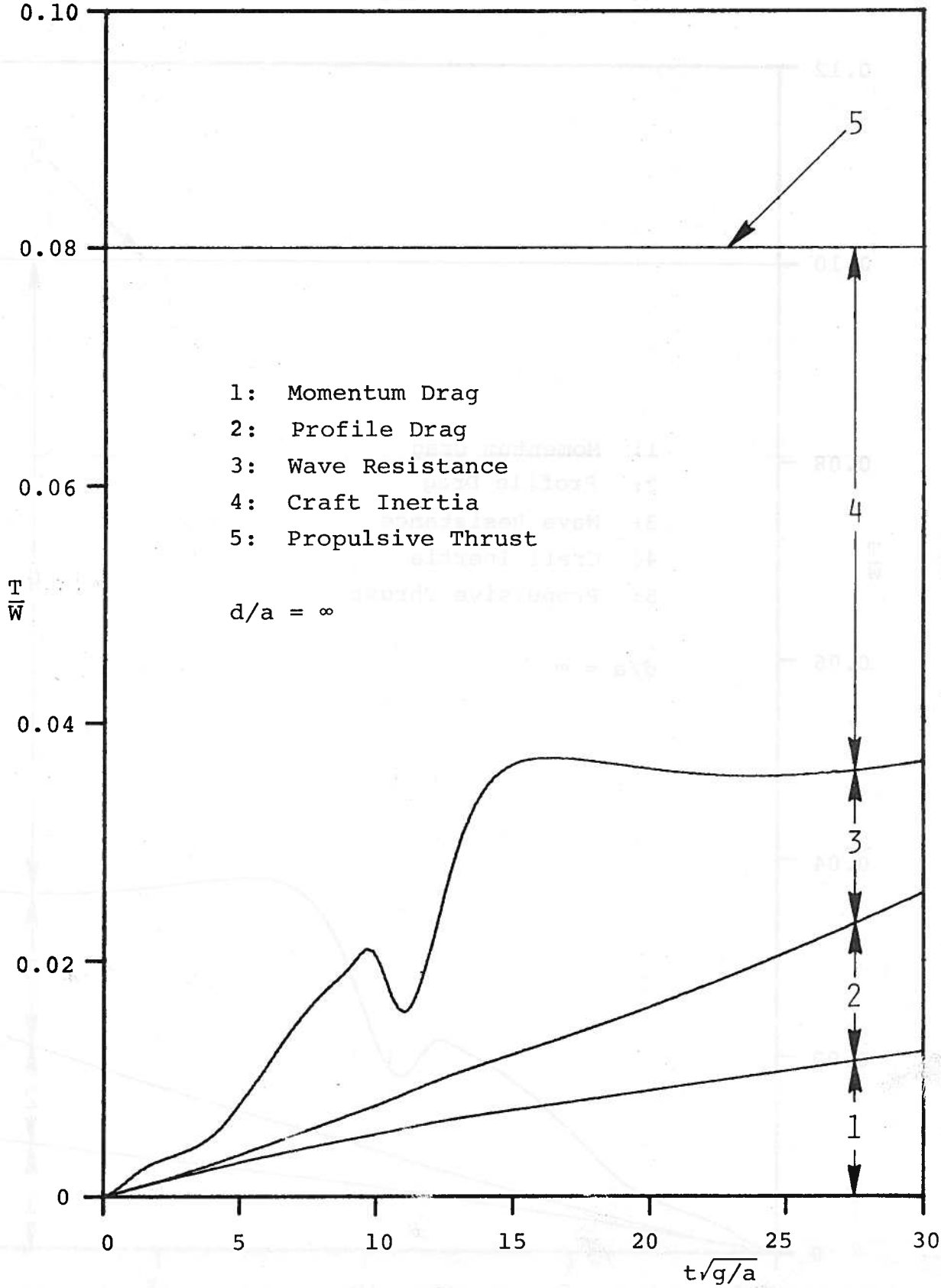

Fig. 24 (cont.) (b) T/W = 0.08

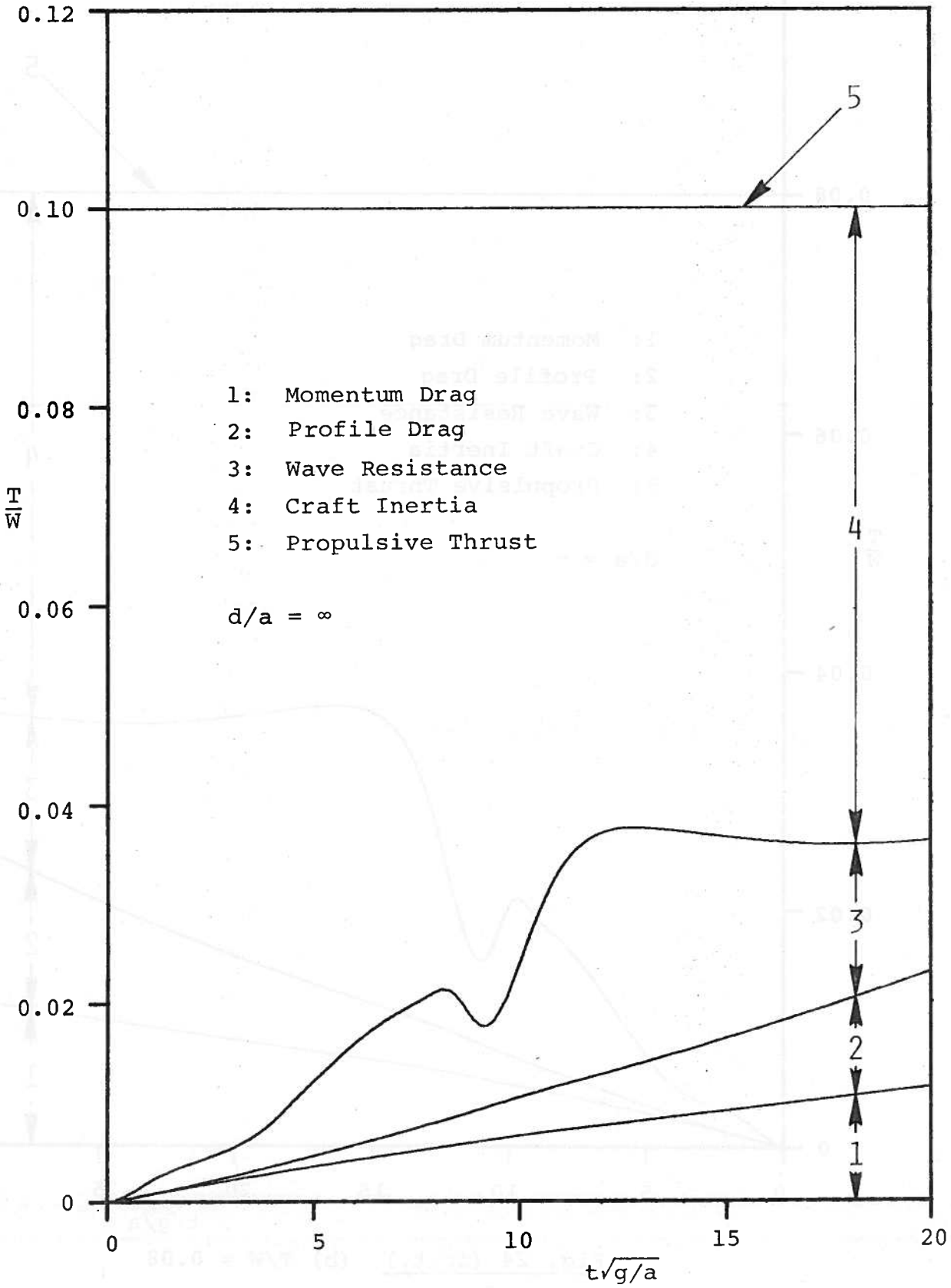

Fig. 24 (cont.) (c) T/W = 0.1

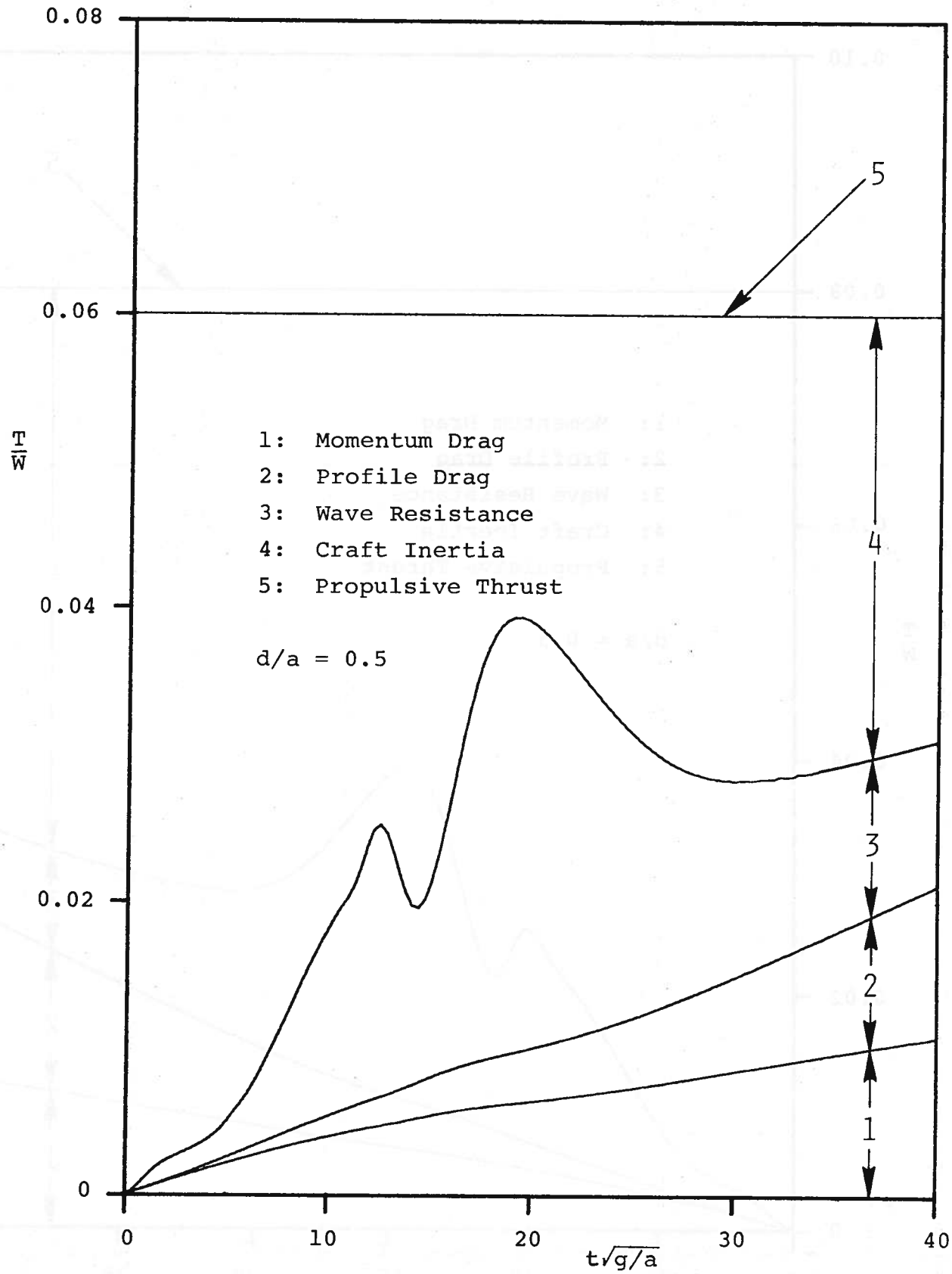

Fig. 25 Drag Components in Finite Depth (Constant Thrust)
(a) T/W = 0.06

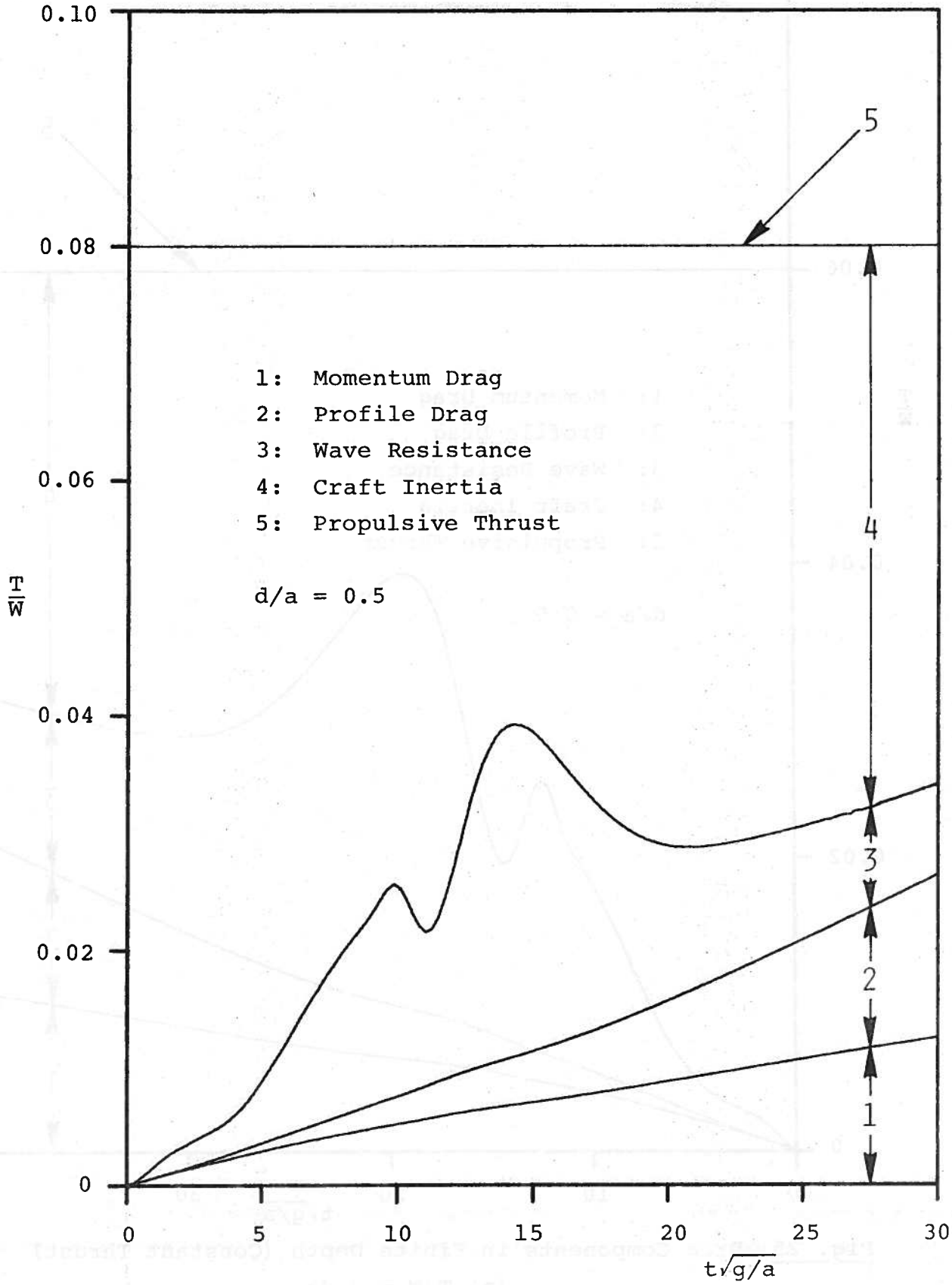

Fig. 25 (cont.) (b) T/W = 0.08

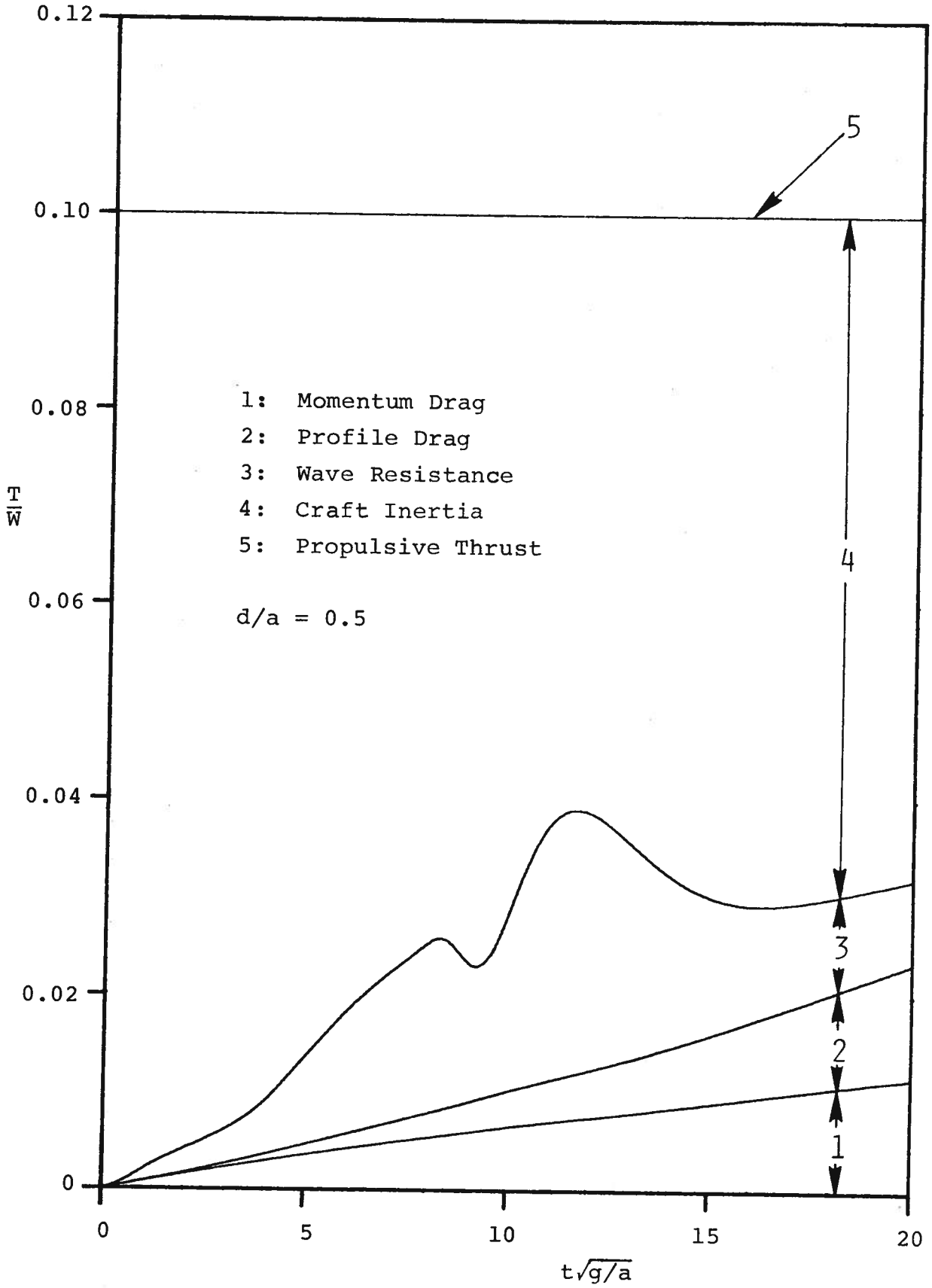

Fig. 25 (cont.) (c) T/W = 0.1

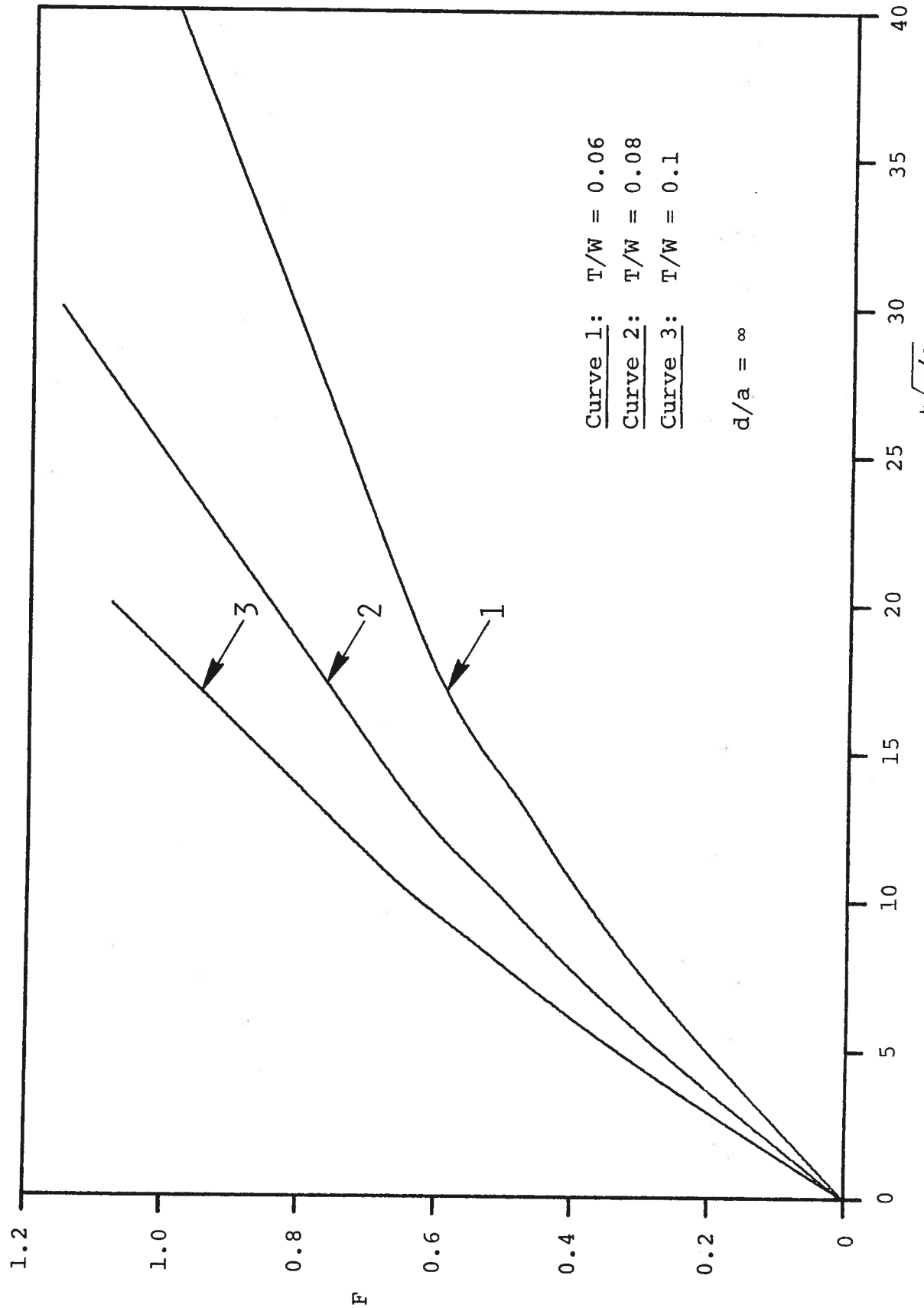

Fig. 26 Velocity Pattern in Deep Water (Constant Thrust)

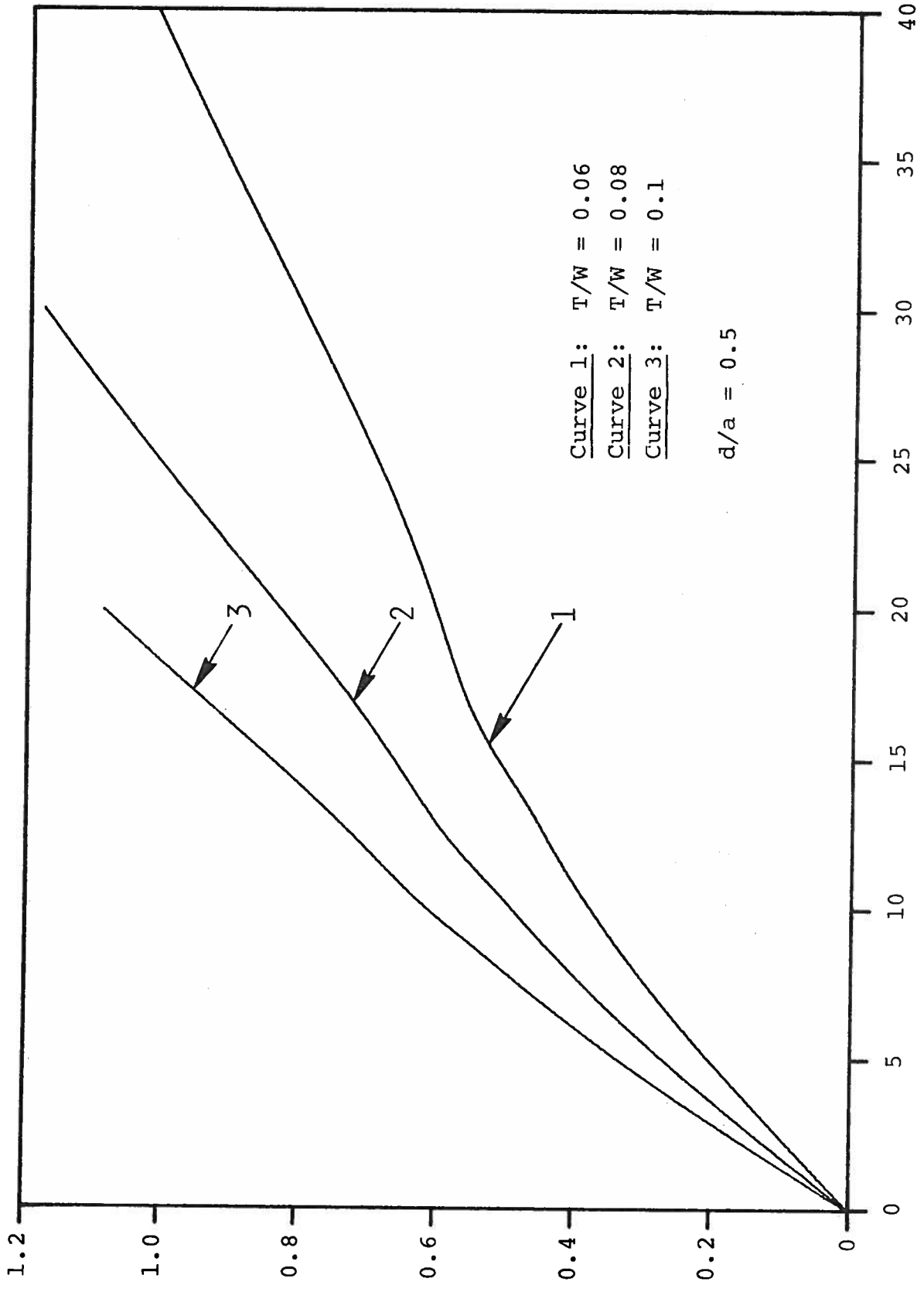

Fig. 27 Velocity Pattern in Finite Depth (Constant Thrust)

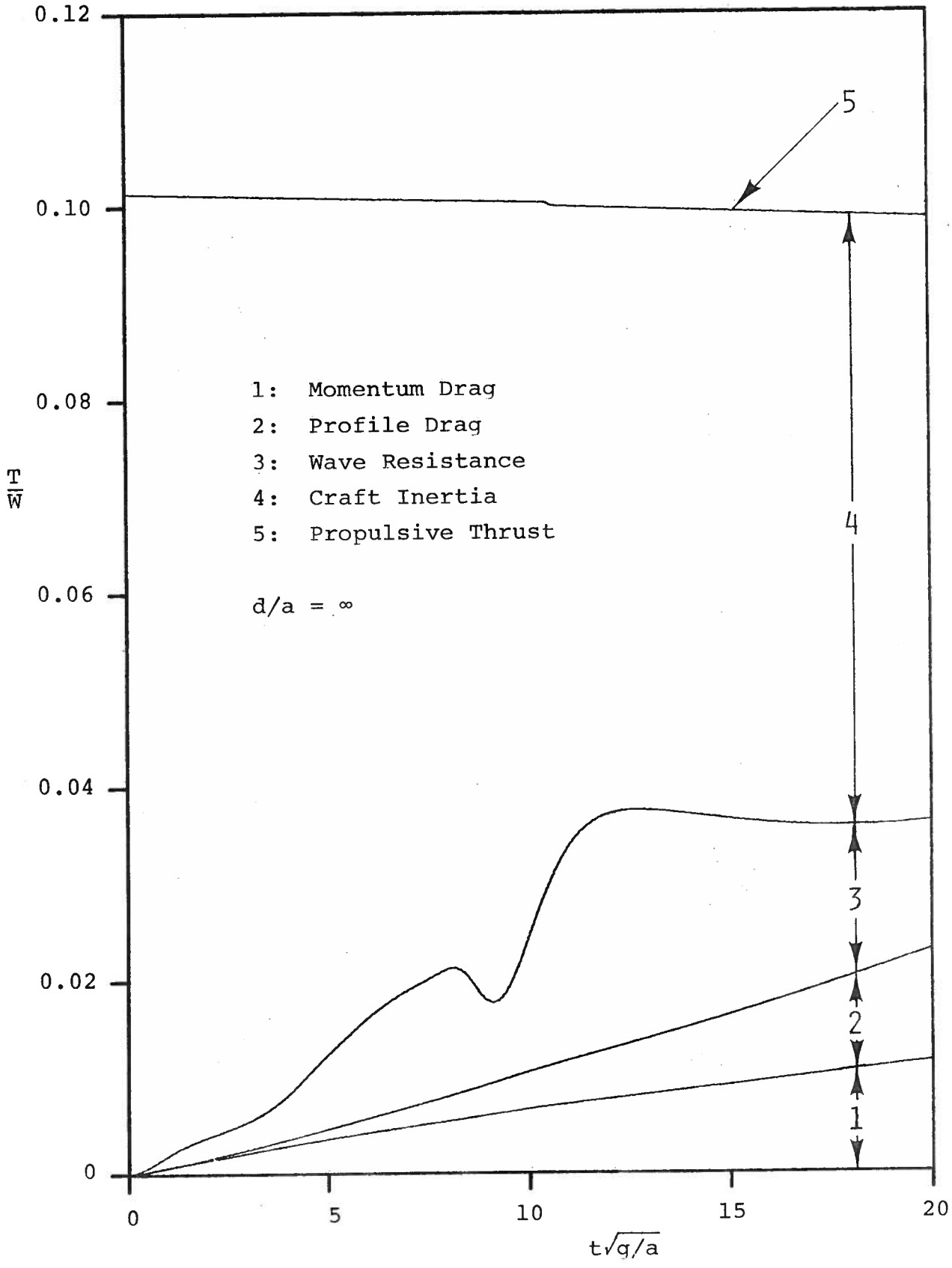

Fig. 28 Drag Components in Deep Water (Constant Prop. Power)

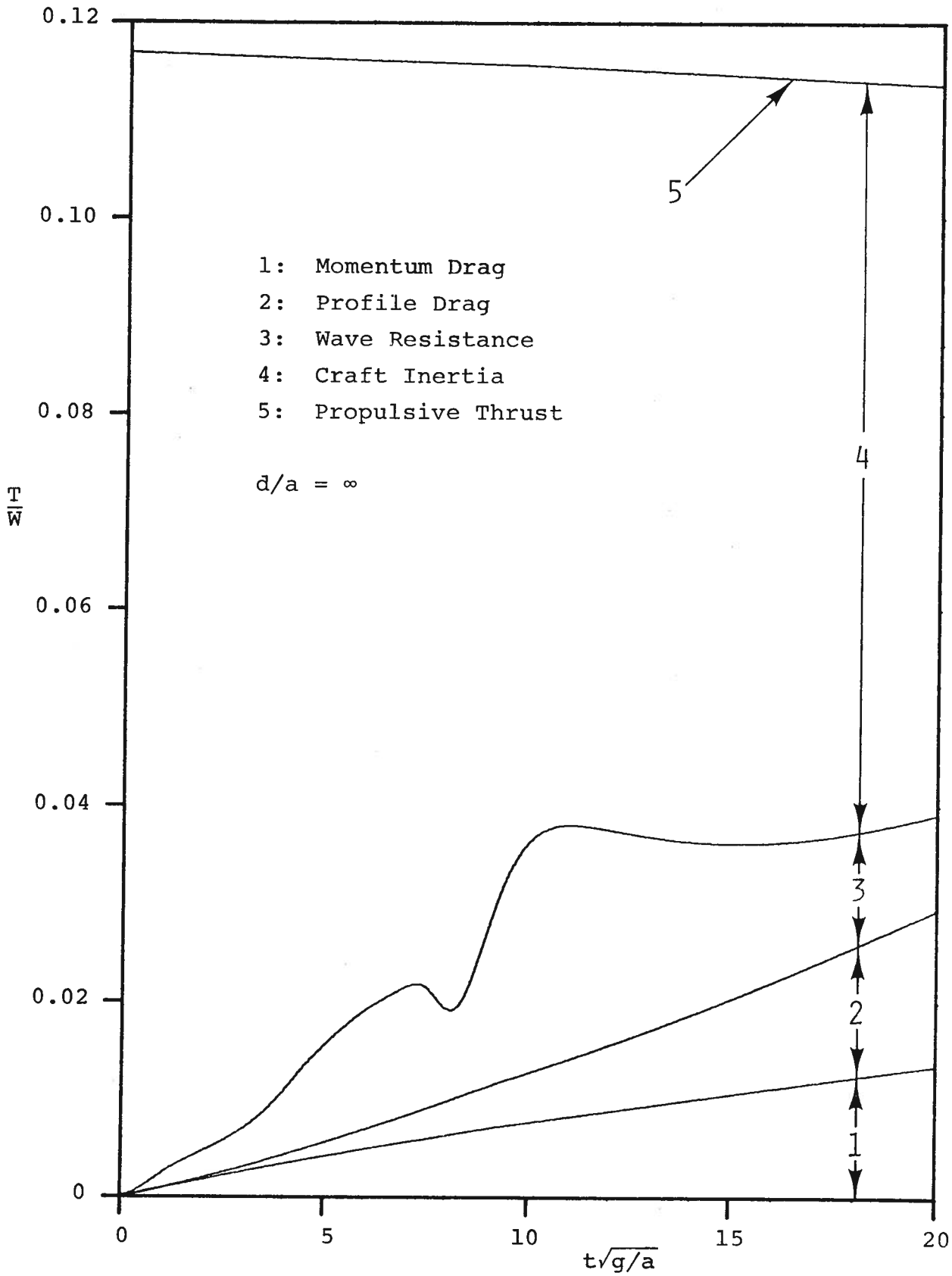

Fig. 29 Drag Components in Deep Water (Constant. Prop. Revs.)
(a) Normal Load

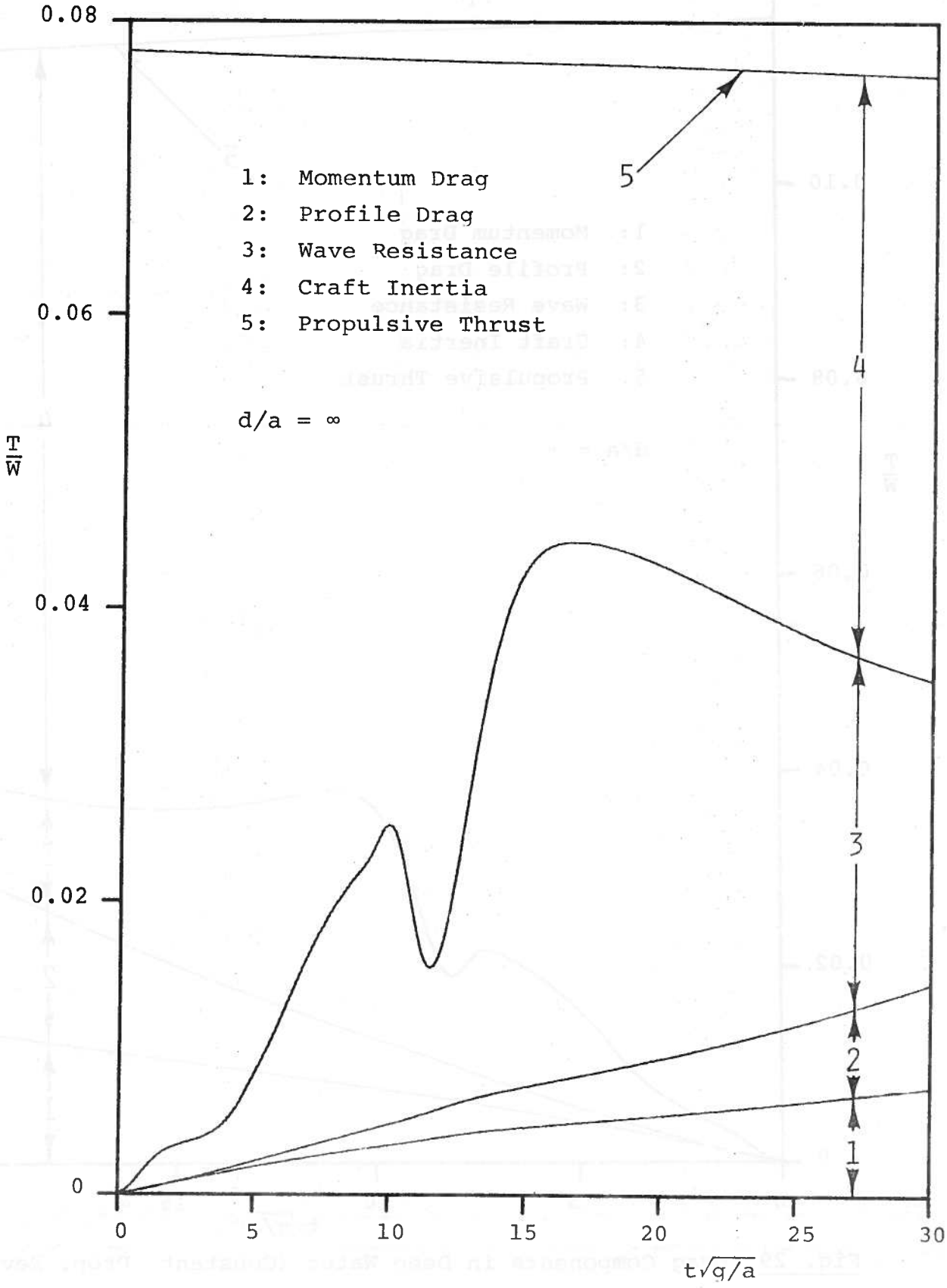

Fig. 29 (cont.) (b) 50% Overload

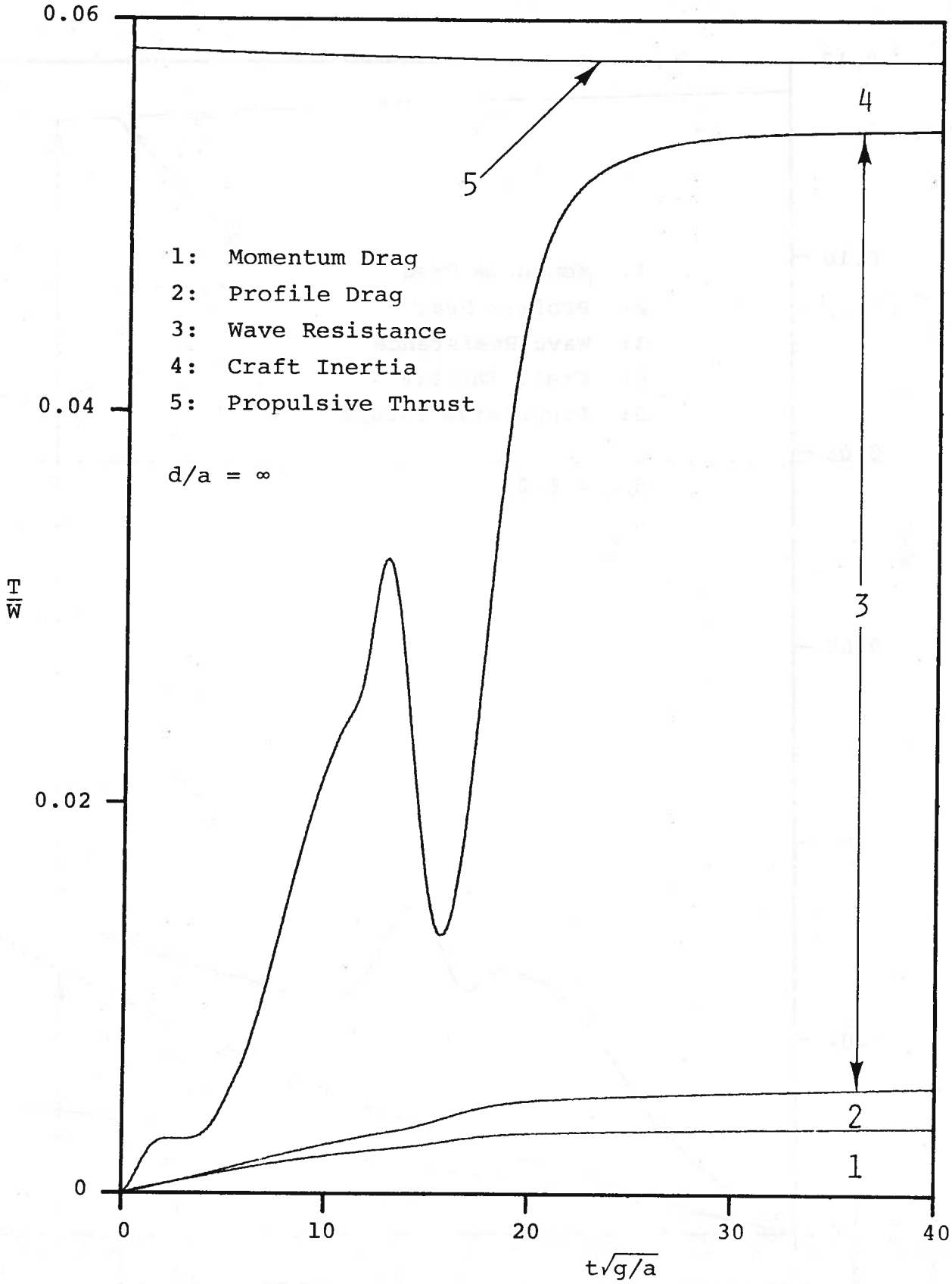

Fig. 29 (cont.) (c) 100% Overload

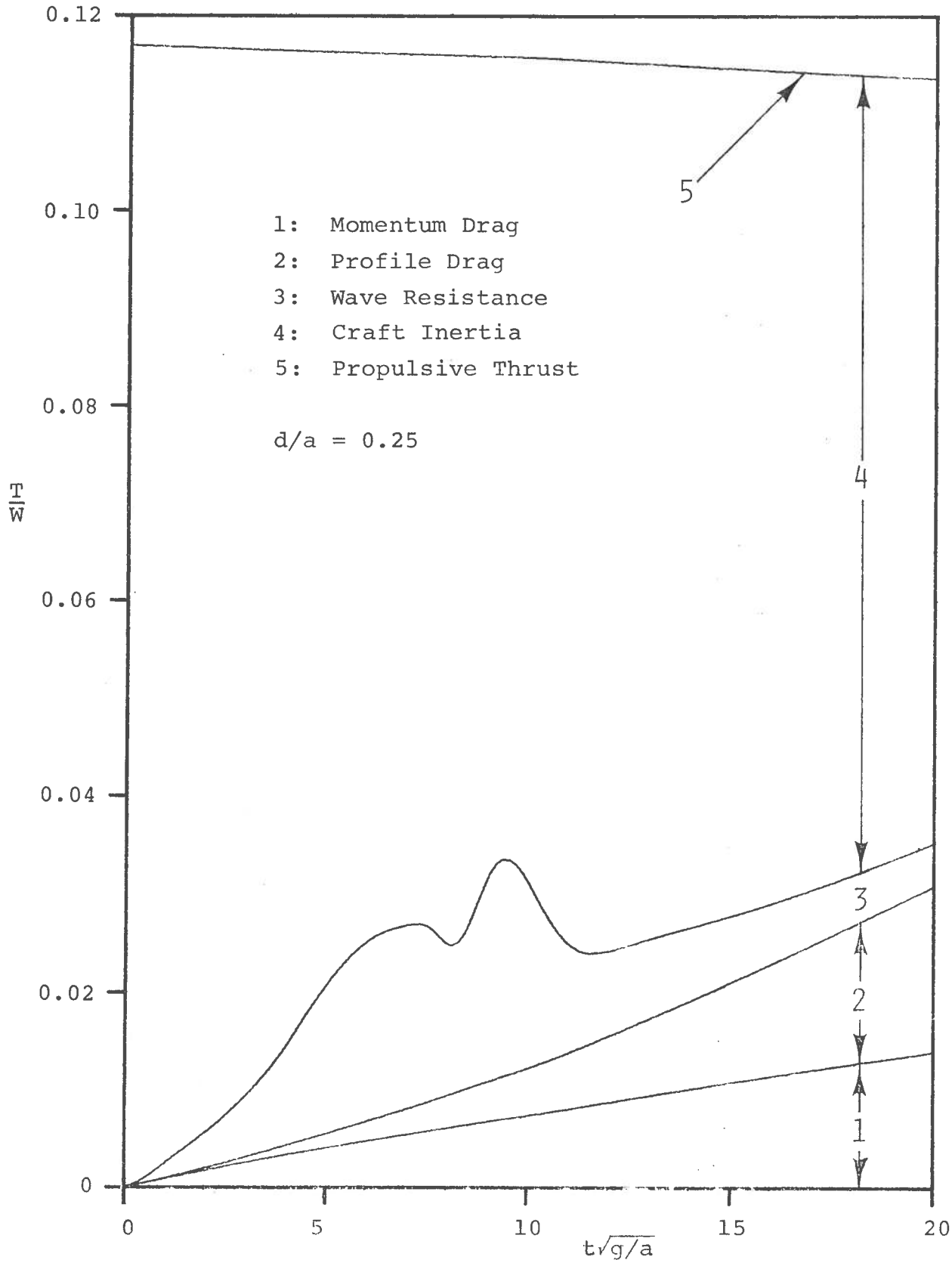

Fig. 30 Drag Components in Finite Depth (Constant Prop. Revs.)
(a) Normal Load

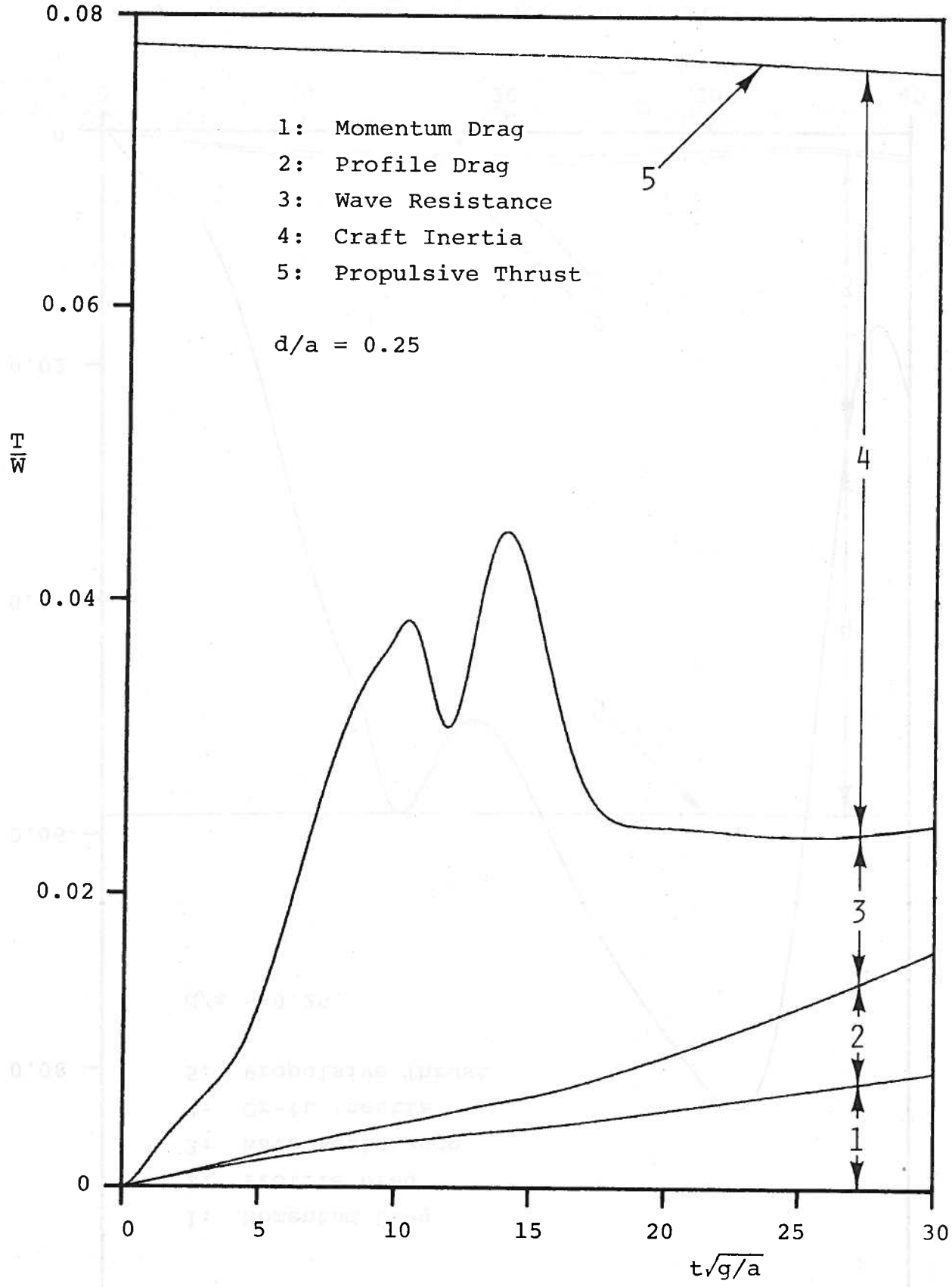

Fig. 30 (cont.) (b) 50% Overload

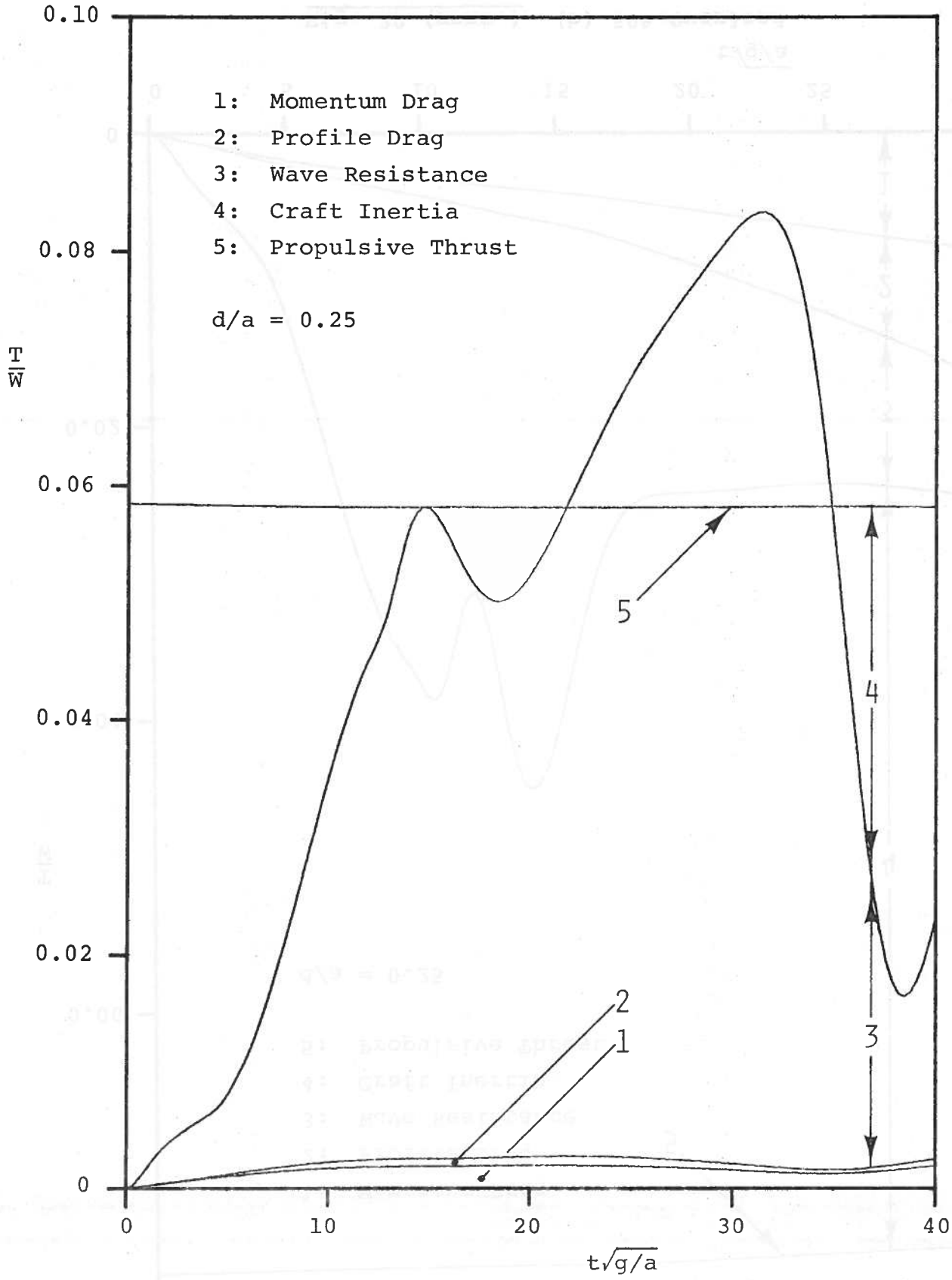

Fig. 30 (cont.) (c) 100% Overload

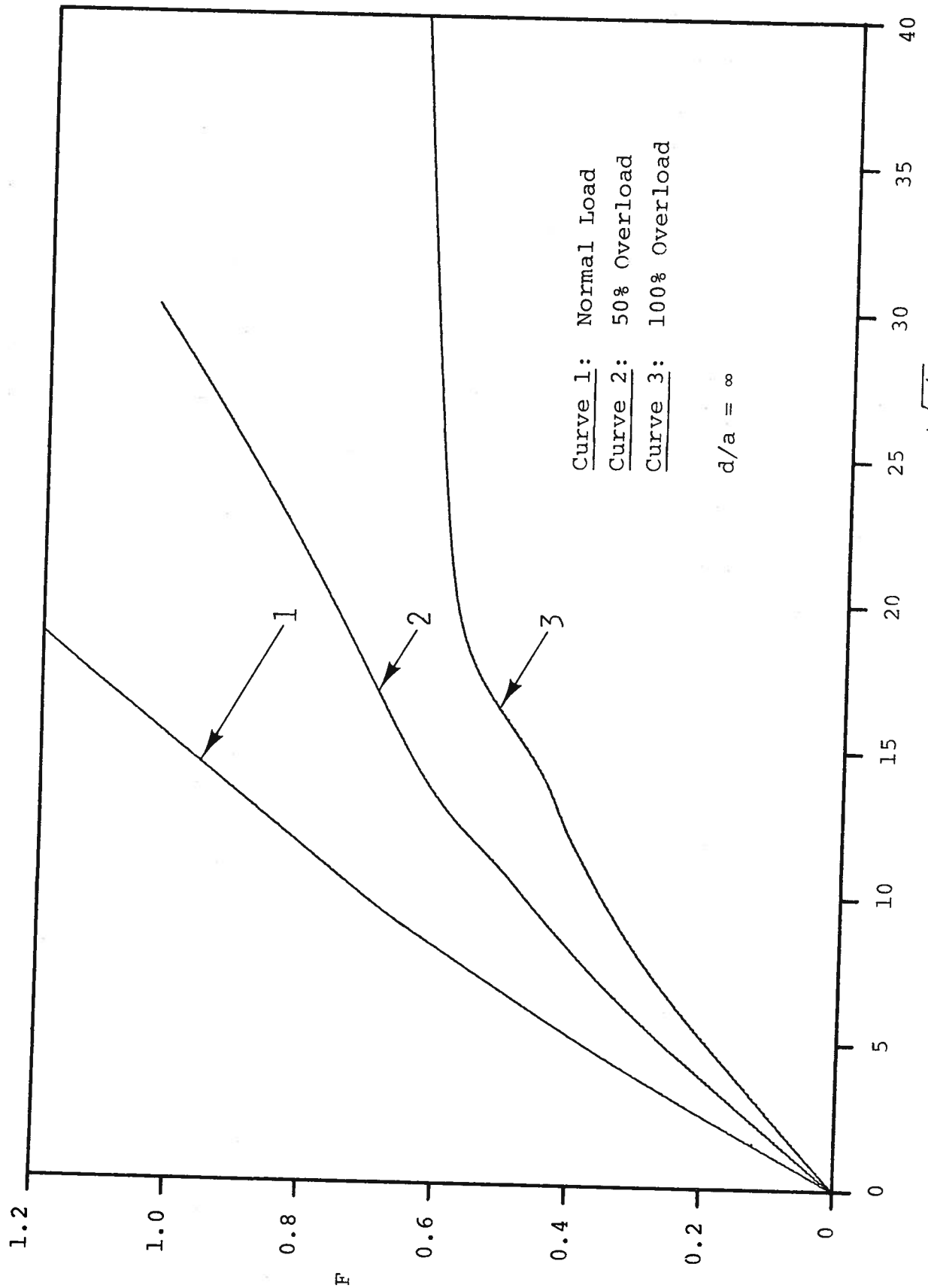

Fig. 31 Velocity Pattern in Deep Water (Constant Propeller Revolutions)

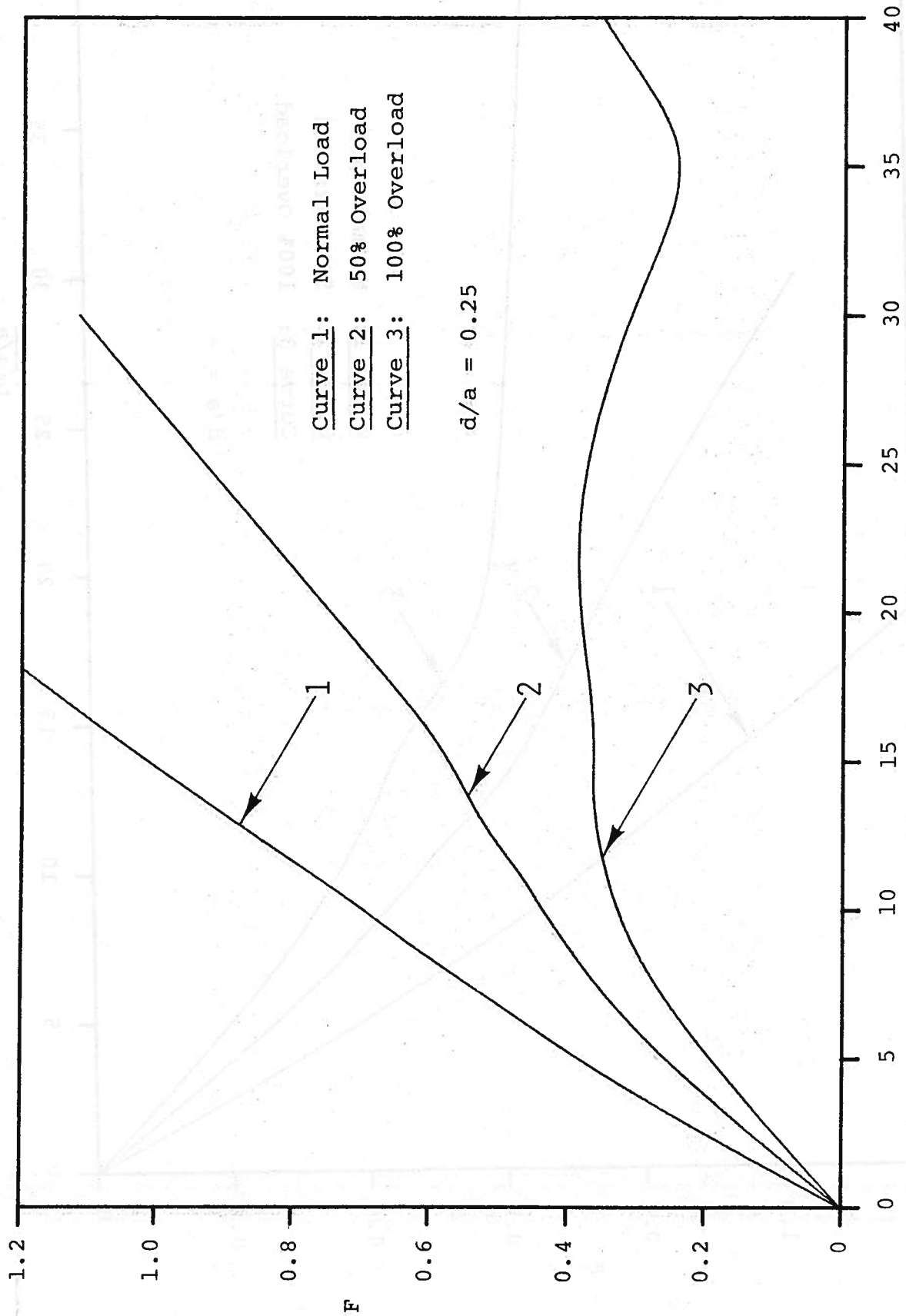

Fig. 32 Velocity Pattern in Finite Depth (Constant Propeller Revolutions)

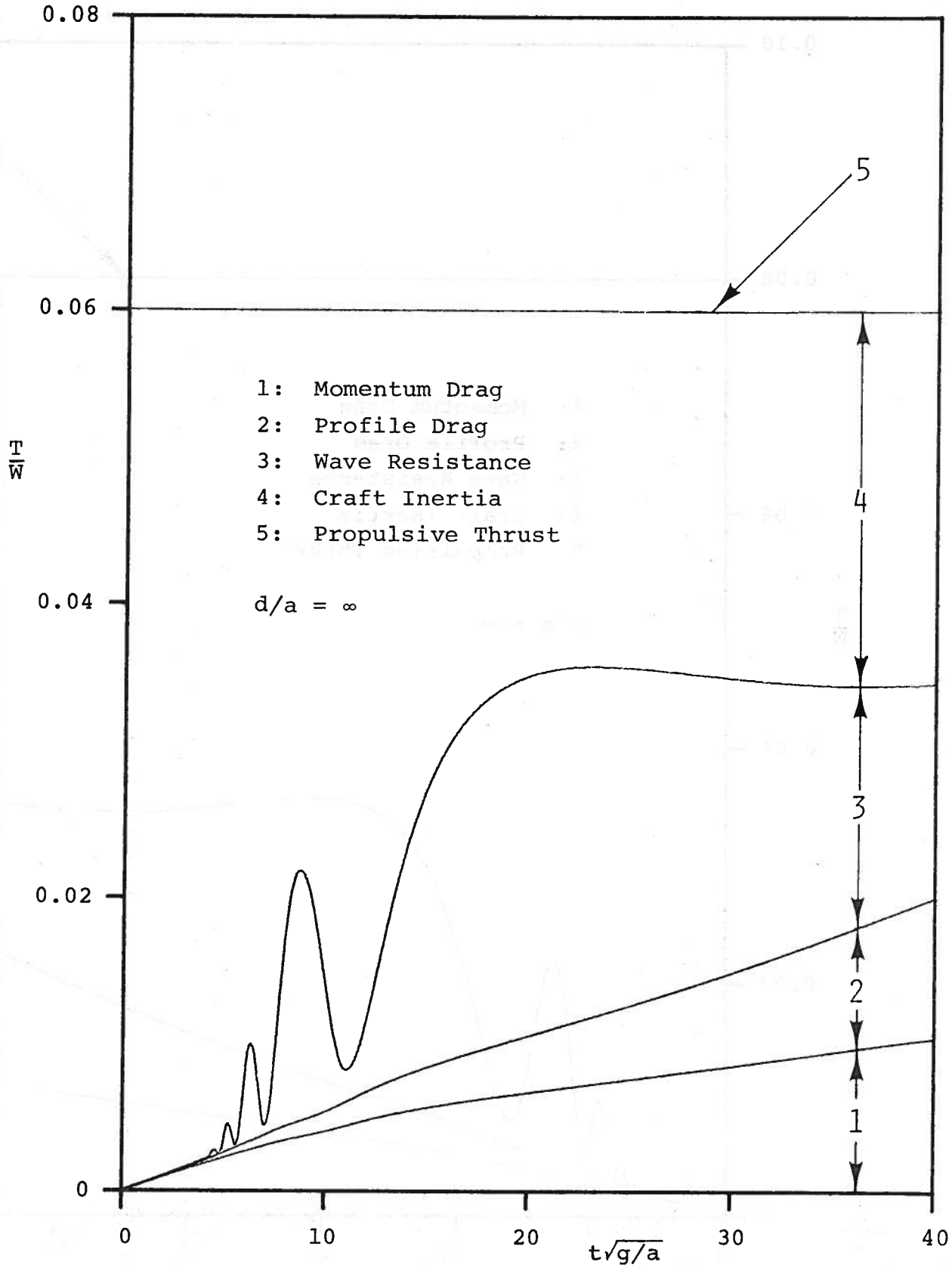

Fig. 33 QS Drag Components in Deep Water (Constant Thrust)
(a) T/W = 0.06

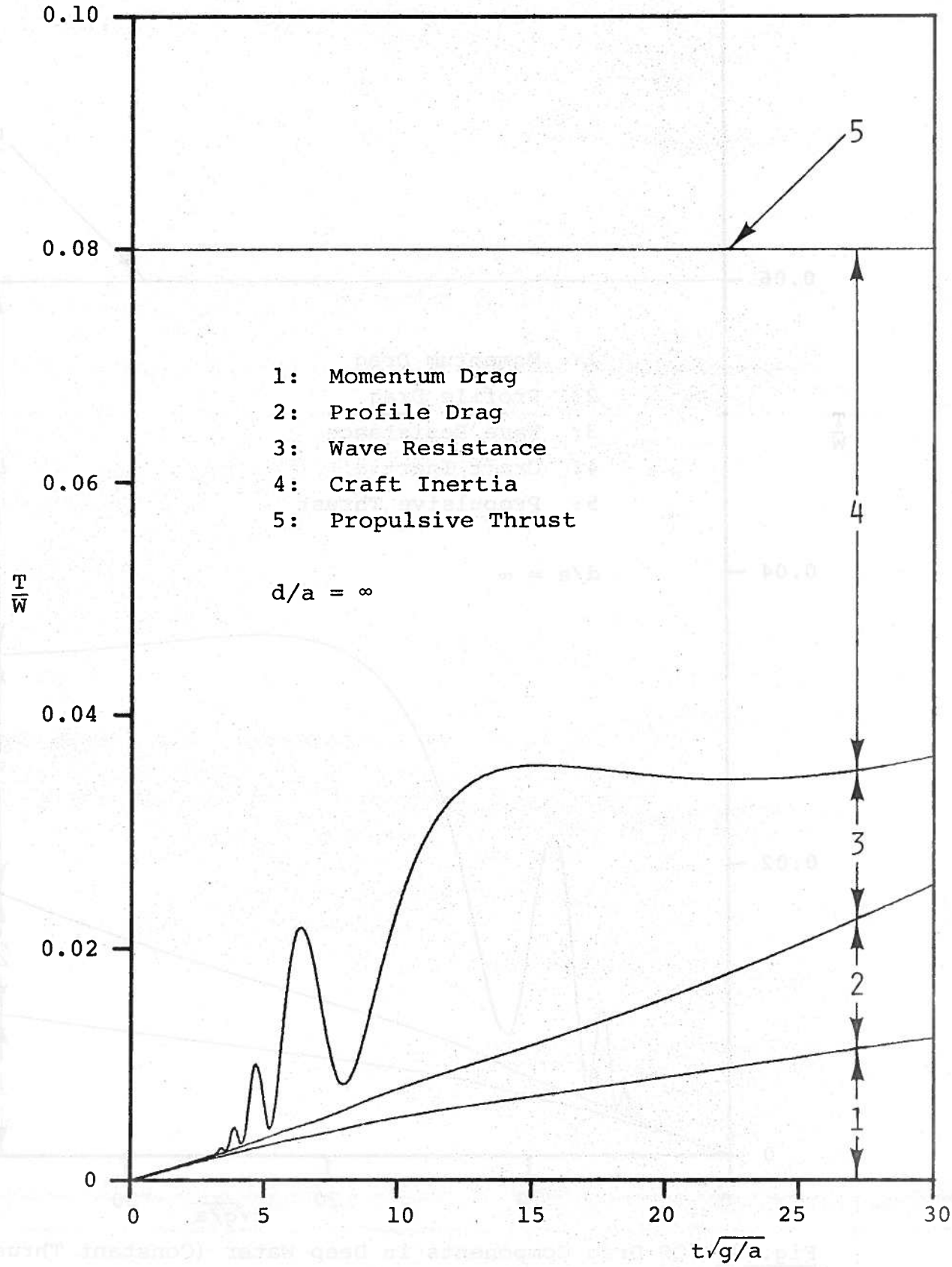

Fig. 33 (cont.) (b) T/W = 0.08

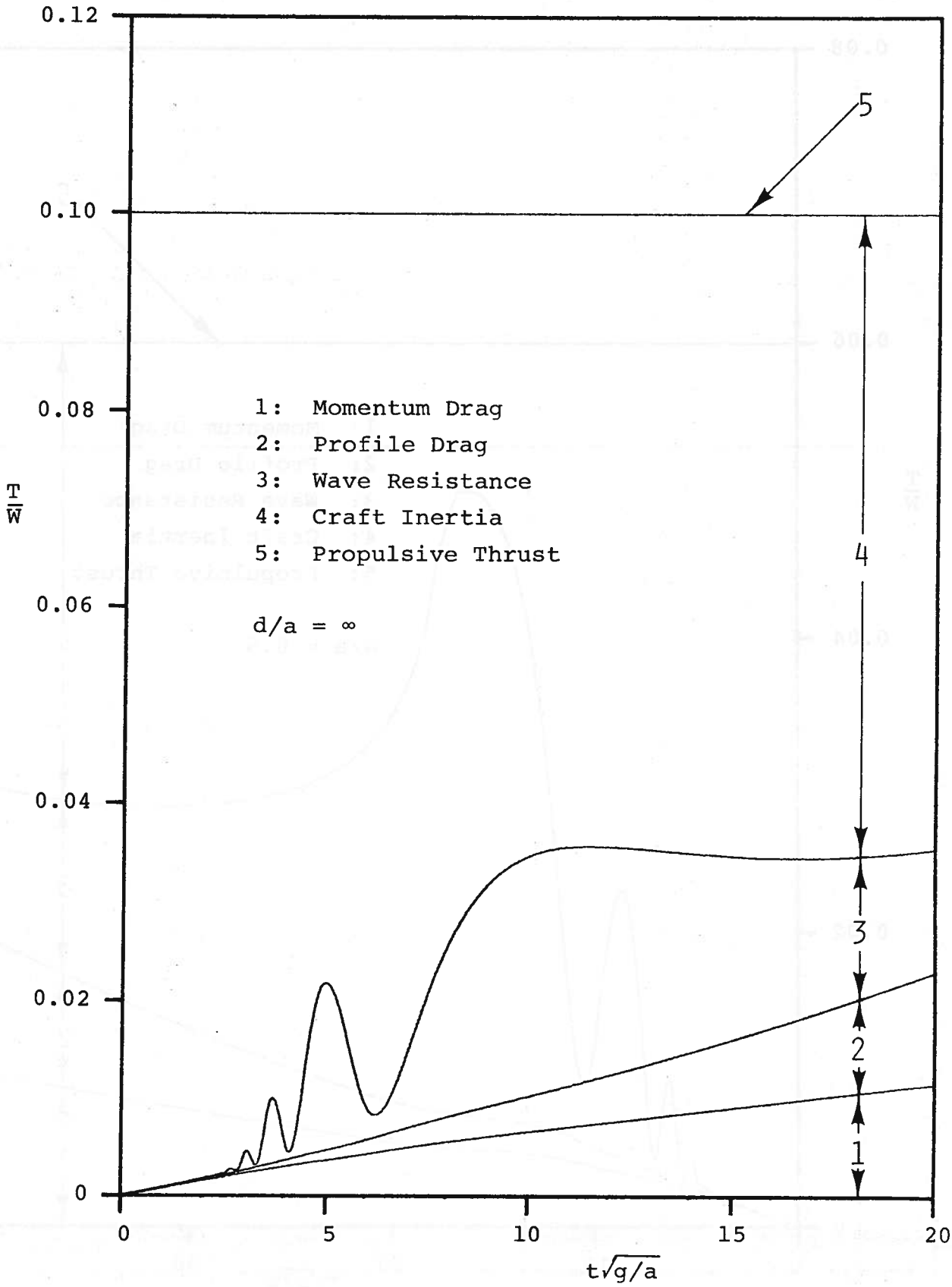

Fig. 33 (cont.) (c) T/W = 0.1

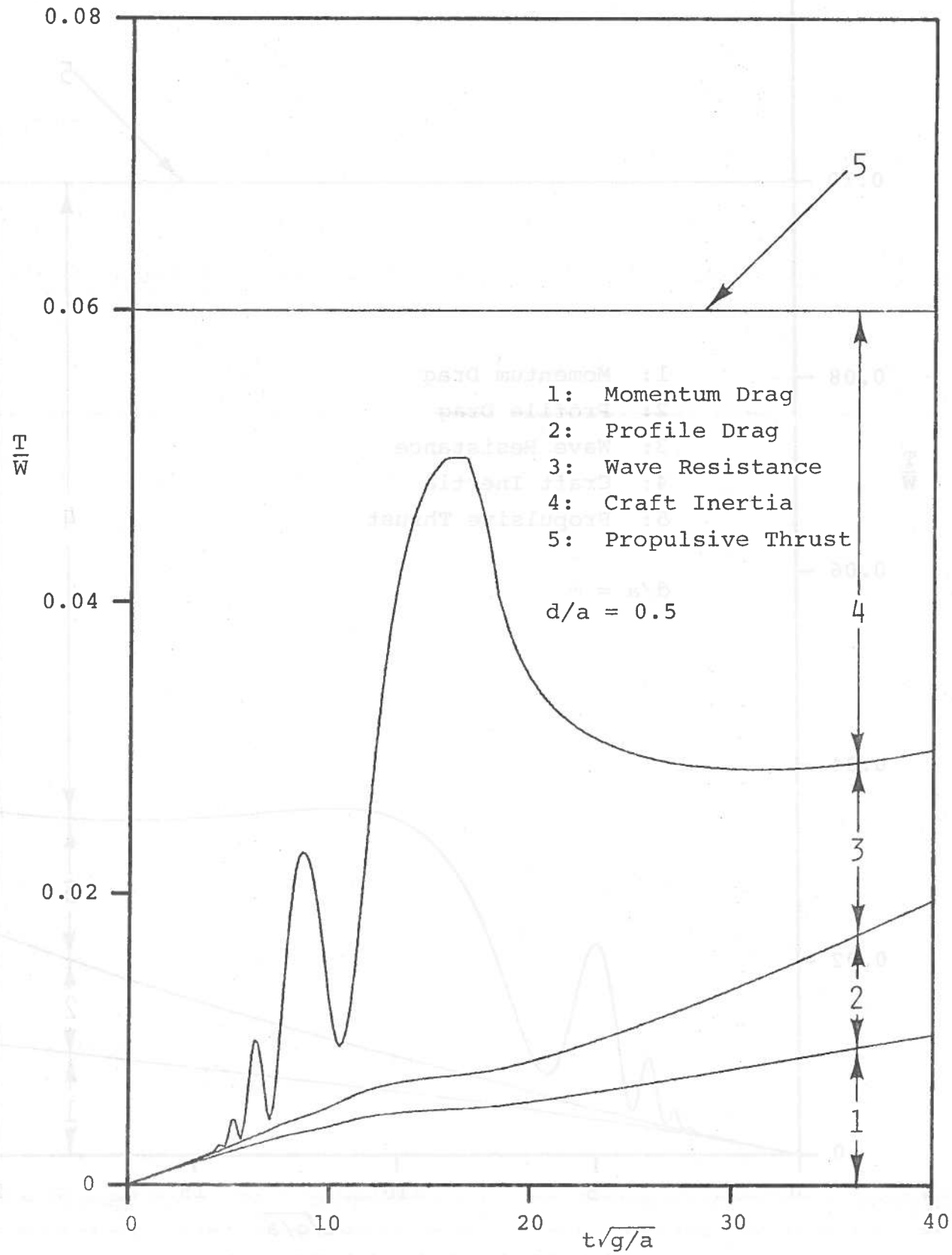

Fig. 34 QS Drag Components in Finite Depth (Constant Thrust)
(a) T/W = 0.06

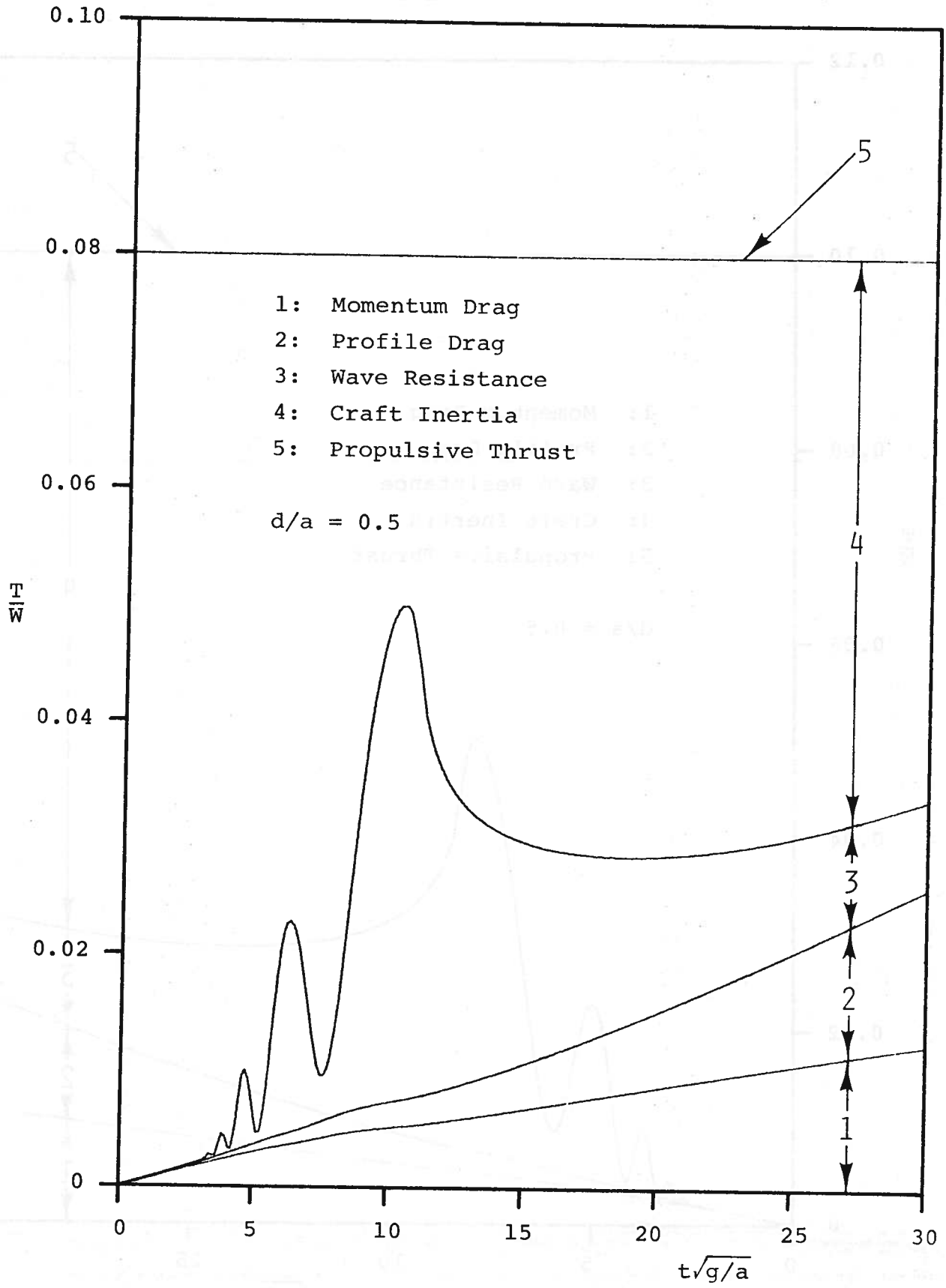

Fig. 34 (cont.) (b) T/W = 0.8

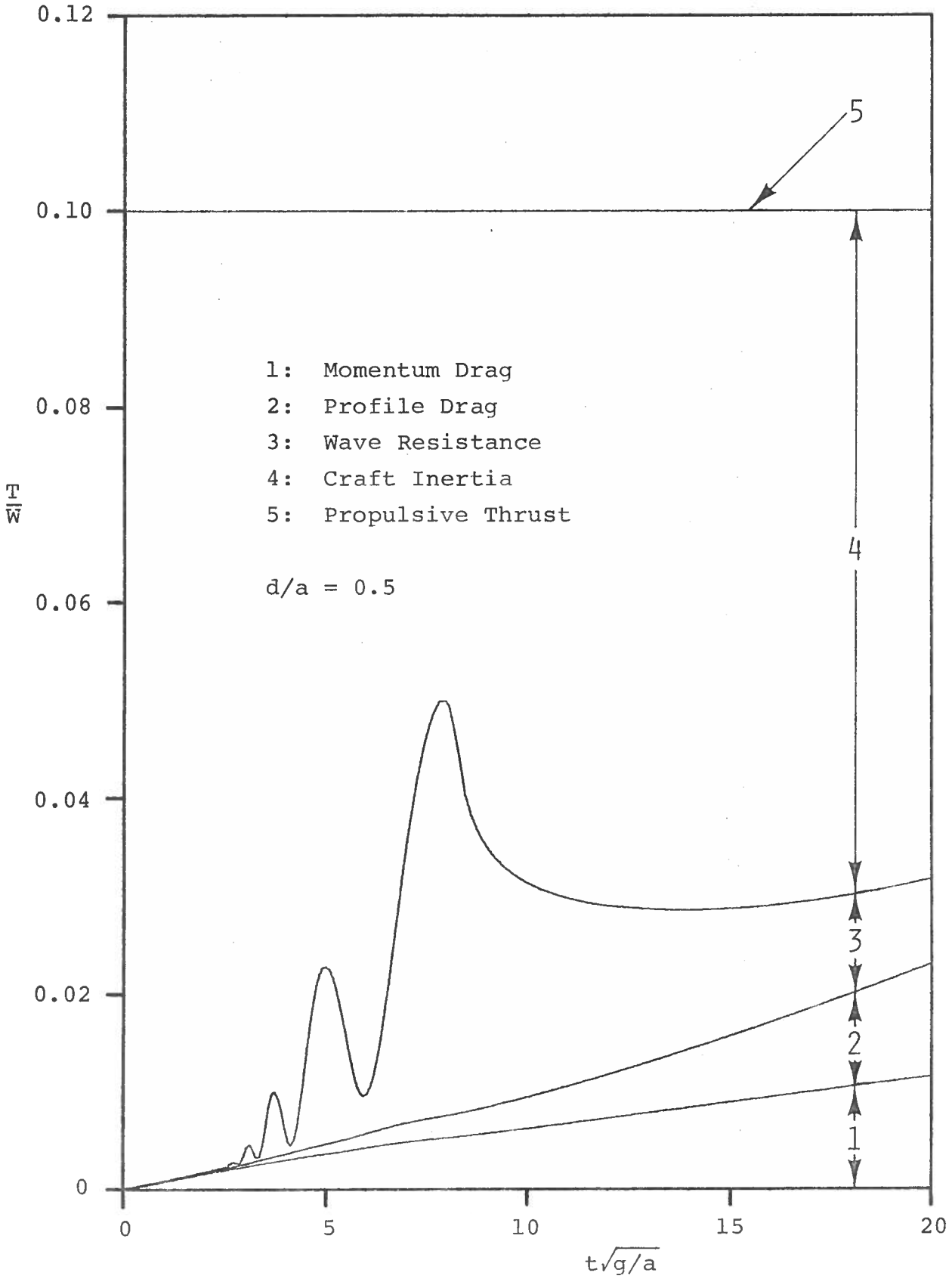

Fig. 34 (cont.) (c) T/W = 0.1

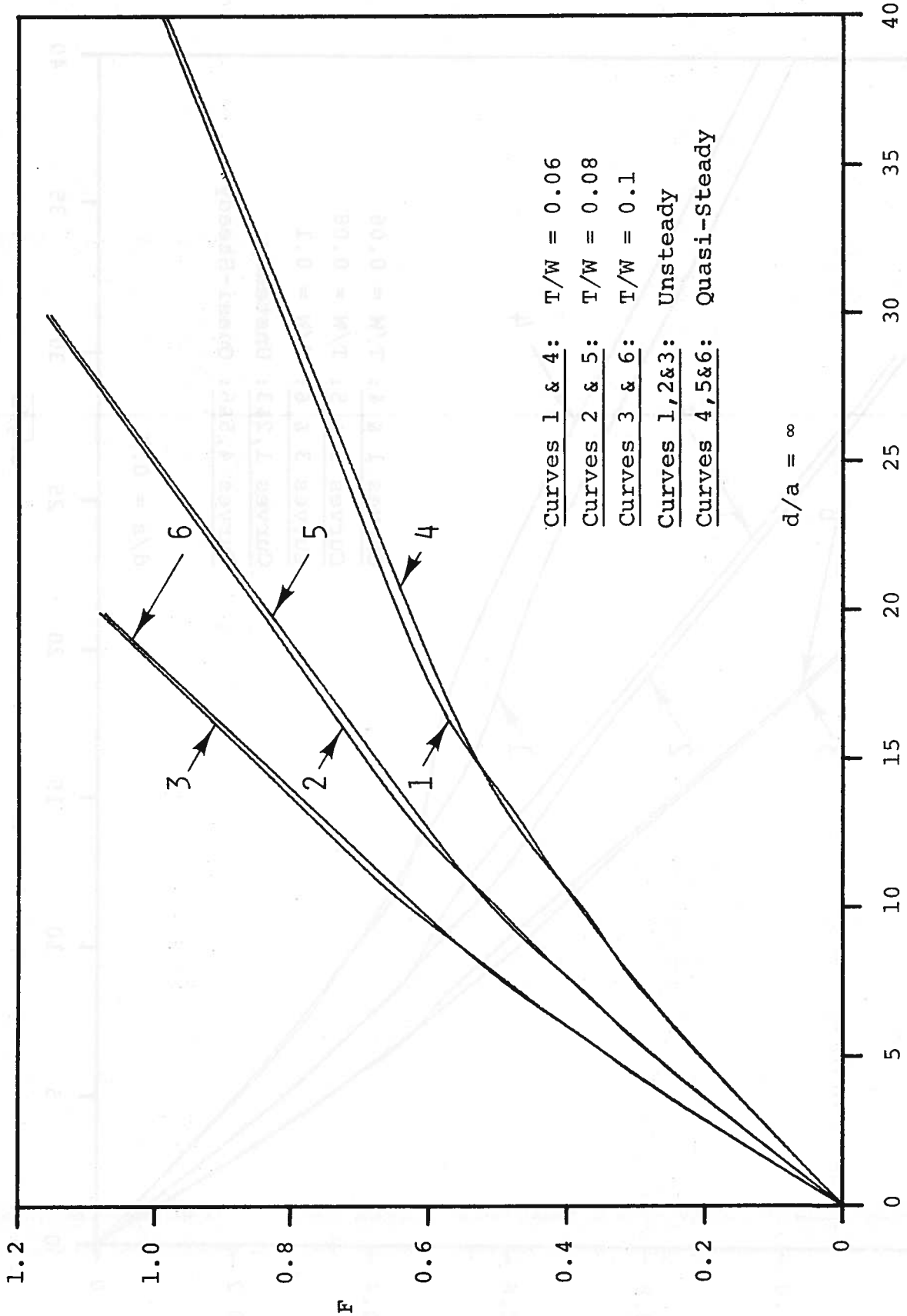

Fig. 35 Quasi-Steady and Unsteady Velocity Patterns in Deep Water (Constant Thrust)

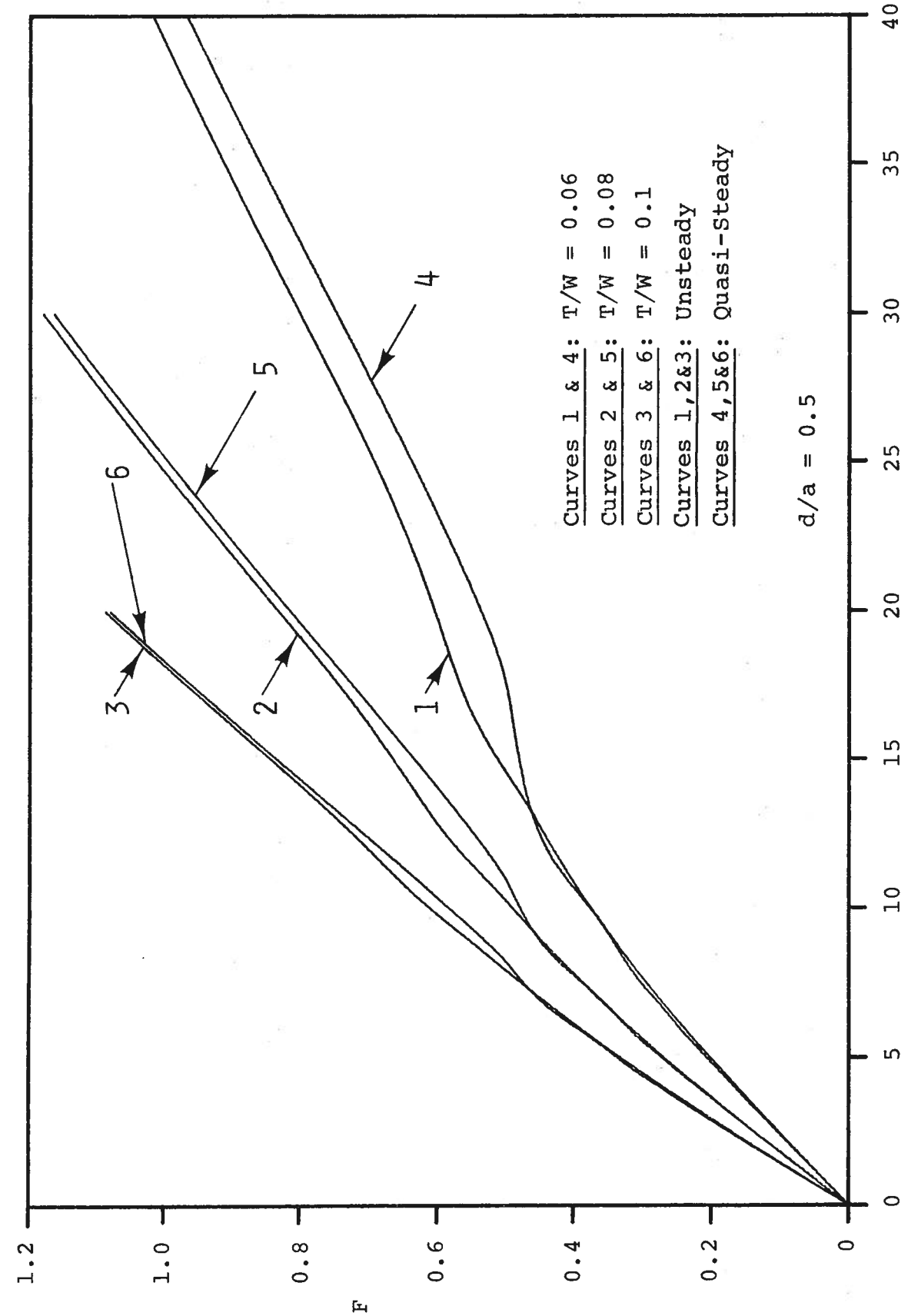

Fig. 36 Quasi-Steady and Unsteady Velocity Patterns in Finite Depth (Constant Thrust)

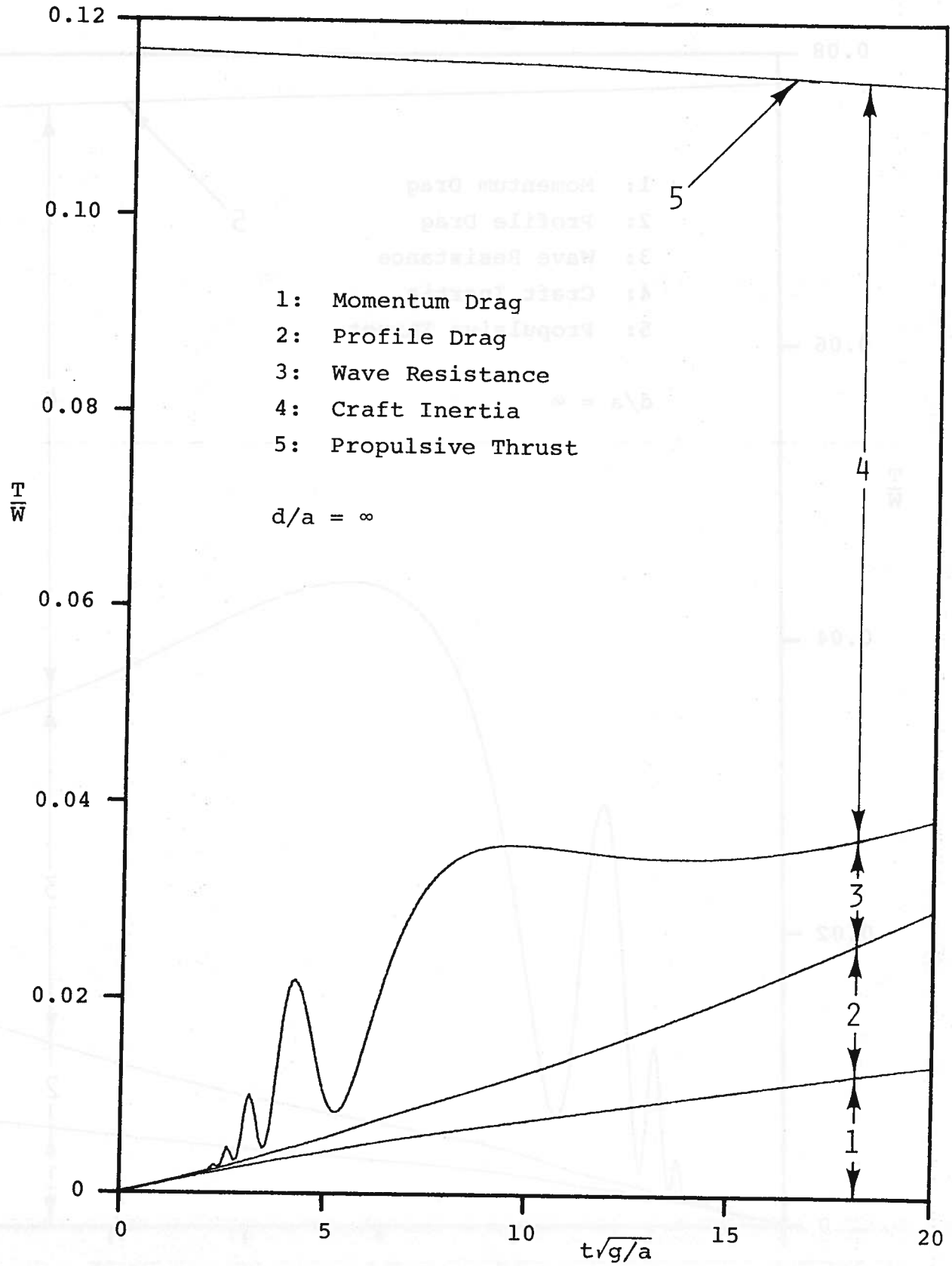

Fig. 37 QS Drag Components in Deep Water (Const. Prop. Revs.)
(a) Normal Load

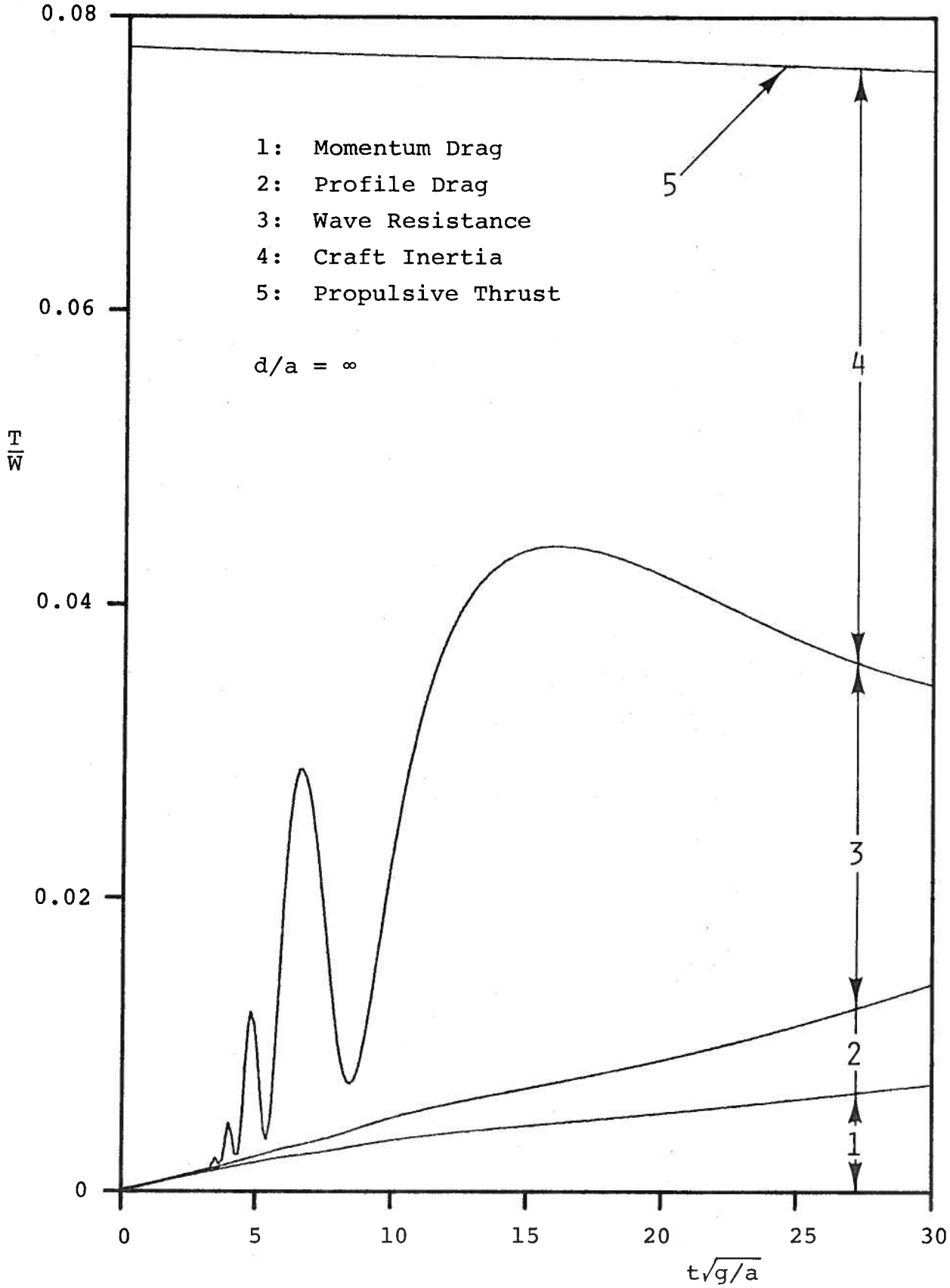

Fig. 37 (cont.) (b) 50% Overload

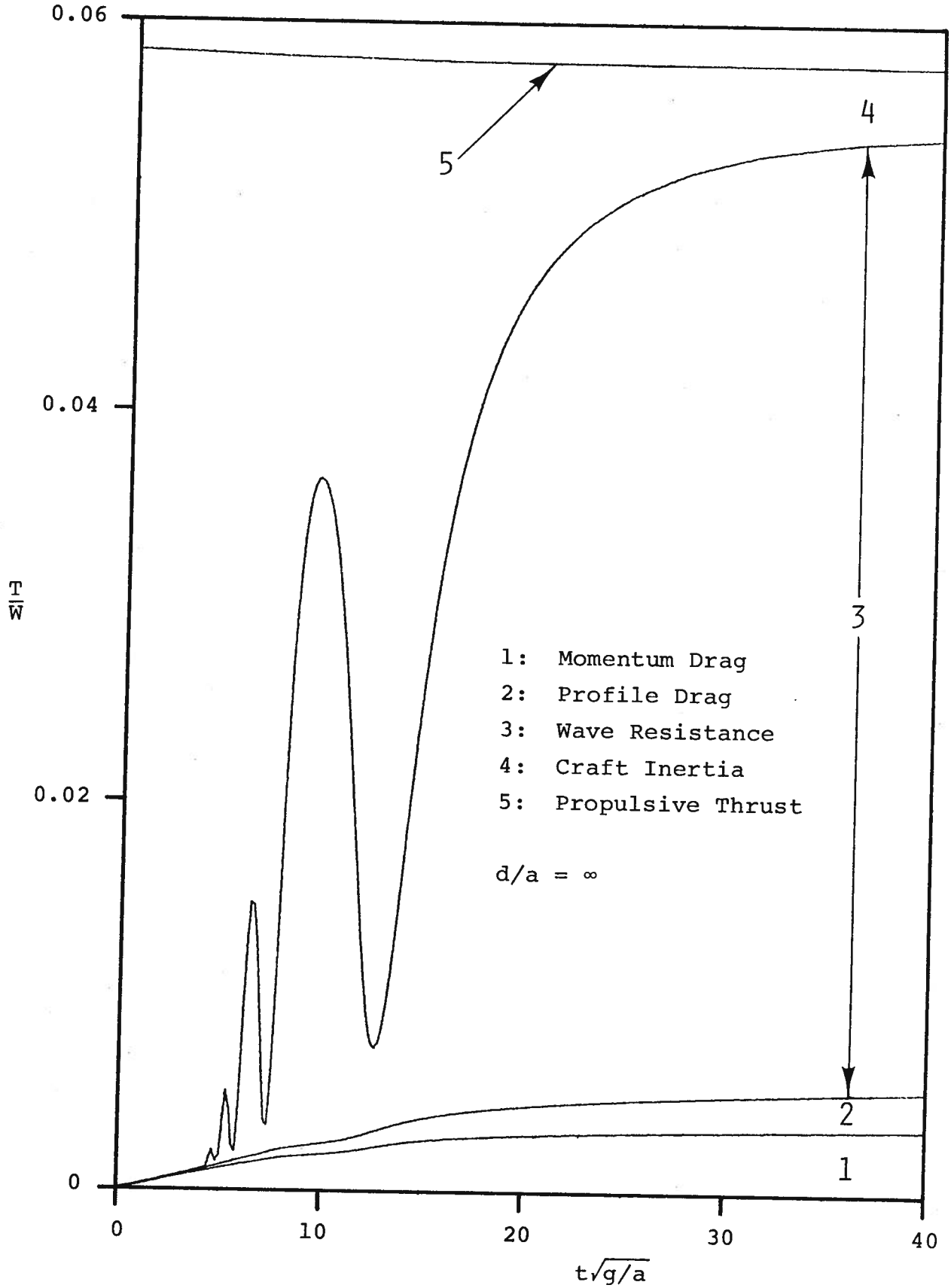

Fig. 37 (cont.) (c) 100% Overload

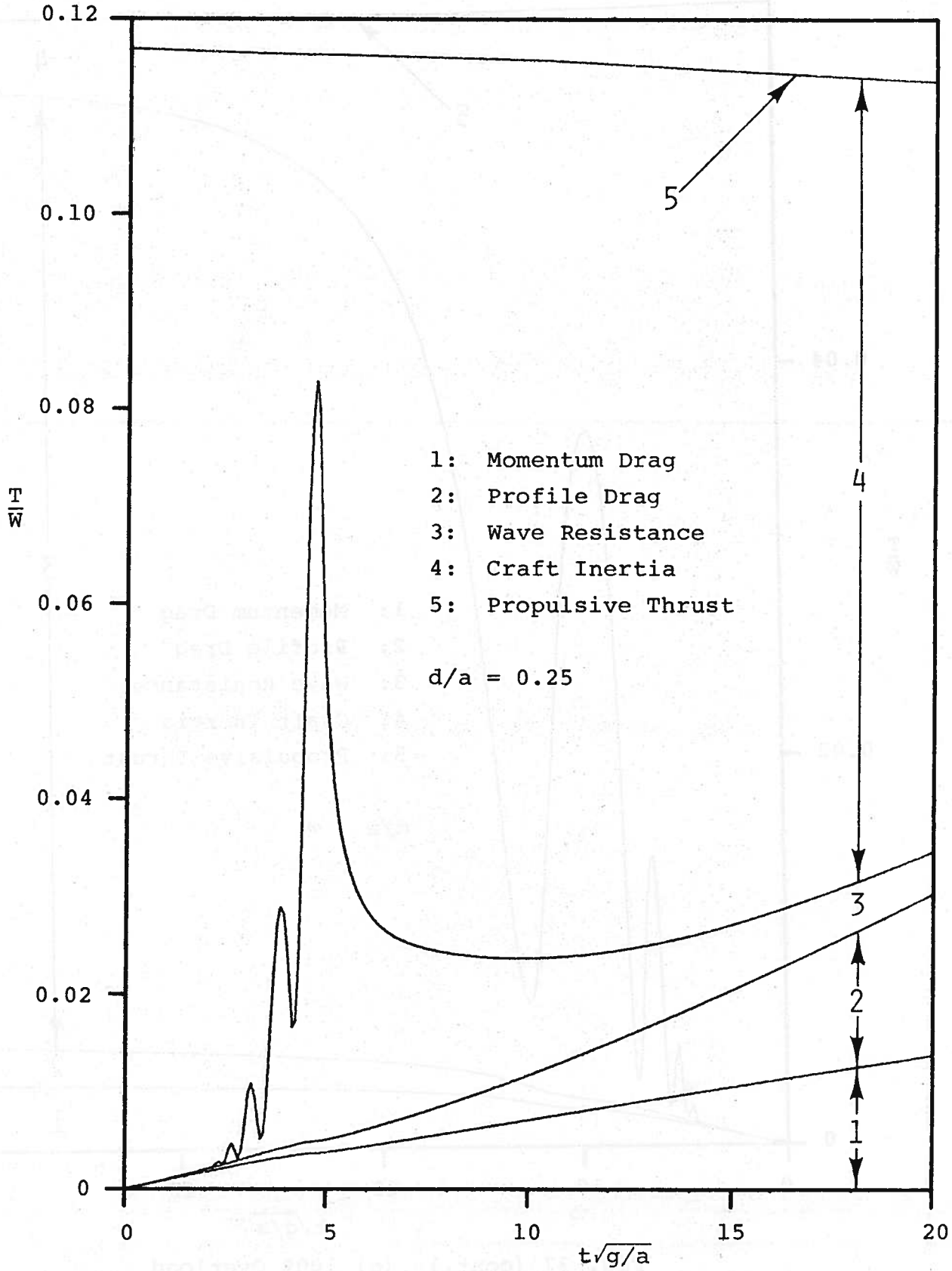

Fig. 38 QS Drag Components in Finite Depth (Const. Prop. Revs.)
(a) Normal Load

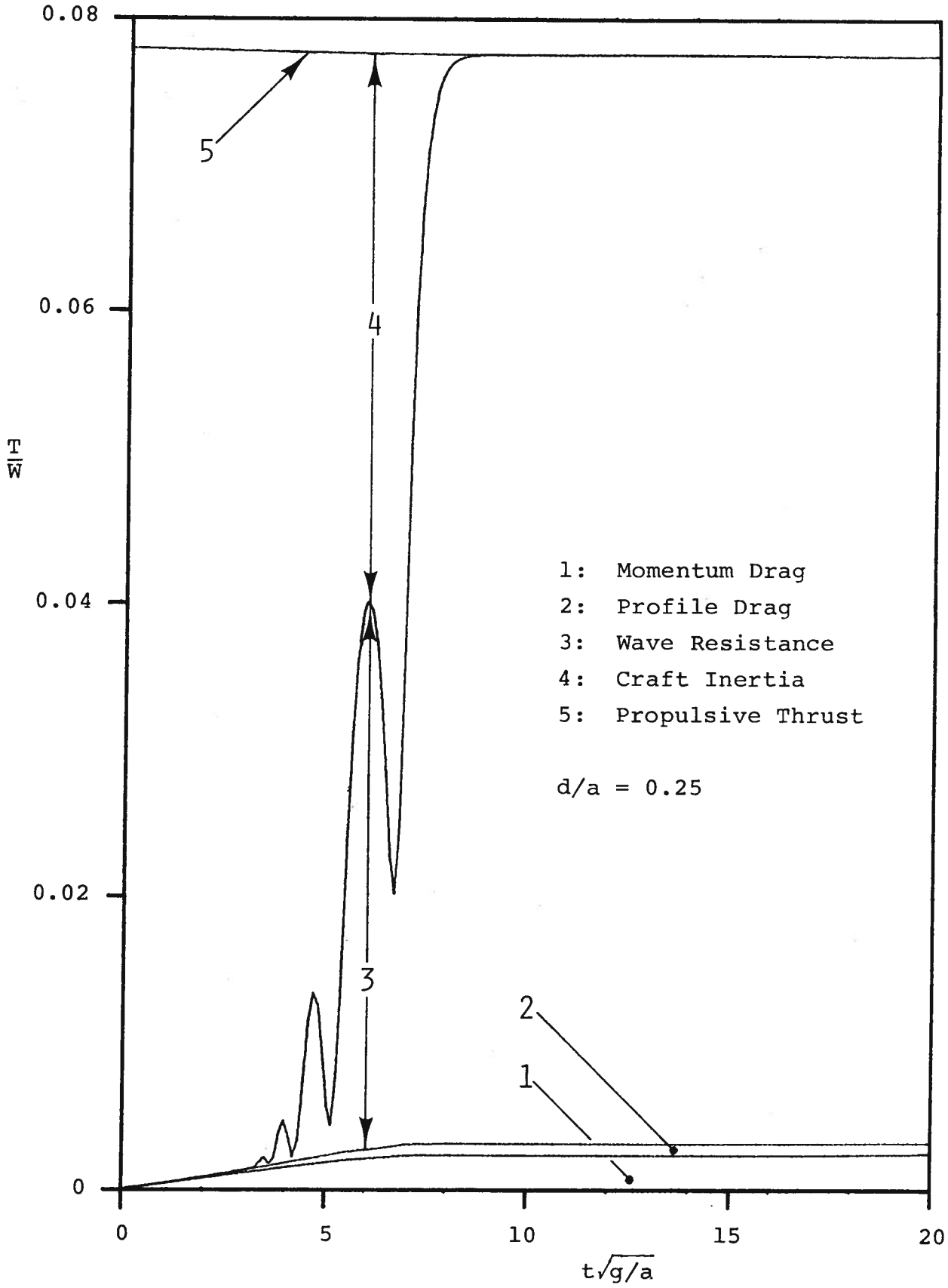

Fig. 38 (cont.) (b) 50% Overload

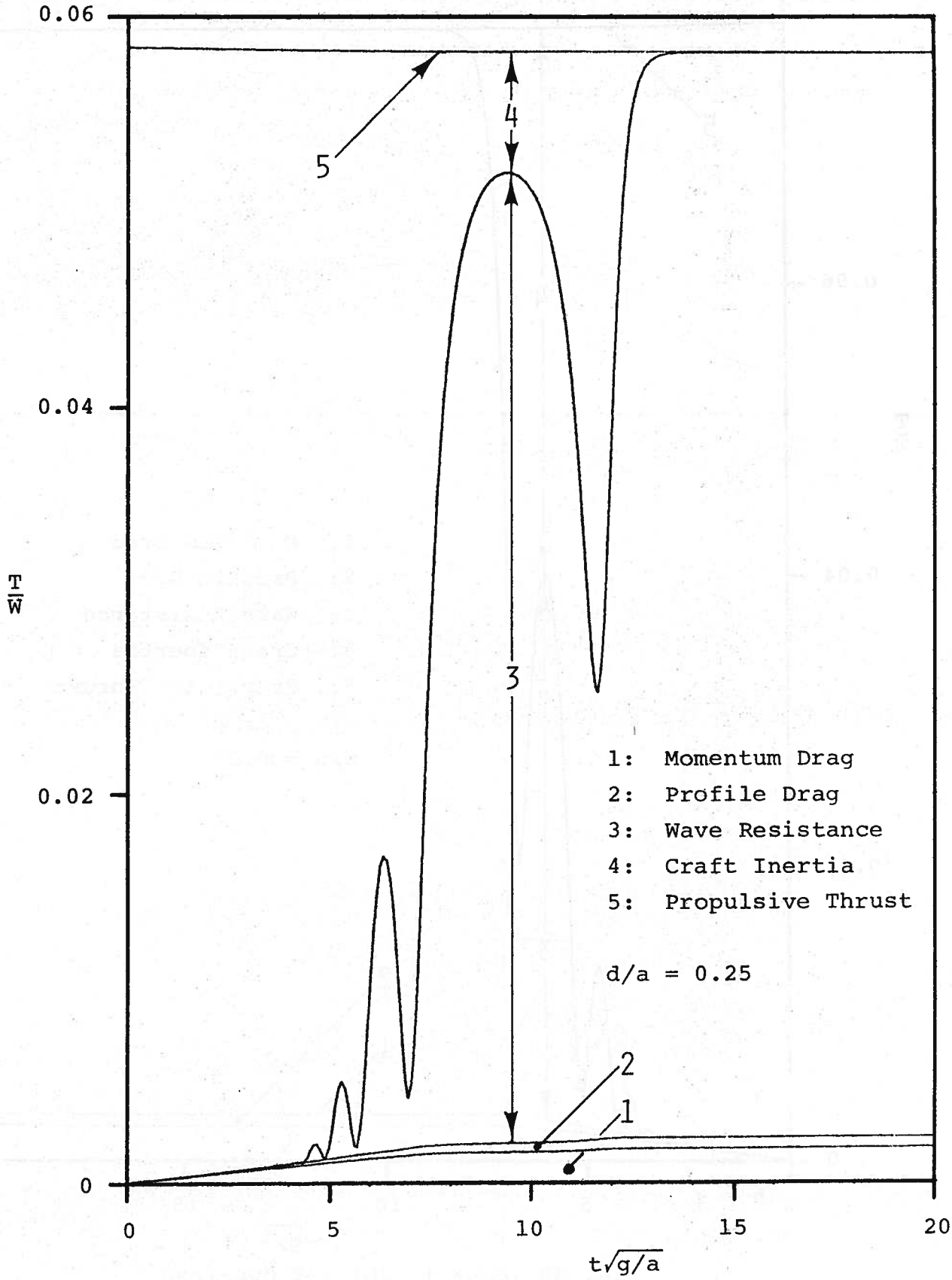

Fig. 38 (cont.) (c) 100% Overload

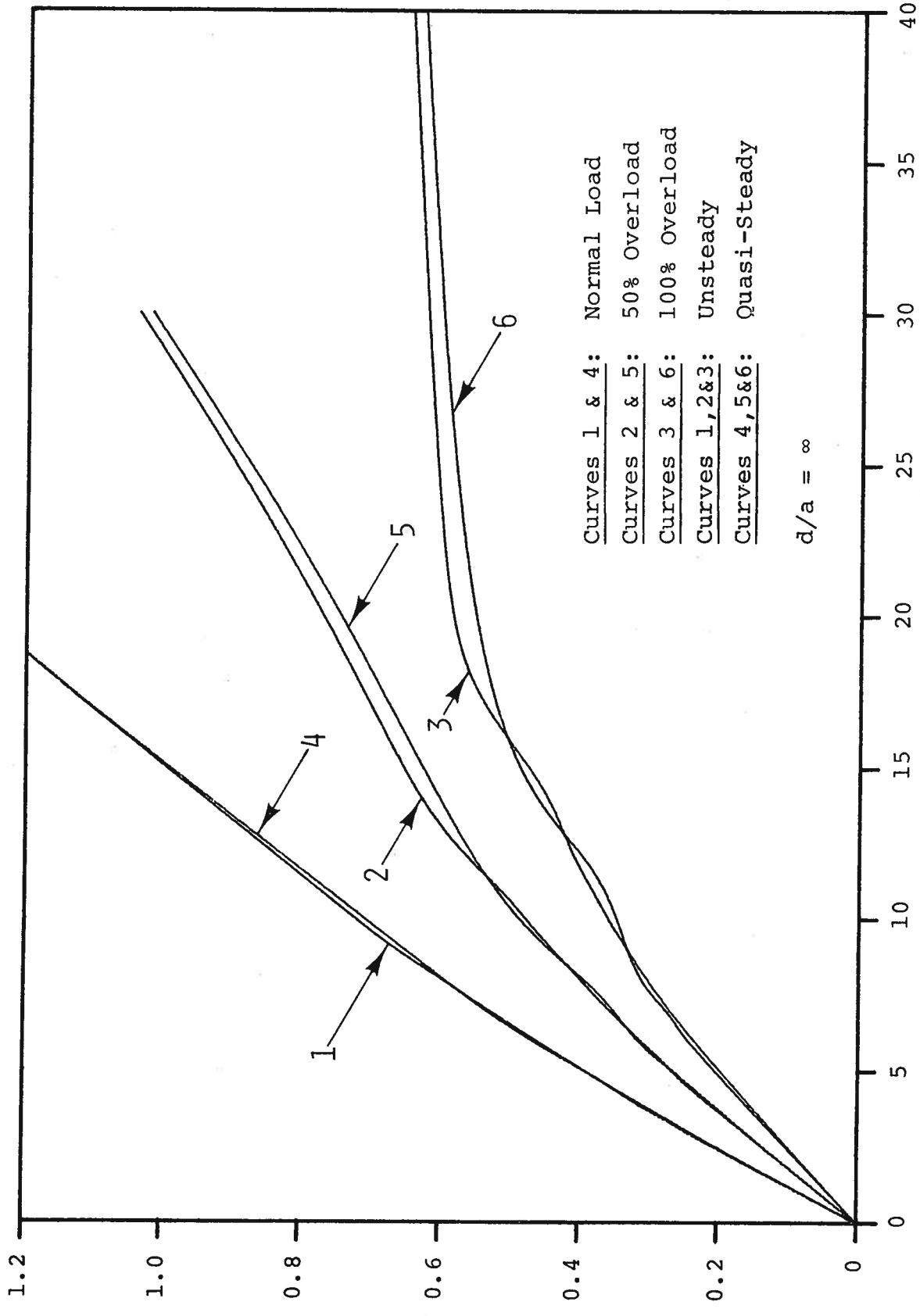

Fig. 39 QS and Unsteady Velocity Patterns in Deep Water (Constant Propeller Revolutions)

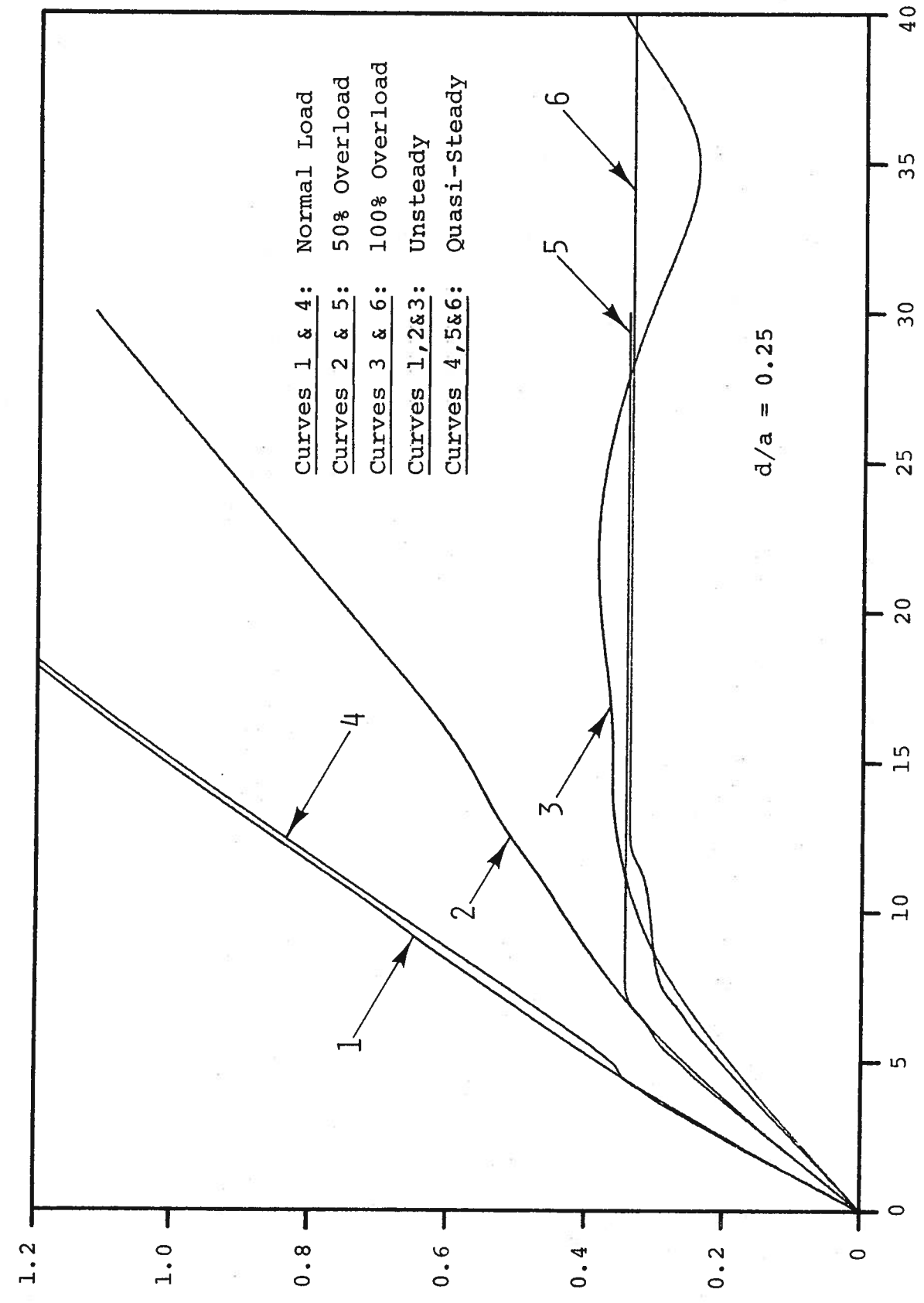

Fig. 40 QS and Unsteady Velocity Patterns in Finite Depth (Constant Propeller Revolutions)

Security Classification

DOCUMENT CONTROL DATA - R & D

(Security classification of title, body of abstract and indexing annotation must be entered when the overall report is classified)

1. ORIGINATING ACTIVITY *(Corporate author)*

Department of Naval Architecture and Marine Engineering, University of Michigan, Ann Arbor, Michigan 48104

2a. REPORT SECURITY CLASSIFICATION

Unclassified

2b. GROUP

3. REPORT TITLE

THE WAVE RESISTANCE OF AN AIR-CUSHION VEHICLE IN ACCELERATED MOTION

4. DESCRIPTIVE NOTES *(Type of report and inclusive dates)*

Technical Report

5. AUTHOR(S) *(First name, middle initial, last name)*

Lawrence J. Doctors and Som D. Sharma

6. REPORT DATE	7a. TOTAL NO. OF PAGES	7b. NO. OF REFS
December 1970	196	41

8a. CONTRACT OR GRANT NO.

N00014-67-A-0181-0018

b. PROJECT NO.

NR 062-420 (Code 438)

c.

d.

9a. ORIGINATOR'S REPORT NUMBER(S)

099

9b. OTHER REPORT NO(S) *(Any other numbers that may be assigned this report)*

10. DISTRIBUTION STATEMENT

Distribution of this report is unlimited

11. SUPPLEMENTARY NOTES

12. SPONSORING MILITARY ACTIVITY

Office of Naval Research
U.S. Department of Defense
Washington, D.C.

13. ABSTRACT

This report is concerned with the theoretical wave resistance of an air-cushion vehicle (ACV) traveling over water of uniform finite or infinite depth, in steady or unsteady motion. Referring first to steady motion, it is shown that the unrealistic oscillations in the wave resistance curve at low Froude numbers found by previous workers can be eliminated by using a smoothed out pressure distribution rather than one with sharp edges studied exclusively in the past. The main result of unsteady motion calculations is that the peak wave resistance in shallow water, even in moderately accelerated motion, is appreciably less than the corresponding steady-state value. In fact, cases have been found where an ACV starting from rest under the action of a constant thrust would seem to be unable to cross the critical depth Froude number on the basis of quasi-steady estimates of wave resistance, while the more elaborate unsteady calculations show that it has sufficient power to reach its final supercritical cruising speed. An interesting feature of unsteady motion is that besides wave resistance there is another mechanism transferring energy to the free surface which is here called the dynamic sustention power. Contrary to intuition, the wave resistance in unsteady motion over finite depth sometimes becomes negative at supercritical Froude numbers before finally approaching zero at infinite speed.

DD FORM 1 NOV 65 1473

Unclassified

Security Classification

Security Classification

14. KEY WORDS	LINK A		LINK B		LINK C	
	ROLE	WT	ROLE	WT	ROLE	WT
Air-Cushion Vehicle						
Wave Resistance						
Accelerated Motion						
Finite Depth						
Sustention Power						
Pressure Distribution						
Free-Surface Effects						
Unsteady Motion						
Shallow Water						

Unclassified

Security Classification

October 1970

APPROVED DISTRIBUTION LIST FOR
UNCLASSIFIED TECHNICAL REPORTS
ISSUED UNDER CONTRACT N00014-67-A-0181-0018
ONR TASK NO. NR062-420

Technical Library
Building 131
Aberdeen Proving Ground
Maryland 21005

Defense Documentation Center
Cameron Station (20)
Alexandria, Virginia 22314

Technical Library
Naval Ship Research and
Development Center
Annapolis Division
Annapolis, Maryland 21402

Professor Bruce Johnson
Engineering Department
Naval Academy
Annapolis, Maryland 21402

Library
Naval Academy
Annapolis, Maryland 21402

Professor W. P. Graebel
Department of Engineering
Mechanics
The University of Michigan
College of Engineering
Ann Arbor, Michigan 48104

Professor W. R. Debler
Department of Engineering
Mechanics
University of Michigan
Ann Arbor, Michigan 48104

Dr. Francis Ogilvie
Department of Naval Arch.
and Marine Engineering
University of Michigan
Ann Arbor, Michigan 48104

Professor S. D. Sharma
Department of Naval Architec-
ture and Marine Engineering
University of Michigan
Ann Arbor, Michigan 48104

Professor W. W. Willmarth
Department of Aerospace
Engineering
University of Michigan
Ann Arbor, Michigan 48104

Professor Finn C. Michelsen
Naval Architecture and Marine
Engineering
445 West Engineering Bldg.
University of Michigan
Ann Arbor, Michigan 48104

AFOSR (REM)
1400 Wilson Boulevard
Arlington, Virginia 22204

Dr. J. Menkes
Institute for Defense Analyses
400 Army-Navy Drive
Arlington, Virginia 22204

Professor S. Corrsin
Mechanics Department
The Johns Hopkins University
Baltimore, Maryland 20910

Professor O. M. Phillips
The Johns Hopkins University
Baltimore, Maryland 20910

Professor L. S. G. Kovasznay
The Johns Hopkins University
Baltimore, Maryland 20910

Librarian
Department of Naval Architec-
ture
University of California
Berkeley, California 94720

Professor P. Lieber
Department of Mechanical Engineering
University of California
Institute of Engineering Research
Berkeley, California 94720

Professor M. Holt
Division of Aeronautical Sciences
University of California
Berkeley, California 94720

Professor J. V. Wehausen
Department of Naval Architecture
University of California
Berkeley, California 94720

Professor J. R. Paulling
Department of Naval Architecture
University of California
Berkeley, California 94720

Professor E. V. Laitone
Department of Mechanical Engineering
University of California
Berkeley, California 94720

School of Applied Mathematics
Indiana University
Bloomington, Indiana 47401

Commander
Boston Naval Shipyard
Boston, Massachusetts 02129

Director
Office of Naval Research
Branch Office
495 Summer Street
Boston, Massachusetts 02210

Professor M. S. Uberoi
Department of Aeronautical Engineering
University of Colorado
Boulder, Colorado 80303

Naval Applied Science Laboratory
Technical Library
Bldg. 1 Code 222
Flushing and Washington Aves.
Brooklyn, New York 11251

Professor J. J. Foody
Chairman, Engineering Department
State University of New York
Maritime College
Bronx, New York 10465

Dr. Irving C. Statler, Head
Applied Mechanics Department
Cornell Aeronautical Laboratory, Inc.
P. O. Box 235
Buffalo, New York 14221

Dr. Alfred Ritter
Assistant Head, Applied Mechanics Department
Cornell Aeronautical Laboratory, Inc.
Buffalo, New York 14221

Professor G. Birkhoff
Department of Mathematics
Harvard University
Cambridge, Massachusetts 02138

Commanding Officer
NROTC Naval Administrative Unit
Massachusetts Institute of Technology
Cambridge, Massachusetts 02139

Professor N. Newman
Department of Naval Architecture and Marine Engineering
Massachusetts Institute of Technology
Cambridge, Massachusetts 02139

Professor A. H. Shapiro
Department of Mechanical Engineering
Massachusetts Institute of Technology
Cambridge, Massachusetts 02139

Professor C. C. Lin
Department of Mathematics
Massachusetts Institute
of Technology
Cambridge, Massachusetts 02139

Professor E. W. Merrill
Department of Mathematics
Massachusetts Institute of
Technology
Cambridge, Massachusetts 02139

Professor M. A. Abkowitz
Department of Naval Architec-
ture and Marine Engineering
Massachusetts Institute of
Technology
Cambridge, Massachusetts 02139

Professor G. H. Carrier
Department of Engineering and
Applied Physics
Harvard University
Cambridge, Massachusetts 02139

Professor E. Mollo-Christensen
Room 54-1722
Massachusetts Institute
of Technology
Cambridge, Massachusetts 02139

Professor A. T. Ippen
Department of Civil Engineering
Massachusetts Institute of
Technology
Cambridge, Massachusetts 02139

Commander
Charleston Naval Shipyard
U. S. Naval Base
Charleston, South Carolina
29408

A. R. Kuhlthau, Director
Research Laboratories for the
Engineering Sciences
Thorton Hall, University of
Virginia
Charlottesville, Virginia
22903

Director
Office of Naval Research
Branch Office
219 Dearborn Street
Chicago, Illinois 60604

Library
Naval Weapons Center
China Lake, California 93557

Library MS 60-3
NASA Lewis Research Center
21000 Brookpark Road
Cleveland, Ohio 44135

Professor J. M. Burgers
Institute of Fluid Dynamics
and Applied Mathematics
University of Maryland
College Park, Maryland 20742

Acquisition Director
NASA Scientific & Technical
Information
P. O. Box 33
College Park, Maryland 20740

Professor Pai
Institute for Fluid Dynamics
and Applied Mathematics
University of Maryland
College Park, Maryland 20740

Technical Library
Naval Weapons Laboratory
Dahlgren, Virginia 22448

Computation & Analyses
Laboratory
Naval Weapons Laboratory
Dahlgren, Virginia 22448

Professor C. S. Wells
LTV Research Center
Dallas, Texas 75222

Dr. R. H. Kraichnan
Dublin, New Hampshire 03444

Commanding Officer
Army Research Office
Box CM, Duke Station
Durham, North Carolina 27706

Professor A. Charnes
The Technological Institute
Northwestern University
Evanston, Illinois 60201

Dr. Martim H. Bloom
Polytechnic Institute of
Brooklyn - Graduate Center,
Department of Aerospace
Engineering and Applied
Mechanics
Farmingdale, New York 11735

Technical Documents Center
Building 315
U. S. Army Mobility Equipment
Research and Development Center
Fort Belvoir, Virginia 22060

Professor J. E. Cermak
College of Engineering
Colorado State University
Ft. Collins, Colorado 80521

Technical Library
Webb Institute of Naval
Architecture
Glen Cove, Long Island,
New York 11542

Professor E. V. Lewis
Webb Institute of Naval
Architecture
Glen Cove, Long Island
New York 11542

Library MS 185
NASA, Langley Research Center
Langley Station
Hampton, Virginia 23365

Dr. B. N. Pridmore Brown
Northrop Corporation
NORAIR-Div.
Hawthorne, California 90250

Dr. J. P. Breslin
Stevens Institute of Technology
Davidson Laboratory
Hoboken, New Jersey 07030

Mr. D. Savitsky
Stevens Institute of Technology
Davidson Laboratory
Hoboken, New Jersey 07030

Mr. C. H. Henry
Stevens Institute of Technology
Davidson Laboratory
Hoboken, New Jersey 07030

Professor J. F. Kennedy, Director
Iowa Institute of Hydraulic
Research
State University of Iowa
Iowa City, Iowa 52240

Professor L. Landweber
Iowa Institute of Hydraulic
Research
State University of Iowa
Iowa City, Iowa 52240

Professor E. L. Resler
Graduate School of Aeronautical
Engineering
Cornell University
Ithaca, New York 14851

Professor John Miles
I.G.P.P.
University of California,
San Diego
La Jolla, California 92038

Director
Scripps Institution of
Oceanography
University of California
La Jolla, California 92037

Dr. B. Sternlicht
Mechanical Technology Incorporated
968 Albany-Shaker Road
Latham, New York 12110

Mr. P. Eisenberg, President
Hydronautics
Pindell School Road
Howard County
Laurel, Maryland 20810

Professor A. Ellis
University of California
San Diego
Department of Aerospace and
Mechanical Engineering Science
La Jolla, California 92037

Mr. Alfonso Alcedan L. Director
Laboratorio Nacional
De Hydraulics
Antigui Cameno A. Ancon
Casilla Jostal 682
Lima, Peru

Commander
Long Beach Naval Shipyard
Long Beach, California 90802

Professor John Laufer
Department of Aerospace
Engineering
University Park
Los Angeles, California 90007

Professor J. Ripkin
St. Anthony Falls
Hydraulic Laboratory
University of Minnesota
Minneapolis, Minnesota 55414

Professor J. M. Killen
St. Anthony Falls
Hydraulic Laboratory
University of Minnesota
Minneapolis, Minnesota 55414

Lorenz G. Straub Library
St. Anthony Falls
Hydraulic Laboratory
Mississippi River at 3rd Ave.SE
Minneapolis, Minnesota 55414

Dr. E. Silberman
St. Anthony Falls
Hydraulic Laboratory
University of Minnesota
Minneapolis, Minnesota 55414

Superintendent
Naval Postgraduate School
Library Code 0212
Monterey, California 93940

Professor A. B. Metzner
University of Delaware
Newark, New Jersey 19711

Technical Library
USN Underwater Weapons
Research & Engineering Station
Newport, Rhode Island 02840

Technical Library
Underwater Sound Laboratory
Fort Trumbull
New London, Connecticut 06321

Professor J. J. Stoker
Institute of Mathematical
Sciences
New York University
251 Mercer Street
New York, New York 10003

Engineering Societies Library
345 East 47th Street
New York, New York 10017

Office of Naval Research
New York Area Office
207 W. 24th Street
New York, New York 10011

Commanding Officer
Office of Naval Research
Branch Office
Box 39
FPO New York, New York 09510 (25)

Professor H. Elrod
Department of Mechanical
Engineering
Columbia University
New York, New York 10027

Society of Naval Architects
and Marine Engineering
74 Trinity Place
New York, New York 10006

United States Atomic Energy Commission
Division of Technical Information Extension
P. O. Box 62
Oak Ridge, Tennessee 37830

Miss O. M. Leach, Librarian
National Research Council
Aeronautical Library
Montreal Road
Ottawa 7, Canada

Technical Library
Naval Ship Research and Development Center
Panaman City, Florida 32401

Library
Jet Propulsion Laboratory
California Institute of Technology
4800 Oak Grove Avenue
Pasadena, California 91109

Professor M. S. Plesset
Engineering Division
California Institute of Technology
Pasadena, California 91109

Professor H. Liepmann
Department of Aeronautics
California Institute of Technology
Pasadena, California 91109

Technical Library
Naval Undersea Research and Development Center
3202 E. Foothill Boulevard
Pasadena, California 91107

Dr. J. W. Hoyt
Naval Undersea Research and Development Center
3202 E. Foothill Boulevard
Pasadena, California 91107

Professor T. Y. Wu
Department of Engineering
California Institute of Technology
Pasadena, California 91109

Director
Office of Naval Research
Branch Office
1030 E. Green Street
Pasadena, California 91101

Professor A. Acosta
Department of Mechanical Engineering
California Institute of Technology
Pasadena, California 91109

Naval Ship Engineering Center
Philadelphia Division
Technical Library
Philadelphia, Pennsylvania 19112

Technical Library (Code 249B)
Philadelphia Naval Shipyard
Philadelphia, Pennsylvania 19112

Professor R. C. Mac Camy
Department of Mathematics
Carnegie Institute of Technology
Pittsburgh, Pennsylvania 15213

Dr. Paul Kaplan
Oceanics, Inc.
Plainview, Long Island,
New York 11803

Technical Library
Naval Missile Center
Point Mugu, California 93441

Technical Library
Naval Civil Engineering Lab.
Port Hueneme, California 93041

Commander
Portsmouth Naval Shipyard
Postsmouth, New Hampshire 03801

Commander
Norfolk Naval Shipyard
Portsmouth, Virginia 23709

Professor F. E. Bisshopp
Division of Engineering
Brown University
Providence, Rhode Island 02912

Dr. L. L. Higgins
TRW Space Technology Labs, Inc.
One Space Park
Redondo Beach, California 90278

Redstone Scientific Information Center
Attn: Chief, Document Section
Army Missile Command
Redstone Arsenal, Alabama 35809

Dr. H. N. Abramson
Southwest Research Institute
8500 Culebra Road
San Antonio, Texas 78228

Editor
Applied Mechanics Review
Southwest Research Institute
8500 Culebra Road
San Antonio, Texas 78206

Librarian
Naval Command Control Communications Laboratory Center
San Diego, California 92152

Library & Information Services
General Dynamics-Convair
P. O. Box 1128
San Diego, California 92112

Commander (Code 246P)
Pearl Harbor Naval Shipyard
Box 400
FPO San Francisco, California 96610

Technical Library (Code H245C-3)
Hunters Point Division
San Francisco Bay Naval Shipyard
San Francisco, California 94135

Office of Naval Research
San Francisco Area Office
50 Fell Street
San Francisco, California 94103

Dr. A. May
Naval Ordnance Laboratory
White Oak
Silver Spring, Maryland 20910

Fenton Kennedy Document Library
The Johns Hopkins University
Applied Physics Laboratory
8621 Georgia Avenue
Silver Spring, Maryland 20910

Librarian
Naval Ordnance Laboratory
White Oak
Silver Spring, Maryland 20910

Dr. Bryne Perry
Department of Civil Engineering
Stanford University
Stanford, California 94305

Professor Milton Van Dyke
Department of Aeronautical Engineering
Stanford University
Stanford, California 94305

Professor E. Y. Hsu
Department of Civil Engineering
Stanford University
Stanford, California 94305

Dr. R. L. Street
Department of Civil Engineering
Stanford University
Stanford, California 94305

Professor S. Eskinazi
Department of Mechanical Engineering
Syracuse University
Syracuse, New York 13210

Professor R. Pfeffer
Florida State University
Geophysical Fluid Dynamics Institute
Tallahassee, Florida 32306

Professor J. Foa
Department of Aeronautical Engineering
Rennsselaer Polytechnic Institute
Troy, New York 12180

Professor R. C. Di Prima
Department of Mathematics
Rennsselaer Polytechnic Institute
Troy, New York 12180

Dr. M. Sevik
Ordnance Research Laboratory
Pennsylvania State University
University Park, Pennsylvania
16801

Professor J. Lumley
Ordnance Research Laboratory
Pennsylvania State University
University Park, Pennsylvania
16801

Dr. J. M. Robertson
Department of Theoretical and
Applied Mechanics
University of Illinois
Urbana, Illinois 61803

Shipyard Technical Library
Code 130L7 Building 746
San Francisco Bay Naval Shipyard
Vallejo, California 94592

Code L42
Naval Ship Research and
Development Center
Washington, D. C. 20007

Code 800
Naval Ship Research and
Development Center
Washington, D. C. 20007

Code 2027
U. S. Naval Research Laboratory
Washington, D. C. 20390 (6)

Chief of Naval Research
(Code 438)
Department of the Navy
Arlington, Virginia 22217 (3)

Code 513
Naval Ship Research and
Development Center
Washington, D. C. 20007

Science & Technology Division
Library of Congress
Washington, D. C. 20540

ORD 913 (Library)
Naval Ordnance Systems Command
Washington, D. C. 20360

Code 6420
Naval Ship Engineering Center
Concept Design Division
Washington, D. C. 20360

Code 500
Naval Ship Research and
Development Center
Washington, D. C. 20007

Code 901
Naval Ship Research and
Development Center
Washington, D. C. 20007

Code 520
Naval Ship Research and
Development Center
Washington, D. C. 20007

Code 0341
Naval Ship Systems Command
Department of the Navy
Washington, D. C. 20360

Code 2052 (Technical Library)
Naval Ship Systems Command
Department of the Navy
Washington, D. C. 20360

Mr. J. L. Schuler (Code 03412)
Naval Ship Systems Command
Department of the Navy
Washington, D. C. 20360

Dr. J. H. Huth (Code 031)
Naval Ship Systems Command
Department of the Navy
Washington, D. C. 20360

Code 461
Chief of Naval Research
Department of the Navy
Washington, D. C. 20360

Code 530
Naval Ship Research and
Development Center
Washington, D. C. 20360

Code 466
Chief of Naval Research
Department of the Navy
Washington, D. C. 20360

Office of Research and
Development
Maritime Administration
441 G. Street, NW
Washington, D. C. 20235

Code 463
Chief of Naval Research
Department of the Navy
Washington, D. C. 20360

National Science Foundation
Engineering Division
1800 G. Street, NW
Washington, D.C. 20550

Dr. G. Kulin
National Bureau of Standards
Washington, D. C. 20234

Department of the Army
Coastal Engineering Research
Center
5201 Little Falls Road, NW
Washington, D. C. 20011

Code 521
Naval Ship Research and
Development Center
Washington, D. C. 20007

Code 481
Chief of Naval Research
Department of the Navy
Washington, D.C. 20390

Code 421
Chief of Naval Research
Department of the Navy
Washington, D. C. 20360

Commander
Naval Ordnance Systems Command
Code ORD 035
Washington, D.C. 20360

Librarian Station 5-2
Coast Guard Headquarters
1300 E. Street, NW
Washington, D.C. 20226

Division of Ship Design
Maritime Administration
441 G. Street, NW
Washington, D.C. 20235

HQ USAF (AFRSTD)
Room 1D 377
The Pentagon
Washington, D.C. 20330

Commander
Naval Ship Systems Command
Code 6644C
Washington, D.C. 20360

Dr. A. Powell (Code 01)
Naval Ship Research and
Development Center
Washington, D.C. 20007

Director of Research Code RR
National Aeronautics &
Space Administration
600 Independence Avenue, SW
Washington, D.C. 20546

Commander
Naval Ordnance Systems Command
Code 03
Washington, D.C. 20360

Code ORD 05411
Naval Ordnance Systems Command
Washington, D.C. 20360

AIR 5301
Naval Air Systems Command
Department of the Navy
Washington, D.C. 20360

AIR 604
Naval Air Systems Command
Department of the Navy
Washington, D.C. 20360

Dr. John Craven (PM 1100)
Deep Submergence Systems
Project
Department of the Navy
Washington, D.C. 20360

Code 522
Naval Ship Research and
Development Center
Washington, D.C. 20007

Commander
Naval Oceanographic Office
Washington, D.C. 20390

Chief of Research & Development
Office of Chief of Staff
Department of the Army
The Pentagon
Washington, D.C. 20310

Code 6342A
Naval Ship Systems Command
Department of the Navy
Washington, D.C. 20360

Code 468
Chief of Naval Research
Department of the Navy
Washington, D.C. 20360

Director
U.S. Naval Research Laboratory
Code 6170
Washington, D.C. 20390

Code 473
Chief of Naval Research
Department of the Navy
Washington, D.C. 20360

Code 6100
Naval Ship Engineering Center
Department of the Navy
Washington, D.C. 20360

Mr. Ralph Lacey (Code 6114)
Naval Ship Engineering Center
Department of the Navy
Washington, D.C. 20360

Dr. A. S. Iberall, President
General Technical Services, Inc.
451 Penn Street
Yeadon, Pennsylvania 19050

Dr. H. Cohen
IBM Research Center
P.O. Box 218
Yorktown Heights, New York
10598

Professor S. A. Piascek
Department of Engineering
Mechanics
University of Notre Dame
Notre Dame, Indiana 46556

Security Classification

DOCUMENT CONTROL DATA - R & D

(Security classification of title, body of abstract and indexing annotation must be entered when the overall report is classified)

1. ORIGINATING ACTIVITY *(Corporate author)*	2a. REPORT SECURITY CLASSIFICATION
Department of Naval Architecture and Marine Engineering, University of Michigan, Ann Arbor, Michigan 48104	Unclassified
	2b. GROUP

3. REPORT TITLE

THE WAVE RESISTANCE OF AN AIR-CUSHION VEHICLE IN ACCELERATED MOTION

4. DESCRIPTIVE NOTES *(Type of report and inclusive dates)*

Technical Report

5. AUTHOR(S) *(First name, middle initial, last name)*

Lawrence J. Doctors and Som D. Sharma

6. REPORT DATE	7a. TOTAL NO. OF PAGES	7b. NO. OF REFS
December 1970	196	41

8a. CONTRACT OR GRANT NO.	9a. ORIGINATOR'S REPORT NUMBER(S)
N00014-67-A-0181-0018	
b. PROJECT NO. NR 062-420 (Code 438)	099
c.	9b. OTHER REPORT NO(S) *(Any other numbers that may be assigned this report)*
d.	

10. DISTRIBUTION STATEMENT

Distribution of this report is unlimited

11. SUPPLEMENTARY NOTES	12. SPONSORING MILITARY ACTIVITY
	Office of Naval Research U.S. Department of Defense Washington, D.C.

13. ABSTRACT

This report is concerned with the theoretical wave resistance of an air-cushion vehicle (ACV) traveling over water of uniform finite or infinite depth, in steady or unsteady motion. Referring first to steady motion, it is shown that the unrealistic oscillations in the wave resistance curve at low Froude numbers found by previous workers can be eliminated by using a smoothed out pressure distribution rather than one with sharp edges studied exclusively in the past. The main result of unsteady motion calculations is that the peak wave resistance in shallow water, even in moderately accelerated motion, is appreciably less than the corresponding steady-state value. In fact, cases have been found where an ACV starting from rest under the action of a constant thrust would seem to be unable to cross the critical depth Froude number on the basis of quasi-steady estimates of wave resistance, while the more elaborate unsteady calculations show that it has sufficient power to reach its final supercritical cruising speed. An interesting feature of unsteady motion is that besides wave resistance there is another mechanism transferring energy to the free surface which is here called the dynamic sustention power. Contrary to intuition, the wave resistance in unsteady motion over finite depth sometimes becomes negative at supercritical Froude numbers before finally approaching zero at infinite speed.

DD FORM 1 NOV 65 1473

Unclassified

Security Classification

14. KEY WORDS	LINK A		LINK B		LINK C	
	ROLE	WT	ROLE	WT	ROLE	WT
Air-Cushion Vehicle						
Wave Resistance						
Accelerated Motion						
Finite Depth						
Sustention Power						
Pressure Distribution						
Free-Surface Effects						
Unsteady Motion						
Shallow Water						